The University of Canterbury

Finite Elements for Yarn Mechanics

by

Wayne Alistair Munro

A thesis submitted in partial

fulfillment of the requirements

for the degree of

Doctor of Philosophy.

Department of Civil Engineering

Christchurch, New Zealand

1995

Abstract

Finite element analysis is applied in a rigorous manner to the field of yarn mechanics. Unlike previous numerical yarn analyses this approach does not restrict the possible yarn deformations or loading conditions. The model can represent yarn deformation in extension, torsion, bending or any combination of these actions. A finite element is developed to overcome the difficulties introduced by a fibrous material such as nonlinearities from both geometry and material properties as well as a high degree of material anisotropy.

The concept of basing a continuum analysis on a two contact point bending element was investigated. It is found that the lack of fibre direction continuity between bending elements is unrealistic. Attempts to compensate for the energy loss using statistical methods prove unsuccessful.

A finite element is developed which exploits the anisotropic properties of the material to simplify the element formulation. A system of modal decomposition is used to form the properties of the element in a coordinate system based on the deformation modes of the element. This allows the various structural properties of the fibre and those of the continuum to be defined individually. The properties can also be variable allowing a nonlinear material definition. Theory defining the transformation of the element properties between the modal coordinate system and the conventional nodal coordinate system was derived.

A two dimensional finite element program using the modal approach was written. Deformation results were favourably verified against an array of springs.

Modal analysis was extended into three dimensions using a finite element based on a six faced block. Results from the three dimensional analysis demonstrate that the model can represent the deformation of a yarn in a variety of states.

Acknowledgements

The Author thanks the Wool Research Organisation of New Zealand for both financial support through a doctoral fellowship and technical support, the lack of either would have made this project impossible.

This project was conducted under the supervision of Dr Athol Carr[1], Dr Garth Carnaby[2], Dr Peter Moss[1] and Dr Surinder Tandon[2] who all need to be thanked for their ideas, insights and enthusiasm when the project was going well and for their understanding when it was not.

Friends and family deserve accolades for tolerating what was sometimes an erratic character, the support from these sources was invaluable and prevented the development of a bitter twisted individual. Although there is insufficient space to name all those who have helped over the years, special mention must be made of a few. Roger Vreugdenhil, Grant Ryan, Nathan Schmidt, Gavin Macaulay, Amanda Hastrop and Craig Allan have all contributed in some way to the final state of this project for which they have the Author's gratitude.

Thanks to the Civil Engineering Department for their assistance over the years and specifically the computing staff for allowing the Author a high degree of freedom on the computer systems. The staff from the University Computer Services Centre are also thanked for their understanding.

---

[1] University of Canterbury, Civil Engineering Department.

[2] Wool Research Organisation of New Zealand.

Contents

List of Figures

1 Introduction

To design woollen structures such as carpets or fabrics an understanding of the internal workings of the woollen yarn is required. Increasing industrial competition demands more and more from fibrous textile designers and in turn they demand better knowledge of their material. The development of new methods of investigating fibrous actions is critical. The quest for better understanding of fibrous problems is also motivated by the more academic desire of research to increase the knowledge of a subject.

Research into yarn mechanics is not new, the field of research has been active for decades and during that time both numerical methods and analytical methods have been used. Variations of finite element analyses have been applied to yarn problems in the past but none have provided a general element suitable for use in loading patterns other than those investigated. These numerical analyses suffer from the difficulty that affects most analytic approaches, they are limited in the type of problem to which they can be applied. A correctly configured finite element can be applied to a wide range of situations and the fibrous analysis *tool box* could be considered incomplete not to have a rigorous finite element analysis at call.

This project set out to develop a general finite element for yarn mechanics. Such a model should be able to predict the actions of a yarn under general deformations in that any combination of extension, torsion, bending or lateral compression could be applied to the yarn model.

The finite element was to be developed to model woollen yarns, introducing a number of complications to the process. Woollen yarns consist of staple fibres so they have highly nonlinear material properties and in addition the fibre material itself is also nonlinear. Yarns undergo large scale deformation, adding another degree of complicating nonlinearity to the analysis. In order to apply the finite element approach the yarn must be modelled as a continuum which presents further problems as the stiffness of the continuum in the fibre direction can be many orders of magnitude different from those in other directions. Due to computational limitations numerical processes tend to have difficulty with such large differences in stiffness.

A number of alternatives were investigated before an approach was selected for the yarn mechanics finite element. A system of modal decomposition was used to form the properties of the element in a coordinate system based on the deformation modes of the element. This allows the various structural properties of the fibre and those of the continuum to be defined individually. The properties can also be fully variable allowing a nonlinear material definition. The necessary theory defining the transformation of the element properties between the modal coordinate system and the conventional nodal coordinate system was derived.

For simplicity an analysis was developed based on treating the fibres as continuous elastic helices. This is clearly a poor representation of the time dependent visco-elastic nature of the fibre material and also ignores the possibility of slippage of the staple fibres. More realistic properties could be substituted after a functional analysis system had been developed.

A two dimensional finite element model was programmed using the modal theory. To verify the model an array of springs were deformed and the displacement data from the springs matched against the results from the numerical model. Good agreement was found between the two data sets.

The three dimensional modal element was based on a general six faced block. The added complications of three dimensions caused difficulties for this element. Three dimensions introduced fibre torsion which was not present in the two dimensional analysis and it proved difficult to find a satisfactory model for this deformation. The definition of the element resistance to the lateral contraction of the fibre assembly (jamming) was also difficult in three dimensions due to the extra degrees of freedom involved.

Due to an unsatisfactory resolution of the definition of the lateral jamming the modal element is restricted in the range of problems to which it can be applied. A series of results are presented which show that the element jamming is a significant problem but also that the fibrous finite element model has some potential. A proposal for a five faced (triangular prism) three dimensional element would solve this jamming problem and open the full range of yarn mechanics problems to investigation using a finite element analysis.

Thesis Overview

Chapter Two

A brief review of the literature on both yarn mechanics and unit cell theory.

Chapter Three

An outline of the theory of continuum mechanics and finite element analysis.

Chapter Four

An example of the derivation of a simple three dimensional finite element is presented. The limitations of two previous numerical yarn models are discussed.

Chapter Five

Developmental work for the yarn model is presented. The section is mostly concerned with investigation of the properties of a single fibre under deformation. The limitations of an analysis based on single fibre bending models is discussed.

Chapter Six

The concept of having fibres fixed rigidly within a continuum material is introduced. A proposal for a conventional finite element model based on this approach quickly becomes cumbersome and the development is discontinued.

Chapter Seven

An alternative approach to applying the finite element method to a continuum is investigated. The conceptual and theoretical development of the modal analysis method is presented.

Chapter Eight

The definition of the two dimensional modal finite element is given. The various degrees of freedom for the element are defined, as are the equations linking the degrees of freedom in the different coordinate spaces (the modal coordinates or the conventional cartesian coordinates).

Chapter Nine

The two dimensional modal model is verified against an array of springs. Deformation plots from the springs are overlaid with the matching finite element mesh for comparison.

Chapter Ten

A description of the first stage of the development of the three dimensional modal finite element model is given. The element degrees of freedom are defined in a manner similar to that of the two dimensional model. An equation solver was written to overcome a difficulty with the arrangement of the system equations. The torsion resistance of the model proved to be faulty which severely restricted the situations that the model could be used. A simple twisting under tension test was run which gave a good comparison with a theoretical result.

Chapter Eleven

The development of the three dimensional model is continued, a solution for the torsion resistance problem of the element implemented. A range of yarn deformation problems are tested with the element and the results are presented. The tests reveal that finding a stable solution to the element lateral jamming is critical to the continuation of the fibrous finite element model development.

Chapter Twelve

This chapter briefly reviews the thesis, presents the conclusions and points the way forward to the next fibrous finite element model.

2 Literature Review

2.1 Yarn Mechanics

Galileo [13] in 1638 wondered about the mechanism by which a long, strong rope may be made out of many pieces which individually represent only a tiny portion of the total length. An accurate model of this process has still not been achieved although much progress has been made during the last few decades. The mechanisms which allow a staple fibre yarn to 'self-lock' are now understood and successive models are continually improving in accuracy.

All new studies must start with the simplest case available and work slowly towards an all-encompassing theory. How a process such as this has lead to modern day yarn mechanics is outlined below.

In the analysis the yarn as a whole may be treated either as an assembly of interacting discrete units or an *equivalent* continuous material. Both of these methods involve assumptions and put restrictions on the analysis. These restrictions are discussed. A yarn is defined as a collection of roughly aligned fibres which have been twisted to form a structure. In continuous fibre yarn every fibre stretches from one end of the yarn to the other, in contrast, staple fibre yarns are formed from large numbers of fibre pieces, each considerably shorter than the yarn.

2.1.1 Yarn Mechanics Development

The simplest experiment to perform on a yarn is to extend it under tension. This is part of the reason why all of the early yarn models were concerned only with the actions under tension. Observation methods that are available also play a part in deciding the form of the model. When the first researchers were developing models, they were restricted to inspection of the exterior of the yarn and hence early models tended to be very simplistic.

Gégauff [14] was responsible for the first yarn model in 1907 but his work did not come to light until it had already been independently duplicated by Platt [46] in 1950. Consistent with the external appearance of a yarn, their models assumed that the yarn was made of a series of helical fibres, each fibre being identical to its neighbours except

for a displacement and rotation along and about the yarn axis. All fibres were infinitely long with uniform cross section and uniform mechanical properties. There was no interaction allowed between fibres and they were assumed to be slender, therefore allowing only tensile forces. Gégauff and Platt both formulated the relationship between fibre and yarn strain:

$$\epsilon_f = \epsilon_y \cos^2\alpha \qquad (2\text{-}1)$$

Where: ϵ_f = the fibre strain

ϵ_y = the yarn strain

α = fibre helix angle

Platt [44] later modified his theory to incorporate the effects of a helix angle which varies with yarn extension. He showed that for helix angles of less than 45° and continuous filament yarns the difference in the strain is insignificant. He also showed that the modified version of his equation is identical to one calculated in an analysis of yarn bending fibre strains by Backer [1] in 1952. The effects of lateral forces were ignored during these analyses. Lateral contraction was considered but a constant volume stretch was assumed for simplicity. This gave lower fibre strains, by 10% at a 25° helix angle with the difference decreasing with increasing helix angle.

Hearle [16] gave an analysis of yarns which included transverse forces (assuming a hydrostatic pressure distribution), but not lateral contraction. He showed that the transverse forces play an important part in determining the properties of the yarn.
In 1961 Hearle *et. al.* [21] reworked this previous paper - a hydrostatic pressure distribution in the lateral direction was still assumed. The effects of lateral contraction were taken into account by a constant volume relationship. An equation for filament extension was derived which was equivalent to one given by Platt [47] in 1954. Hearle's analysis gave good results for low yarn strains, but failed to give any predictions better than the theory of Platt and Gégauff when yarn rupture was approached.

The methods developed by Hearle above are sometimes called stress methods and they yield detailed information about the internal stresses. However, it is very difficult to combine the effect of both radial contraction and lateral forces using this method. Therefore Treloar and Riding [57] developed an 'energy analysis' method in which the internal elastic energy is expressed in terms of the yarn extension and is then

differentiated with respect to the yarn extension to give the yarn tensile force (this is the virtual work method). The advantages of this energy method are that it can easily cope with large yarn strains, non linear fibre tensile behaviour, radial contraction and lateral forces. The yarn is assumed to extend without any change in volume and this is consistent with experimental results for continuous filament yarns. A uniform packing density is also assumed. A small strain approximation to this analysis shows it to be similar to that of Hearle, El Behery, and Thakur [21].

All of the analyses which had been developed at this stage were valid only for continuous filament yarns. This was because every fibre was assumed to maintain a constant radial position at all cross sections. For a staple fibre yarn this would mean that the fibres on the surface would fall from the yarn. It would be impossible for the yarn to build up any transverse pressures and it would collapse. The effects of fibre migration were first avoided in theoretical analyses. For example, Sullivan [54] in 1942 developed transverse pressures by introducing an arbitrary pressure on the yarn surface. Holdaway [23] in 1965 used an 'ineffective outer layer' to build up transverse pressures. For one solution Pierce [42] proposed that the fibres are a random 'tangle' within the yarn giving it the required cohesion. Morton and Yen [37], after using a tracer fibre technique on a staple fibre yarn proposed regular fibre migration. Riding [50] also found that there was fibre migration in continuous yarns.

Morton [36] suggested that migration may be caused by differential tensions in the fibres, caused by feeding all fibres at the same rate to differing radii in the yarn. The tension mechanism of migration was confirmed in experimentation by Hearle and Merchant [19] on a seven ply yarn and by measurement of migration against yarn twist and yarn count made by Morton [35].

An alternative geometrical mechanism was proposed by Hearle and Bose [17]. Filaments were presented for spinning in a ribbon form and it was proposed that the producer's twist in the ribbon combined with the formation of a wrapped ribbon form caused fibre migration. This mechanism explains the relationship between the period of producer's twist and that of migration, which Riding found unexplainable [49].

Hearle et al [18] discuss the possibility that migration is a simultaneous combination of both mechanisms while Hickie and Chaikin [22] suggested that the tension mechanism is the more important of the two.

Hearle, Gupta, and Merchant [20] developed equations for fibre migration based on a linear variation of the square of the radius with the length along the fibre. An idealized geometry was proposed where every fibre migrates from the surface to the axis and then back to the surface. Migration is assumed to occur slowly so that over a small section of yarn length ideal helical geometry may be assumed for the fibres. Migration is characterized in terms of an analogy with electric current using mean fibre position, rms deviation, and mean migration intensity. An actual migration pattern can then be represented in terms of an idealized pattern.

Treloar [56] modified his earlier energy analysis for ideal migration and came to the same conclusion as Hearle *et. al.* [20] but his solutions made a shortcoming of the theory more obvious. Near the axial region one of their initial assumptions must be abandoned for a solution that is either that all fibres have identical paths or that there is a constant packing density throughout the yarn.

The equations developed are valid for continuous filament yarns (the assumption of constant packing density is not valid for staple fibre yarns), Treloar shows that the difference in yarn strength between migration theory and idealized helical theory is negligible for continuous fibre yarns. It was shown that if the migration period is extended to infinity then the equations tend to the idealized helical theory as expected.

Carnaby and Grosberg [4] used Treloar and Ridings energy method for staple fibre yarns. They tested yarns at short gauge lengths (25mm) to separate the effects of slippage. There was a considerable difference between the results from the experiment and the analysis. The conclusion was that the assumptions of this theory were too restrictive for staple fibre yarns. For example, the packing density is radially dependent and much lower than for a continuous fibre yarn and therefore the assumption of constant volume (or any other uniform lateral contraction) is untenable. The yarn model must be allowed to assume its own geometry, for example, by the use of a radially dependent Poissons ratio. To achieve this it is necessary to define the mechanism which controls the lateral movements of the fibre, for example, the resistance of the fibres to close packing.

Carnaby and Grosberg used a Van Wyk type relationship which defined the pressure as a function of specific volume. Their model was divided into concentric zones as the stresses and strains are non-linear in the radial direction. During the analysis each fibre remains within its original zone. The energy in each zone is calculated from the tensile deformation and close packing in terms of the material properties, the yarn extension,

and the two radii of the cylinder. The strain energy is then expressed as a function of the unknown parameters and minimised to find the equilibrium geometry. The minimum energy is then differentiated with respect to the incremental yarn extension to yield the yarn tensile force. This model agrees with the results of short gauge length studies up to a strain of 12%.

Van Luijk [58] used a form of the finite element method to re-work the model of Carnaby and Grosberg into a stress analysis problem incorporating both the effects of transverse forces and transverse contraction. A uniform hydrostatic stress field was maintained in the transverse plane within each element throughout the analysis. This assumption is not valid for staple fibre yarns because it implies the redistribution of fibre mass without shear resistance. The equilibrium equation was used to match the pressure found from a van Wyk type relationship with that caused by the tensioned helically wound fibres. This was applied within each element and gave sufficient information to allow the solution of the equations. This approach allowed the element to deform laterally without changing the tension, even though the volume had changed. The element stiffness matrix was therefore non-conservative.

An analysis which would be valid for gauge lengths longer than the fibre length was sought. The effects of fibre migration and slippage were then included into the analysis. The assumptions made were that each fibre in the yarn follows an identical path except for a shift in position or rotation, that the starting points are equally distributed along the z axis, and that the twist is constant throughout the yarn. The same equilibrium equations were used for this analysis as in the previous one, ignoring the small difference in the inclination of the fibres due to the migration angle.

The results of the staple fibre analysis with parameters set such that there would be no slippage, showed negligible difference with a continuous filament analysis. This finding agreed with the previous work of Treloar [56].

In the evaluation of the staple fibre analysis with slippage the values of the slippage parameters were not known. They were therefore treated as unknowns and used to find a best fit between the experimental and theoretical results. Good agreement was found in only one case, with some cases being of similar form, but not precise.

The development of models for yarn bending has not been given as much attention as yarn extension, however some progress has been made. Backer [1] proposed an ideal geometry for the bending of a continuous yarn into a torus. Analyses were only

developed for the extreme cases of complete freedom or lack of freedom of movement between fibres during bending. During the analysis with complete freedom the fibres slip past one another to minimize their tensile load. Consequently almost all of the bending is due to the contributions from the bending and torsion in the fibres. When there is no inter-fibre slippage the yarn bends as an elastic rod and the contribution from fibre tension is the most significant contribution. It is thought that the situation in a real yarn lies somewhere between these two extremes.

In an analysis by Platt, Klein, and Hamburger [43] the effects of fibre 'clustering' was shown to increase the yarn bending rigidity (compared to complete freedom of fibre movement). The same result as that of Backer was given for the case of no freedom of movement, but a much simpler bending theory was used to demonstrate it. It was shown that the bending rigidity with no freedom of movement decreases with increasing helix angle. This is also shown for complete freedom, but is more significant for the former case.

The problem of the modelling of yarn torsion has also been given only limited treatment in the literature. In an analysis by Platt, Klein, and Hamburger [45] the torque in a singles yarn is defined in terms of only the bending and the torque in the fibre elements.

In a later study by Postle, Burton, and Chaikin [48] an equation for yarn torque in terms of fibre bending, torsion and tension was derived. This is an addition to the analysis by Platt *et. al.* which ignored the contribution from fibre tension. The relationship between yarn and fibre strain as derived by Platt and Gégauff, equation (2-1), is assumed and the contribution to yarn torsion due to fibre tension is calculated in terms of a general fibre stress-strain relationship. With the assumption of Hooke's law for the fibres, the first order binomial approximations for each of the three contributions to yarn torque are calculated. Over a commercial range of yarn twist the contribution from fibre tension is found to be vastly greater than that from fibre torsion. The fibre bending contribution is relatively insignificant. The total yarn torsion is found to be almost double that derived from experiment. The proposed explanation for this error is yarn relaxation during the time required for twisting. However a more significant contribution to the error may have been due to ignoring the lateral contraction of the yarn.

Analyses have been discussed that model each of yarn extension, bending and torsion. Some models have been developed that can represent two or more of these actions.

Thwaites [55] proposed a method in which the yarn is a solid rod. The material is assumed to be transversely anisotropic with the 'fibre' axis inclination dependent on radial position, similar to the idealized helical model. The analysis is limited to the case of elastic fibre properties.

The analysis starts from the general equations for equilibrium in cylindrical coordinates. The stresses on a yarn element are considered for an element inclined from the yarn axis, radius r and at a rotation of θ. To aid the mathematical calculations it was assumed that the yarn material was incompressible, which is valid for textile polymeric materials. It was also assumed that the radial stress is zero at the yarn surface. The equations for yarn tension and axial torque were derived. The analysis showed that the tensile modulus decreases with increasing twist angle while the torsional rigidity increases with increasing twist. The axial stress component was found to dominate the torsional rigidity at high twists. Increasing the shear modulus increases both the tensile modulus and the torsional rigidity.

2.1.2 Discrete or Continuous Analysis

At first sight the discrete analyses seem to bear more relevance to the yarn, they represent the actual fibres that compose the yarn. However it would be impossible to have a discrete fibre analysis that incorporates the effect of the position of every fibre as it lies in the yarn, therefore some approximations must be made. These may be better or worse than those made for a continuous analysis, however there are other factors.

Most discrete fibre yarn analyses developed have been created to model a specific loading situation. For example, the tension models of Gégauff and Hearle or the bending model of Backer. For each new situation a new analysis must be created or an old analysis modified. A successful continuum analysis should be valid for all loading situations, for which the constitutive material matrix of the unit cell would be the same for each analysis.

The assumptions necessary for the solution of yarn problems using a discrete fibre approach makes them useful only for continuous fibre yarns or for staple fibre yarn where slippage is confined to near the fibre ends. The analysis of a staple fibre yarn near rupture would require including the effects of significant fibre slippage, making a discrete analysis impracticable.

It is probable however that any useful continuum analysis will be both an incremental and iterative procedure and therefore it is likely that more computation would be required for a continuum analysis. This problem may not be a consideration due to the rate at which available, low cost computing power is increasing.

2.2 Unit Cell

The previous section indicated that a promising path for the analysis of staple fibre yarns would be to achieve a continuum model. The use of this method requires detailed knowledge of the relationship between stress and strain for a unit cell of the yarn material. A history of the development of such a Unit Cell, by both theoretical and experimental means is presented here.

2.2.1 Unit Cell Development

The compression of a mass of fibres is one of the easiest experiments to perform and has had the most attention in the literature, starting prior to 1946.

One of the earliest workers to adopt some form of unit cell approach to fibrous assemblies was Van Wyk in 1946 [59]. From his experimental work Van Wyk proposed a relationship between the pressure and volume of a random assembly of the form:

$$p = A\left(\frac{1}{V^3} - \frac{1}{V_0^3}\right) \qquad \textbf{(2-2)}$$

Where: p = applied pressure on the assembly
A = a constant
V = current specific volume of assembly
V_o= specific volume when p=0

Van Wyk used a three point bending element to build a model of his assembly as a *pile of rods*, regularly spaced at right angles. Beam theory shows that for small strains:

$$F = \frac{24iY}{b^3}y \qquad \textbf{(2-3)}$$

F=Force at the midpoint
i=Moment of inertia of rod in bending
Y=Youngs modulus of fibre
2b=Length of rod
y=The deflection of the rod at the midpoint

The **24** in this equation was replaced by a factor **k,** the difference of this factor from 24 accounted for the irregular spaceing of the contact points and the possibility that the forces may not regularly alternate in direction.

Van Wyk gave two methods of calculating **b**, the mean distance between fibre-to-fibre contacts which is sometimes called the projected fibre length method, and the projected fibre area method. Later work by Duckett and Cheng [7] showed the two methods to be identical.

With these assumptions it can be shown (if the element length **b** is decreased as the pressure increases):

$$p = \frac{kYm^3}{\rho^3}\left(\frac{1}{V^3} - \frac{1}{V_0^3}\right) \qquad \textbf{(2-4)}$$

in excellent agreement with van Wyk's experimental results.
The Van Wyk equation is a special case of an equation proposed earlier by M and J Eggert [10].

Dunlop [8] investigated the compression behaviour of various wools by measuring the values of the constants A and V_0 from equation (2-2). He found only moderate agreement with van Wyk's theory. This was because of various causes one of which was frictional slippage effects.

Later Dunlop [9] measured the dynamic bulk modulus by an acoustic impedance technique, minimising the effects of friction and slippage. This produced similar results to the Van Wyk equation. However the experimental value of **k** was only 5-10% of the theoretical value proposed by Van Wyk.

Dunlop et al [9] showed that the assumption of a Poisson distribution for the fibre lengths allowed the theoretical value **k** to be low enough and therefore the discrepancy may be put down to the limitations of the theory of van Wyk. A more thorough investigation of the effects of aspects of the model on the value of **k** was carried out by Lee, Carnaby, Carr, and Moss [31]. It was assumed that x_k, the distance between neighbouring contact points has an exponential density. It was then assumed that a contact point deflects as a beam with clamped ends, equation (2-3) and it was subsequently reasoned that the effect of assuming a constant segment length makes the value of 'k' at most six times larger. The effect of a varying number of loading points between contacts was also found to make for a more flexible model. After some simplifications it was concluded that the resistance of this model would be greater than one quarter of (but less than) the model of Van Wyk.

Anisotropy in the orientation of the fibres at higher compressions causes the number of fibre-to-fibre contacts calculated by van Wyk to become inaccurate. Stearn [52] modified the theory to account for this effect by assuming a relationship for the movement of the fibres during compression.

Kallmes and Corte [24] suggested a statistical geometry for paper. They derived the total number of fibre contacts in a unit area of a two dimensional sheet. The elasticity of the paper was derived by Onogi and Sasaguri [39] assuming that the tensile deformation of the sheet was due to the bending and tension of the fibres. Slippage was ignored which is of little consequence for paper but is not a good assumption for a textile fibre assembly.

Komori and Makishima [25] developed a theory based on an orientation density function for fibre segments. They proved the generality of their theory by deriving the results of van Wyk [59] and Kallmes and Corte [24] as special cases of their theory.

Lee and Lee [30] developed a more comprehensive analysis of fibrous assemblies. They also proposed that the external compressive strain of the assembly is translated directly into fibre bending strains. They derived an initial compression modulus and Poissons ratio in terms of the packing density and the orientation density function.

Pan and Carnaby [40] developed a model which incorporates the effects of slippage, an important mechanism of the assembly in reducing bending energy. The model uses a critical slipping angle to decide whether the contact points slip or do not slip.

A complete knowledge of the unit cell requires knowing more than just the actions under compression, both tension and shear are also factors which must be considered.

Carnaby and Curiskis [3] used the single fibre withdrawal theory of Grosberg [15] to develop a model of an assembly under extension. By using a fibre length distribution function and average tensile properties as well as the fibre withdrawal properties, a model was formed based on a proportion of the fibres slipping at each load increment. The distribution could then be updated ready for the next increment. A satisfactory comparison with experiment was found.

Pan and Carnaby [40] also developed the initial shear modulus of a fibre assembly by extending the work of Lee and Lee. The model ignored the effects of slippage. Later the effects of slippage were included [41] to give a more complete shear model. This model was checked using simple symmetry rules relating the mechanical constants.

Djaja [6] included the shear modulus derived by Pan and Carnaby [40] together with the linear mechanical property constants from Lee and Lee [30]. The constitutive material property matrix for the untwisted unit cell was assembled using an analogy with a set of parallel springs. No effects due to slippage were included in the analysis.

Almost all unit cell models have resolved external actions into the bending of a fibre segment. Most analyses have been based on the three contact point bending element first proposed by van Wyk [40]. In recent years, a new basic element has been trialed by D. H. Lee and G. A. Carnaby [29] which has only two contact points. Carnaby and Lee developed a compression model for the unit cell based on this two point element. Independent continuous length and orientation probability density functions were assumed for the elements. All elements were assumed to have the same initial curvature and each element was allowed to bend in uniform curvature. Each fibre segment was assumed to be elastic, homogeneous, and to have a circular cross section. Only the bending energy of the fibre segments was considered, any fibre which mathematically should have extended was allowed to slip. This was a more realistic assumption than allowing for axial extension of the segment. For a compressive strain the energy was minimised with respect to the assembly Poisson's ratio. In part II of the paper [28] the method was assessed. A relationship to update the orientation density function after a compressive increment was derived and it is shown to be a generalisation of a relationship found by Stearn [52]. A gamma function was assumed for the fibre segment length distribution. Satisfactory evaluation studies were carried out although no quantitative evaluation was performed.

Some theoretical justification has been given by Lee, Carnaby, Carr and Moss for the two point element rather than the three point element [31]. An investigation was made into the way that vertical strains are defined in two unit cell models. A comparison was made between an inclined pile of logs (a development on the Van Wyk theory) and the definition of continuum strain of the Lee and Lee model [30]. Fundamental differences were found between these two definitions of the same strain. However, it is demonstrated that a solution to this strain definition problem was not required as it was found that the three point bending element cannot be assembled to form a continuum without including some void space between the elements. The definitions of continuum strain with the two point element are considerably simpler to derive than those of the three point elements. This in itself is a good enough reason for any new theory to use this element.

Not only are strains easier to derive with a two point element. Although the three point element is restricted to bending, the two point element can easily account for the

contributions from all the various deformation modes that a fibre segment may be subjected to.

This new two point element represents the likely direction of theoretical unit cell development in the near future.

2.2.2 Experimental

The theoretical approach to the unit cell is possibly not the only path to a useful unit cell algorithm. It is possible in theory to take a bundle of fibres and subject it to various load cases, measuring strains or forces as appropriate. In this way it could be possible to develop a large database of information that could describe the response of the unit cell. Although this approach may be possible, it is very unlikely that it would be feasible, because of various contributory factors.

The unit cell database required for a satisfactory model would be immense, the number of possible strain states is very large and it is highly possible that the resulting method would be too unwieldy for practical use. The collection of the experimental results would be a long and tedious process. The data collected would be particular to the fibres being tested, preventing any convenient transfer of data from one fibre type to another.

Even if a solution is found for all of the difficulties listed above, the actual experiments required are difficult to devise and awkward to perform. For example, in an attempt to find a value for the Poisson's ratio of a fibre assembly, uniaxial compression tests are performed with and without sidewalls. The intention being that the compression modulus measured from the case with the sidewalls may be used with the results from the other test to find the Poisson's ratio. Unfortunately, only the tangent compression modulus is found and this is a function of the present strain state, the two tests only have the same strain state before the start of testing, making it impossible to evaluate the Poisson's ratio in this way. As another example of test difficulties, when attempting to measure the Poisson's ratio and the tensile modulus of an assembly by an axial extension test, several problems are encountered. Holding the fibres at the ends requires the use of clamps which introduces significant lateral compression local to the end regions. The measurement of the Poisson's ratio requires the definition of the surface. The surface of a fibrous assembly is difficult to define and some arbitrary decision must be made as to what constitutes the surface. This problem is common to many experiments and has not yet been satisfactorily resolved. Measuring the shear modulus

of the unit cell also causes significant difficulties as no satisfactory test has yet been devised for measuring the property of shear in a fibrous assembly.

Ignoring the problems with the experimental approach, the method still lacks the completeness, flexibility and the insights into the micro mechanical workings that are given by the theoretical approach. It must not be forgotten however that experiment can not be ignored as results are still required against which to compare new theoretical treatments.

3 Continuum Mechanics and Finite Element Analysis

The previous chapter has presented a case for the use of continuum mechanics through a finite element formulation, this chapter will give a brief introduction to both continuum mechanics and finite element theories. Both of these topics are responsible for a vast array of publications, volumes would be required to give a complete description of either, so only a limited description will be given. For a more complete introduction the reader is directed towards the references quoted, [51, 26, 12, 32, 33, 5, 60, 53, 38, 34, 27].

3.1 Continuum Mechanics

It has been discovered that all materials may be considered to be composed of a large collection of very small structural units or particles. A complete analysis of such a structure would require taking into account the effect that every one of these minute units has on the entire assembly. However for most materials the size of the particle is so small in comparison to the whole that an effective and useful discrete particle analysis is impractical to perform. A theory was developed where this assembly may be treated as a solid object and the stresses and strains in the material were defined to be continuous functions. This allowed the tools of calculus to be used to solve the problems. This process leads to what is now known as continuum mechanics.

For most materials, steel for example, it is intuitive that the assumption of a continuum would not seem to be significantly in error. However the theory is sometimes applied to materials where the contribution to the whole from one structural unit is much greater, the validity of assuming a continuum in these cases is sometimes doubtful. The general question of the validity of continuum mechanics is discussed below. The mathematical theory that is the practical side of continuum mechanics is also presented.

3.1.1 The Continuum Assumption

The validity of assuming that a material is a continuum is not something which has been given a lot of treatment in much of the literature on continuum mechanics. It would appear that there is even some debate over whether the issue is statistical or philosophical.

The point is often made in some form or another, that the smallest volume that can be considered to be a continuum is one that contains enough particles that the statistical average of their effects are independent of the state of the particles. In other words the particle has no significance in the continuum, resulting in properties that vary smoothly in both space and time. This comment however is almost only ever stated in a qualitative sense, no simple method of testing the validity of the assumption is offered.

Scipio [51], attempts a less qualitative description of the minimum volume that may be considered to be a continuum. He considers that the mass and therefore the density, is characteristic of a continuum. A hypothetical plot is made of the density (mass divided by volume) calculated in a region V as V tends to zero. If the material were truly a continuum, the density would approach a definite limit as the volume tended to zero. However in the hypothetical plot once the volume decreases below a certain point the effects of the distribution and movements of individual molecules become significant and the density fluctuates between limits which increase as the volume decreases. Scipio defines this point as the *continuum limit* and proposes that this is the smallest region that may be called a continuum. This volume would not easily be given a numerical quantity and would probably vary with material and orientation along with many other factors but it does give a better image of the requirements of a continuum material.

Lai, Rubin, and Krempl [26] point out that more than a hundred years of tests have justified such a theory in a wide variety of situations. It would seem that the most complete way of testing the validity of using the theory on a new material would be to attempt an analysis and see how the results compare with those measured from experiment.

3.1.2 Continuum Equations

In the field of continuum mechanics there are two main types of equations that are dealt with, those that are general to all materials, and those which are specific to one type of material. The general equations, which are the definitions of stress and strain will be presented first followed by the equations which define the constitutive properties of the material.

3.1.3 Stress

Consider a closed surface S, within a material continuum. A unit normal vector ν is normal to ΔS, a small part of S. The direction of ν is towards the outside of S. The part

of the material on the outside of ΔS exerts a force $\Delta \mathbf{F}$ on the other part. The force depends on the location, size and orientation of ΔS. As ΔS tends to zero, the ratio of $\Delta \mathbf{F}$ over ΔS tends to a limit $\mathbf{dF}/dS$, it is assumed that the moment of the force acting on ΔS about any force acting on ΔS vanishes in the limit. Define the *traction* (force per unit area) when the normal to the surface is ν as:

$$\underline{T}_{\nu} = \frac{d\underline{F}}{dS} \tag{3-1}$$

Consider the special case where the surface ΔS_k, k=1,2,3 is parallel to one of the coordinate planes, let the stress vector acting on ΔS_k be denoted by $\underline{T}^k$, with three components along the direction coordinate axes.

$$\text{Define:} \quad T_1^k = \tau_{k1} \;,\; T_2^k = \tau_{k2} \;,\; T_3^k = \tau_{k3} \tag{3-2}$$

We can show that the stress tensor may be written as:

	component of stress 1	2	3				
suface normal to x_1	τ_{11}	τ_{12}	τ_{13}		σ_x	τ_{xy}	τ_{xz}
surface normal to x_2	τ_{21}	τ_{22}	τ_{23}	or	τ_{yx}	σ_y	τ_{yz}
surface normal to x_3	τ_{31}	τ_{32}	τ_{33}		τ_{zx}	τ_{zy}	σ_z

(3-3)

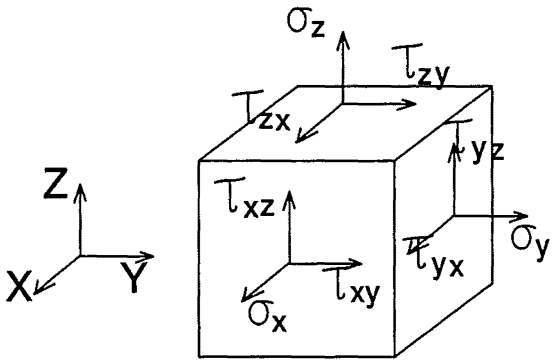

Figure 3-1 *Components of Stress*

The equations of equilibrium can be derived by considering the equilibrium of the small cube shown below. X_1, X_2, X_3 are the body forces acting over this volume of the continuum.

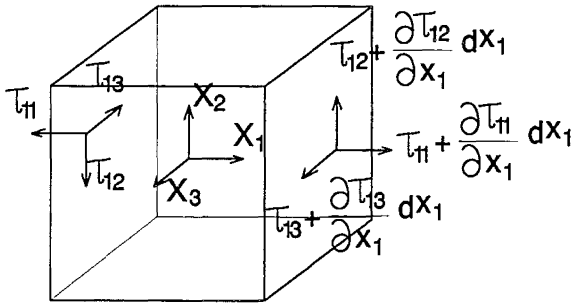

Figure 3-2 *Body Forces.*

By ensuring equilibrium of forces in each of the three axis directions, can arrive at the three equations represented by:

$$\frac{\partial \tau_{ij}}{\partial x_j} + X_i = 0 \qquad \textbf{(3-4)}$$

and by consideration of the moment equilibrium of this infinitesimal segment, it can be shown that the stress tensor is symmetric:

$$\tau_{ij} = \tau_{ji} \qquad \textbf{(3-5)}$$

3.1.4 Strain

Strain is a measure of the deformation of a continuum, a representation of the relative displacements of two points. This is evident as a rigid body rotation or translation produces large displacements but no relative displacements or strains. The Lagrangian and Eulerian strain tensors are shown here and the simplifications for infinitesimal strain are also given.

Consider a point in space which is initially defined by the coordinates (a_1, a_2, a_3) that deforms to be the point (x_1, x_2, x_3). This is a mapping from the a's to the x's, the continuum assumption ensures that the deformation is continuous and the mapping is one-to-one. By consideration of an infinitesimal segment ds_o, which deforms to ds, the strain tensors based on the change in the square of the length of this segment can be easily derived.

$$ds^2 - ds_0^2 = \left(\delta_{\alpha\beta}\frac{\partial x_\alpha}{\partial a_i}\frac{\partial x_\beta}{\partial a_j} - \delta_{ij}\right)da_i da_j = 2E_{ij}da_i da_j$$

$$E_{ij} = \frac{1}{2}\left(\delta_{\alpha\beta}\frac{\partial x_\alpha}{\partial a_i}\frac{\partial x_\beta}{\partial a_j} - \delta_{ij}\right) \qquad \textbf{(3-6)}$$

E_{ij} is called the Greens strain tensor, it is written in the Lagrangian form which means that the displacements are associated with particles in the original position. Similarly the strain tensor can be written in the Eulerian form where displacements are associated with particles in the deformed position.

$$ds^2 - ds_o^2 = \left(\delta_{ij} - \delta_{\alpha\beta}\frac{\partial a_\alpha}{\partial x_i}\frac{\partial a_\beta}{\partial x_j}\right)dx_i dx_j = 2e_{ij}dx_i dx_j$$

$$e_{ij} = \frac{1}{2}\left(\delta_{ij} - \delta_{\alpha\beta}\frac{\partial a_\alpha}{\partial x_i}\frac{\partial x_\beta}{\partial x_j}\right) \qquad \textbf{(3-7)}$$

e_{ij} is called Alamansi's strain tensor. It is obvious that the strain tensors are symmetric.

$$E_{ij} = E_{ji} \qquad e_{ij} = e_{ji} \qquad \textbf{(3-8)}$$

In rectangular cartesian coordinates, the strain tensors may be re-written in terms of the displacement vector **u**, which is defined as:

$$u_\alpha = x_\alpha - a_\alpha$$

$$\therefore \frac{\partial x_\alpha}{\partial a_i} = \frac{\partial u_\alpha}{\partial a_i} + \delta_{\alpha i} \qquad \frac{\partial a_\alpha}{\partial x_i} = \delta_{\alpha i} - \frac{\partial u_\alpha}{\partial x_i} \qquad \textbf{(3-9)}$$

which leads to the tensors:

$$E_{ij} = \frac{1}{2}\left[\frac{\partial u_j}{\partial a_i} + \frac{\partial u_i}{\partial a_j} + \frac{\partial u_\alpha}{\partial a_i}\frac{\partial u_\alpha}{\partial a_j}\right]$$

$$e_{ij} = \frac{1}{2}\left[\frac{\partial u_j}{\partial x_i} + \frac{\partial u_i}{\partial x_j} - \frac{\partial u_\alpha}{\partial x_i}\frac{\partial u_\alpha}{\partial x_j}\right] \qquad \textbf{(3-10)}$$

If the components of **u** are such that the first derivatives are small, then e_{ij} simplifies to Cauchy's infinitesimal strain tensor.

$$e_{ij} = \frac{1}{2}\left[\frac{\partial u_j}{\partial x_i} + \frac{\partial u_i}{\partial x_j}\right] = \tfrac{1}{2}\left(u_{i,j} + u_{j,i}\right) \qquad \textbf{(3-11)}$$

For infinitesimal displacements, the distinction between the Lagrangian and the Eulerian displacements disappears.

The small spin tensor, which represents infinitesimal rigid body rotations, can be shown to be:

$$w_{ij} = \frac{1}{2}\left(\frac{\partial u_j}{\partial x_i} - \frac{\partial u_i}{\partial x_j}\right) = \tfrac{1}{2}\left(u_{i,j} - u_{j,i}\right) \qquad \textbf{(3-12)}$$

In an infinitesimal displacement field for which the strain tensor vanishes at a point P, the rotation of a neighbourhood of P, is given by **w**, where:

$$w_k = \tfrac{1}{2} e_{ijk} w_{ij}$$

$$e_{111} = e_{222} = e_{333} = e_{112} = e_{113} = e_{221} = e_{223} = e_{331} = e_{332} = 0 \qquad \textbf{(3-13)}$$

$$e_{123} = e_{231} = e_{312} = 1$$

$$e_{213} = e_{321} = e_{132} = -1$$

The strain tensor need not be derived based on the change in the square of the distances. The change in the length ds may have been chosen as a starting point. Other well known deformation measures are Cauchy's deformation tensor (c_{ij}) and Green's deformation tensor (C_{ij}) as defined below.

$$c_{ij} = \frac{\partial a_j}{\partial x_k}\frac{\partial a_j}{\partial x_m} \qquad C_{ij} = \frac{\partial x_k}{\partial a_i}\frac{\partial x_k}{\partial a_j} \qquad \textbf{(3-14)}$$

For the case of a rigid body translation the deformation tensors above do not give zero components as do the strain tensors, they actually become unit tensors, described by:

$$c_{ij} = \delta_{ij} \qquad C_{ij} = \delta_{ij} \qquad \textbf{(3-15)}$$

This means that the constitutive equations used for such a formulation must be such that no internal stresses are produced by a rigid body movement.

It has been shown that the six strain components may be found from the three displacement components, however finding the three displacements from the six strains requires the use of compatibility equations. The displacements may only be found within a rigid body rotation as the strains represent only relative displacements. The compatibility equations for infinitesimal strains can be found to be :

$$\begin{aligned} e_{11,22}+e_{22,11} &= e_{12,12} & -e_{23,11}+e_{31,21}+e_{12,31} &= 2e_{11,23} \\ e_{22,33}+e_{33,22} &= e_{23,23} & e_{23,12}-e_{31,22}+e_{12,32} &= 2e_{22,31} \\ e_{33,11}+e_{11,33} &= e_{13,13} & e_{23,13}+e_{31,23}-e_{12,33} &= 2e_{33,12} \end{aligned} \qquad \textbf{(3-16)}$$

3.1.5 Large Displacement Stress

The writing of the equilibrium conditions requires the use of conjugate stress and strain relations in the present configuration. When an Eulerian formulation is used for the strain calculations the appropriate stress tensor is the earlier defined Cauchy stress tensor, equation (3-3), as the strain is defined in the deformed state. If a Lagrangian formulation such as the Greens strain tensor is used then the Cauchy stress must be altered to a form appropriate to the undeformed state. Two methods for this are described below.

In the first method, the Piola-Kirchhoff stress, the stress at a point in the deformed state is transformed back to the undeformed state using the same force present in the deformed state but divided by an area which has been transformed to the undeformed state. This may be written in terms of the Cauchy stress [32] as:

$$T_{ji}^{0} = \frac{\rho_0}{\rho}\frac{\partial a_j}{\partial x_r}\sigma_{ri} \qquad \textbf{(3-17)}$$

This stress definition has the disadvantage that the tensor produced is unsymmetric.

In the second Piola-Kirchhoff stress tensor the force as well as the area is transformed back to the undeformed state. This may be written as equation (3-18).

The stress tensor σ is the Cauchy stress in the deformed position. The second Piola-Kirchhoff tensor has the advantage of being symmetric.

$$S_{ij} = |J| \sigma_{rs} \frac{\partial a_i}{\partial x_r} \frac{\partial a_j}{\partial x_s} \qquad \text{(3-18)}$$

$$\text{Where} \quad |J| = \left| \frac{\partial x_i}{\partial a_j} \right|$$

It can be shown [32] that only certain stress-strain pairings represent valid expressions for the internal strain energy, these are conjugate pairs. The pair for the first Piola-Kirchhoff tensor is the transpose of J (defined above). The second Piola-Kirchhoff tensor conveniently pairs with Green's strain tensor.

The internal strain energy may now be written using the second Piola-Kirchhoff stress as:

$$U = \frac{1}{2} \int_{V_0} S_{ij} E_{ij} dV_0 \qquad \text{(3-19)}$$

3.1.6 Constitutive Equations

The relationships derived so far indicate that in a general three dimensional continuum there will be fifteen unknowns, three displacements, six strains and six stresses. Nine equations have been presented to allow for the solution of these unknowns, three equilibrium equations and six strain-displacement equations. Therefore, six more equations are required for the solution of the system, these are relationships between the six stresses and strains and can be written very concisely for the case of an elastic solid as:

$$\sigma_{ij} = C_{ijkl} e_{kl} \qquad \text{(3-20)}$$

C_{ijkl} is a rank four tensor which can represent 81 elastic constants. However, due to the symmetry restrictions on σ and e which restrict each of them to 6 independent values,

C_{ijkl} represents merely 36 constants. A more conventional representation is given in matrix notation as:

$$\{\sigma\} = [K]\{\varepsilon\} \quad \underline{or} \quad \{\varepsilon\} = [C]\{\sigma\}$$

where: $\{\sigma\}$ = *six stress components*
$\{\varepsilon\}$ = *six strain components*
$[K]$ = $6x6$ *stiffness matrix*
$[C]$ = $6x6$ *compliance matrix*

(3-21)

The above relations indicate that at each point in the material the stresses are linearly related to the strains (linear elastic material). Although this has produced good results for many problems it will not always be true for real materials as most materials will demonstrate some nonlinear mechanical behaviour to some degree. Therefore the components of the constitutive matrix are dependent on the strain in the deformed state. An incremental technique can be developed where the components of the constitutive matrix may be assumed to be constant within any one increment but the values are based on the material state at the start of the increment. Ignoring numerical difficulties in the limit as the size of an increment tends to zero this method will give exact results. However, this limit is impossible to achieve and numerical techniques for arriving at satisfactory results with a finite increment size will be discussed later.

$$\Delta\underline{\varepsilon} = \left[C_T\left(\underline{\sigma}_0, \underline{\varepsilon}_0\right)\right]\Delta\underline{\sigma}$$

Where: $[C_T]$ *is the* ***tangent*** *compliance matrix*

(3-22)

Types of material isotropy can dramatically reduce the number of independent constants within the constitutive equations. For a fully isotropic material the material properties should be identical whatever the orientation. This means that the tensor C_{ijkl} must be identical under any orthogonal coordinate transformation. This statement can be used along with tensor algebra to prove that the number of independent constants in such a material is exactly two. It may also be shown that nine, six or five independent values are needed if the situation being represented is one of orthotropy, degenerate square symmetry, or transverse orthotropy, respectively.

3.1.7 Boundary Conditions

Knowing the internal workings of a continuum alone is inadequate for the complete solution of the problem. A sufficient number of conditions must be placed on the region boundary to establish a unique solution. It is most common that the boundary conditions are specified as either a stress or a displacement boundary condition. The specified stress along a boundary is often referred to as a 'traction' and models any surface forces which are applied to the system. Tractions are often given in terms of components both parallel to and normal to the surface and a rotation of these components is often required to align them with the coordinate system existing within the continuum. The specification of the displacement is usually required at a minimum of one point within the system as without that a solution could only be found to within a rigid body displacement, giving an infinite number of permissible solutions.

3.1.8 Polar Coordinates

Often in continuum problems, the rectangular cartesian coordinate system is not the most concise system available, using a curvilinear coordinate system may allow considerable simplification to the equations governing the problem. One such curvilinear system which is in popular use is that of cylindrical polar coordinates, the equations relevant to an analysis using this system are presented below.

The cylindrical polar coordinate system is based on r, θ, and z, where r is in the radial direction, θ the rotational, and z is aligned with the axis of the cylinder. The relationships between stresses in a rectangular cartesian system and those in a cylindrical polar system may be easily derived by tensor transformation as:

$$\sigma_x = \sigma_r\cos^2\theta + \sigma_\theta\sin^2\theta - \tau_{r\theta}\sin 2\theta \qquad \tau_{xy} = (\sigma_r - \sigma_\theta)\sin\theta\cos\theta + \tau_{r\theta}(\cos^2\theta - \sin^2\theta)$$

$$\sigma_y = \sigma_r\sin^2\theta + \sigma_\theta\cos^2\theta + \tau_{r\theta}\sin 2\theta \qquad \tau_{zx} = \tau_{zr}\cos\theta - \tau_{z\theta}\sin\theta$$

$$\sigma_z = \sigma_z \qquad \tau_{zy} = \tau_{zr}\sin\theta + \tau_{z\theta}\cos\theta$$

(3-23)

The cylindrical polar infinitesimal strain-displacement relationships can be shown to be:

$$\varepsilon_{rr} = \frac{\partial u_r}{\partial r} \qquad \varepsilon_{zr} = \frac{1}{2}\left(\frac{\partial u_r}{\partial z} + \frac{\partial u_z}{\partial r}\right)$$

$$\varepsilon_{\theta\theta} = \frac{u_r}{r} + \frac{1}{r}\frac{\partial u_\theta}{\partial \theta} \qquad \varepsilon_{z\theta} = \frac{1}{2}\left(\frac{1}{r}\frac{\partial u_z}{\partial \theta} + \frac{\partial u_\theta}{\partial z}\right) \qquad \textbf{(3-24)}$$

$$\varepsilon_{r\theta} = \frac{1}{2}\left(\frac{1}{r}\frac{\partial u_r}{\partial \theta} + \frac{\partial u_\theta}{\partial r} - \frac{u_\theta}{r}\right) \qquad \varepsilon_{zz} = \frac{\partial u_z}{\partial z}$$

3.2 Finite Element Analysis

The real world is not something that analytical methods have ever been very good at dealing with as any real situation possesses a complexity for which a complete analysis is beyond the ability of even modern computers. An analysis method may be developed which models the problem in a form similar enough to the real situation so that the differences are negligible but simple enough that a solution may be found in a reasonable time frame. This idea has been around for centuries and has been developed into methods like the Rayleigh-Ritz-Galerkin method from which the Finite Element Method can be viewed as an extension.

The modern form of the Finite Element Method will be outlined with specific reference to the displacement based isoparametric finite elements. Discussion will be given on the special problems associated with large displacement geometries and nonlinear material constitutive equations.

3.2.1 Finite Element Development

In the Rayleigh-Ritz-Galerkin method, the idea is to choose a finite number of trial functions $N_1,\ldots,N_n$, and form their linear combination with the weights q_j, $\sum q_j N_j$. The Ritz approximation is to find the values of the weights which produces the minimum potential energy for the system. Therefore the goal is to choose trial functions such that the potential energy may be easily computed and minimized and that are general enough that they may sufficiently approximate the real solution. These two objectives had been found to be very difficult to satisfy simultaneously but the finite element method can be looked at as providing a solution to the problem.

The first step of the finite element method is to divide the solution region by a series of imaginary lines or surfaces into a collection of sub-regions. The solution functions are then chosen such that they can be non-zero only within one sub-region or element. Therefore the solution is made up of a combination of small piecewise functions which are usually chosen to be low order polynomials to satisfy the simplicity requirements. The shape of these functions is fully described by the values at nodes on the boundary of each element and the entire problem may be assembled simply by stitching these elements together at the nodes.

The functions described above will be used in a problem to approximate one or more of the dependent variables, such as displacement or stress. The discussion to follow

however will be based on elements where only the displacement field is approximated by the functions, the so called displacement elements. Displacement elements are to be used because not only are they in popular use, but also because they make the understanding of the method much simpler. Low order polynomials are almost always used for finite elements and their use will be assumed here.

3.2.2 Shape Function Criteria

In order to ensure that a solution will tend towards the correct solution with mesh refinement (convergence), the displacement functions (or shape functions) must satisfy certain criteria:

a. There can be no resultant internal strain energy when the element is subjected to a rigid body translation or rotation.

b. The element must satisfy the patch test which required that if the nodes of an element are given displacements corresponding to a state of constant strain, the displacement field must represent a state of constant strain.

c. The displacement field must maintain continuity within the element and across element boundaries of derivatives of up to one order less than that contained in the variational formula. This is to prevent the loss of energy from the system by the infinite levels of energy which would result from integrating the derivative of a discontinuous function.

d. The displacements along an edge must be controlled by only the nodes along that edge. This is the condition of compatibility which ensures that the solution actually remains as a continuum.

It was found that it was very difficult to satisfy the requirements of d above for quadrilateral elements unless all of the sides were parallel to a coordinate axis, to overcome this problem parametric elements were developed. The element is based on a 'unit' configuration where all sides are parallel to the coordinate axes. The geometry of this configuration is then mapped to a non-standard geometry. This arrangement satisfies the compatibility condition as well as allowing for a wide variety of geometries including curved sides. If the mapping functions which are used are the shape functions then the possession of 'rigid body modes' is ensured and condition a above is satisfied. This element is then an isoparametric element.

3.2.3 Nonlinearity

The real world is fundamentally nonlinear. Fortunately many of the problems which need solution may be satisfactorily approximated by a linear relationship. However some physical situations present nonlinearities too large to be ignored and it is only in recent decades that the processing power has been available to attempt the numerical solution of complex nonlinear systems.

In general a time independent problem may be symbolized as:

$$[K]\{D\} = \{R\} \tag{3-25}$$

For a linear analysis both [K] the stiffness matrix and {R} the load vector are considered to be independent of the displacement vector {D}. A nonlinear problem produces a dependence on {D} of both [K] and/or {R}. This nonlinearity is usually from one or both of two sources, either geometrical or material nonlinearity.

Geometrical nonlinearity is when the deformations within the structure are such that the solution must be based on the deformed configuration to be sufficiently accurate and finite displacement continuum mechanics must be used.

Material nonlinearity is caused by the components of the material constitutive matrix at a point being dependent on the loading history and the strain states at that point.

3.2.4 Geometrically Nonlinear Element Formulation

The element displacements are defined in terms of the nodal displacements $\mathbf{u}_I$ by the shape functions **N**. This may be written in matrix notation as:

$$\{u(x)\} = [N(x)]\ \{u_I\} \tag{3-26}$$

The strain vector $\{e\}$ can be split into parts representing its small $\{\varepsilon\}$ and large $\{\eta\}$ displacement components and may be represented in three dimensional cartesian coordinates as:

$$\{e\} = \{\varepsilon\} + \{\eta\} \tag{3-27}$$

$$\begin{Bmatrix} \varepsilon_x \\ \varepsilon_y \\ \varepsilon_z \\ \gamma_{xy} \\ \gamma_{yz} \\ \gamma_{xz} \end{Bmatrix} = \begin{Bmatrix} \frac{\partial u}{\partial x} \\ \frac{\partial v}{\partial y} \\ \frac{\partial w}{\partial z} \\ \frac{\partial u}{\partial y}+\frac{\partial v}{\partial x} \\ \frac{\partial u}{\partial z}+\frac{\partial w}{\partial y} \\ \frac{\partial w}{\partial x}+\frac{\partial u}{\partial z} \end{Bmatrix} + \frac{1}{2} \begin{Bmatrix} \left(\frac{\partial u}{\partial x}\right)^2+\left(\frac{\partial v}{\partial x}\right)^2+\left(\frac{\partial w}{\partial x}\right)^2 \\ \left(\frac{\partial u}{\partial y}\right)^2+\left(\frac{\partial v}{\partial y}\right)^2+\left(\frac{\partial w}{\partial y}\right)^2 \\ \left(\frac{\partial u}{\partial z}\right)^2+\left(\frac{\partial v}{\partial z}\right)^2+\left(\frac{\partial w}{\partial z}\right)^2 \\ 2\left(\frac{\partial u}{\partial y}\frac{\partial u}{\partial x}+\frac{\partial v}{\partial y}\frac{\partial v}{\partial x}+\frac{\partial w}{\partial y}\frac{\partial w}{\partial x}\right) \\ 2\left(\frac{\partial u}{\partial y}\frac{\partial u}{\partial z}+\frac{\partial v}{\partial y}\frac{\partial v}{\partial z}+\frac{\partial w}{\partial y}\frac{\partial w}{\partial z}\right) \\ 2\left(\frac{\partial u}{\partial x}\frac{\partial u}{\partial z}+\frac{\partial v}{\partial x}\frac{\partial v}{\partial z}+\frac{\partial w}{\partial x}\frac{\partial w}{\partial z}\right) \end{Bmatrix} \quad \textbf{(3-28)}$$

Then the matrix [B] may be defined, giving the strain vector in terms of the nodal displacements in each of the three directions ($\mathbf{u_I}$,$\mathbf{v_I}$,$\mathbf{w_I}$).

The small displacement component may be written as:

$$\{\varepsilon\} = \begin{bmatrix} N_{,x} & 0 & 0 \\ 0 & N_{,y} & 0 \\ 0 & 0 & N_{,z} \\ N_{,y} & N_{,x} & 0 \\ N_{,z} & 0 & N_{,x} \\ 0 & N_{,z} & N_{,y} \end{bmatrix} \begin{Bmatrix} u_I \\ v_I \\ w_I \end{Bmatrix} = [B_0] \begin{Bmatrix} u_I \\ v_I \\ w_I \end{Bmatrix} \quad \textbf{(3-29)}$$

$$\text{Where } [N_{,x}] = \left[\frac{\partial N}{\partial x}\right] = \left[\frac{\partial N_1}{\partial x} \quad \frac{\partial N_2}{\partial x} \quad \cdots \quad \frac{\partial N_n}{\partial x}\right]$$

The variation of ε may be written:

$$\{d\varepsilon\} = [B_0] \begin{Bmatrix} du_I \\ dv_I \\ dw_I \end{Bmatrix} \quad \textbf{(3-30)}$$

The large displacement part of e may also be written in matrix notation:

$$\{\eta\} = \frac{1}{2}\begin{bmatrix} \theta_x^T & 0 & 0 \\ 0 & \theta_y^T & 0 \\ 0 & 0 & \theta_z^T \\ \theta_y^T & \theta_x^T & 0 \\ \theta_z^T & 0 & \theta_x^T \\ 0 & \theta_z^T & \theta_y^T \end{bmatrix} \begin{Bmatrix} \theta_x \\ \theta_y \\ \theta_z \end{Bmatrix} = \tfrac{1}{2}[A]\{\theta\} \qquad \textbf{(3-31)}$$

$$\text{Where} \quad \theta_x^T = \begin{bmatrix} \frac{\partial u}{\partial x} & \frac{\partial v}{\partial x} & \frac{\partial w}{\partial x} \end{bmatrix}$$

In terms of nodal displacements, $\{\theta\}$ may be written as:

$$\{\theta\} = \begin{bmatrix} N_{,x} & 0 & 0 \\ 0 & N_{,y} & 0 \\ 0 & 0 & N_{,z} \\ N_{,x} & 0 & 0 \\ 0 & N_{,y} & 0 \\ 0 & 0 & N_{,z} \\ N_{,x} & 0 & 0 \\ 0 & N_{,y} & 0 \\ 0 & 0 & N_{,z} \end{bmatrix} \begin{Bmatrix} u_I \\ v_I \\ w_I \end{Bmatrix} = [G]\begin{Bmatrix} u_I \\ v_I \\ w_I \end{Bmatrix} = [G]\{\delta\} \qquad \textbf{(3-32)}$$

Define:

$$\{\eta\} = \tfrac{1}{2}[A][G]\{\delta\} = \tfrac{1}{2}[B_L]\{\delta\}$$

$$\text{Where} \quad \{\delta\} = \begin{Bmatrix} u_I \\ v_I \\ w_I \end{Bmatrix} \qquad \textbf{(3-33)}$$

The matrix $[B_L]$ above is a function of the nodal displacements $\{\delta\}$.

The variation of η is calculated to be:

$$\begin{aligned} \{d\eta\} &= \tfrac{1}{2}[dA]\{\theta\} + \tfrac{1}{2}[A]\{d\theta\} = [A]\{d\theta\} \\ &= [A][G]\{d\delta\} \\ &= [B_L]\{d\delta\} \end{aligned} \tag{3-34}$$

The equation for the internal strain energy may be calculated in terms of the strain vector and the appropriate stress vector {S} for this Lagrangian large displacement formulation as:

$$U = \tfrac{1}{2}\int_V \{e\}^T\{S\}\,dV \tag{3-35}$$

With the substitution of equations (3-17) and (3-24) this becomes:

$$\begin{aligned} U &= \tfrac{1}{2}\int_V \{e\}^T[C]\{e\}\,dV \\ &= \tfrac{1}{2}\int_V \{\varepsilon+\eta\}^T[C]\{\varepsilon+\eta\}\,dV \\ &= \tfrac{1}{2}\int_V (\{\varepsilon\}^T[C]\{\varepsilon\} + \{\eta\}^T[C]\{\varepsilon\} + \{\varepsilon\}^T[C]\{\eta\} + \{\eta\}^T[C]\{\eta\})\,dV \end{aligned} \tag{3-36}$$

Incorporating the shape functions by substitution of equations (3-30) and (3-26) yields:

$$\begin{aligned} U &= \tfrac{1}{2}\{\delta\}^T\int_V [\bar{B}]^T[C][\bar{B}]\,dV\{\delta\} \\ &= \tfrac{1}{2}\{\delta\}^T \int_V [B_0]^T[C][B_0] + \tfrac{1}{2}[B_L]^T[C][B_0] + \tfrac{1}{2}[B_0]^T[C][B_L] + \tfrac{1}{4}[B_L]^T[C][B_L]\,dV\,\{\delta\} \end{aligned} \tag{3-37}$$

Where: $[\bar{B}] = [B_0] + \tfrac{1}{2}[B_L]$

By taking into account the effects of body forces, nodal forces, and surface tractions by the vector R_F, the equilibrium equation can be written as (3-38).

The variation of ψ is found to be (3-39).

$$\{\psi\} = \int_V [B]^T[C][B]dV\{\delta\}$$

$$= \int_V \left([B_0]^T[C][B_0] + [B_L]^T[C][B_0] + [B_0]^T[C][B_L] + [B_L]^T[C][B_L]\right)dV\{\delta\} - \{R_F\} = 0 \quad \textbf{(3-38)}$$

Where $[B] = [B_0] + [B_L]$

$$\{d\psi\} = \int_V [dB_L]^T\{S\}dV + \left([K_0] + [K_L]\right)\{d\delta\}$$
$$= \left([K_\sigma] + [K_0] + [K_L]\right)\{d\delta\} \quad \textbf{(3-39)}$$

$[K_0]$ is the small displacement matrix that would be found in conventional linear theory, $[K_\sigma]$ is a matrix dependent on the state of stress (geometric or initial stress matrix) and $[K_L]$ is dependent linearly and quadratically on the displacement, as defined below.

$$[K_0] = \int_V [B_0]^T[C][B_0]dV$$

$$[K_\sigma]\{d\delta\} = \int_V [dB_L]^T\{S\}dV \quad \textbf{(3-40)}$$

$$[K_L] = \int_V [B_L]^T[C][B_0] + [B_0]^T[C][B_L] + [B_L]^T[C][B_L]\ dV$$

$[K_\sigma]$ is not presented above in a form which can be easily calculated. A property of the matrix [A] can be used to evaluate $[K_\sigma]$ as:

$$[K_\sigma] = \int_V [G]^T[M][G]dV$$

$$\text{Where } [M] = \begin{bmatrix} \sigma_x I_3 & \tau_{xy} I_3 & \tau_{xz} I_3 \\ \tau_{xy} I_3 & \sigma_y I_3 & \tau_{yz} I_3 \\ \tau_{xz} I_3 & \tau_{yz} I_3 & \sigma_z I_3 \end{bmatrix} \tag{3-41}$$

$$\{S\} = \{\sigma_x \ \sigma_y \ \sigma_z \ \tau_{xy} \ \tau_{xz} \ \tau_{yz}\}^T$$

$$[I_3] = \begin{bmatrix} 1 & 0 & 0 \\ 0 & 1 & 0 \\ 0 & 0 & 1 \end{bmatrix}$$

Two formulations are popular for the way that the tangent stiffness matrix $[K_T]$ is formed. Where $[K_T]$ is found from the variation of ψ, and is used in the incremental equilibrium equation:

$$[K_T]\{\Delta\delta\} - \{\Delta R_F\} = \{0\} \tag{3-42}$$

In the derivation shown, the tangent stiffness matrix is formed as:

$$[K_T] = [K_0] + [K_\sigma] + [K_L] \tag{3-43}$$

As an alternative, the tangent stiffness matrix can be made up from:

$$[K_T] = [K_0] + [N_1] + [N_2] \tag{3-44}$$

Where $[K_0]$ is the small displacement matrix, $[N_1]$ is a matrix linearly dependent on the displacement, and $[N_2]$ is a matrix quadratically dependent on the displacement. It can be shown that the definitions of the matrices $[N_1]$ and $[N_2]$ are not unique [11], and that forms may be found which repeat in the total potential energy, the equilibrium, and the linear incremental equilibrium equations.

3.2.5 Method of Weighted Residuals

An alternative method (to the variational method of the previous section) of generating the element matrices is given by the method of weighted residuals. The residual caused by the governing equation being inexactly satisfied by the solution functions is distributed according to certain weighting functions.

If the governing equation for a problem is given as:

$$\mathrm{L}(U) = f \tag{3-45}$$

where L is a differential operator and U is an exact solution, then for an approximate solution the residual may be written:

$$\mathrm{R}(x) = \mathrm{L}(u) - f \tag{3-46}$$

For three dimensional elasto-statics the residual equation may be written from the equilibrium equations as:

$$\mathrm{R} = \sigma_{kj,j} + b_k \tag{3-47}$$

A variety of weighted residual methods are possible [2], the differences being the weighting functions which are used, some of these method are listed below.

a) Point Collocation - the residual is set to zero at a number of points within the domain, using these functions is similar to finite difference methods.

b) Subdomain Collocation - the domain is divided into subdomains, and the integral of the residual over each subdomain is set to zero.

c) Galerkin - the functions used here are the same functions which are used for the displacements, a self-adjoint problem should give the same results for the Galerkin method, and the variational method.

The Galerkin method will be used here to show the formulation of the tangent stiffness matrices using weighted residuals. The controlling equation is then written [2]:

$$\int_V (\sigma_{kj,j} + b_k) w_k dV = 0 \qquad \textbf{(3-48)}$$

where w are the displacement type weighting functions, and b are the body forces. An integration by parts of equation (3-48) assuming linear steps within each increment yields:

$$-\int_V \sigma_{kj} e^*_{kj} dV + \int_V b_k w_k dV = -\int_S p_k w_k dS \qquad \textbf{(3-49)}$$

The functions e^* are the strains related to the weighting functions, p are the traction boundary conditions which are related to the stresses through the direction cosines defining the slope of the boundary surface.

Equation (3-49) may be rewritten as:

$$\int_V [B]^T [C][B] dV\{\delta\} - \int_V b_k w_k dV + \int_S p_k w_k dS = 0 \qquad \textbf{(3-50)}$$

Noting the similarity between this equation and equation (3-38), it can be seen that this method will give the same results for the formulation of the incremental stiffness matrices. However, an explicit expression for the force vector $\{R_F\}$ is obtained in terms of the shape functions, the body forces and the surface tractions.

3.2.6 Isoparametric Element

The above formulations ignored the earlier discussed problems which require the use of isoparametric geometry mappings, it will be shown that the inclusion of these mappings produces no significant differences in the formulation of the stiffness matrices.

Assume that the three dimensional element is mapped to the 'unit' reference configuration of a cube of edge length two in rectangular cartesian coordinates of α, β, and γ. As the element is isoparametric, the shape functions which were used for the deformation are also used for the geometry mapping.

The derivatives of the shape functions with respect to the x,y,z coordinates are required for the construction of the matrices [B] and [G], these may be related to the derivatives of the displacements with respect to the α, β, γ coordinates by the Jacobian matrix [J].

$$\begin{bmatrix} \frac{\partial N}{\partial \alpha} \\ \frac{\partial N}{\partial \beta} \\ \frac{\partial N}{\partial \gamma} \end{bmatrix} = \begin{bmatrix} \frac{\partial x}{\partial \alpha} & \frac{\partial y}{\partial \alpha} & \frac{\partial z}{\partial \alpha} \\ \frac{\partial x}{\partial \beta} & \frac{\partial y}{\partial \beta} & \frac{\partial z}{\partial \beta} \\ \frac{\partial x}{\partial \gamma} & \frac{\partial y}{\partial \gamma} & \frac{\partial z}{\partial \gamma} \end{bmatrix} \begin{bmatrix} \frac{\partial N}{\partial x} \\ \frac{\partial N}{\partial y} \\ \frac{\partial N}{\partial z} \end{bmatrix} = [J] \begin{bmatrix} \frac{\partial N}{\partial x} \\ \frac{\partial N}{\partial y} \\ \frac{\partial N}{\partial z} \end{bmatrix} \tag{3-51}$$

$$\text{Therefore} \quad \begin{bmatrix} \frac{\partial N}{\partial x} \\ \frac{\partial N}{\partial y} \\ \frac{\partial N}{\partial z} \end{bmatrix} = [J^{-1}] \begin{bmatrix} \frac{\partial N}{\partial \alpha} \\ \frac{\partial N}{\partial \beta} \\ \frac{\partial N}{\partial \gamma} \end{bmatrix}$$

Unfortunately the inverse of the Jacobian is rarely known in closed form and numerical integration is required to be performed with the Jacobian being evaluated and inverted at each integration point. The Jacobian may be easily calculated as:

$$[J] = \begin{bmatrix} \frac{\partial N}{\partial \alpha} \\ \frac{\partial N}{\partial \beta} \\ \frac{\partial N}{\partial \gamma} \end{bmatrix} \begin{bmatrix} x_I & y_I & z_I \end{bmatrix} \tag{3-52}$$

(x_I, y_I, z_I) are the coordinates of the nodal points.

With the means to calculate the [B] and [G] matrices, and the inclusion of the determinant of the Jacobian, the stiffness matrices may now be calculated by an integral over the *unit* configuration.

$$[K_0] = \int_V [B_0]^T [C][B_0] dV = \int_{-1}^{1}\int_{-1}^{1}\int_{-1}^{1} [B_0]^T [C][B_0] |J| \, d\alpha \, d\beta \, d\gamma \tag{3-53}$$

Similar modifications are carried out for the other contributions to the tangent stiffness matrix.

3.2.7 Material Nonlinearity

When a problem exhibits material nonlinearity, the only difference to the formulation is that the constitutive matrix is a function of the strain and therefore a function of the nodal displacements. In a lot of problems involving material nonlinearity the properties are a function of not only the present state of the material but also the history. This means that the solution of the problem is path dependent and the complete solution path must be found.

In an analysis with linear constitutive properties the solution can be shown to be unique, when the material has nonlinear properties the solution is much harder to find. Although there will be many states which satisfy the equilibrium equations only one is correct, to find this one solution the entire loading path must be traced.

3.2.8 Solution of Incremental Equilibrium Equations

The solution strategies for nonlinear equations are many and varied, no one method will be both efficient and accurate for all problems and a strategy which is flexible is necessary. Some methods will be discussed here and a combination of these could be put together as part of a solution package.

In general, due to the nonlinear material properties, a solution method must be found which produces the entire loading path. An incremental method is usually implemented where the load is put onto the system in a series of small steps and the equilibrium equation is assumed to be linear within each incremental step. The linear incremental tangent stiffness matrix $[K_T]$ as already derived is suitable for such an incremental step as set out by equation (3-42). Errors in this simple incremental method quickly compound as shown in Figure 3-3(a) for a simple one degree of freedom case.

Many techniques are available for improving the method shown above. The problem can be given a more mathematical basis by interpreting it as the solution of a system of nonlinear differential equations. The method shown above can be looked on as an explicit Euler method and other explicit methods are available which give better solutions such as explicit Runge-Kutta methods or explicit Linear Multistep methods. Although these better methods will give superior results the work required is greater and the computer storage requirements increase very quickly. To ensure a good solution with explicit methods a prohibitively small step size is often required and often a more efficient solution is given by using an implicit method.

The use of an implicit method requires the solution of a system of nonlinear equations at each load step. This may be looked upon as applying an equilibrium correction within each load step. An implicit Euler method is shown in Figure 3-3(b). As with the explicit method, higher order methods are available, often implicit versions of the Runge-Kutta, and the Linear Multistep methods.

The solution of the system of nonlinear equations within each increment must be performed by an iterative method. A few methods are in popular use, the method which has the fastest convergence but requires the most work is the Newton-Raphson method. The stiffness matrix, which in the context of a system of nonlinear equations is the Jacobian matrix, is reformulated at each iteration, this method is illustrated in Figure 3-3(c). The modified Newton method is shown in Figure 3-3(d), the Jacobian matrix is kept constant for all iterations, requiring much less work but giving only linear convergence as compared to the quadratic convergence of the Newton-Raphson method. The modified Newton method is sometimes also called constant stiffness iteration. Quasi-Newton methods such as Broydens method may be used. The Jacobian matrix is adjusted between iterations rather than completely reformulated. These methods usually give convergence rates between that of Newton-Raphson and Modified Newton methods.

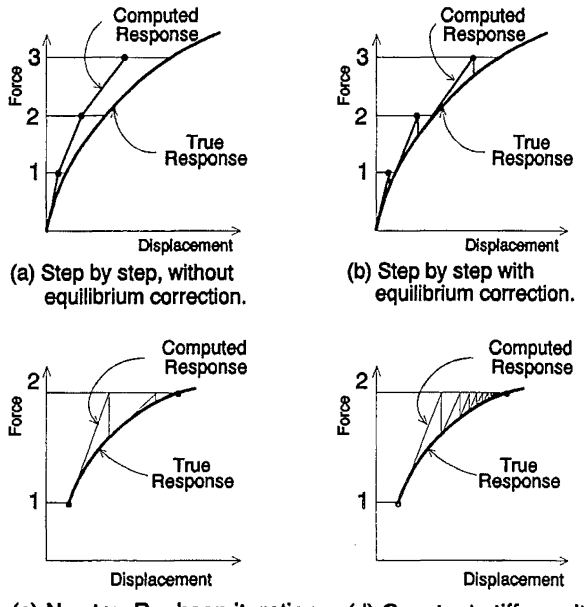

Figure 3-3 *Incremental and iterative techniques.*

The most efficient method for the solution of a system of nonlinear equations may be given by a mixture of the techniques described above, perhaps a modified Newtons method with the Newton-Raphson applied once every few iterations.

When a problem is highly nonlinear, smaller step sizes must be used and the Newton-Raphson method tends to be the most stable method within each loading increment.

4 Examples

This chapter sets out to provide a more tangible look at fibrous finite element analysis, as well as indicating why starting a new analysis may be more beneficial than extending a previous one. A simple general finite element is demonstrated and two previous analyses are investigated.

In the next section a simple example of a small displacement, three dimensional, plane stress element is given. This example will show how element displacement functions are used and how element matrices are formulated.

Sections 4.2 and 4.3 describe analyses which were performed by Van Luijk and Djaja respectively. Some of the faults in these models are indicated and reasons are given for each as to why it would not be profitable to spend time on their extension and refinement.

4.1 Finite Element Analysis Example

To illustrate a very simple example of the formulation of the stiffness matrix for a finite element an eight noded, linear elastic, isoparametric finite element is used.

The element will be generated in cartesian coordinates, (x,y,z), with the displacements being u,v and w in the three axis directions respectively. The reference state of the element in (r,s,t) coordinates, and the element shape after mapping, are shown in Figure 4-1.

The x, y and z coordinates for each node are described by the vectors X_I Y_I and Z_I as shown:

$$\{X_I\} = \begin{Bmatrix} x_1 \\ x_2 \\ \vdots \\ x_8 \end{Bmatrix} \quad \{Y_I\} = \begin{Bmatrix} y_1 \\ y_2 \\ \vdots \\ y_8 \end{Bmatrix} \quad \{Z_I\} = \begin{Bmatrix} z_1 \\ z_2 \\ \vdots \\ z_8 \end{Bmatrix} \qquad \textbf{(4-1)}$$

The displacements at each node, U_I, V_I and W_I, are defined similarly.

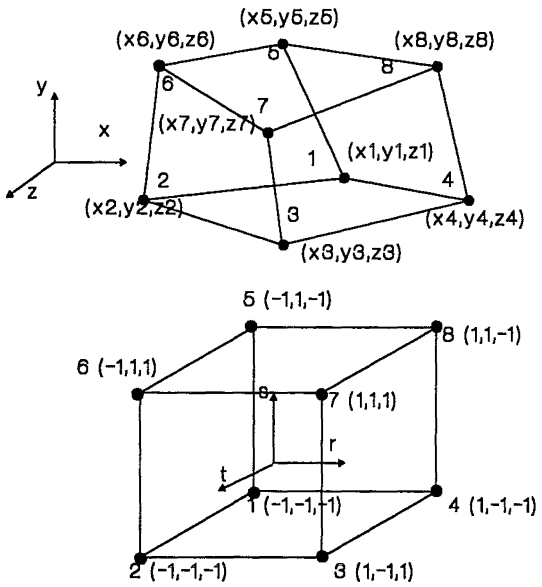

Figure 4-1 *Mapped and reference states of 8-node isoparametric element.*

The linear shape functions, N, are defined as (4-2).

$$N_i = \frac{1}{8}(1+rr_i)(1+ss_i)(1+tt_i)$$

$$\{N\} = \{N_1 \;\; N_2 \;\; N_3 \;\; N_4 \;\; N_5 \;\; N_6 \;\; N_7 \;\; N_8\}$$

$$= \frac{1}{8}\begin{Bmatrix}(1-r)(1-s)(1-t)\\(1-r)(1-s)(1+t)\\(1+r)(1-s)(1+t)\\(1+r)(1-s)(1-t)\\(1-r)(1+s)(1-t)\\(1-r)(1+s)(1+t)\\(1+r)(1+s)(1+t)\\(1+r)(1+s)(1-t)\end{Bmatrix}^T \qquad \textbf{(4-2)}$$

Therefore, the displacements and coordinates within the element are given in terms of the shape functions, which are functions of r,s and t, by:

$$\begin{Bmatrix} x \\ y \\ z \end{Bmatrix} = \begin{bmatrix} N & 0 & 0 \\ 0 & N & 0 \\ 0 & 0 & N \end{bmatrix} \begin{Bmatrix} X_I \\ Y_I \\ Z_I \end{Bmatrix} \qquad \begin{Bmatrix} u \\ v \\ w \end{Bmatrix} = \begin{bmatrix} N & 0 & 0 \\ 0 & N & 0 \\ 0 & 0 & N \end{bmatrix} \begin{Bmatrix} U_I \\ V_I \\ W_I \end{Bmatrix} \tag{4-3}$$

The strains for this three dimensional small displacement case are described by:

$$\{e\} = \{\varepsilon\} = \begin{Bmatrix} \varepsilon_x \\ \varepsilon_y \\ \varepsilon_z \\ \gamma_{xy} \\ \gamma_{xz} \\ \gamma_{yx} \end{Bmatrix} = \begin{bmatrix} N_{,x} & 0 & 0 \\ 0 & N_{,y} & 0 \\ 0 & 0 & N_{,z} \\ N_{,y} & N_{,x} & 0 \\ N_{,z} & 0 & N_{,x} \\ 0 & N_{,z} & N_{,y} \end{bmatrix} \begin{Bmatrix} U_I \\ V_I \\ W_I \end{Bmatrix} = [B_0] \begin{Bmatrix} U_I \\ V_I \\ W_I \end{Bmatrix} \tag{4-4}$$

To calculate the derivatives of the shape functions with respect to x,y and z coordinates, the inverse of the Jacobian must be found.

$$\begin{Bmatrix} N_{,x} \\ N_{,y} \\ N_{,z} \end{Bmatrix} = \begin{Bmatrix} \frac{\partial N}{\partial x} \\ \frac{\partial N}{\partial y} \\ \frac{\partial N}{\partial z} \end{Bmatrix} = [J^{-1}] \begin{Bmatrix} \frac{\partial N}{\partial r} \\ \frac{\partial N}{\partial s} \\ \frac{\partial N}{\partial t} \end{Bmatrix} \tag{4-5}$$

Where the Jacobian is defined and evaluated as equation (4-6).

As the inverse of J can not in general be found in closed form, numerical integration is used. The integration points are described by the indices j,k, and each have a weighting of W_{jk}. At each integration point, the numerical value of the Jacobian is found and inverted. The appropriate derivatives are then calculated, allowing the formation of the B matrix at that point. The stiffness matrix is then formed, as

$$[J] = \begin{bmatrix} \frac{\partial x}{\partial r} & \frac{\partial y}{\partial r} & \frac{\partial z}{\partial r} \\ \frac{\partial x}{\partial s} & \frac{\partial y}{\partial s} & \frac{\partial z}{\partial s} \\ \frac{\partial x}{\partial t} & \frac{\partial y}{\partial t} & \frac{\partial z}{\partial t} \end{bmatrix} = \begin{bmatrix} \frac{\partial N}{\partial r} \\ \frac{\partial N}{\partial s} \\ \frac{\partial N}{\partial t} \end{bmatrix} [X_I \;\; Y_I \;\; Z_I]$$

$$= \frac{1}{8} \begin{bmatrix} -(1-s)(1-t) & -(1-r)(1-t) & -(1-r)(1-s) \\ -(1-s)(1+t) & -(1-r)(1+t) & (1-r)(1-s) \\ (1-s)(1+t) & -(1+r)(1+t) & (1+r)(1-s) \\ (1-s)(1-t) & -(1+r)(1-t) & -(1+r)(1-s) \\ -(1+s)(1-t) & (1-r)(1-t) & -(1-r)(1+s) \\ -(1+s)(1+t) & (1-r)(1+t) & (1-r)(1+s) \\ (1+s)(1+t) & (1+r)(1+t) & (1+r)(1+s) \\ (1+s)(1-t) & (1+r)(1-t) & -(1+r)(1+s) \end{bmatrix}^T [X_I \;\; Y_I \;\; Z_I] \qquad \textbf{(4-6)}$$

described in chapter 3, by an integral over the volume. Due to the numerical integration, the integral is actually represented by a summation over the integration points.

$$[K_0] = \int_{Volume} [B_0]^T [C][B_0] dVolume$$

$$= \int_{-1}^{1}\int_{-1}^{1}\int_{-1}^{1} [B_0]^T [C][B_0] |J| \, dr\,ds\,dt \qquad \textbf{(4-7)}$$

$$= \sum_j \sum_k \sum_l W_{jkl} [B_{jkl}]^T [C][B_{jkl}] |J|$$

Where B_{jkl} is B_0 evaluated at the point represented by j,k,l.

4.2 Van Luijk Analysis

4.2.1 Continuous Fibre Model

Van Luijk [58] commenced his study by re-working the continuous fibre analysis of Carnaby to a computationally more efficient energy formulation based on the finite element displacement method. The same analysis based around a less formal stress analysis method is then repeated. The continuous fibre analysis was modified to include the effects of staple fibres and the fibre migration necessary for the strength of a staple fibre yarn.

All of the models used assumed that the fibre properties do not change along the fibre and that the properties of the yarn are independent of its length. The nonlinear fibre axial properties are approximated by a piecewise linear function. All non-migration models assume that fibres are arranged at constant radius and follow uniform helical paths.

The lateral compression behaviour of the yarn model was assumed to be governed by the Van Wyk equation which relates volume change to pressure. This pressure is effectively matched to the lateral compressive stress generated by the axial forces in the helical fibres.

The first stage of the finite element analysis is to assume the yarn material is a continuum. The lateral stresses as defined by the Van Wyk equation are suitable for this situation. The axial stress in the fibres must be modified for the assumption as the continuum stress is defined as continuous over the voids between the fibres.

The yarn was meshed by assuming element boundaries which were concentric cylinders and linear displacement functions were used in both the radial and axial directions. The number of fibres within each element varied between elements but the fibre density was assumed uniform within an element. Only one layer of elements were used in the axial direction due to the assumption of uniformity in this direction.

In the energy formulation, the principal of virtual work (variational approach) was used to form the system equilibrium equations. The yarn stress in the lagrangian coordinate system is written in terms of the nodal displacements and the use of a constitutive material matrix was avoided by writing the stresses directly as a nonlinear function of

the nodal displacements rather than more conventionally as a function of the strains. The element nodal force vector (f) is formed from the derivatives of the strains and the stresses (S), using the principal of virtual work, equation (4-8), in terms of the nodal displacements. The element nodal force vectors were then assembled to form the global force vectors (F) and therefore the equilibrium equations (4-9) where P is the system global node vector. Due to the nonlinear equations involved the solution demanded an iterative solution technique but not necessarily an incremental one as the problem was not path dependent. Newton-Raphson iteration was used and the tangent stiffness matrix, as the derivatives of the vector F with respect to the nodal displacements was required.

$$\{f\} = \int_{V_0} \frac{\partial \{e\}^T}{\partial \{u\}} \{S\} dV_0 \tag{4-8}$$

$$\{P\} = \{F\} \tag{4-9}$$

The stress analysis differs from the energy analysis in the governing equation. The stress method directly balances the lateral stress calculated from the Van Wyk relationship with that calculated from the axial forces in the helical fibres. Both of these expressions are formed in terms of the nodal displacements. The governing equation is the equilibrium relationship between the two.

A problem is found in forming the governing equation in that there is more than one way to define the lateral pressure from the helical fibres within the element. The pressure from the Van Wyk equation is dependent on the volume change within the element, hence is constant within the element. The lateral pressure from the fibres is defined such that it is radially dependent, therefore the two pressures can not be directly compared. Five possible relations, of varying complexity, were tested and compared with the results obtained from the energy analysis. The various relations were compared on the basis of error from the energy solution and the computational effort required for their use. The solution procedure for the stress analysis is similar to that for the energy analysis except that the yarn force must be calculated separately using equilibrium check in the axial direction after each increment.

4.2.2 Staple Fibre Model

The staple fibre model has two main differences to the continuous fibre model, the slippage of the fibres near the fibre ends must be considered and it must include the effects of fibre migration if it is to have any significant strength.

Van Luijk modified the ideal migration model used by Hearle and Treloar to include variable fibre packing density in the radial direction. The model assumes that all fibres are identical except for a translation along the yarn axis and a rotation around the yarn axis. It was found that an analytic solution could only be derived for the case when the packing density was discontinuous across the yarn and was directly related to the inverse of the radius within each element.

The stress method described above was modified for the migration model as it was felt that to include the slipping energy in the energy approach would be too difficult if not impossible. In the stress method the slipping energy does not effect the governing equations. The slipping energy need only be taken into consideration when the yarn force is calculated using a virtual work principal with numerically evaluated derivatives after each increment. The other main difference from the continuous fibre analysis is that the fibre mass within each element must be updated after each increment due to fibre mass transport across the boundaries during fibre slippage. This causes the problem to be path dependent.

Fibres were assumed to be surrounded by a imaginary tube, the tube extended with the yarn and the fibre either extended with the tube or slipped inside it. The axial force at a point in a fibre was calculated using the simple assumption to use the minimum of the maximum force possible due to frictional restraints and the force if the fibre extends with its tube. The maximum frictional force was calculated using Grosbergs single fibre withdrawal formula, modified by a correction C which was dependent on the shape of the migration path, to account for the fact that not all frictional forces at contact points will act in an opposing direction.

4.2.3 Comments

There are reasons why a fresh start on the problem would be more desirable than working on an extension to the analysis of Van Luijk. Some of the reasons listed below have come about due to the greater computational power and more flexible computer programmes that are now available and also developments in the field have also suggested better paths for the development of the theory.

Van Luijk designed his migration model for uniaxial monotonic loading and it would be more desirable to have a model which applied to a general situation. Computing improvements are such that a general analysis is much more likely to be feasible. The way in which Van Luijk's analysis was formed makes it very inflexible for extension to more complex loadings, such as bending or other nonsymmetric situations. Part of the reason for this is that Van Luijk's analysis was developed as a modification to a continuous fibre theory. The finite element model was made by subdivision of a yarn model, rather than by being built up from continuum properties as is both conventional and more versatile. Unfortunately the incorporation of migration and slippage effects in such an analysis would require radical changes from the methods used by Van Luijk.

The energy model was formed to comply with most of the requirements of finite element analysis, the stress model, however, has significant departures from the mathematical rigor required. The problem with the non-unique definition for the governing equation has already been covered, Van Luijk gets around this problem for the case without migration by comparing various choices with the energy method solutions to find the best option. This option was then used in the migration analysis. Although this was the best method available theoretical justification is lacking. The second technical difficulty with the migration analysis is that it was shown that the simple method assumed for calculating the fibre axial force when slippage was a possibility does not actually apply in some cases. Although for the simple loading case used on the model this assumption was shown to have negligible effect, in an analysis involving more general loadings, this assumption could be a source of significant error.

Van Luijk, like Carnaby previously, used the Van Wyk equation to govern the lateral compression of the yarn and this was a considerable improvement over previous assumptions such as constant volume deformation. The Van Wyk relationship was originally justified by experimental tests with random fibre assemblies and then derived theoretically by using rods stacked at right angles. It was used here to approximate an assembly of aligned fibres, this is not an assumption that seems very justified, except that at the time it was the best available. Other theories have now been developed, based on a fibre orientation density function, that may provide a better solution than the Van Wyk equation.

A further problem with the relationship governing the lateral compression of the yarn meant that the stiffness matrix of the system was unconservative. The transverse stress is changed by the extension of the yarn as the volume of the element changes (Van Wyk relationship is based on the volume). It is possible to deform the element laterally and

change the volume without adjusting the tension, causing the stiffness matrix to become unsymmetric and therefore unconservative.

There are some assumptions made in the model which are adjusted for a manageable solution. During the majority of the analysis the packing density of the fibres is assumed to be constant within each element and yet for solution of the ideal migration equations the packing density is defined to vary with the inverse of the radius. Although this is a small point which probably makes little difference to the solution, it would be desirable to have analysis where the assumptions are consistent throughout.

The initial stresses in the model were assumed to be zero. This was explained by assuming that stress relaxation during storage would reduce them. Although this may be the case, the issue of initial stresses deserves some consideration.

4.3 Djaja Analysis

4.3.1 Unit Cell Model

Djaja [6] developed a model for the twisting and extension of a cylinder of aligned fibres. The model is valid for small strain and assumed elastic fibre properties. A uniform helix was used to model the fibre crimp. The analysis was based on the mechanical constants derived by Lee and Lee, and the shear moduli of Pan and Carnaby, all of which are defined using the fibre orientation density function of Komori and Makishima. The constants are based on the three point bending element, therefore only fibre bending energy is considered, the fixed end conditions were assumed to ensure slope continuity along the fibre. The helix angle, the volume fraction, and the orientation factor were updated at the end of each increment.

As the problem was axisymmetric, only a one thirty-sixth segment of the cylinder was analysed, one element was used in the axial direction as the assembly was considered uniform in the axial direction. Two sets of boundary conditions were considered for the model, the first was the more theoretically correct, it involved fixing all bottom surface nodes in the axial and rotational directions, all axial nodes in the radial direction, and all top surface nodes were linked so as to have common axial and rotational components. The second set of boundary conditions were the same except that a common axial component was no longer maintained on the top surface.

4.3.2 Comments

The analysis of Djaja has addressed some of the faults that the model of Van Luijk possessed, however other problems were created in the process.

This model is capable of more flexible usage than that of Van Luijk as conventional finite element methods were used throughout, for example, the material constitutive matrix was actually written. This flexibility would allow this model to be easily modified for a much more general loading, such as non-axisymmetric problems like bending.

Some doubt may also be cast on the correctness of the micromechanical basis for the analysis. The relationships used for generating the mechanical properties were based on the three contact point bending element where a theoretical objection has been raised to this element, (section 2.2.1) and a two point element would now be preferred for study. Another problem with the micromechanics is that the assumptions made are far from consistent, the fibres are assumed to be aligned uniform helices and to maintain that shape throughout deformation. However, the model assumes that there are multiple contact points along the fibre. Also, as the model is extended in tension, all of the helices are assumed to reduce in radius, yet the number of contact points increases, this is inconsistent.

This model also fails to take into consideration the possibility of strain energy other than that of bending, nonlinear fibre properties, or the effects of fibre slippage, all of which would be required for a complete answer.

The restraints placed on the model may have been insufficient. The object was to model an assembly, uniform in the axial direction, when subject to twisting. If such a situation is imagined, then it is obvious that the rotational displacement of any point must be a linear function of the axial position. This model allows for a quadratic displacement in the rotational direction, thereby allowing the model to be more flexible than it should be. An extra restriction should have been placed on the mid-side nodes on the sides in the axial direction linking them to the corner nodes on that side so as to enforce a linear variation of rotational displacement in the axial direction. This would ensure a state of uniform shear at constant radial position, as expected with such a twist.

5 Single Fibre Studies

The indications coming from the review of the literature were that the most likely path for the development of fibrous analysis would be based around the two point bending element. This chapter starts to explore the application of the two point element to the problem being considered.

Limitations were found in the two point element mostly due to the element deformation being based solely on the strain field. Some attempts are made to investigate ways of overcoming these difficulties but it was eventually decided that these were not worth the added complexity. Consequently the two point bending element was abandoned.

5.1 Two Point Bending Elements

The two point bending element was developed for use in the modelling of the compression of a random fibre assembly and in this situation it performed well. It was proposed that the same approach could be used to develop a model for an aligned assembly.

Conceptually the two point bending element is generated from a continuous fibre within an assembly. The points where this fibre touches any other fibre or where other forces are applied to the fibre are identified, these are called contact points. All contact points are then assumed to be rigidly fixed to the continuum. The small piece of fibre between any two contact points forms the bending element which is then treated as an independent[3] unit, free to rotate at the contact points.

It is the independence of these bending elements which makes them so attractive for the compression problem but it is this same 'feature' which will cause trouble when it comes to more complicated systems. In an aligned system the continuity of the fibre plays a far more important role in the structural action of the assembly than it does in

[3] The elements are not actually independent as they are still linked through the continuum strain field - they are independent in the sense that they no longer have direct connection to their neighbours on the fibre, and their properties are defined solely by the global strain field.

the random fibre assembly and this fibre continuity is not maintained by the independent units.

There are two obvious implications of this loss of fibre continuity which will seriously affect the performance of the model. The first is the response of the element when the deformation is principally bending in the element, and the second relates to the slippage between fibres at the contact points.

When the bending response of an element is the major factor in the deformation of the system (because the ends of an element are free to rotate), this will have a significant effect on the results.

Consider the very simple case of two elements with a lateral load on the centre node. If the elements are to act independently then there will be no force induced from the bending stiffness. However if continuity is maintained, a significant contribution to the lateral force resistance will come from the bending (see Figure 5-1).

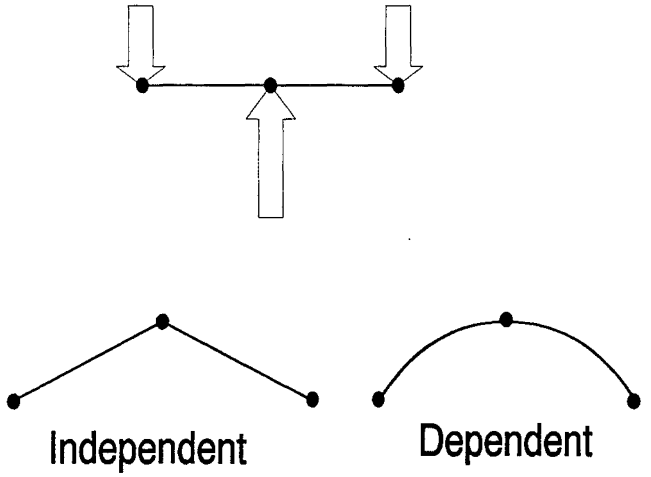

Figure 5-1 *Lateral force on independent and dependent 'element' pairs.*

The independent units fail to match the correct deformation pattern at all. This effect would possibly be minimal in the random assembly as only fibres which are perpendicular to the loading (or enforced deformation) would be affected and those in line with the force would assume a bent configuration as required. But within an assembly where the fibres are aligned situations could easily come about where the error of this approximation would be unacceptable.

The second apparent problem with the two point bending element is the slippage of a fibre against a number of other fibres. In this situation, the criteria governing whether or not a fibre will slip is based on the amount of force which is being transmitted across the contact. This force in turn, is dependent on the level of the axial force within the fibre itself. Because of the way that slippage occurs, the axial force in a fibre will decrease towards the ends of the fibre, therefore a fibre piece acting independently cannot recreate this effect. The normal force at a contact point in a two point element can be dependent only on the amount of bending in the segment. If the fibre is in tension it will be straight and the normal component of the force will be zero.

5.2 Fibre Continuity, Energy Approach

The problem of ensuring fibre continuity for an individual segment without considering the fibre as a whole (to preserve the independent status) is complicated. In fact it is likely to be impossible but it should be possible to get a far better approximation than simply allowing every end to rotate without restraint.

When a fibre segment is deformed the energy within that segment is adjusted, either increased or decreased[4]. Controlling the deformation of a segment such that all continuity requirements within the fibre are met is a very difficult task if the segment ends are free to rotate. However if the segment ends are constrained to maintain the same slope which they had at the start of the increment, then continuity will be maintained throughout deformation. It is assumed that the geometry definition given in the undeformed state does indeed represent a continuous state. This deformation however would make the system artificially stiff, putting considerably more energy into each segment than there would be if the correct contact point continuity conditions were maintained.

The other deformation method which is easily calculated is when the segment ends are free to rotate, but no continuity is enforced at the ends. This could be called a 'free' segment. Therefore this system would be too flexible, each segment containing less than the required energy.

However the two deformation descriptions present upper and lower bounds to the correct energy for the system. It was hoped that some relationship could be found that

[4] note that the energy content may only be increased from an undeformed state.

would allow the correct energy level to be estimated as a function of the upper and lower bounds.

This relationship would depend on many different variables; the number of independent segments within a fibre, the length distribution of the segments, the slenderness of the segments, the fibre constitutive properties, the geometry of the fibre, the actual strains of the continuum, and even the position of the segment along the fibre as a whole.

This problem was dealt with on the assumption there was no slippage and as if it were only valid for small values of continuum strain (which may well be the case). As there is no slippage the contact points can be assumed to be fixed to the continuum. This is the only link of the fibre to the continuum properties.

The method initially ignores most of the effects which could be factors in the desired relationship by assuming a 'random' model with a variety of segment lengths and by using only constant continuum strain.

Once each model is assembled and contact points have been chosen, three analyses are carried out for each valid continuum strain movement.

- Each segment acts as an independent unit and no continuity is maintained - this gives the lower bound for the total internal energy.
- Full continuity is maintained and contact points are allowed to rotate - this gives the 'correct' value for total internal energy.
- Continuity is maintained, but contact points are not allowed to rotate - an upper bound on the energy is found.

These analyses should be repeated for a series of 'random' fibres, for various strain situations within each fibre. Also the increment from one deformed state to another may be considered. The analyses would actually have been performed using the nonlinear finite element package ABAQUS.

Analysis of these results may allow the desired relationship to be found and the use of uniform strains in testing allows the entire fibre to be considered to be 'at a point'.

The first few attempts at this type of analysis were performed with for small number of elements (about six), and the geometries were manually generated simple patterns. It was found that there was insufficient variation between the resultant energy values.

Some runs would have the same value of energy for both of the first two cases and a much higher value for the third, and in some other runs the second case would be exactly the same as the third. This situation was obviously not going to result in data suitable for the intended purpose. New test assemblies were proposed which were randomly generated, but arranged to basically approximate a line. An example of one test to give some idea of the type of geometry which was generated is shown (Figure 5-2).

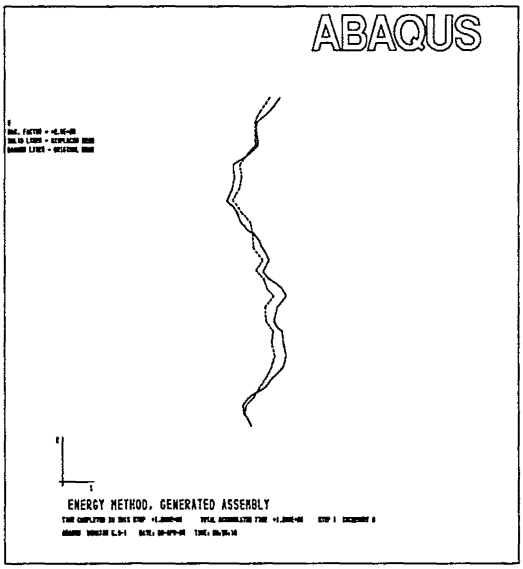

Figure 5-2 *Example of randomly generated test assembly.*

An ULTRIX script routine was written ('fenergy') which accepted as input the parameters which control the formation and loading of the 'random' assembly. These parameters are:

- The number of nodes in the assembly.
- The number of nodal points in each fibre (not counting the first).
- The radius of a fibre.
- The Young's modulus of a fibre.
- The Poissons ratio of a fibre.
- The top limit of horizontal displacement, the x position of one node compared to the previous one is allowed to be plus or minus this value.
- The top and bottom limits of the vertical displacements, the y position of one node as compared to the previous one is allowed to vary between these limits, if both are positive and greater than zero (usual case) this ensures that the fibre progresses in a strictly upward direction, avoiding problems with

backtracking or zero length fibres. This also means that the resultant shape is basically a line in the y direction.

- Top and bottom limits for the x strain to be imposed on the assembly, as well as the number of increments to be made between those limits.
- Similar limits et cetera for y and shear strain.
- Number of tests to be made at each level.

Each node in the assembly is then randomly generated based on the x and y direction steps from one node to the next being equally distributed within the limits given in the input. Cubic displacement beam finite elements are then used to connect each node to the next. Then the key nodes (those which form the boundaries of the fibre segments) are restrained such that they remain fixed to the constant continuum strain which is to be enforced for that run.

The script routine then controls the execution of a large number of ABAQUS analyses. The routine has asked the user for both the ranges of the various strain parameters which are to be tested and the number of tests to be executed at each strain value. A data file is created listing the values for each test.

A FORTRAN program ('random') takes the data files from the script routine as they are created, this program then produces three input files ready for ABAQUS execution. The files represent the three energy cases as described above.

The script routine then executes each of the three ABAQUS jobs in turn. The Unix functions 'grep' and 'nawk'[5] are used to pick out the one energy result which is required from each ABAQUS output data file, these results are then listed in the output file which contains the output from all tests. This process is repeated until all required tests are completed.

The first analyses of the energy approach were for the cases of a fixed x strain of 20% or a fixed y strain of 10%, 31 nodes and 2 nodal points per nodal segment. Histograms were plotted for the frequency distributions of the ratio value (a measure of the placement of the case 2 energy between the case 1 and the case 3). The histograms were discretised into either 10 or 20 steps, the 20 step plots showed some bumps, but both indicated that a definite distribution was present as opposed to merely a random arrangement (Figure 5-3).

---

[5] 'grep' is a UNIX command for pattern matching, and 'nawk' is a useful UNIX based data extraction language.

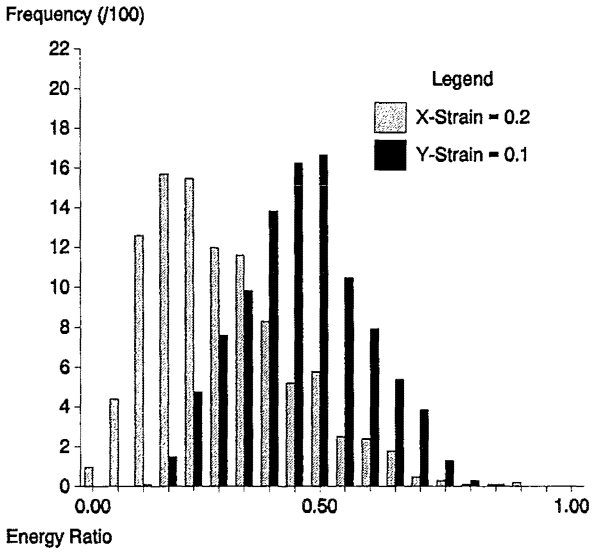

Figure 5-3 *Frequency Distribution at y-strain=0.1 and x-strain=0.2*

Investigation of the data suggested that a source of the 'bumps' in the histograms (not apparent in the 10 step plot due to the coarse discretisation) may be due to the restricted accuracy of the ABAQUS energy output. This low accuracy may be reducing some of the results to be meaningless, most often only 3 significant figures are obtained from ABAQUS, the value is then formed as the ratio of two differences in energy levels between different cases. As the differences in energies between cases are commonly less than 10% of the total, this lack of accuracy can lead to the situation where the relationship between the values of the ratio is such that only a small number of possible values are present between 0 and 1 for the ratio. This means that the results of the discretised histogram are biased towards the sections which contain the lower order fractions.

The accuracy of the energy terms is a problem because the programmers of ABAQUS did not anticipate the output being used as it is here. The energy values would be calculated to a greater accuracy within the program but are not displayed, there is little that can be done to extract this information from within the program. In a more complete attempt, specialist software would allow accurate energy calculation.

Two methods were developed to solve this problem with the data. One was to have some form of smoothing of every result, this method however could be relatively complicated and has the disadvantage of some bias still remaining in the results. The second method was to decide which data were of dubious accuracy and simply not to include these data in the results. There was the possibility however that this process

itself may introduce some bias, which would occur if there were any link between the energy level of the data and the ratio value. However a plot of energy against ratio value for 500 data points indicated that no such link was evident. Therefore it was decided that the suspect points could simply be 'dropped' from the results. This was tried over a series of tests and comparison of smoothed histograms resulting from 'fixed' and the 'unfixed' results indicate that only a small, if not negligible difference was made. It did however make the production of results considerably more difficult and tedious, consequently it was decided to drop this correction.

More analyses were performed and then plotted, the most complete concerns the variation in the value of the x-strain in the situation outlined above. The frequency distributions of these are shown. A plot of the means and standard deviations are also given.

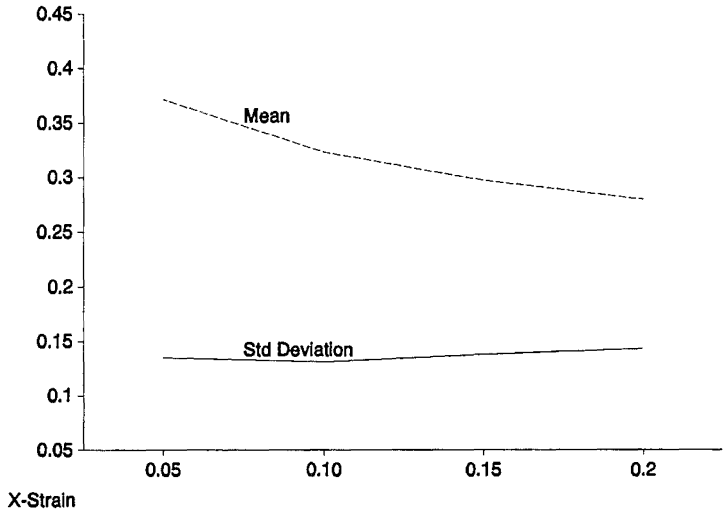

Figure 5-4 *Mean and standard deviation at various x-strains.*

Conclusions

These test runs remain incomplete, it was decided that the research should take an alternative direction but it is felt that enough has been done that some qualitative conclusions may be drawn.

This approach will not result in a formula which will give an exact solution under all situations, but an approximation could be found which would be better than either of the two extreme cases. The output from the program showed that in many cases the

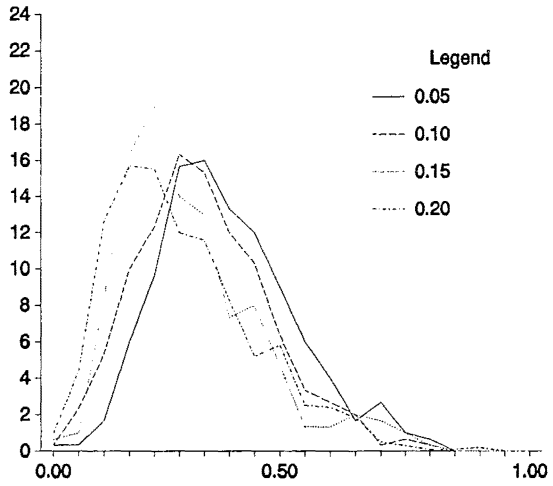

Figure 5-5 *Frequency distributions at various x-strains*

energy differences between the two extreme cases has been as much as a factor of two, indicating that if the two point bending element were to be used, a fix for continuity based on this approach could be useful.

If this approach was to be continued it would be necessary to find a different way of calculating the energy values of the system. A special program could be designed which could take advantage of the fact that nearly the same analysis is being done three times for each random configuration. It would then also be possible for the energy values of the system to be output with a greater degree of accuracy. This program would give much better results, and would operate considerably quicker than using ABAQUS.

5.3 Lateral Compression of Sinusoidal Fibres

The problem with the two point bending element when slippage is being considered is that the normal contact point force of a fibre can not be known. This is because this force is a function of the axial force in the fibre, which in turn depends on the position of the segment within the whole fibre and this information is unknown to the fibre segment.

Attempting to find a solution to this general problem would be an excessive initial step and the task set was to solve a similar problem in a much more restricted system. It was decided to work with the two dimensional situation of the lateral deformation of a sinusoidal fibre, this being the projection of a three dimensional helix into a two

dimensional plane. The sinusoidal fibre was theoretically compressed laterally between two flat plates, the resistance forces from the fibre to the plates being the forces of interest. This was modelled using the nonlinear finite element package ABAQUS. Contact points between the fibre and the plates were represented by slippage interfaces with rigid surfaces. Note that the use of slippage surfaces does indeed make the problem one requiring nonlinear solution techniques.

The first fibre model contained 6 cycles of the sinusoidal shape. Significant convergence difficulties were found with this mesh. In an attempt to get results the slenderness of the fibre was increased and another mesh was drawn which had twice as many elements within each wave. Softened contact was also assumed at the contact points, which means that some overclosure and some negative pressures are allowed at contacts. Convergence criteria were considerably lowered as it was found that previous limits were greater than the contact forces, making these early results unusable. The minimum size of an increment was reduced in the hope that the analysis was merely striking regions of slow convergence and this extra flexibility might overcome these spots. This was found to help in some cases.

In the light of the problems with convergence a new start was proposed, beginning with a much simpler system and seeing what effect variation of the input parameters have on the convergence or otherwise of the solution. Symmetry was used in all cases to lower the computational effort. The first and the simplest model possible was a single cycle of a sinusoidal curve, which due to symmetry requires consideration of only half of a cycle. This was modelled with four B22 ABAQUS elements. One rigid surface and one interface element were required. The parameters varied were:

- coefficient of friction
- fibre diameter
- size of half wave
- elastic properties (Young's modulus and Poisson's ratio)

When results were obtained, the analysis was extended to include more waves, symmetry always being used to reduce the size of the problem.

Plots of the lateral force variation at the contact points of fibres of models representing up to five waves were investigated. The plots indicated that a common form was

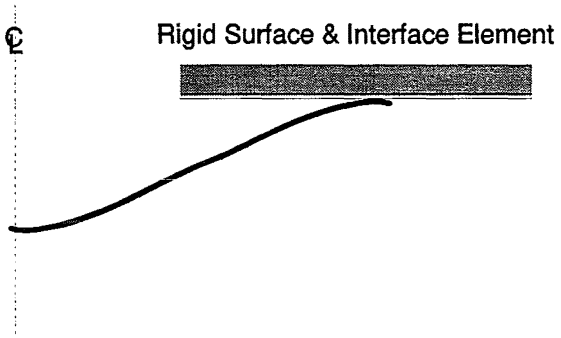

Figure 5-6 *Element arrangement, one wave, using symmetry.*

developing for the lateral forces at the contact points between the fibre and the rigid plates.

For the simpler models (less than five waves) full studies varying both fibre radius and lateral strain were carried out. On the five wave problem this became impossible due to solution convergence difficulties. Plots of the form of the normal force variation along the fibre length were obtained, and how that distribution changed for one sample. It was found that for a *normalised*[6] plot, all of the lateral forces showed identical values at each contact point for all values of the lateral strain and the fibre radius. This meant that the full parameter study was unnecessary for each arrangement. Subsequent models were tested at only one value of lateral strain and fibre radius. The strain value was chosen as low as possible without giving bad results due to numerical difficulties (and ensuring that slippage occurred), as this made convergence significantly more likely.

Results were then able to be obtained for the cases of six, seven and eight waves, until convergence difficulties made it impossible to attain results at larger numbers of waves.

The points however were plotted, polynomial curves of degree two, three and four were fitted to all of the data points with the cubic and quartic curves being almost identical, for this reason, the simple cubic curve (which is significantly different from the quadratic) was chosen (Figure 5-7).

Where f(x) is the proportion of the peak normal force and x is the proportion of the distance along the fibre from the midpoint.

---

[6] The normal force plots were normalised such that the normal force at the middle point equalled one, therefore these plots represent the degradation of the normal force along the fibre length.

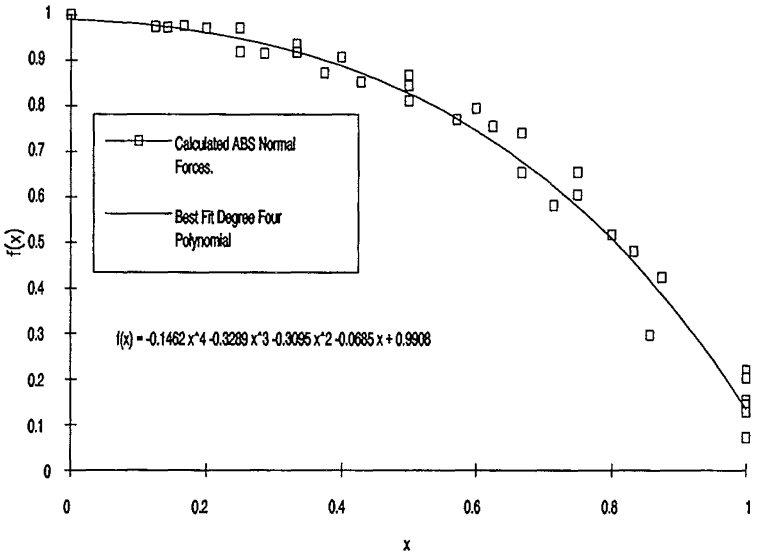

Figure 5-7 *Polynomial fit to lateral forces.*

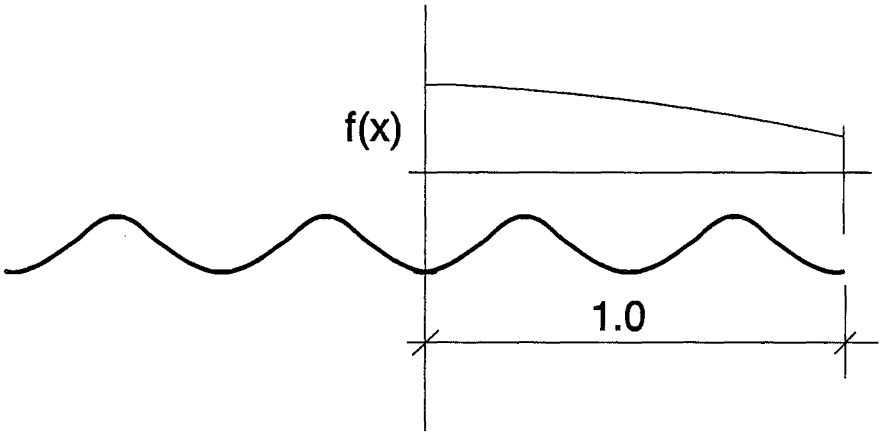

Figure 5-8 *Lateral force distribution.*

Conclusions

Like the previous approach to the solution of the problems with the two point bending element, a change in the research direction away from this element meant that the conclusions are restricted to qualitative and directional assessments.

From the small number of analyses, it seems that it would be possible to define a relationship for the form of the normal force along a fibre. This would mean that for the case of a sinusoidal fibre laterally compressed at a constant strain along the length, the normal forces (at the contact points) for a two point segment could be found with

only knowledge of the position of that segment along the fibre. For this approach to be useful, a vast amount of further study must be done, involving three dimensional configurations and many other permutations of fibre shapes and loading systems.

5.4 Continuum Strain

If the two point fibre segment were to be used in a continuum analysis, it would be necessary to develop the relationship between the strain properties of the continuum and the chord strain of the fibre segment. These relationships are derived below for the cases of both large and small displacement continuum mechanics.

Small Displacement

A fibre segment is defined to be the *free* piece of a fibre between two contact points with other fibres. If the contact points are assumed not to slip and to undergo an affine deformation then the change in the chord length of the fibre segment may be defined in terms of the appropriate strain parameters. In three dimensional cartesian coordinates these are three normal and three shear strain components:

$$\varepsilon_x,\ \varepsilon_y,\ \varepsilon_z,\ \varepsilon_{xy},\ \varepsilon_{yz},\ \varepsilon_{xz} \tag{5-1}$$

Define the fibre segment chord such that one end is at the origin and the other at the coordinates (x', y', z'). The chord length is then r', where:

$$r'^2 = x'^2 + y'^2 + z'^2 \tag{5-2}$$

The small displacement relationships can be written as:

$$\varepsilon_{ij} = \frac{1}{2}\left(\frac{\partial u_i}{\partial x_j'} + \frac{\partial u_j}{\partial x_i'}\right) \tag{5-3}$$

where u, the displacement vector is the difference between the deformed and the undeformed coordinates. The deformed coordinates are (x, y, z), therefore:

$$u_1 = x - x' \quad u_2 = y - y' \quad u_3 = z - z' \tag{5-4}$$

Define the mapping from the undeformed to the deformed coordinates to be defined by the set of equations:

$$\begin{aligned} x &= Ax' + By' + Cz' \\ y &= Dx' + Ey' + Fz' \\ z &= Gx' + Hy' + Iz' \end{aligned} \tag{5-5}$$

However, the mere stipulation of a value for the shear strain does not give a unique definition of deformation, some assumptions about the form of the shear deformation must be drawn. The assumption made regarding the shear deformation in the x'-y' plane is shown in Figure 5-9. This assumption reduces to the statement that within the x'-y' plane, deformation due to shear is independent of the x' coordinate therefore the value of D in (5-5) is set to zero. Similar assumptions may be made in the other two planes which lead to:

$$D=0 \quad G=0 \quad H=0 \tag{5-6}$$

There is a physical reason that some assumption has to be made about the deformation of the system. Any three dimensional body has six modes of deformation which will allow movement of the body as a rigid body, these are called the *rigid body modes*. The first three are the most obvious and are the movements of the whole along each of the three coordinate axes (translation modes). The second three modes relate to the rotation of the body about the axes (rotation modes).

When the system of equations were assembled the translation modes were deliberately excluded, if they were included there should have been an extra constant added to each line of the equation (5-5). This is not the same as setting the amount of rigid body translation to zero, but this value has been constrained to the extent that it is now a function of the strain parameters. This constraint could have been introduced in other ways but would have no effect on the result (as a rigid body motion can not effect the fibre segment chord strain), and would simply lead to more complicated algebra.

In the case of the rotation modes, three constraints have to be introduced for their removal. The restraints were chosen in such a way as to minimise the complexity of the equations.

Substitution among the previous equations easily lead to the statement that:

$$\begin{aligned} A &= \varepsilon_x + 1 & E &= \varepsilon_y + 1 \\ B &= 2\varepsilon_{xy} & F &= 2\varepsilon_{yz} \\ C &= 2\varepsilon_{xz} & I &= \varepsilon_z + 1 \end{aligned} \tag{5-7}$$

Which then can be re-worked to the set of equations:

$$\begin{aligned} x &= (\varepsilon_x+1)x' + (2\varepsilon_{xy})y' + (2\varepsilon_{xz})z' \\ y &= (\varepsilon_y+1)y' + (2\varepsilon_{yz})z' \\ z &= (\varepsilon_z+1)z' \end{aligned} \tag{5-8}$$

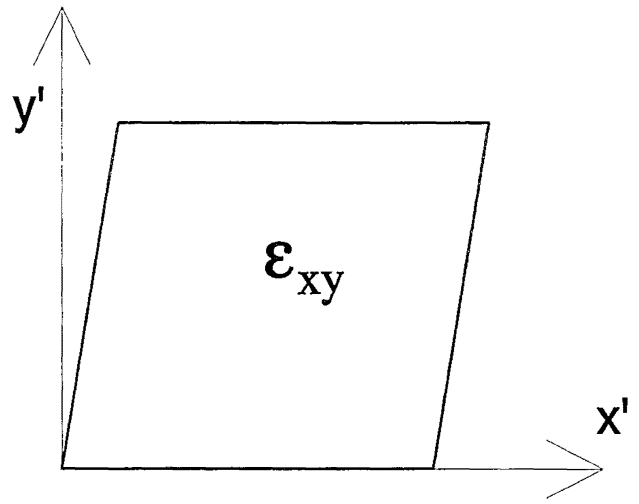

Figure 5-9 *Deformation assumption for shear in the x'-y' plane.*

The strain in the fibre segment chord may now be written as:

$$(1+e_j) = \left(1+\frac{\delta r'}{r'}\right) = \frac{(r'+\delta r')}{r'} = \frac{r}{r'} = \frac{\sqrt{x^2+y^2+z^2}}{\sqrt{x'^2+y'^2+z'^2}} \qquad \textbf{(5-9)}$$

Therefore with substitution:

$$\begin{aligned}(1+e_j)^2 = {} & \left((\varepsilon_x+1) C_x + (2\varepsilon_{xy}) C_y + (2\varepsilon_{xz}) C_z \right)^2 \\ & + \left((\varepsilon_y+1) C_y + (2\varepsilon_{yz}) C_z \right)^2 \\ & + \left((\varepsilon_z+1) C_z \right)^2\end{aligned} \qquad \textbf{(5-10)}$$

Where the C terms in these equations are the direction cosines in the appropriate directions.

Note that the two dimensional case is obtained by setting all of the z-terms are set to zero:

$$\begin{aligned}(1+e_j)^2 = {} & \left((\varepsilon_x+1) C_x + (2\varepsilon_{xy}) C_y \right)^2 \\ & + \left((\varepsilon_y+1) C_y \right)^2\end{aligned} \qquad \textbf{(5-11)}$$

Large Deformation

For large deformations the strain tensor is defined as (in the Lagrangian system, and using tensor notation):

$$\varepsilon_{ij} = \frac{1}{2}\left(\frac{\partial u_i}{\partial x_j} + \frac{\partial u_j}{\partial x_i} + \frac{\partial u_k}{\partial x_i}\frac{\partial u_k}{\partial x_j}\right) \tag{5-12}$$

The same assumptions regarding the form of the shear deformation are made for the large displacement case as for the small displacement case, and after some manipulation result in:

$$A = \sqrt{2\,\varepsilon_x + 1} \tag{5-13}$$

$$B = \frac{2\,\varepsilon_{xy}}{\sqrt{2\,\varepsilon_x + 1}} \tag{5-14}$$

$$C = \frac{2\,\varepsilon_{xz}}{\sqrt{2\,\varepsilon_x + 1}} \tag{5-15}$$

$$E = \sqrt{2\,\varepsilon_y + 1 - \frac{4\,\varepsilon_{xy}^2}{2\,\varepsilon_x + 1}} \tag{5-16}$$

$$I = \sqrt{2\,\varepsilon_z + 1 - \frac{4\,\varepsilon_{xz}^2}{2\,\varepsilon_x + 1} - \frac{\left(2\,\varepsilon_{yz} - \frac{4\,\varepsilon_{xy}\varepsilon_{xz}}{2\,\varepsilon_x + 1}\right)^2}{2\,\varepsilon_y + 1 - \frac{4\,\varepsilon_{xy}^2}{2\,\varepsilon_x + 1}}} \tag{5-17}$$

$$F = \frac{2\,\varepsilon_{yz} - \frac{4\,\varepsilon_{xy}\varepsilon_{xz}}{2\,\varepsilon_x + 1}}{\sqrt{2\,\varepsilon_y + 1 - \frac{4\,\varepsilon_{xy}^2}{2\,\varepsilon_x + 1}}} \tag{5-18}$$

It may then be written that:

$$(1 + e_j)^2 = (A C_x + B C_y + C C_z)^2 + (E C_y + F C_z)^2 + (I C_z)^2 \qquad \textbf{(5-19)}$$

This (after appropriate substitution) gives the desired relationship for the strain in the chord of the bending element in terms of the global strain parameters.

6 Fibres Fixed Within Continua

The previous chapter discussed the limitations of the two point bending element. Within this chapter an alternate approach based on each fibre being rigidly attached to a continuum is outlined, developed, and discarded.

6.1 Use of Continuum Analysis

An approach to continuum analysis of fibrous assemblies is explained. The approach is one of many possible definitions of a continuum analysis. The method avoids the use of the two point bending element.

The continuum analysis envisaged here would be analogous to an assembly of fibres that have been set into jelly. The properties of this jelly are only such that they merely maintain the topological position of each fibre with respect to its neighbouring fibres. An important point here is that every position in the length of the fibre is constrained to move with the continuum and there can be no fibre deformation possible without deformation of the continuum. This can be contrasted with another possible scenario where the fibres are only attached to the continuum at particular points along their length, the contact points. This second continuum definition would behave differently from the first.

The positive results from a discrete fibre yarn torsion model at WRONZ posed the question why a similar approach could not be used within a continuum model. The discrete fibre model was based on the shortest path principle, in which a fibre is assumed to take the shortest path between two points if under tension. Continuum realisation of this principle would be an energy minimisation procedure. The shortest path for a fibre in tension would also correspond closely with the minimum energy configuration. Therefore a method based on consideration of fibre energies (and therefore continuum energies) was investigated.

The decision to make the continuum assumption for the yarn problem can be arrived at in many ways. The decision can be justified by reasons of either simply attempting to get a model to more correctly represent the amount of energy in the system, or to allow simple solution for the system parameters. Some of these lines of reasoning are

briefly described below, along with the more obvious advantages and disadvantages of these approaches.

The first major reason for treating the system as a continuum was dissatisfaction with the two point bending element. As discussed in the previous section, the application of this element fails to conserve fibre direction continuity at the contact points. If the fibres were treated as fixed rigidly to a continuum, then this continuity would be automatically satisfied.

Along with this continuity effect, it was thought that with the two point bending element, the structural actions would be dominated by the contact point distributions. In an assembly that is predominantly aligned most of the energy of deformation will be generated from the gross system deformations. Gross system deformations would be those that concern a greater length of the fibre, over many contact points. The small length of fibre between the contact points would be contributing similar actions to its neighbours. This would imply that the effect of any individual contact point could be ignored, and the structural actions of the system taken simply from the path of the fibre as a whole.

A very simple example of how the two point bending element behaves badly if used within a continuum analysis is shown by the case of a helical yarn under tension and torsion. As the yarn deforms, any fibres initially near the outside of the yarn move in towards the centre of the yarn to reduce fibre tension. In the real situation the fibres cannot attain a position of zero internal elastic energy because the reduction in tension will be balanced by an increase in the bending and torsion in the fibre. With the two point bending element however, the internal stress is defined only by the chord length of the element. Fibre pieces may then simply move in towards the yarn axis to a position where the chord lengths are the same as that in the undeformed state, giving zero internal strain energy. It is also important to note that the deformation of the two point element is in a single plane, therefore there can be no elastic energy generated through a fibre torsion action whereas there would be in an actual helical yarn.

A second reason for assuming the system to be a continuum is so that available system solution methods may be used. For continua, there is a veritable plethora of variations of solution techniques and commercial packages available for solution. Once the problem has been formulated so that it can be solved within one of these packages, then a variety of systems may be solved. Solutions based on a discrete fibre model are likely to be restricted to a very small class of problem that are geometrically equivalent to the

initial problem. The advantage is not just being able to use commercial packages, this is an extension of the fact that once a continuum is assumed, the wealth of knowledge that has been developed in the field of continuum mechanics regarding problem solution is applicable.

It would be wrong to assume that the conversion to a continuum is without loss. There are disadvantages in making this assumption. One restriction is a topological consideration, a fibre that is next to another fibre in the continuum will always remain next to the same fibre. The distance between these two fibres, or the angle between them at some particular point may change, but no other fibre can move into the continuum space between them.

It is also impossible for any part of a continuum to overlap. In a real fibre structure a group of fibres might merge with another group. Merging could be done (without violating the above restriction on the consistent topology) if the continua were allowed to overlap or to fold onto one another. This still maintains the same topology because the topology is defined in the direction of the continuum rather than the apparent geometric position. However such continuum folding is not allowed in almost any conventional analysis, therefore this restriction on the assembly deformation is introduced.

The use of the continuum approach would put more restrictions on the deformation patterns in the final analysis than merely those listed above. Because the problem solution would be performed using a numeric method (such as finite element analysis) it would be impossible to deal with the infinite number of deformation patterns possible in a real system. A subset of patterns must be chosen which will reduce the total number of degrees of freedom to a finite number. This will have an effect on the solution; it is possible that the *correct* solution to the problem cannot actually be represented by any combination of the chosen deformation patterns. In this instance an approximation would have to be chosen.

6.2 Continuum Fibre Model Assumptions

The assumptions under which the initial continuum model was developed are outlined. These assumptions are simplistic, as is appropriate for a model under development. The

extension of the model to more complicated situations will be left until the gross features have been successfully applied to a simple case.

The system shall be formed as a *solid* material, the properties of which mimic arrangements of fibres rigidly fixed to the continuum. The fibre material shall be initially assumed to be linear elastic and the fibre itself to be a uniform circular rod in the undeformed state.

Energy of the fibrous system is assumed to be contributed solely from the elastic energy stored within the fibres from tension, bending and torsion[7].

The movement of the fibres perpendicular to their direction is critical to the development of the correct system action. This is because any jamming of one fibre against another involves this deformation. However, in the simplistic model, any energy gains from this type of deformation will not initially be considered.

6.3 Initial Approach

6.3.1 Introduction

The approach that was initially taken to the creation of a continuum model is outlined below. The method is described using only a two dimensional case. This is for simplicity but extension to three dimensions could be performed. The two dimensional assumption is simple not only because of the reduction in the number of variables, but also because of the exclusion of the possibility of torsion in the fibres.

At a local level the fibres are assumed to be uniformly aligned at a constant angle (this is not a necessary simplification and may be easily relaxed later) and of constant material density, radius and elastic properties. An element may then be taken from the continuum as shown in Figure 6.1, the local fibre orientation is at the angle Θ.

---

[7] Torsion in the fibre will only be present in a three dimensional model, fibres in a plane (as in two dimensional model) can not have any twist.

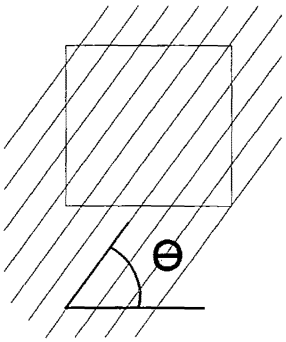

Figure 6.1 *Undeformed fibre continuum.*

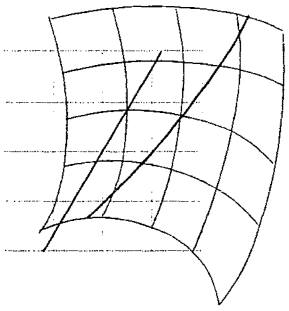

Figure 6.2 *Deformed fibre continuum.*

Figure 6.2 shows how a fibre that in its undeformed state is at an angle of Θ could deform to a state where a variety of orientations may exist along its length.

Each fibre within the continuum described above, will have at every point along its length a curvature (ϕ) and bending stiffness (k_b) where one or both are a function of the arc length (s). Assuming that only the curvature varies with position along the fibre, the total bending energy in the length (L_o) of all the fibres that pass through the piece of continuum being considered may now be calculated as:

$$E_{bf} = \int_{L_o} \frac{1}{2} k_b \phi^2 ds \qquad \textbf{(6-1)}$$

There are similar relationships for all of the other contributions to the element energy.

The relationship between the density of the continuum and the density of the fibre is defined as below. It can be noted that although only two dimensions are being used, a volume of unit thickness is implicit to keep consistent units.

$$\rho_c = \frac{\rho_f \pi D^2 s}{4V} = \frac{\rho_f \pi D^2 L_o}{4V_o} \qquad \textbf{(6-2)}$$

ρ_c = Continuum Density
ρ_f = Fibre Density
D = Fibre Diameter

It may then be written that:

$$ds = \frac{\rho_c}{\rho_f} \frac{2}{\pi D^2} k_b \phi^2 dV$$

$$\therefore E_b = \int_{V_o} \frac{\rho_c}{\rho_f} \frac{2}{\pi D^2} k_b \phi^2 dV \qquad \textbf{(6-3)}$$

6.3.2 Deformation Description

In order to calculate the curvatures of the fibres, the continuum deformation must be described.

If initially deformation in just the x direction is considered. Then the deformation from the undeformed state (x) to the deformed state (x') can be expressed as:

$$x' = x + u \tag{6-4}$$

and the derivatives are calculated:

$$\begin{aligned} dx' &= \frac{\partial x'}{\partial x}dx + \frac{\partial x'}{\partial y}dy + \frac{\partial x'}{\partial z}dz \\ &= \left(1 + \frac{\partial u}{\partial x}\right)dx + \frac{\partial u}{\partial y}dy + \frac{\partial u}{\partial z}dz \end{aligned} \tag{6-5}$$

and similarly for the other directions (y and z). For the two dimensional case the relationship can be written in matrix form:

$$\begin{Bmatrix} dx' \\ dy' \end{Bmatrix} = \begin{bmatrix} \left(1+\frac{\partial u}{\partial x}\right) & \frac{\partial u}{\partial y} \\ \frac{\partial v}{\partial x} & \left(1+\frac{\partial v}{\partial y}\right) \end{bmatrix} \begin{Bmatrix} dx \\ dy \end{Bmatrix} = \begin{bmatrix} A & B \\ D & E \end{bmatrix} \begin{Bmatrix} dx \\ dy \end{Bmatrix} \tag{6-6}$$

Note that the letter C has been omitted from the matrix. This is for two reasons, firstly to avoid confusion when C is used later for the direction cosines of the fibre direction and secondly to be consistent with the three dimensional extension of this matrix.

Assuming that the initial direction of the fibre is known at a point in the continuum then it is necessary to know what that direction is after deformation. Let the unit vector representing the initial fibre direction be û and after deformation û'. Then the unit vectors may be written as the vector sum of the direction cosines:

$$\begin{aligned} \hat{u} &= C_x\hat{i} + C_y\hat{j} \\ \hat{u}' &= C_x'\hat{i} + C_y'\hat{j} \end{aligned} \tag{6-7}$$

Then the transformation of one direction cosine to the deformed state may be clearly calculated in terms of the known parameters (6-8), with a similar equation for C_y' the deformed fibre direction may be calculated.

$$C_x' = \frac{dx'}{ds'} = \frac{dx'}{\sqrt{dx'^2 + dy'^2}} = \frac{A\,dx + B\,dy}{\sqrt{(A\,dx + B\,dy)^2 + (D\,dx + E\,dy)^2}} \tag{6-8}$$

6.3.3 Curvature Calculation

The curvature of a fibre in the continuum is not explicitly known. It is necessary to develop this value in terms of the quantities that will be known to the system. These are both the strain parameters at a point and the initial conditions at that point.

Assume that a point in the undeformed continuum has fibre orientation û and fibre position s, in the deformed configuration these change to û' and s' respectively. As the curvature is merely a measure of the rate of change of û', then:

$$\phi' = \left\| \frac{d\hat{u}'}{ds'} \right\| = \left\| \frac{\partial \hat{u}'}{\partial x'} \frac{dx'}{ds'} + \frac{\partial \hat{u}'}{\partial y'} \frac{dy'}{ds'} \right\| \tag{6-9}$$

and simplifying some terms from this equation leads to:

$$\frac{dx'}{ds'} = C_x' \qquad \frac{dy'}{ds'} = C_y' \tag{6-10}$$

While expanding others:

$$\frac{\partial \hat{u}'}{\partial x'} = \frac{\partial C_x'}{\partial x'} \hat{i} + \frac{\partial C_y'}{\partial x'} \hat{j} = \frac{1}{A} \frac{\partial C_x'}{\partial x} \hat{i} + \frac{1}{A} \frac{\partial C'}{\partial x} \hat{j} \tag{6-11}$$

leading to the relationship for the curvature of the fibre in the deformed continuum:

$$\phi' = \left\| \left(\frac{C_x'}{A} \frac{\partial C_x'}{\partial x} + \frac{C_y'}{E} \frac{\partial C_x'}{\partial y} \right) \hat{i} + \left(\frac{C_x'}{A} \frac{\partial C_y'}{\partial x} + \frac{C_y'}{E} \frac{\partial C_y'}{\partial y} \right) \hat{j} \right\| \tag{6-12}$$

and a simpler relationship for the fibre curvature in the undeformed state:

$$\phi = \left\| \left(C_x \frac{\partial C_x}{\partial x} + C_y \frac{\partial C_x}{\partial y} \right) \hat{i} + \left(C_x \frac{\partial C_y}{\partial x} + C_y \frac{\partial C_y}{\partial y} \right) \hat{j} \right\| \tag{6-13}$$

Note that both relationships contain derivatives with respect to only the undeformed coordinates. This is vital to the successful formulation of the equation system. It is also

important that as required the equation for the curvature in the undeformed state will be zero in the event that the direction cosines are constant everywhere in the element (i.e. the fibres are all straight).

6.3.4 Extension Calculation

In a manner similar to that in the above calculation for the bending curvature, the amount of extension of the fibre at any point in the continuum must be found. The extension is defined as the ratio of the length of a piece of deformed fibre to the length of the same section in the undeformed state less one:

$$\frac{\Delta l}{l} = \frac{ds'}{ds} - 1 \tag{6-14}$$

$$\begin{aligned} \frac{ds'}{ds} - 1 &= \sqrt{\frac{dx'^2 + dy'^2}{dx^2 + dy^2}} - 1 \\ &= \sqrt{\frac{(A\,dx + B\,dy)^2 + (D\,dx + E\,dy)^2}{dx^2 + dy^2}} - 1 \\ &= \sqrt{(A^2+D^2)\,C_x^2 + 2\,(AB+DE)\,C_x C_y + (B^2+E^2)\,C_y^2} - 1 \end{aligned} \tag{6-15}$$

Similar reasoning for the case of axial extension, where k_t is the axial deformation stiffness, leads to:

$$E_t = \int_{V_o} \frac{\rho_c}{\rho_f} \frac{2}{\pi D^2} k_t \left(\frac{ds'}{ds} - 1 \right)^2 dV \tag{6-16}$$

6.3.5 Element Energy

The expression for the total energy of the element can then by found be adding the calculated values of the bending and extension contributions and integrating over the volume (V_o). The volume element represented in this formula is not an element in the sense of finite element analysis. It merely calculates the energy of any volume and of any size of a fibrous assembly.

$$E = \int_{V_o} \frac{\rho_c}{\rho_f} \frac{2}{\pi D^2} \left[\phi^2 k_b + \left(\frac{\partial s'}{\partial s} - 1 \right)^2 k_t \right] dV \tag{6-17}$$

As an example of what this equation means consider Figure 6.3 which shows two assemblies with fibre orientations perpendicular to each other (a) and (c). When both are deformed into the same displaced shape (b) will have a significant portion of both bending energy and extension energy due to the curvatures in the fibre paths and the length changes. In contrast (d) will deform with no energy increase at all, none of the fibres bend giving the total energy integral as zero.

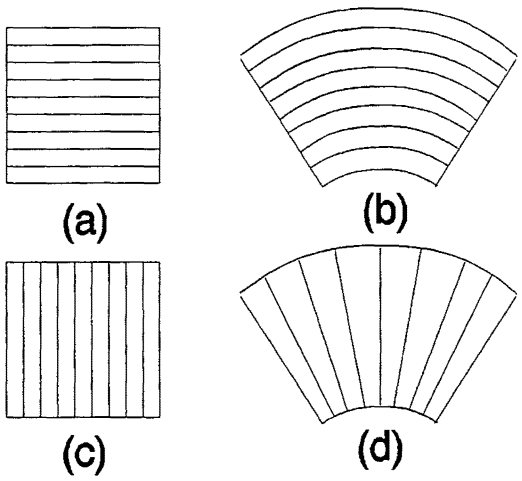

Figure 6.3 *Example deformations of fibrous assembly.*

With a formula capable of finding the total energy over a given volume of fibrous assembly, a start may be made on finding the properties of a finite element.

Initially it must be shown that the total energy of a finite element can be calculated. Assume that the volume in space representing the finite element has been chosen, along with suitable nodes, degrees of freedom, and displacement functions.

The nature of the equations is such that a nonlinear approach is required for system solution. This is seen from either the formula for the extension or the formula for the bending energy. The values represented by the letters A,B,D and E are functions of the displacement parameters. If they are included in the final equations in anything more than a linear fashion then an iterative solution method would have to be used.

For the purposes of showing how the energy calculation would proceed, it will be assumed that the solution process is partially completed and non-zero displacements are present. The integration over the element may not be performed analytically therefore numerical integration is used. The total energy is summed over a series of integration

points, the number of which will have an impact on the accuracy of the numerical approximation.

The easier of the two calculations is that of the extension energy, the values A,B,D and E, may be calculated in terms of the present displacement values. These displacements are interpolated from the nodal degrees of freedom to the calculation points. Integration may then proceed as all other components of the equation are known initial conditions, such as initial fibre directions, which are defined only at the nodal points. These are interpolated to the calculation points using the element displacement functions.

The calculation of the bending energy presents more difficulties. This is due to the inclusion of the spatial derivatives of the deformed direction cosines at the calculation points. The deformed fibre direction cosines are calculated at the nodal points and the interpolated to the calculation points. Spatial derivatives of these values are based on the derivatives of the element shape functions and interpolated to the calculation points. This involves some degree of approximation but it is of no greater significance than that being applied already.

6.3.6 Element Stiffness Matrix

It has been implied that once a formula was found for the total energy of the finite element then the element stiffness matrix may be calculated. It will be explained how one leads to the other, in addition to how the abundance of algebra was performed.

The terms of a finite element stiffness matrix are simply found as the second derivatives of the element total energy with respect to the element degrees of freedom:

$$K_{ij} = \frac{\partial^2 E}{\partial \delta_i \partial \delta_j} \qquad \textbf{(6-18)}$$

It can be seen from this that the stiffness matrix is symmetric, as is required for energy conservation under deformation.

The calculation of the energy as outlined in a previous section involves a large amount of algebra even when only considering the value at one integration point. Consequently a symbolic algebra package MAPLE[8] was used for the manipulation of the formulae. MAPLE allowed the value of the energy at an integration point to be explicitly defined

[8] MAPLE usage and code is outlined in later sections.

in terms of the nodal degrees of freedom and the initial conditions. MAPLE then calculates the matrix of second derivatives of the energy with respect to the input parameters and the element stiffness matrix is calculated symbolically. This gives the contribution from one calculation point, which has to be summed over the element to give the full matrix.

After these formulae were symbolically generated, MAPLE was again used to generate FORTRAN source code to evaluate them numerically. The same system was also used for the calculation of the vector of first derivatives of the energy. This vector represents the system force vector. It is worth noting that even for the very simple system being discussed here, the output from MAPLE was already becoming large. If MAPLE had not been capable of output in a popular programming language, the symbolic results would have been unusable, simply because accurately manipulating formulae of this size would be physically impossible.

The solution process could now proceed, a pseudo-code algorithm for one load increment is given below. It is likely that in any scheme used, many increments would be required. The applied loading or some enforced boundary condition would be increased (or changed) between increments.

- Start increment.
- Iterate.
  - Evaluate A,B,D,E values at element nodes.
  - Calculate values of deformed direction cosines at nodes.
  - For each calculation point, DO:
    - Find interpolated A,B,D,E at calculation point.
    - Find deformed and undeformed direction cosines.
    - Find spatial derivatives of direction cosines.
    - Evaluate energy derivatives from MAPLE FORTRAN.
    - Add in contribution to element stiffness matrix.
    - Add in contribution to element force vector.
  - End DO.
  - Assemble global stiffness.
  - Enforce boundary conditions and loadings.
  - Solve for new displacements.
- End iteration upon satisfying convergence criteria.
- End increment

6.3.7 Results and Projections

This method was never fully implemented. An element was generated to the stage where deformations could be applied and the energy at any point within the element area could be calculated. This was then used to evaluate the total element energies. The element seemed to perform exactly as expected although the size of the MAPLE output code was very large. Some derivative terms were calculated, but it quickly became obvious that using the resulting formulae and code could be described, at best, as unwieldy.

For several reasons to be mentioned in the next section this approach was discontinued before completion. This was mainly due to anticipation that the method would become impossible well before a satisfactory result was obtained with present computing facilities. Despite this, some projections for the future are listed below, these might become viable with either increased computing power or an ingenious simplifying assumption.

It should be possible for multiple fibre paths to pass through one local continuum area, each with a different orientation. As all obey the continuum assumption at every point and are governed by the deformations at the same nodal points then their respective energies could be summed when integrating element properties. Many multiple paths could be used and could be summed to give an orientation distribution with a proportion of the fibres initially pointing in each direction.

If multiple paths are introduced then the way is open for a slippage analysis based on fibre migration. The lateral pressure between fibres in the continuum could be used in combination with some frictional law to generate criteria for the stick or slippage of fibres. This would introduce further nonlinear aspect to the analysis.

6.4 Towards a Modal Approach

It can be seen that this approach quickly becomes very cumbersome and many difficulties with the system have not yet been dealt with. A difficulty yet to be included could be the stiffness and resistance of the lateral jamming of the fibres (a critical piece of the resistance mechanism of the fibrous assembly). The approach that has been used to include the effects of the fibre properties would not be amenable for applying the system properties such as the lateral jamming or the shear resistance.

If it was attempted to continue along this path it would be likely that the system would quickly become impractical. This is more obvious when it is considered that the extension of the system to three dimensions has yet to be made. This extension will also bring in complicating torsion effects.

The next attempt at a solution to this fibrous assembly problem must be less complicated and two ways were anticipated for achieving this. Either the generality of the solution must be reduced or a better approach must be found. It was decided to partially implement both simplifications. The problem being solved was reduced to highly aligned fibrous systems, aligned to such a degree that the fibres could be assumed not to cross. A finite element could be developed where the fibres are all aligned with the element sides. A new approach to the problem was also developed involving the decomposition of the modes of deformation of the element. This approach is discussed more fully in the following chapters but was implemented for reasons of simplicity and ease of dealing with *all* element energy types, including transverse compression and shear stiffness.

7 Modal Analysis

7.1 Conceptual Development

7.1.1 Introduction

The previous chapter described the development of a general fibrous assembly element. The resulting solution was too cumbersome and complicated to use. This chapter will introduce a different approach to solving a less general problem, which met with more success. The concepts and thoughts that lead to the modal approach will be outlined, giving a better understanding of this method.

It has been explained that the generality of the problem was reduced by restricting the fibre direction within the finite element. Fibres are restricted to being aligned with a pair of the element sides. The element is then deformed and the fibres remain aligned, but this does not mean that they will remain straight. If the sides of an element bend then the fibres will also bend. The amount of deformation of the fibres within the element is varied across the element as the fibres on either side are allowed to be aligned with their respective sides.

After the difficulties of the previous approach, it was decided that a new and more careful start must be made on the problem. A consideration of the energy change in the fibrous system with deformation was the starting point for the new analysis.

It was ensured that there was provision made within the system for *any* type of energy generating mechanism. The previous analysis looked to deal competently with the energies from the bending and extension deformations. However, significant complications were likely to result when more complicated mechanisms were included. One example of these mechanisms could be the *jamming* energies that build up from the interaction of two (or any number of) fibres under lateral compression. Deformations such as shear between fibres could also be included here.

A two dimensional, four-sided assembly section is presented for discussion. The fibres within being oriented horizontally, and aligned parametrically with two opposite element sides. A sketch of this piece is shown in Figure 7-1. Deformed shapes are also shown to give some idea what is meant by the fibres remaining aligned.

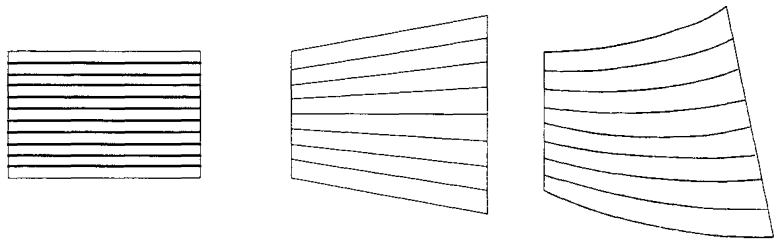

Figure 7-1 *A section of assembly and some deformed patterns.*

For a simple discussion the assumption is made that the only types of energy to be generated in this system are from bending and extension of the constituent fibres. There are an infinite number of shapes into which the four-sided section can deform. Most of these shapes will involve a combination of extension or bending of the fibres. An important point is that not *all* the modes will involve an energy gain. A second point is that there will be a subset of deformations that involve only one type of energy gain, either bending or extension. One possibility for each of these is shown in Figure 7-2.

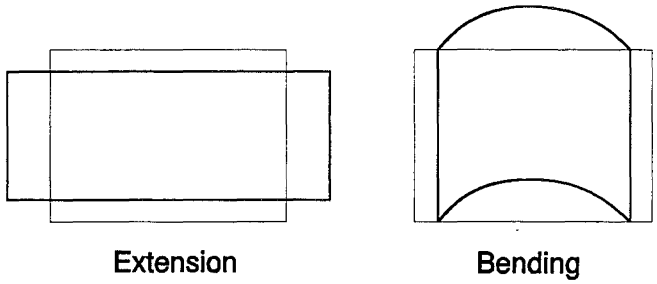

Figure 7-2 *Deformations which involve only one energy type.*

The deformations shown here are not unique. As well as being able to apply a scaling factor to these, there is a veritable smorgasbord of other options that will give *pure* deformations. This would be an extremely difficult problem to deal with when considering the complete continuum representation of the assembly section under discussion. Difficulties come from the infinite number of degrees of freedom of movement that the section has. If the section is assumed to be represented by a finite element then the situation becomes much more manageable. A finite element has a finite (and often small) number of degrees of freedom. It is possible to calculate which

combination of degrees of freedom will give deformation involving only one energy type.

7.1.2 Eigenvalue Analysis and Basis Sets

The next stage of development involved extension of an eigenvalue analysis, an idea taken from conventional finite element analysis. This analysis and how it applies to finite elements will be briefly explained, both for the necessary background and the insight provided on the development of modal analysis.

A vector space representing n degrees of freedom has a coordinate system defined by n linearly independent vectors. For example, the vector space of the two dimensional plane has two degrees of freedom. This means that exactly two values are sufficient to define a position on the plane. What the two numbers would be depends on the basis vectors chosen for the coordinate system. Conventional Cartesian coordinates are the most obvious and natural basis set.

$$\begin{Bmatrix} x \\ y \end{Bmatrix} = \left(\begin{Bmatrix} 1 \\ 0 \end{Bmatrix}, \begin{Bmatrix} 0 \\ 1 \end{Bmatrix} \right) \tag{7-1}$$

Any number of other sets might also be chosen, for example polar coordinates are simply the use of a different set of basis vectors. Different values would then be given for the same position in the plane, but the basis vector sets can be used to transform between sets of point values.

Consider now a finite element with n degrees of freedom. It could be said that the natural set of basis vectors for such an element are those that are similar to the natural Cartesian coordinates described above.

$$\left\{ \begin{matrix} 1 \\ 0 \\ 0 \\ \vdots \\ 0 \end{matrix} \right\}, \left\{ \begin{matrix} 0 \\ 1 \\ 0 \\ \vdots \\ 0 \end{matrix} \right\}, \cdots, \left\{ \begin{matrix} 0 \\ 0 \\ 0 \\ \vdots \\ 1 \end{matrix} \right\} \tag{7-2}$$

For various reasons this simple basis set is used to generate the stiffness matrix of the element. However, if required the stiffness matrix can be generated with any set of valid basis vectors.

Often a completed element stiffness matrix will be analyzed to find the eigenvalues and associated eigenvectors. These can be used to reveal some fundamental problems with

an element. The eigenvectors represent the stiffnesses of the deformation mode shape described by the relevant eigenvector. This process could be viewed as transforming the element into a new coordinate system. A system where the basis vectors have been specifically chosen such that the element stiffness matrix in this coordinate system would be diagonal.

This is used in finite element analysis to detect any fundamental problems with an element. The eigenvectors immediately reveal the number of modes of the element that generate zero energy. This is the number of zero eigenvalues, as these are deformation modes with zero stiffness. An element must have a specific number of such modes, more or less will violate some requirements of finite element formulations.

7.1.3 Modal Basis Sets

It is the idea of applying the eigenvalue analysis in reverse that has grown up into the modal analysis method now used. The idea is to start with the diagonal stiffness matrix and a set of basis vectors, and transform back to get the matrix in more conventional coordinates.

It was the idea that each basis vector could represent one mode incorporating one type of energy. Then the associated single stiffness value will be the stiffness of that one mode. This value should be easily calculable because of the restricted energy types contributing to it.

It is clear that when including the more complicated effects (such as shear and lateral fibre jamming) this modal approach would have some significant advantages. These effects could be separated into their own deformation modes as easily as could the bending and extension effects. Stiffnesses could then be assigned to the modes as required before the matrices are transformed.

Ensuring that the element has the required number of zero stiffness rigid body modes is also a simple matter. The modes could be assigned a basis vector, and purposefully be given a stiffness of zero. It is easy to ensure that the element has no more zero energy modes, by checking that all other stiffnesses have a non zero value.

7.2 Modelling and Theory Development

This section describes the process that culminated in a more formal statement of the modal analysis method. The models developed during this process are discussed only qualitatively, emphasis being placed on the method rather than the particular element. Although the model development was simultaneous, the description will be left until the next chapter.

7.2.1 Transformation Matrix

Initially it was thought that the key to modal analysis would be the coordinate transformation matrix. A matrix defining the transformation from the coordinate system based on the conventional (nodal) degrees of freedom, to that based on the modal degrees of freedom. This expectation came from analogy with the element eigenvalue analysis. The transformation of the stiffness matrix and supporting vectors was expected to proceed as outlined below.

Define the transformation matrix [A]:

$$[A]\{\beta\} = \{\delta\}\ , \quad \therefore \{\beta\} = [A^{-1}]\{\delta\} \tag{7-3}$$

Then the transformation may be made, starting from the modal equation and finishing with the nodal equation:

$$\begin{aligned} [K']\{\beta\} &= \{q\} \\ [K'][A^{-1}]\{\delta\} &= \{q\} \\ [A^{-1}]^T[K'][A^{-1}]\{\delta\} &= [A^{-1}]^T\{q\} \\ [K]\{\delta\} &= \{Q\} \end{aligned} \tag{7-4}$$

The stiffness matrix and force vector transformations are then defined as:

$$\begin{aligned} [K] &= [A^{-1}]^T[K'][A^{-1}] \\ \{Q\} &= [A^{-1}]^T\{q\} \end{aligned} \tag{7-5}$$

Note that the symmetry of the stiffness matrix is preserved throughout this transformation.

The next task would be the generation of the terms of the transformation matrix. The first element to which this was applied was a six noded rectangular element. It was found that the shapes of the modes could be written almost intuitively. Because each column of the transformation matrix represents the factored displacements from one mode shape, it was thought that each column could be written from the knowledge of what the mode was physically like.

The transformation matrix [A] was formed as described above. It was found that it was impossible to write the terms of the equations explicitly. This was because the way in which one mode deformed could depend on the magnitude of that mode, or any number of other modes. For example consider a beam element capable of bending. The amount of displacement at each node that further bending would induce is very dependent on the level of bending present in the beam. Similarly, but more complicated is the extension mode of this beam. The direction for further extension without extra bending depends not on the present level of extension, but on the amount of bending. This causes the transformation matrix [A] to have a nonlinear nature. The [A] matrix is required to find the amount of each mode, but the modal amounts are in turn required for the calculation of the [A] matrix. This is a situation requiring an iterative or incremental solution process.

A series of unknown factors was introduced into the [A] matrix, these allowed modelling of the nonlinear behaviour described above. Initially the matrix was formed including these factors. The matrix was then inverted symbolically, giving a way of finding the modal amounts, given the coordinates. Once these are found, the new unknown factors can be calculated as these can all be defined as a function of the modal amounts. The inverse of [A] can then be reassessed, and the iterations proceed until satisfied. This iterative process would result in the [A] matrix, given any reasonable set of nodal coordinates.

Care was required in the formulation of the equations. It is essential that each modal deformation increase only the amount of that mode and none other. This requirement introduced more factors into the equations, but the system matrix was still able to be inverted (non-singular).

The generation of an element stiffness matrix as described above was coded in FORTRAN. This was then included within a complete analysis. The results were unsatisfactory, apart from the process being computationally intensive (due to the iterative solutions required to find the [A] matrix), the answers were incorrect. This is despite the fact that only the very simple model of a single element was being used.

7.2.2 Tangent Properties

A reason was found for the undesirable results from the previous model. The [A] matrix that was used was more appropriate for a linear system, than for a nonlinear

system. This is similar to the situation that results in a tangent stiffness matrix being used for systems, and a description of this is used to ease explanation.

A conventional stiffness matrix is used within the system:

$$[K]\{\delta\} = \{Q\} \tag{7-6}$$

Where $\{\delta\}$ are the displacements and $\{Q\}$ are the applied forces. In an iterative system this is insufficient, the variables must be the increments of the displacements and forces and the tangent stiffness must be used.

$$[K_T]\{\partial\delta\} = \{\partial Q\} \tag{7-7}$$

In a linear system these two equations are identical and no problem arises.

For the case of the transformation matrix the comparison between the linear and the nonlinear systems may be made. The definition of the matrix may be reformulated for the nonlinear iterative system in which it is expected to operate.

$$\{\partial\delta\} = [A]\{\partial\beta\} \tag{7-8}$$

Which may then be rewritten to define the matrix as:

$$[A] = \left[\frac{\partial\delta}{\partial\beta}\right] \tag{7-9}$$

Support for this equation also comes from the definition of the force vector. The force vectors in both nodal and modal coordinates may be written in terms of energy derivatives as:

$$\{Q\} = \left\{\frac{\partial E}{\partial\delta}\right\} \qquad \{q\} = \left\{\frac{\partial E}{\partial\beta}\right\} \tag{7-10}$$

And the transformation of the force vectors by the [A] matrix is:

$$\{Q\} = [A^{-1}]^T\{q\} \quad or \quad \{Q\}^T = \{q\}^T[A^{-1}] \tag{7-11}$$

This transformation can also clearly be written in terms of the energy terms:

$$\left\{\frac{\partial E}{\partial \delta}\right\} = \left\{\frac{\partial E}{\partial \beta}\right\}\left[\frac{\partial \beta}{\partial \delta}\right] \qquad \textbf{(7-12)}$$

A comparison between the latter part of equation (7-11) and equation (7-12) gives a definition of [A] in agreement with above.

$$[A^{-1}] = \left[\frac{\partial \beta}{\partial \delta}\right] \quad or \quad [A] = \left[\frac{\partial \delta}{\partial \beta}\right] \qquad \textbf{(7-13)}$$

This new representation was then coded into the analysis. Each column of the matrix was found by using the procedure for calculating the coordinates that would be represented by the present modal values. A particular modal value would be adjusted up and down from its present value, and the coordinates calculated. A finite difference approximation would then be used to evaluate the various derivatives contributing to the terms of that column of the matrix.

The procedure above gave the matrix [A]; the inverse of this matrix was required in the stiffness matrix transformation equation. Rather than perform the costly numerical inversion of [A], the transformation equation was carried out as a series of equation system solutions. This saved both computational time and improved the numerical accuracy of the answer.

This system was seen to give significantly better results than those attained previously. The analysis was still very complicated and computationally expensive due to the numerical derivative calculations and the iterative solution required. A closer look at the new definition of the transformation matrix solved both problems. The inverse of the [A] matrix is the derivative of the modal amount with respect to the nodal displacements. Therefore if the modal amounts could be written as a function of the nodal variables, then the inverse of [A] could be calculated directly saving a vast amount of computational effort.

It can be seen that writing the equations describing the modal amounts in terms of the nodal variables is simpler than any previous description of this relationship. The directions of deformation are not being explicitly defined but are automatically calculated in the derivatives. This means that the previous complicated procedure

needed to ensure that the deformations of each mode contain none of any other modes is now unnecessary.

The equations require more information that just the nodal displacements. For example, the initial coordinates of all the nodes have to be supplied. All these inputs are constants within the equations and are incidental.

7.2.3 Formal Transformation Definition

With the vast computational simplifications introduced after the new definition of [A], the analysis testing progressed beyond the single element stage. Although the single element was found to perform well under deformation, this good performance was not carried over into more complicated multiple element models.

The models all performed as expected at small deformations, however, as deformations increased the element would become increasingly unstable. This instability would increase until some critical point was achieved and the iterative solution would abruptly diverge in an oscillatory manner. A few methods were attempted to stabilize the solution process.

The first method was to apply damping procedures and sophisticated line search algorithms onto the nonlinear equation solution. These met with limited success, solutions were found at greater deformations than previously possible, but only slightly so. The computational cost of this operation was great, with the solution step size for stability sometimes decreasing to such a small size that a result would never be achieved within a reasonable period.

An attempt was made to treat the system as dynamic. Introducing inertial and damping forces into the equations. The controlling parameters could be adjusted to give better results than were possible in the static system. However, the results were not significantly better and similar comments could be made as those about the numerical damping procedures.

Stiffness adjustments were made to some modes in order to increase stability. This was introduced as it was noticed that as the extension increased, the bending modes would oscillate uncontrollably. Adjustments were made such as increasing the stiffness of the bending modes depending on the extension. This was by far the most successful of the

attempts to improve stability. The solution still depended on some arbitrary parameters and was far from being stable in all situations.

During this process the test element had moved from a six noded rectangle through various stages to a two noded beam. This very simple model exhibited the same problems at large deformation. Using this simple model it was possible for a direct comparison to be made between the modal theory and conventional finite element theory. The same approximations were used in both cases. This meant that if the modal model was correctly formulated, the stiffness matrices generated from both systems should be identical. A better description of this check is given in section 7.4. The result was that the matrices were identical at zero deformation, in all other situations the differences in the matrices increased with increasing deformation.

The equations transforming the stiffness matrix were investigated more closely. It was attempted to show what the transformation should be in terms of the energy derivatives as had been done for the force vectors.

The tangent stiffness matrix in terms of the nodal displacements can be written as;

$$[K_T] = \left[\frac{\partial^2 E}{\partial \delta^2}\right] \tag{7-14}$$

or in simpler tensor notation:

$$K_{Tij} = \frac{\partial^2 E}{\partial \delta_i \partial \delta_j} \tag{7-15}$$

and the coordinate conversion may now be written as:

$$\begin{aligned}
\frac{\partial^2 E}{\partial \delta_i \partial \delta_j} &= \frac{\partial}{\partial \delta_i}\left(\frac{\partial E}{\partial \delta_j}\right) \\
&= \frac{\partial}{\partial \delta_i}\left(\frac{\partial E}{\partial \beta_k}\frac{\partial \beta_k}{\partial \delta_j}\right) \\
&= \frac{\partial^2 E}{\partial \delta_i \partial \beta_k}\frac{\partial \beta_k}{\partial \delta_j} + \frac{\partial E}{\partial \beta_k}\frac{\partial^2 \beta_k}{\partial \delta_i \partial \delta_j} \\
&= \frac{\partial^2 E}{\partial \beta_l \partial \beta_k}\frac{\partial \beta_l}{\partial \delta_i}\frac{\partial \beta_k}{\partial \delta_j} + \frac{\partial E}{\partial \beta_k}\frac{\partial^2 \beta_k}{\partial \delta_i \partial \delta_j}
\end{aligned} \tag{7-16}$$

If the matrix definition is made:

$$\left[AJ_k^{-1}\right] = \left[\frac{\partial^2 \beta_k}{\partial \delta^2}\right] \tag{7-17}$$

Then equation (7-16) may also be written in matrix form:

$$[K_T] = [A^{-1}]^T [K_T'][A^{-1}] + \sum_{k=1}^{n} \left(q_k [A J_k^{-1}] \right) \qquad \textbf{(7-18)}$$

This more formal definition of the transformation clearly shows the inadequacies of the previous formulation. The transformation is identical except for one extra term. It is important to note that the extra term in the equation has the modal force vector as a multiplier. The extra term is a modifier on the stiffness to account for the forces present within the system. This is a very similar adjustment to the bending mode stiffness adjustment that was tried above to solve the stability problem. This term applies the correction much more thoroughly than could have ever been achieved manually.

It is interesting that the symmetry of the stiffness matrix is maintained, as the extra term is itself symmetric.

The modified transformation was then compared against the conventional beam, and was found to compare satisfactorily. This is shown more fully in section 7.4.

The beam element based on this new transformation was found to behave well under deformation.

7.3 Modal Example

This section will clarify the workings of the proposed modal approach. A simple two degree of freedom system will be modelled and the various matrices calculated. The simplicity of this system makes the approach seem cumbersome, but a more complicated system would make it difficult to understand or show what is happening.

The system is a straight rod attached to a point in two dimensional space by a hinge. The two degrees of freedom of the system are the x and y direction displacements of the free end. The hinge and the lack of a rotational degree of freedom imply that the rod will always remain straight. The constraint to two dimensions eliminates the possibility of any torsion in the rod. Extension of the rod remains as the only means of energy storage.

As the system has two degrees of freedom, two deformation modes are required. The first shall represent the rotation of the rod. The remaining mode should be the extension of the rod and this is therefore the only energy contributing mode.

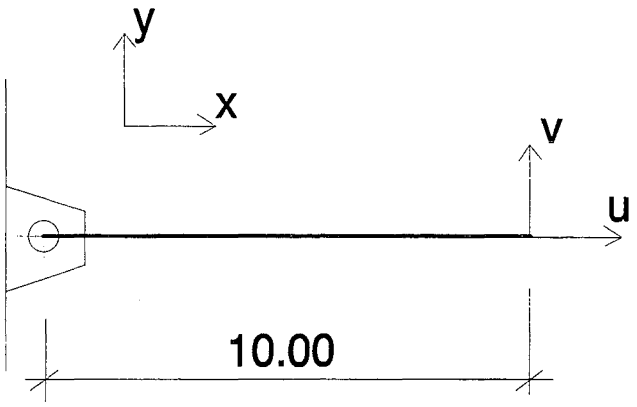

Figure 7-3 *Simple two degree of freedom model.*

Note that a normal two dimensional element should have three modes that generate zero energy. Two of these modes (the rigid translation modes) are restricted from movement by one end of the rod being fixed. The third rigid body mode (the rigid rotation) is the one in evidence.

The hinge end of the rod is assumed to be rigidly fixed at coordinates (0,0). Modal amounts may now be written in terms of the initial position, and the displacements.

$$\begin{aligned} \beta_1 &= \tan^{-1}\left(\frac{y+v}{x+u}\right) = \tan^{-1}\left(\frac{y'}{x'}\right) \\ \beta_2 &= \frac{\sqrt{x'^2+y'^2}}{\sqrt{x^2+y^2}} \end{aligned} \tag{7-19}$$

The derivative matrices may now be calculated:

$$\left[A^{-1}\right] = \begin{bmatrix} \dfrac{-y'}{x'^2+y'^2} & \dfrac{x'}{x'^2+y'^2} \\ \dfrac{x'}{\sqrt{x'^2+y'^2}\sqrt{x^2+y^2}} & \dfrac{y'}{\sqrt{x'^2+y'^2}\sqrt{x^2+y^2}} \end{bmatrix} \tag{7-20}$$

$$\left[AJ_1^{-1}\right] = \frac{1}{(x'^2+y'^2)^2}\begin{bmatrix} 2x'y' & -x'^2+y'^2 \\ -x'^2+y'^2 & -2x'y' \end{bmatrix} \tag{7-21}$$

$$\left[AJ_2^{-1}\right] = \frac{1}{\left(x'^2+y'^2\right)^{\frac{3}{2}}\left(x^2+y^2\right)^{\frac{1}{2}}}\begin{bmatrix} y'^2 & x'y' \\ x'y' & x'^2 \end{bmatrix} \qquad \textbf{(7-22)}$$

These equations are still quite comprehensible, however this is one of the simplest systems possible.

The numerical values of these matrices were calculated for two states (starting with zero deformation) and the results are displayed below. The transformation matrix is calculated as the inverse of the derivative matrix.

$$\text{For}\begin{Bmatrix} x=10.0 \\ y=0.0 \\ u=0.0 \\ v=0.0 \end{Bmatrix} \quad \left[A^{-1}\right] = \begin{bmatrix} 0.0 & 0.1 \\ 0.1 & 0.0 \end{bmatrix} \quad [A] = \begin{bmatrix} 0.0 & 10.0 \\ 10.0 & 0.0 \end{bmatrix} \quad \textbf{(7-23)}$$

$$\left[AJ_1^{-1}\right] = \begin{bmatrix} 0.0 & -0.01 \\ -0.01 & 0.0 \end{bmatrix} \quad \left[AJ_2^{-1}\right] = \begin{bmatrix} 0.0 & 0.0 \\ 0.0 & 0.01 \end{bmatrix}$$

Of interest here is the transformation matrix [A]. The columns of this matrix represent the mode shapes of each of the two modes.

$$\text{For}\begin{Bmatrix} x=10.0 \\ y=0.0 \\ u=0.0 \\ v=10.0 \end{Bmatrix} \quad \left[A^{-1}\right] = \begin{bmatrix} -0.05 & 0.05 \\ 0.07071 & 0.07071 \end{bmatrix} \quad [A] = \begin{bmatrix} -10.0 & 7.071 \\ 10.0 & 7.071 \end{bmatrix}$$

$$\left[AJ_1^{-1}\right] = \begin{bmatrix} 0.005 & 0.0 \\ 0.0 & -0.005 \end{bmatrix} \quad \left[AJ_2^{-1}\right] = \begin{bmatrix} 0.0035 & -0.0035 \\ -0.0035 & 0.0035 \end{bmatrix} \qquad \textbf{(7-24)}$$

Consider the undeformed case. The first column of this matrix represents a horizontal movement of zero and a vertical movement of 10. This is the direction that would give a pure rotation from this state (which is the first mode). The second column is a deformation in only the horizontal direction, a pure extension.

It is important to note that the magnitudes of these modes are not without meaning. In the extension mode, the magnitude of the mode shape vector is exactly a displacement that would give a unit increase to the amount of the mode.

The second deformation case above has the rod at an angle of 45 degrees from the horizontal. The mode shapes must change accordingly. It can be seen that the rotation mode direction is still perpendicular to the rod direction and the extension mode is parallel to the rod direction as required.

The modal stiffness matrix and force vector must be calculated. It will be assumed that the rod is linearly elastic with a stiffness of k.

$$[K'] = \begin{bmatrix} 0 & 0 \\ 0 & k \end{bmatrix} \quad \{q\} = \begin{Bmatrix} 0 \\ k\frac{\Delta}{L} \end{Bmatrix} \tag{7-25}$$

For the second example case above, the force vector is evaluated as:

$$\{q\} = \begin{Bmatrix} 0 \\ k(\sqrt{2}-1) \end{Bmatrix} = \begin{Bmatrix} 0 \\ 0.4142\,k \end{Bmatrix} \tag{7-26}$$

Then the nodal stiffness matrix may be calculated using equation (7-18) and the transformation matrices given above.

$$\begin{aligned} [K] &= \begin{bmatrix} -0.05 & 0.07071 \\ 0.05 & 0.07071 \end{bmatrix} \begin{bmatrix} 0 & 0 \\ 0 & k \end{bmatrix} \begin{bmatrix} -0.05 & 0.05 \\ 0.07071 & 0.07071 \end{bmatrix} \\ &\quad + 0.4142\,k \begin{bmatrix} 0.0035 & -0.0035 \\ -0.0035 & 0.0035 \end{bmatrix} \\ &= k \begin{bmatrix} 0.00646 & 0.00354 \\ 0.00354 & 0.00646 \end{bmatrix} \end{aligned} \tag{7-27}$$

The force vector is similarly transformed.

$$\{Q\} = \begin{bmatrix} -0.05 & 0.07071 \\ 0.05 & 0.07071 \end{bmatrix} \begin{Bmatrix} 0 \\ 0.4142k \end{Bmatrix} = \begin{Bmatrix} 0.02929k \\ 0.02929k \end{Bmatrix} \tag{7-28}$$

All that remains is the assembly of all elements, the addition of any applied loadings or boundary conditions and solution of the system of equations. All of these steps are standard finite element procedures.

7.4 Verification With Traditional Methods

This section presents a verification of the modal analysis method with conventional finite element analysis. This comparison was the first proof that the method as originally proposed was incorrect and was also used to show when the correct formulation was found.

For comparison, a two noded beam finite element was used. Each node had three degrees of freedom, two translation and one rotation. Therefore the element had six degrees of freedom, and could represent a cubic displacement pattern along the length (Figure 7-4).

Figure 7-4 *Degrees of freedom of the beam test element.*

The test element had stiffness in only the extension mode. This simplification made calculation of the matrix simple in both modal and conventional methods.

The calculation of the element stiffness by the modal approach went exactly as for the simple example of the previous section. Here there were six mode shapes (as there were six degrees of freedom). The mode shapes used for the element were, two rigid body translations, a rigid body rotation, an extension mode and two bending modes. A representation of the displaced shapes of these modes from their initial positions is shown in Figure 7-5.

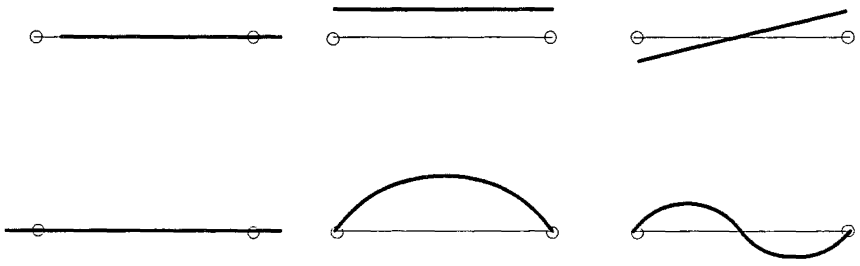

Figure 7-5 *Modes of the beam test element.*

The nodal approach to calculating the stiffness matrix was simple in this case, mainly due to the small number of degrees of freedom and the restriction to extension stiffness only. An equation was generated for the arc length of the beam, in terms of the initial

coordinates and the displacements. This equation was then differentiated twice with respect to the displacements, giving the relevant stiffness matrix directly.

The test element was then forced to take a variety of deformed shapes, the element stiffness matrix was calculated for each deformed shape. Comparisons between the matrix values calculated from the two methods were identical for all eight displayed decimal places over all 36 terms in the matrix, and for all deformations attempted. One deformed shape that was used is shown in Figure 7-6.

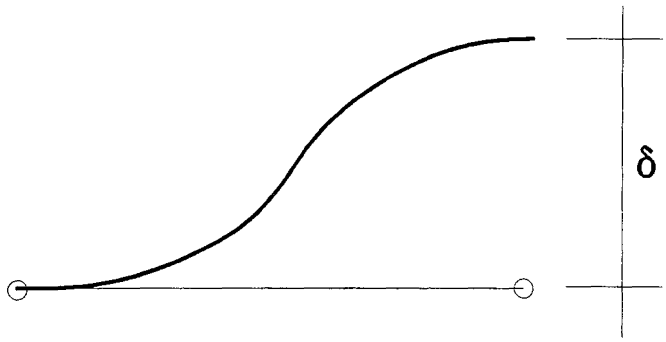

Figure 7-6 *Deformation in d.o.f. 4 of the test beam.*

The contributions to the element stiffness matrix from the modal method can be thought of in two parts. A *linear* part comes from the first term of equation (7-18), and a *geometric* contribution that comes from the latter term of the same equation. The total stiffness is formed as the sum of the two parts. For the deformed shape shown above, the stiffness matrices were recorded as the element was displaced. Plots of selected stiffness terms against deformation are shown below. The separate components of the stiffness are also shown on the plots.

The matrix terms chosen for viewing were all diagonal terms from the matrix. These terms will give a good idea of how an element will perform. The three terms chosen are all the degrees of freedom from one end of the element. Stiffness terms from the other end of the element were identical.

In all cases the geometric part of the stiffness gives a significant contribution to the total. This explains why the initial models performed so badly without this term included, it is no minor correction. The importance of this term is clearly shown in

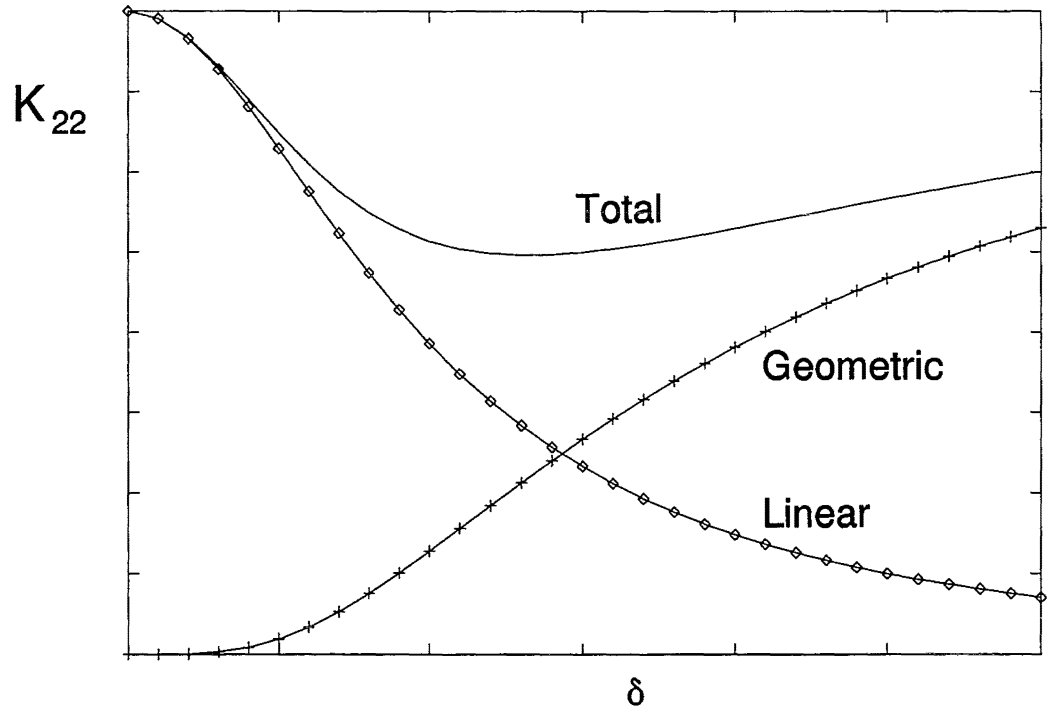

Figure 7-7 *Contributions to stiffness component (2,2) with deformation.*

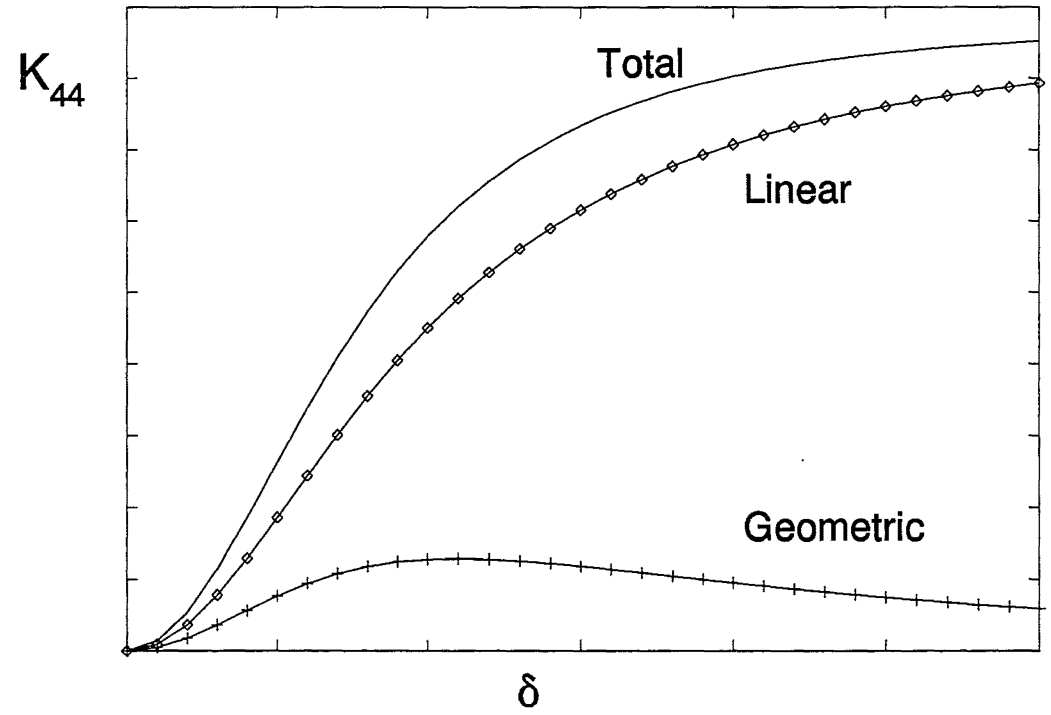

Figure 7-8 *Contributions to stiffness component (4,4) with deformation.*

Figure 7-9, the geometric contribution forms the majority of the stiffness and changes the sign of the result at large deformations.

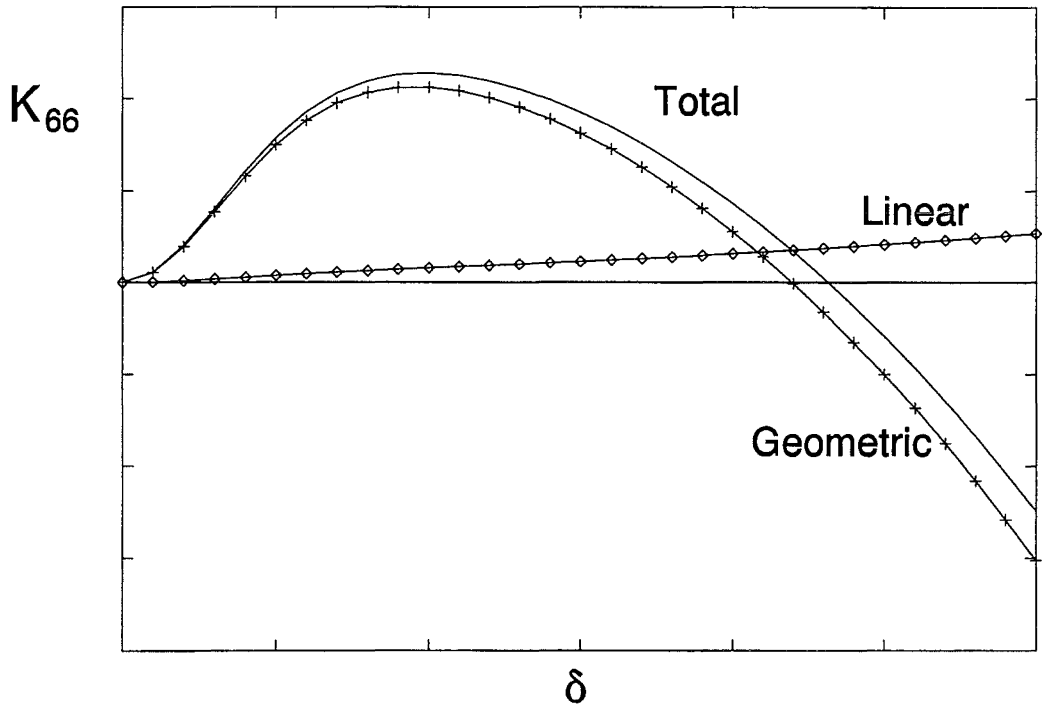

Figure 7-9 *Contributions to stiffness component (6,6) with deformation.*

7.5 Structural Dynamics

Modal methods in conventional finite elements are not restricted to the element diagnosis mentioned earlier. A modal method is also used in structural dynamics that uses the change of basis system outlined above for modal elements.

The structural dynamic modes are taken as the eigenvectors of the system matrix. The modes are then used to transform the system matrices (such as the stiffness and mass matrices) to a new coordinate system. This is to facilitate easy calculation of the deformation of the system with time dependent (or periodic) loadings or displacements.

For various reasons this method is only used for linear systems that explains why the geometric part of the stiffness is not included. For linear systems where the modes are also linear combinations of the displacements, this part is always equal to zero. This can be seen as one multiplier in the geometric part is the term:

$$\frac{\partial^2 \beta_k}{\partial \delta_i \partial \delta_j} \tag{7-29}$$

Which is the second derivative of the mode shapes with respect to the displacements. If the mode shape is a linear function of the displacements (as happens for eigenvectors of a linear system), then this term is always zero.

8 Two Dimensional Model

A two dimensional fibrous finite element model is developed. Modal techniques (as explained in previous chapters) are used to generate the element properties. The resulting model is then successfully tested against experimental results.

8.1 Degrees of Freedom

A finite element is defined by the degrees of freedom of movement that it has. The range of possible deformations of the element is controlled by the number and variation of the degrees of freedom present. The first stage in designing a new element is the selection of the degrees of freedom.

Conventional finite elements require the definition of one set of degrees of freedom, modal elements require two sets. A description of the element modes provides the extra set. Element modes represent a different coordinate set for the description of the deformation and relationships must be provided to give a unique transformation between the two systems.

8.1.1 Nodal Degrees of Freedom

Many finite elements could be used for any material. The elements could vary in the number of nodes, number of degrees of freedom, and general complexity. For practical reasons the simplest element that will model the fibrous continuum will be selected.

The selection of the nodal degrees of freedom of an element is subject to few rules, the two most significant would be compatibility and suitability. Compatibility is a general restriction on all finite elements and it can be reduced to the requirement that the deformation of any edge of an element depends only on values at the nodes along that edge. Satisfaction of this rule ensures that if any other element is joined to the first, the two will deform together. Suitability requires that the element deform appropriately for the material, that is, it must be possible to form deformation patterns to generate all the energy mechanisms that the continuum material can.

The first two conditions on the element are that it is initially rectangular and that it is in two dimensions. The two dimensional nature of the element restricts the number of types of degrees of freedom that are available for each node, movement is only allowed within the plane of the element. Rectangular elements must have at least four nodes, more than this is possible which would allow elements with curved sides. A minimum configuration for the element is therefore a four noded rectangle with two degrees of freedom per node. Two degrees of freedom are required per node to allow the rectangle to assume any four-sided shape within the two dimensional space, see Figure 8-1 for some example deformations.

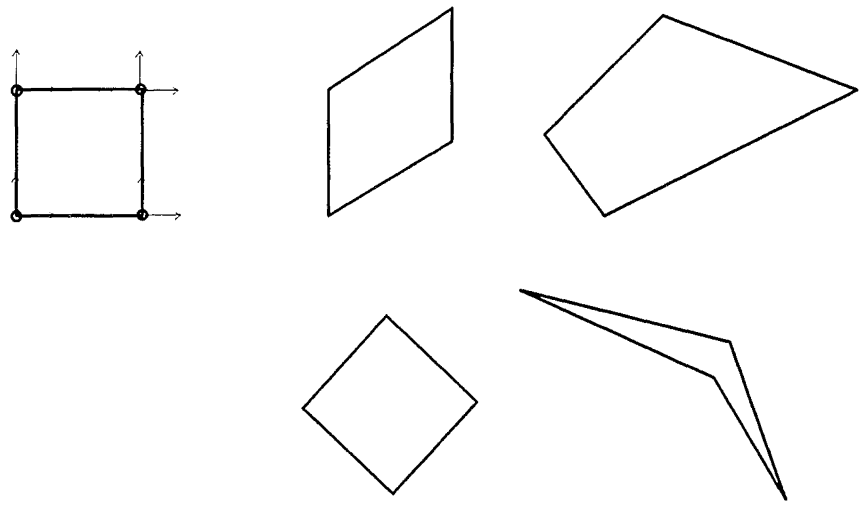

Figure 8-1 *Four noded rectangular element, and possible deformed shapes.*

A rectangular element will not produce any bending in the fibre. Any fibre that was straight in the initial state will remain straight after the continuum deforms into any of the shapes described above. This is because the four noded element enforces linear deformation and a higher order deformation is required to produce bending.

An additional degree of freedom would be sufficient to introduce bending to the element, although two would be the minimum to avoid violating the compatibility requirement. Figure 8-2 demonstrates this, the element with one extra degree of freedom cannot independently bend the top and bottom edges of the element. The constraint introduced means that the actions along either of the edges will affect the other edge, violating the compatibility requirement. An element with just one extra degree of freedom but only one bending edge would not violate compatibility, but this would not be a useful element either.

The ten degree of freedom element was chosen for the next stage of development. The code was written to calculate the energy generated from a single element under

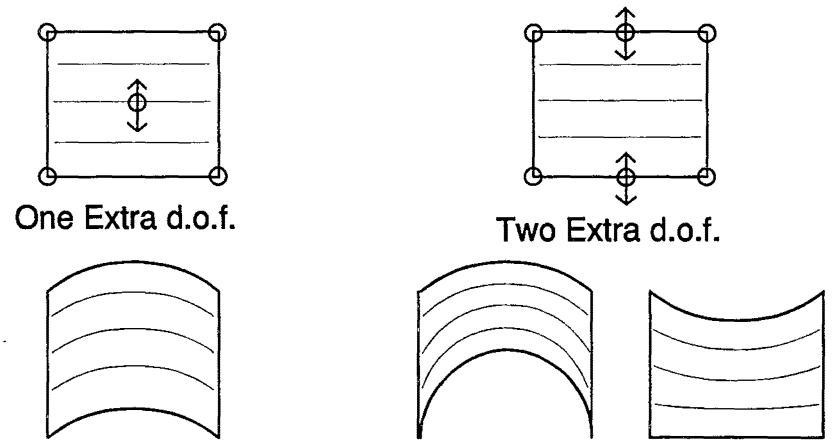

Figure 8-2 *Extra degrees of freedom to allow fibre bending.*

deformation. Results from this element were promising, the energy distributions across the element behaved as expected.

Assemblies of multiple elements were then tested, the element failed in this situation. It was found that the two bending degrees of freedom were insufficient to give the minimum necessary variation in bending to represent the bending mechanism of the continuum. The reason is best described in terms of fibre continuity. The nodes on the ends of the element described above have only translation degrees of freedom, the elements connected to the ends will agree in only translation. Fibre direction can change instantaneously across the interface between two elements, implying an infinite fibre curvature at the interface. A means for the fibre direction to be maintained across the interface had to be provided, so a rotation degree of freedom was introduced at each of the four corner nodes. The rotation degrees of freedom represent the fibre direction at the corner node, the mid side nodes are no longer required. Rotations of the fibre are specified at each end of the fibre piece, allowing the description of a cubic deformation path for the fibre. The element deformed shapes created by movement in each of the three degrees of freedom at one node are shown in Figure 8-3. The numbering used for the degrees of freedom of the element is shown in Figure 8-4.

Therefore the element that was selected for two dimensional finite element modelling had twelve degrees of freedom, with three degrees of freedom at each of the four nodes.

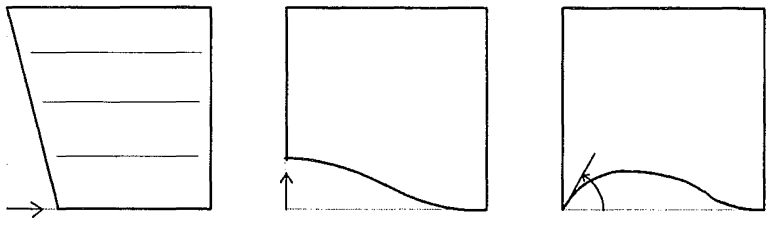

Figure 8-3 *Element shape after deformation of degrees of freedom at one node.*

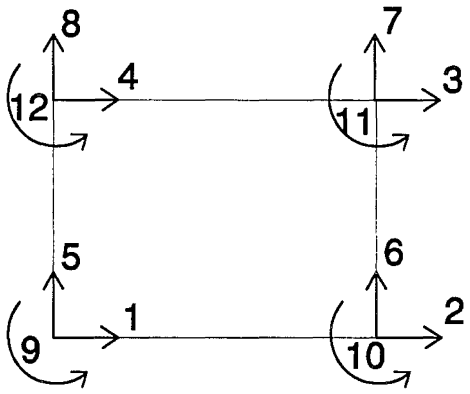

Figure 8-4 *Numbering of degrees of freedom of two dimensional element.*

8.1.2 Modal Degrees of Freedom

It has been explained previously that in addition to the conventional nodal degrees of freedom an equal number of modal degrees of freedom must also be selected. There are as many possibilities for modal degrees of freedom as there are for nodal, the rationale for the modes that were selected are explained below.

The modal analysis method was conceived with the idea that the deformation of each mode would represent one type of deformation energy. In the two dimensional fibrous finite element with the assumptions as have been stated, there are only two mechanisms of generating energy. The two mechanisms are extension and bending of the component fibres. Inclusion of the probable extensions to the element takes the total number of mechanisms to four. The extensions are the element shear (fibre-fibre slippage) and the lateral compression of the fibres. A fifth class of element deformation is introduced, rigid body deformation. Rigid body modes are the three modes (in two dimensions) which must have zero energy associated with their deformation. Consequently there are

five classes of mode and twelve modes, it would be impossible for each mode to represent a separate class of mechanism.

A consequence of having multiple modes for each energy class is that the element modal stiffness matrix cannot be diagonal. The stiffness matrix will be block diagonal instead, each block representing the interaction between the modes dealing with one type of energy mechanism.

The mode shapes for the element will be described for each energy class.

Rigid Body

There are three rigid body modes, the first two representing translations in the x and y directions and the third a rotation. It is important that no energy is associated with these modes because they represent a complete shift of the element, no measurement within the element changes therefore there is no continuum deformation within the element. The three mode shapes are shown in Figure 8-5, noting that the initial fibre direction is horizontal.

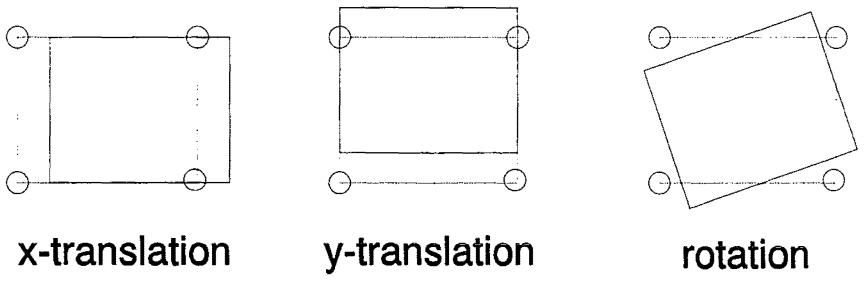

Figure 8-5 *Two dimensional rigid body mode shapes.*

Extension

The deformation of the element is cubic in the direction perpendicular to the fibres, and linear in a direction parallel to the fibres. It is the direction parallel that would affect the extension of the fibres, two modes would be needed to describe fully the linear variation. It was arbitrarily decided that the first of the two modes should represent the equal extension of all the fibres over the width of the element, therefore represent an average element fibre extension. The remaining mode would then be the variation in the fibre length over the element. Diagrams of these modes are shown in Figure 8-6.

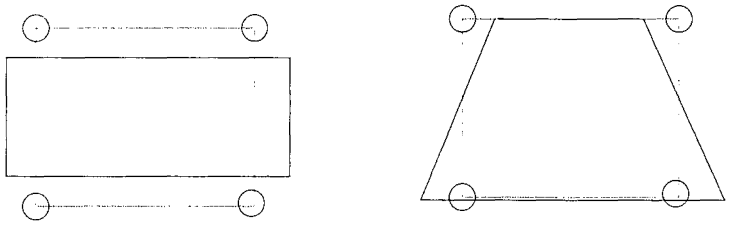

Figure 8-6 *Two dimensional extension modes shapes.*

Bending

There are four rotation degrees of freedom in the element, these are the only degrees of freedom that can induce any bending in the fibre. Consequently four bending modes are sufficient to describe the element bending. An arbitrary system was again used for deciding the shape of each mode (as for the extension modes). The shapes were chosen so that the simpler element bending deformations would be represented by individual modes instead of combinations of them. The element bending modes are shown in Figure 8-7.

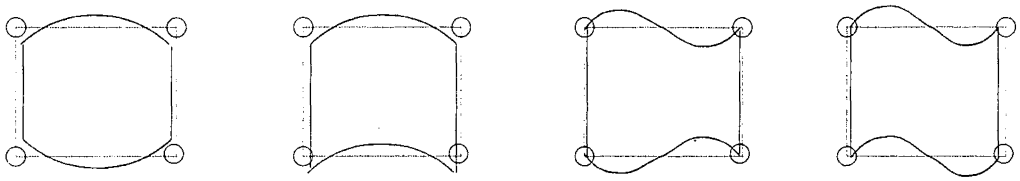

Figure 8-7 *Two dimensional fibrous element bending mode shapes.*

Shear

One mode is enough to describe the shear action of the element. In this context shear is interpreted to be the deformation that creates longitudinal displacements between adjacent fibres in the same element. The mode shape for this is shown in Figure 8-8, the fibres are initially horizontal in these diagrams.

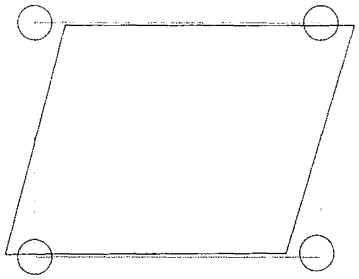

Figure 8-8 *Shape of shear deformation mode.*

Lateral Compression

Two of the twelve modes remain to control the lateral compression action of the element. This energy type represents what happens when the fibres are packed too closely together they will press against one another. The two modes chosen take the measure of the fibre lateral compression from the length of the ends of the element. The second of the two modes represents an average change, the first represents the variation in end length from the average. These modes are shown in Figure 8-9.

All twelve modes can be assigned mode numbers. The mode numbers will give the ordering of the terms of the modal stiffness matrix and modal force vector. The modes have been kept in the same order outlined here, preserving the grouping in energy types. The modal stiffness matrix will be formed from blocks of non zero terms along

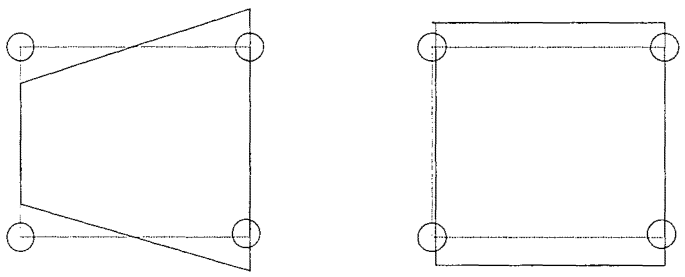

Figure 8-9 *Mode shapes for two dimensional lateral compression.*

the diagonal. All the modes with their numbering are shown in Figure 8-10.

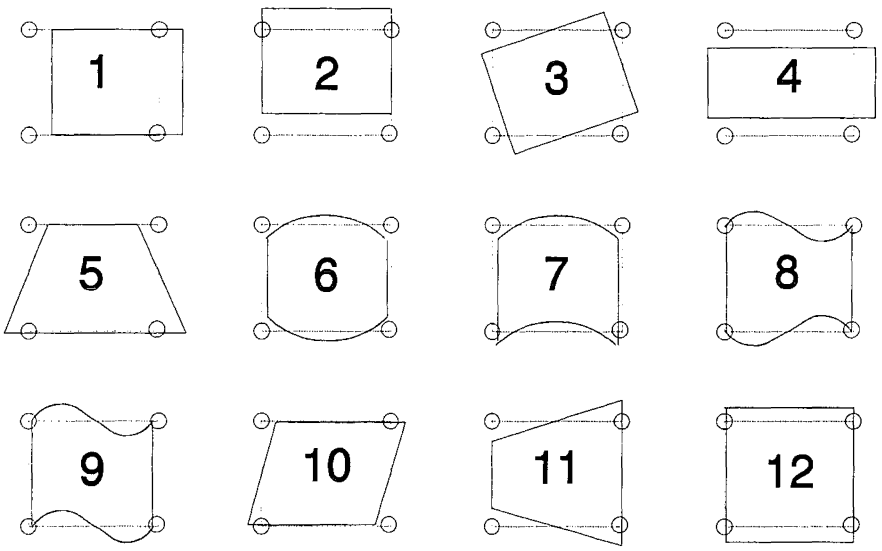

Figure 8-10 *Modes of the two dimensional twelve degree of freedom fibrous element.*

The form of the modal stiffness matrix can be shown. The energy within the element is assumed to be the total of several different types of energy:

$$E = E_1 + E_2 + \ldots \tag{8-1}$$

The modal stiffness matrix is the derivative of the energy with respect to the modal variables:

$$\begin{aligned} K_{ij} &= \frac{\partial^2 E}{\partial \beta_i \partial \beta_j} \\ &= \frac{\partial^2 E_1}{\partial \beta_i \partial \beta_j} + \frac{\partial^2 E_2}{\partial \beta_i \partial \beta_j} + \ldots \end{aligned} \tag{8-2}$$

The element modes have been chosen so that only one type of energy will be generated by deformation of each mode. Equation (8-2) shows that a term in the modal stiffness matrix will be zero unless both of the modes in the derivative are concerned with the same energy mechanism. In diagrammatic form the non zero terms of the modal stiffness matrix are shown in Figure 8-11.

8.2 Transformation Tensors

The degrees of freedom of the fibrous element have been defined in two coordinate systems, this section defines the relationship between the two sets. Once the relationship is fully described, the derivatives may be calculated which form the components of the

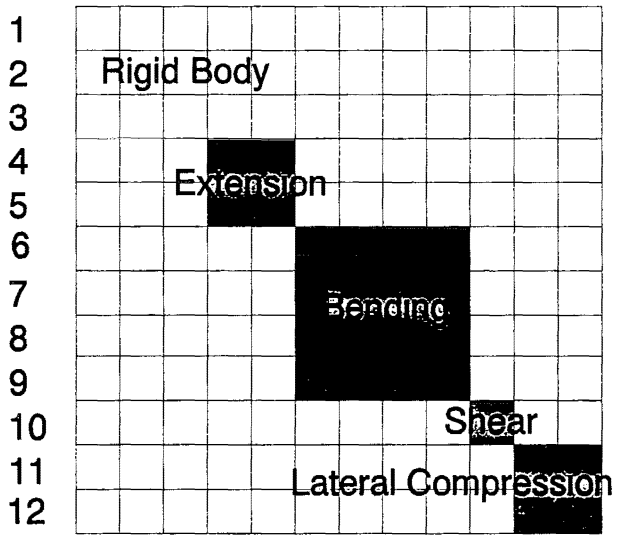

Figure 8-11 *Non-zero terms of the modal stiffness matrix.*

two transformation tensors. With the tensors, the modal stiffness matrix and force vector may be transformed to the nodal stiffness matrix and force vector, ready for conventional finite element assembly and system solution.

8.2.1 Degree of Freedom Naming

Nodal degrees of freedom have been numbered from one to twelve, but this scheme is inconvenient for developing the transformation equations. New names have therefore been assigned to the degrees of freedom based on having two translations and a rotation at each node. The nodes are numbered from one to four. The new scheme makes it more obvious which type of nodal deformation is represented by the name as compared with numbering one through twelve. The names used in the scheme are shown in Figure 8-12.

When discussing the element, certain edges will be called top, bottom and so on. A diagram showing the relationships between these names and the nodal numbering is given in Figure 8-13.

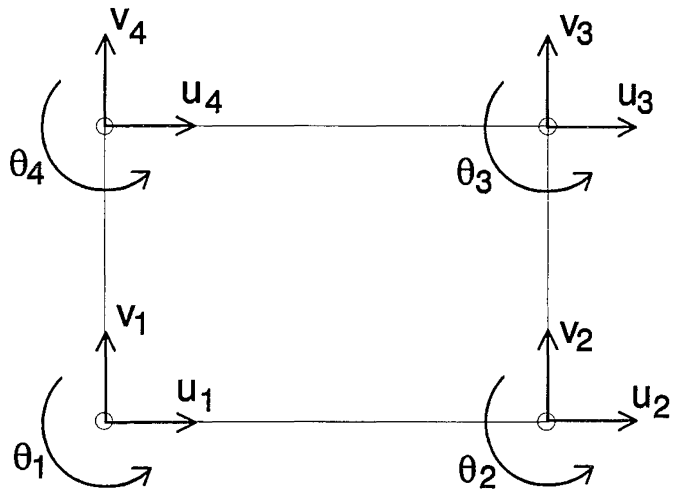

Figure 8-12 *Alternative nodal degree of freedom naming scheme.*

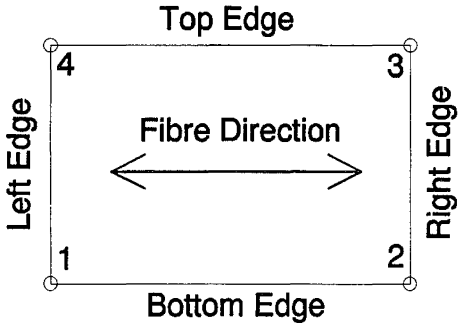

Figure 8-13 *Naming convention for the edges of the two dimensional element.*

8.2.2 Reference Element

For every degree of freedom in an element there must be some state that is the zero value for that degree of freedom. For the set of nodal degrees of freedom the position is obvious. The nodal set measure displacements, therefore the zero state of each must be where there is zero displacement, the initial state. For the set of modal degrees of freedom other definitions are possible.

To explain how the zero state was defined for the fibrous element, examine the measurement of shear in an element. Consider the case of an element that has the shape of a parallelogram in the initial state. A measure of the element could say that there is non zero shear, this is because the measure could be taken assuming that a rectangular element has zero shear. Using such measures for the fibrous element would simplify

the analysis because to calculate the modal values the element need only be compared against a standardised constant element. There would also be significant complications, the modal value at which a mode will have zero energy would be non zero and different for every element in the system. The modal amounts could not then be easily compared between different elements.

An alternative system would be to keep a record of the geometry of every element in the initial state. The calculation of modal values could then be made relative to this state, ensuring that every modal value is zero when it has zero energy. This system would require more storage than the previous one, but the advantages are that the modal values could be compared between elements and could be assigned some consistent physical meaning. For these advantages it was decided to use this relative measurement scheme for the fibrous element.

The concept of a reference element was introduced. This element is geometry in which the element contains zero energy, typically the initial state of the element. A separate reference element was used rather than just the initial state. It was thought possible that when fibre slippage was introduced into the element, the geometry of the reference element might be adjusted to represent any plastic deformation.

The present state is defined as the deformed geometry of the element. The modal amounts of the element can then be found from consideration of only the present and reference states of the element.

8.2.3 Equations of Transformation

Equations can now be given describing the modal amounts in an element in terms of the present and reference element coordinates. The calculations will be carried out mostly using the actual coordinates of the two element states, the present element values will have a superscript P, while the reference element values will use a R. The conversion between the two coordinates sets using the nodal degrees of freedom is given:

$$\begin{aligned}
x_1^P &= x_1^R + u_1 & y_1^P &= y_1^R + v_1 & \Theta_1^P &= \Theta_1^R + \theta_1 \\
x_2^P &= x_2^R + u_2 & y_2^P &= y_2^R + v_2 & \Theta_2^P &= \Theta_2^R + \theta_2 \\
x_3^P &= x_3^R + u_3 & y_3^P &= y_3^R + v_3 & \Theta_3^P &= \Theta_3^R + \theta_3 \\
x_4^P &= x_4^R + u_4 & y_4^P &= y_4^R + v_4 & \Theta_4^P &= \Theta_4^R + \theta_4
\end{aligned} \qquad \textbf{(8-3)}$$

The total rotation of the node Θ (as opposed to the displaced rotation θ) is assumed to have a zero position at the horizontal.

Rigid Body Modes (Modes 1-3)

The first two rigid body modes (translation in the x and y directions) are the simplest to define. Initially consider mode one, two components are calculated, the two are the average x coordinate of each of the present and reference element states.

$$X^P = \frac{1}{4}\left(x_1^P + x_2^P + x_3^P + x_4^P\right)$$
$$X^R = \frac{1}{4}\left(x_1^R + x_2^R + x_3^R + x_4^R\right) \quad \textbf{(8-4)}$$

The modal amount may then be written as the difference of the two components:

$$\beta_1 = X^P - X^R \quad \textbf{(8-5)}$$

Note that substitution leads to a simple expression for this mode in terms of the nodal displacements. A similar expression for translation in the y direction is also shown. No other mode has as simple a definition as that for these first two.

$$\beta_1 = \frac{1}{4}\left(u_1 + u_2 + u_3 + u_4\right)$$
$$\beta_2 = \frac{1}{4}\left(v_1 + v_2 + v_3 + v_4\right) \quad \textbf{(8-6)}$$

The rigid body rotation angle is found by measuring the angle from the horizontal of a chord that passes through the middle of the two element ends. The calculations of the intermediate value for the present element are shown.

$$T^P = \tan^{-1}\left(\frac{-y_1^P + y_2^P + y_3^P - y_4^P}{-x_1^P + x_2^P + x_3^P - x_4^P}\right) \quad \textbf{(8-7)}$$

With a similar term from the reference element, the value for the third mode may be calculated.

$$\beta_3 = T^P - T^R \quad \textbf{(8-8)}$$

Extension Modes (Modes 4-5)

The element extension modes are based on the arc lengths of the fibres at the top and bottom edges. If the modes were concerned with just the chord lengths these modes would be little more complicated than the rigid body modes. Using the arc lengths means that the rotation angles will also have an effect on the modal value. The

calculation of this value involves several steps and intermediate values, these intermediate values will be explained and will be used in calculating later modes.

The rotation angles of the top and bottom chords must be calculated.

$$T_{top}^{P} = \tan^{-1}\left(\frac{y_3^P - y_4^P}{x_3^P - x_4^P}\right) \qquad T_{bot}^{P} = \tan^{-1}\left(\frac{y_2^P - y_1^P}{x_2^P - x_1^P}\right) \tag{8-9}$$

Similar values are found for the reference element.

Deviation angle of the fibre direction from the chord direction may now be calculated.

$$\begin{aligned} r_1^P &= \Theta_1^P - T_{bot}^P \qquad & r_3^P &= \Theta_3^P - T_{top}^P \\ r_2^P &= \Theta_2^P - T_{bot}^P \qquad & r_4^P &= \Theta_4^P - T_{top}^P \end{aligned} \tag{8-10}$$

The definition of these angles can be seen in Figure 8-14. It is evident why these angles greatly affect the arc length of the fibre piece.

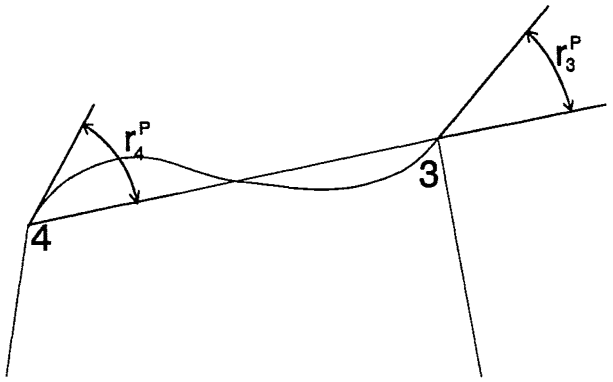

Figure 8-14 *Definition of fibre direction deviation angles.*

The chord lengths of the top and bottom edges must also be known:

$$\begin{aligned} L_{top}^P &= \sqrt{\left(x_3^P - x_4^P\right)^2 + \left(y_3^P - y_4^P\right)^2} \\ L_{bot}^P &= \sqrt{\left(x_2^P - x_1^P\right)^2 + \left(y_2^P - y_1^P\right)^2} \end{aligned} \tag{8-11}$$

Top and bottom fibre arc lengths may be found as a function of the chord lengths and the deviation angles.

$$\begin{aligned} S_{top}^P &= S_{top}^P\left(L_{top}^P, r_3^P, r_4^P\right) \qquad & S_{top}^R &= S_{top}^R\left(L_{top}^R, r_3^R, r_4^R\right) \\ S_{bot}^P &= S_{bot}^P\left(L_{bot}^P, r_1^P, r_2^P\right) \qquad & S_{bot}^R &= S_{bot}^R\left(L_{bot}^R, r_1^R, r_2^R\right) \end{aligned} \tag{8-12}$$

Definition of the arc length will be given in a later section, several options are explored for this relationship before one is chosen.

Both modal amounts are defined in terms of the top and bottom fibre arc lengths.

$$\beta_4 = \frac{1}{2}\left(\frac{S^P_{bot}}{S^R_{bot}} + \frac{S^P_{top}}{S^R_{top}}\right) - 1$$
$$\beta_5 = \frac{1}{2}\left(\frac{S^P_{bot}}{S^R_{bot}} - \frac{S^P_{top}}{S^R_{top}}\right) \qquad \textbf{(8-13)}$$

Bending Modes (Modes 6-9)

The bending modes are defined in terms of the fibre direction deviation values that were calculated with the extension modes.

$$\beta_6 = \frac{1}{4}\left(-r_1^P + r_2^P - r_3^P + r_4^P\right) \qquad \beta_8 = \frac{1}{4}\left(-r_1^P - r_2^P + r_3^P + r_4^P\right)$$
$$\beta_7 = \frac{1}{4}\left(+r_1^P - r_2^P - r_3^P + r_4^P\right) \qquad \beta_9 = \frac{1}{4}\left(+r_1^P + r_2^P + r_3^P + r_4^P\right) \qquad \textbf{(8-14)}$$

The definitions of the bending modes contain no terms calculated from the reference element, this carries the assumption that all fibres are straight in the initial state. This was included to simplify the initial element and introduces no errors since all test assemblies do have straight initial fibres.

Shear Mode (Mode 10)

The shear mode does not describe the conventional shear within the continuum element. It is a measure of the relative slippage between the fibres in the fibre direction. The element shear is calculated based on the midpoints of the chords between the nodes of the element, these points are shown in the first part of Figure 8-15. The later part of the same figure shows the development of the shear value. A line is drawn in the fibre direction between the points on the element ends. The shear value is the distance between the two element side points. The distance is taken in the direction of the fibre direction line. It can be seen that this measure will not change as the fibres are moved apart from one another, it will change only when longitudinal sliding is shown. The modal value is found as the difference from the present and reference states.

$$\beta_{10} = c^P - c^R \qquad \textbf{(8-15)}$$

The equations for the generation of this mode will not be shown, they are cumbersome and would not clarify the definition.

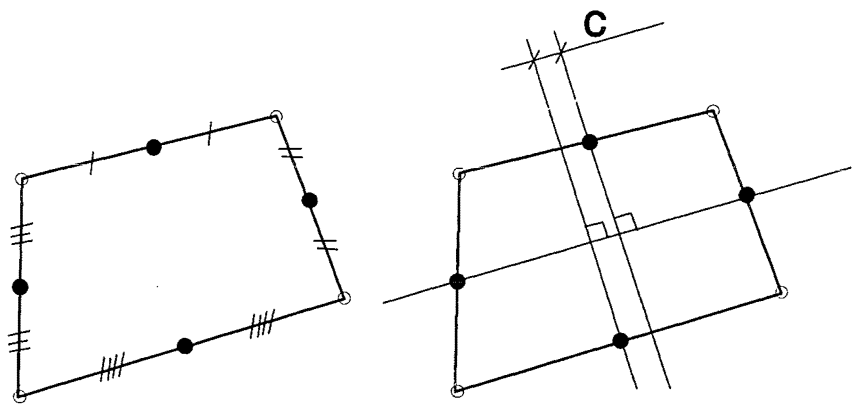

Figure 8-15 *Measurement of the element shear.*

Nodal rotations have no affect on the modal shear. This is a simplification because large nodal displacements could introduce large shear variations over the length of the element. It would be impossible to represent these variations with one shear mode so only gross shear is included. The ignored shear effect is second order and therefore as the element size decreases and the nodal deformations decrease, the error will also decrease.

Lateral Movement (Modes 11-12)

The two remaining modes measure the opening and closing of the gaps between the fibres. Originally these modes were calculated from the length of the projection of the element ends in the direction lateral to the fibres. This was found to give problems to the solution and a more complicated approach based on the nodal rotations was introduced. The problems, the solution and the various resulting formulae are discussed more fully in section 8.3.

8.2.4 MAPLE Programming

The equations outlined in the previous section seem simple, but once they are assembled they become complicated. The algebra required for the calculation of the various first and second derivatives required would be impossible to do manually with speed and reliability. The symbolic algebra package MAPLE was used for almost all algebraic manipulations. An introduction to the package is given with the fourth mode of the element being used for illustration.

The input into MAPLE is as lines of text instructions, all input is case sensitive and the same variable name may be used in upper and lower case to mean different things.

The following lines (Text 8-1) contain the MAPLE code for the evaluation of mode four of the two dimensional fibrous finite element. Variable names used within the MAPLE code do not look exactly like those used in the original equations, this is due to the lack of subscripts and superscripts within the MAPLE syntax.

```
Tr := arctan((yr2+yr3-yr1-yr4)/2,(xr2+xr3-xr1-xr4)/2):
Ttopr := arctan(yr3-yr4,xr3-xr4):
Tbotr := arctan(yr2-yr1,xr2-xr1):
rr1 := tr1-Tbotr:
rr2 := tr2-Tbotr:
rr3 := tr3-Ttopr:
rr4 := tr4-Ttopr:
Ltopr := sqrt((xr3-xr4)^2+(yr3-yr4)^2):
Lbotr := sqrt((xr2-xr1)^2+(yr2-yr1)^2):
Stopr := Ltopr* (1/2+ (( 1 - 1/4*cos(rr3) - 1/4*cos(rr4))**2 +
(-1/4*sin(rr3) - 1/4*sin(rr4))**2)**(1/2)):
Sbotr := Lbotr* (1/2+ (( 1 - 1/4*cos(rr2) - 1/4*cos(rr1))**2 +
(-1/4*sin(rr2) - 1/4*sin(rr1))**2)**(1/2)):

Tp := arctan((yp2+yp3-yp1-yp4)/2,(xp2+xp3-xp1-xp4)/2):
Ttopp := arctan(yp3-yp4,xp3-xp4):
Tbotp := arctan(yp2-yp1,xp2-xp1):
rp1 := tp1-Tbotp:
rp2 := tp2-Tbotp:
rp3 := tp3-Ttopp:
rp4 := tp4-Ttopp:
Ltopp := sqrt((xp3-xp4)^2+(yp3-yp4)^2):
Lbotp := sqrt((xp2-xp1)^2+(yp2-yp1)^2):
Stopp := Ltopp* (1/2+ (( 1 - 1/4*cos(rp3) - 1/4*cos(rp4))**2 +
(-1/4*sin(rp3) - 1/4*sin(rp4))**2)**(1/2)):
Sbotp := Lbotp* (1/2+ (( 1 - 1/4*cos(rp2) - 1/4*cos(rp1))**2 +
(-1/4*sin(rp2) - 1/4*sin(rp1))**2)**(1/2)):

B4 := 1/2*(Stopp/Stopr + Sbotp/Sbotr) - 1:
```

Text 8-1 *MAPLE code for generation of fourth mode.*

When these lines are executed within the MAPLE processor, a formula for the fourth mode in terms of the eighteen inputs is generated. This output is shown in Text 8-2.

The result shown is large, but would not be impossible to calculate by hand. The formula shown is one of the twelve modal formulae that must be calculated. Derivatives of this formula with respect to the input variables must also be calculated, the diff command within MAPLE may be used for this operation. The first derivative of the fourth mode with respect to the first degree of freedom yields over 60 lines of output, this is only one of the 144 such derivatives required. Although not all the terms will be as complicated as that shown above, a large amount of algebra is still required.

```
B4 =

                                                                  2 1/2
     1/2 (xp3^2 - 2 xp3 xp4 + xp4^2 + yp3^2 - 2 yp3 yp4 + yp4^2 )     (1/2
+ (

                                                                 2
           (1 - 1/4 cos(tp3 - %4) - 1/4 cos(tp4 - %4))

                                                                2          /
            + (- 1/4 sin(tp3 - %4) - 1/4 sin(tp4 - %4))^2)^1/2)   /   (
                                                                 /

                                                                  2 1/2
          (xr3^2 - 2 xr3 xr4 + xr4^2 + yr3^2 - 2 yr3 yr4 + yr4^2 )     (1/2
+ (

                                                                 2
           (1 - 1/4 cos(tr3 - %3) - 1/4 cos(tr4 - %3))

                                                                2
            + (- 1/4 sin(tr3 - %3) - 1/4 sin(tr4 - %3))^2)^1/2)) + 1/2

                                                                  2 1/2
          (xp2^2 - 2 xp2 xp1 + xp1^2 + yp2^2 - 2 yp2 yp1 + yp1^2 )     (1/2
+ (

                                                                 2
           (1 - 1/4 cos(tp2 - %2) - 1/4 cos(tp1 - %2))

                                                                2          /
            + (- 1/4 sin(tp2 - %2) - 1/4 sin(tp1 - %2))^2)^1/2)   /   (
                                                                 /

                                                                  2 1/2
          (xr2^2 - 2 xr2 xr1 + xr1^2 + yr2^2 - 2 yr2 yr1 + yr1^2 )     (1/2
+ (

                                                                 2
           (1 - 1/4 cos(tr2 - %1) - 1/4 cos(tr1 - %1))

                                                                2
            + (- 1/4 sin(tr2 - %1) - 1/4 sin(tr1 - %1))^2)^1/2)) - 1

%1 :=                  arctan(yr2 - yr1, xr2 - xr1)
%2 :=                  arctan(yp2 - yp1, xp2 - xp1)
%3 :=                  arctan(yr3 - yr4, xr3 - xr4)
%4 :=                  arctan(yp3 - yp4, xp3 - xp4)
```

Text 8-2 *Formula for mode four of two dimensional element.*

The second derivative terms are also needed. Output from the second derivative of mode four with respect to the first degree of freedom is over 100 lines long. There are 1728 such terms to be found, therefore manual calculation would be prohibitive.

MAPLE can also be used to produce FORTRAN code (or C) ready for inclusion into a subroutine and this option was used to reduce further the chance of mistake.

It was stated above that not all the terms of every matrix will be as complicated as the example given, many terms will be zero. The matrix of first derivative terms can be shown to be only two-thirds populated therefore one third of the terms will be zero whatever the values of the inputs are. A diagram showing the locations of the non zero terms within this matrix is given in Figure 8-16.

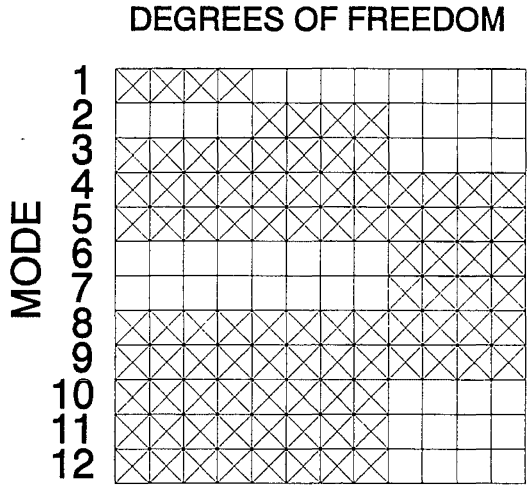

Figure 8-16 *Location of non-zero terms within first derivative matrix.*

The location of the non zero terms within the matrix can be quite instructive. The first two modes are the rigid body translations, the only terms contributing to each of these two modes are the displacement degrees of freedom in their respective directions. The first two bending modes have no derivative component with respect to any of the displacement variables, while the other two bending modes do. This is because of the way that the rotations were combined when assembling the modal values, in the first two bending modes (modes six and seven) the effects from the top and bottom edge rotations cancel.

Two of the most important modes are the extension modes, this is because a fibrous system is orders of magnitudes stiffer in the fibre direction than in any other. It is interesting that the extension modes are two of only four modes that have non zero terms in all degrees of freedom.

The second derivative calculation results in an order three tensor, the non zero terms of this tensor can be displayed using twelve grids similar to that used for the first derivative matrix. These grids are shown in Figure 8-17. This tensor is far from fully populated, only 27 percent of the terms have the potential to be non zero.

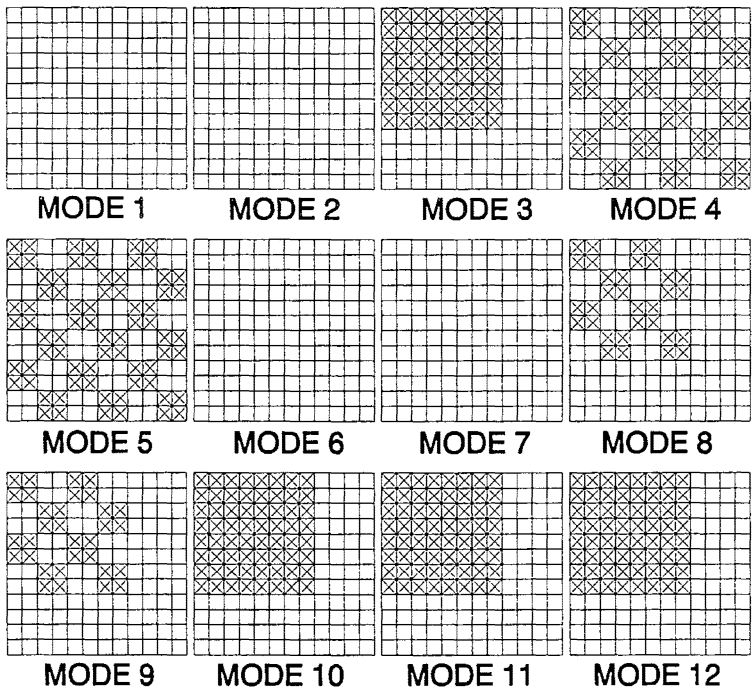

Figure 8-17 *Non-zero terms of the second derivative tensor.*

The absence of any second degree terms for modes one, two, six and seven, is because these modes are related linearly to the nodal degrees of freedom, this is obvious for the first two modes. For the bending modes it is a consequence of the way that the modes were assembled. All terms making up the bending modes are related linearly to the nodal rotations and nonlinearly to the nodal displacements. In the first two bending modes the displacement contributions cancel, resulting in the lack of any second degree terms from these modes. The other two bending modes have second degree terms only with respect to the displacements.

The complexity of the extension modes is again illustrated as they are the only modes that have second derivatives in terms of the rotation degrees of freedom.

MAPLE output can be used to write subroutines to evaluate the various terms required for the transformation equations.

8.3 System Modelling

The remaining steps for generation of a successful two dimensional fibrous finite element stiffness matrix are explained. The definition of the fibre arc length that was

previously excluded is given. Some problems that were found with the final system are discussed and solutions found.

8.3.1 Fibre Arc Length

A definition of the arc length of a single fibre in terms of the variables controlling that fibre had to be found. The first arc length formula to be found was that for the first (and simplest) two dimensional element. In this element there was only one degree of freedom representing bending along the fibre. A more complicated deformation pattern was then introduced and a formula was required for a fibre piece with two bending degrees of freedom.

Several options were tried for the simple element, the formula to be found was of the form:

$$L_{\text{arc}} = L_{\text{arc}}\left(L_{chord}, \delta\right) \tag{8-16}$$

The form of this formula is due to the values for the chord length and the lateral displacement at the midpoint being easily picked from the element degrees of freedom, and the two values fully control the arc length.

It was found that any reasonable formula chosen for the arc length would scale linearly with the chord length, so the chord length could then be taken outside the equation as a multiplier. This left the unknown part of the arc length equation in terms of only one variable, the midpoint displacement:

$$\frac{L_{\text{arc}}}{L_{chord}} = \frac{L_{\text{arc}}}{L_{chord}}(\delta) \tag{8-17}$$

Various types of deformation were attempted including sinusoidal, parabolic, or a series of straight lines. It was found that all of the better approximations could not be evaluated analytically, numerical calculation was required. Because the formula was a function of only one variable it was simple to calculate the arc length for the full range of likely values of the displacement. An approximate curve was then fitted to this data so that within the analysis an arc length value could be quickly calculated.

The parabolic approximation was chosen for use because the form of the deformation was most likely to be able to represent the range of shapes that the fibre might be capable of. The approximation formula was calculated and implemented without trouble. This system was used within the first two dimensional fibrous element and worked well.

It did not undergo exhaustive testing because limitations of the approach were quickly revealed, the fibre would require a minimum of two (rather than one) bending degrees of freedom.

With two bending degrees of freedom per fibre piece, the form of the bending formula is:

$$\frac{L_{arc}}{L_{chord}} = \frac{L_{arc}}{L_{chord}}(r_1, r_2) \qquad \textbf{(8-18)}$$

The first deformation pattern chosen was that of a cubic variation of lateral displacement along the fibre chord (see Figure 8-18). A cubic curve normally requires four degrees of freedom to be fully specified but as the curve is constrained to pass through the nodes at either end of the chord, two degrees of freedom would be sufficient.

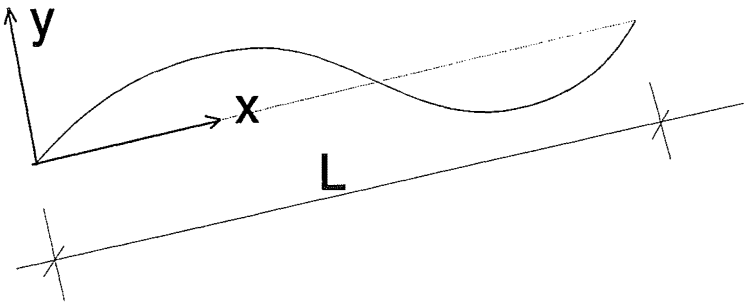

Figure 8-18 *Cubic lateral displacement variation.*

The equation governing the deformation would then be:

$$y = A\left(\frac{x}{L}\right)^3 + B\left(\frac{x}{L}\right)^2 + C\left(\frac{x}{L}\right) \qquad \textbf{(8-19)}$$

$$A + B + C = 0$$

where A, B, and C may be defined from the constraint given and the rotation angles at the nodes.

In a manner similar to the parabolic displacement, the arc length of the cubic curve could not be evaluated analytically and some form of numeric integration would be required. The previous approach of doing the numeric integration once and fitting a simple curve to the result could not be used in this case, the formula depending on two variables is not suitable for such a process. The alternative chosen was to use Simpson's rule integration, but rather than apply it to the numerical values as normal, the symbolic

variables were included in the integration. The result was an approximate formula for the arc length in terms of the input variables. The symbolic processor MAPLE was used for this operation. The resulting formula has many terms and was kept to a manageable size by using at most ten integration points in Simpson's rule.

An element was coded using this bending deformation assumption. The complexity of the approximation was evident when the first and second derivatives of the shape functions were calculated, the code becoming very large although manageable. Under moderate testing the element behaved very well but failed when subjected to extreme test cases. Consider a situation where a piece of fibre is anchored vertically at one end and is subjected to an inclined load (see Figure 8-19).

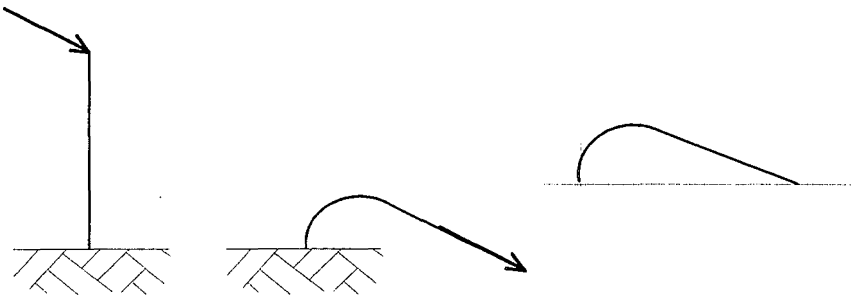

Figure 8-19 *Bending of a vertically anchored fibre.*

The fibre is bent over until the top point passes below the bottom point. If the fibre has been modelled using one element as described above then the analysis will fail at this stage. The reason for failure (as shown in Figure 8-19) is that the displacement pattern required for the fibre can no longer be represented by the cubic displacement function. This test case might seem a little extreme but the important point is that once this limit is crossed the system does not merely give a bad approximation to the solution but it fails to give a solution at all.

A new approximation to the bending was required, which was both simpler and more versatile. The approach was versatile in that it gave a solution under all foreseeable circumstances although not necessarily always a good approximation. The approach was required to be simpler because although the cubic displacement approach did give results, a significant portion of the code and execution time was required to evaluate the approximation and the derivatives at every step.

The simplest possible system that would achieve the desired result was sought. The result was an approximation based on three straight line segments and two rotational springs, and all the fibre bending was accommodated within the springs.

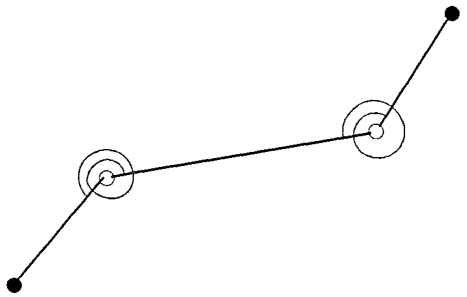

Figure 8-20 *Three segment approximation to fibre bending.*

Before this approximation could be used, two more items needed to be defined, first the relative lengths of each of the line segments and secondly the stiffness of the rotational springs.

The relative lengths of the line segments were chosen for simplicity, the lengths of the two end segments were defined as one quarter of the chord length. The measure was based on the chord length because this is known to the program. If the arc length were used for a basis, then the segment lengths would be required to find the arc length and a nonlinear system results. The value of one quarter was chosen so that in a continuous fibre (constructed from multiple elements), the length of fibre segment between bends would be nearly the same (at least for small displacement), see Figure 8-21 for a diagram displaying this.

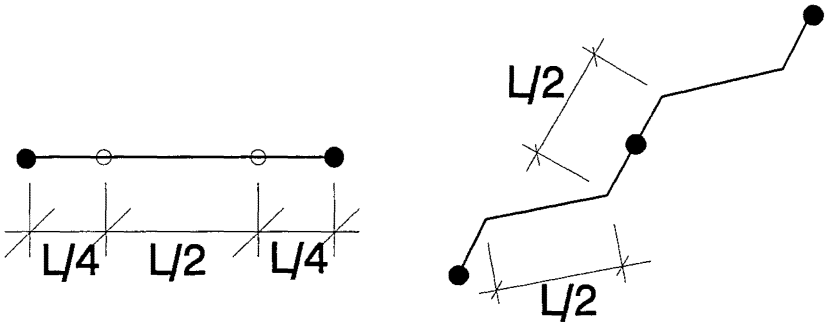

Figure 8-21 *Relative segment length.*

A value had to be found for the stiffness of the rotation springs between the segments of the bent fibre. The value would be a function of at least both the length of the fibre and the bending stiffness of the fibre. A lateral force and a moment were applied to a simple beam then the same force and moment were applied to a single element of the same length. A comparison between the two resulting displacements allowed the calculation of the rotational spring stiffness. These cases were applied initially to small displacement and then the applied moment was given large displacement treatment as well. For each case the comparison can be made by matching any one parameter, both lateral end displacement and end slope were used in separate comparisons.

In all cases the relationship between moment, spring stiffness and spring rotation is defined as:

$$M = K_s \theta \qquad \textbf{(8-20)}$$

Small Displacement, Lateral End Movement, Applied Force.

The case for comparison was a fibre anchored horizontally with a vertical load of P applied to the end.

Figure 8-22 *Small displacement lateral loading comparison case.*

The equations for the lateral end deflection may be written in terms of the appropriate stiffnesses, fibre bending stiffness (K_B) for the continuous fibre and the rotational spring stiffness (K_S) for the approximation.

$$\delta = \frac{1}{3}\frac{PL^3}{K_B} \qquad \delta' = \frac{10}{16}\frac{PL^2}{K_S} \qquad \textbf{(8-21)}$$

Setting the true and approximate deflection to be equal leads to an estimate for the spring stiffness:

$$K_S = \frac{30}{16}\frac{K_B}{L} = 1.875\frac{K_B}{L} \qquad \textbf{(8-22)}$$

Small Displacement, End Slope, Applied Force.

The same case as was previously analysed, but the end slopes are matched rather than the lateral deflections. The two end slopes were:

$$\theta = -\frac{1}{2}\frac{PL^2}{K_B} \qquad \theta' = -\frac{PL}{K_S} \tag{8-23}$$

This similarly leads to a second approximation for the spring stiffness:

$$K_S = 2\frac{K_B}{L} \tag{8-24}$$

Small Displacement, Lateral End Movement, Applied Moment.

This test case was identical to that to which the force was applied except that a moment is applied instead. The end displacements of this system are:

$$\delta = \frac{1}{2}\frac{ML^2}{K_B} \qquad \delta' = \frac{ML}{K_S} \tag{8-25}$$

Leading to another approximation:

$$K_S = 2\frac{K_B}{L} \tag{8-26}$$

Small Displacement, End Slope, Applied Moment.

This is a very simple calculation, principally because the moment is constant along the fibre and is also constant in both springs. The geometries are therefore quite simple and the end slopes are:

$$\theta = \frac{ML}{K_B} \qquad \theta' = 2\frac{M}{K_S} \tag{8-27}$$

The approximation that comes from this is:

$$K_S = 2\frac{K_B}{L} \tag{8-28}$$

Large Displacement, End Slope, Applied Moment.

Only the applied moment case will be used for the large displacement analyses, the simple geometry makes this the simpler option. The equations for the end slope are identical to those for the small displacement case, leading to the same approximation for the spring stiffness.

Large Displacement, Lateral End Movement, Applied Moment.

This case was more complicated, the true lateral deflection may be written in terms of the total rotation angle of the fibre:

$$\delta = [1-\cos(\alpha)]\frac{L}{\alpha} \qquad \text{Where } \alpha = \frac{ML}{K_B} \tag{8-29}$$

The lateral deflection of the approximate beam may be written in terms of the nodal spring rotations as:

$$\delta' = \frac{L}{2}\left(\frac{2+2\sin(\beta)-2\cos^2(\beta)+\sin(2\beta)}{2+\sin(\beta)}\right) \qquad \text{Where } \beta = \frac{M}{K_S} \tag{8-30}$$

Taking series approximations to both deflection equations:

$$\begin{aligned} \delta &= \frac{1}{2}L\alpha - \frac{1}{24}L\alpha^3 + \frac{1}{720}L\alpha^5 + O(\alpha^6) \\ \delta' &= L\beta - \frac{5}{12}L\beta^3 + \frac{1}{120}L\beta^5 + O(\beta^6) \end{aligned} \tag{8-31}$$

Substituting for the rotations in the above series, and setting the first two terms of each to be equal, gives an approximate equation to be solved for the spring stiffness.

$$\frac{1}{2}\frac{ML^2}{K_B} - \frac{1}{24}\frac{M^3L^4}{K_B^3} = \frac{ML}{K_S} - \frac{5}{12}\frac{M^3L}{K_S^3} \tag{8-32}$$

There are three solutions for K_S from this equation, two have significant complex parts and are complex conjugates of one another. The remaining solution is real and can be written as:

$$K_S = 2\frac{K_B}{L} - \frac{1}{24}\frac{LM^2}{K_B} - \frac{7}{576}\frac{L^3M^4}{K_B^3} + O(M^6) \tag{8-33}$$

This equation is in a simpler form when it is rewritten in terms of the fibre rotation:

$$K_S \approx \frac{K_B}{L}\left(2 - \frac{1}{24}\alpha^2 - \frac{7}{576}\alpha^4\right) \tag{8-34}$$

Results

Each approximation that has been found for K_S has been as a multiplier on the ratio of the fibre bending stiffness to the arc length. The results can then be summarised by a list of the various multipliers.

	Match End Displacements	Match End Slopes
Small Displacement Applied Load	$\frac{30}{16} = 1.875$	2
Small Displacement Applied Moment	2	2
Large Displacement Applied Moment	$2 - \frac{1}{24}\alpha^2 - \frac{7}{576}\alpha^4$	2

The decision was made based on these results to use a multiplier of two for the approximation. A plot of the variable large displacement multiplier is shown in Figure 8-23.

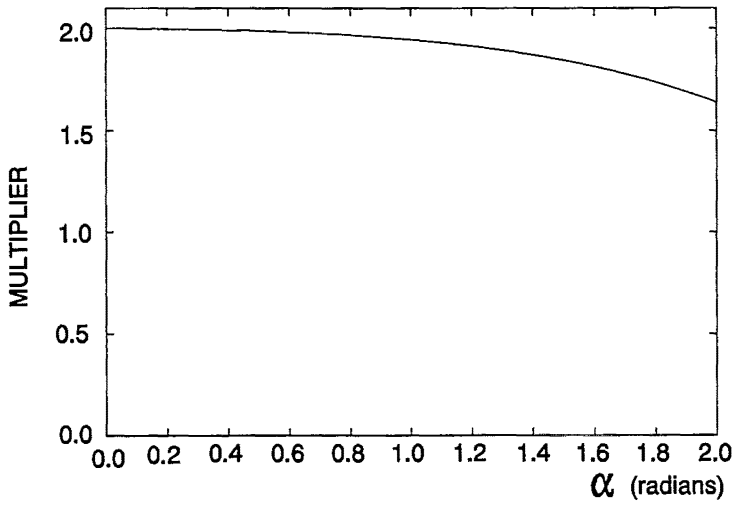

Figure 8-23 *Multiplier on spring stiffness approximation for large displacement.*

8.3.2 Lateral Compression Measures

The lateral compression mode is very important if a system is to model the properties of a fibrous assembly. Many properties of an assembly depend on the friction created when one fibre is pressed against another. Development of the measurement of this mode is explained together with the implications that the different measures have on the analysis. The value of the stiffness that is used for the mode and the importance of this value to the convergence of the total system is also discussed.

The first mode for lateral fibre compression was based on the area of the element. It was thought that the fibres would exhibit no lateral resistance until the element decreases to a size that implies that the fibres are tightly packed. Therefore an element will change size freely until the density passes below a value defined by the initial packing fraction of the continuum, after this point there would be resistance stiffness and force. In practice this method does not function, a series of elements with a point load will deform to a configuration that involves little or no area change for the elements but will often not resemble what a fibrous system would do. Refer to Figure 8-24 for an example of the *zig-zag* pattern that was often found in the results. In this figure two elements are joined end to end (the fibre direction is shown in the figure), lateral forces are applied at the nodes that join the two elements. The elements deform to the state where the nodes overlap, yet the areas of the elements do not significantly change, this configuration does not resemble that expected of an aligned assembly.

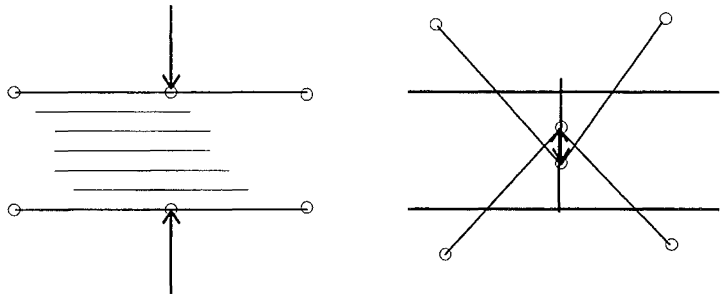

Figure 8-24 *Element deformations with area compression mode.*

A better approach to the fibre transverse compression was sought using two modes to give better control over the deformation. Element area was still used as the control factor for the modes, but each of the two represented only the area of half the element, one end for each mode. Results were superior for this system, but the *zig-zag* effect was still present. The effect was not as strong, nor was it propagated to adjacent elements as easily. The improvements were thought to be due to two modes being used for control, using the element area as a basis was thought to be the reason for the *zig-zag* deformations.

A new measure was developed for the transverse compression, a value representing the space between the fibres was found. The lengths of the ends of the element were measured, and the projection of this length in the direction lateral to the fibre direction was then taken as the fibre lateral compression value. Initial methods assumed the fibres

to be straight and an average of the directions of the element top and bottom chords was used to assess the fibre direction.

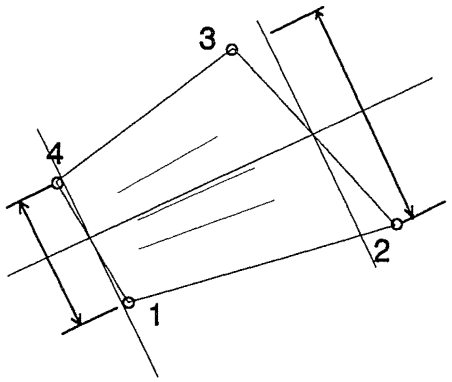

Figure 8-25 *Measurement of the lateral fibre spacing value.*

Significant improvement was again found in the stability of the system, the unusual deformations found previously had disappeared. Other limitations of this method were evident in the solutions. Rotation degrees of freedom have no influence on the transverse measurement, the element direction was used to assess the fibre direction rather than the fibre direction itself. This assumption was found to be an oversimplification, control over the nodal fibre rotation would give a better (though more complicated) solution.

Two methods were proposed for including rotation effects into the transverse fibre spacing measure. Method one changed the direction in which the projection of the end length was taken. Rather than use the average of the top and bottom chord directions, the average of the fibre directions at the nodes on that end was used. Method two involved taking the transverse direction from the element chords as before, but rather than measure the length of the element ends, the length a small length from the node in the direction of the fibre is taken. These methods are illustrated in Figure 8-26.

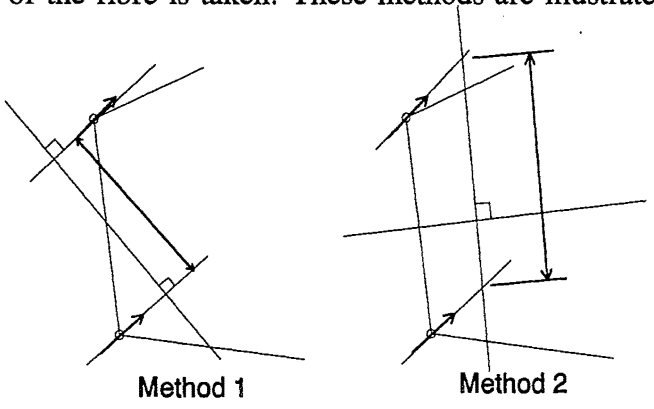

Figure 8-26 *Lateral spacing measure including rotation effects.*

Method two was found the better of these two options, not only was it the simplest option to code but it gave the best results within the analysis. Method two provides the best mechanism for the transferal of a point load at the node into the element, this is partly because the control point for the transverse compression is moved away from the end of the element. In method one the control is at the element end, when two elements are joined end to end there is a degree of redundancy with two similar controls being applied at the same point.

8.3.3 Lateral Compression Stiffness

The changes in the stiffness of the lateral compression mode during deformation together with the large magnitude of these stiffness values causes convergence problems for the analysis. The reasons for each problem are discussed and the solutions that were found are explained.

Stiffness Changes

In simple terms the lateral compression mode exists in one of two states; either the fibres are moving freely or they are jammed against one another.

If the assembly is in the free state then there is space between each fibre, they are free to move laterally without contacting one another. Ideally the stiffness in this state will be zero because there is no resistance to movement, however a small value must be included for numerical reasons, the size of this value is discussed in a later section. It can be said however that there would be many orders of magnitude of difference between the free and compressed states.

The change between the two states must be managed very carefully within the numeric process. In Figure 8-27 two options are shown for how the stiffness and forces might change across the jam point. One option has a step change in stiffness, the other enforces a linear variation in the stiffness.

The step stiffness change was originally used within the analysis but it was found that if the solution was close to the jam point the iterative process would oscillate about that point without convergence. When the system was changed to the linear variation of stiffness the smoother transition made convergence more likely.

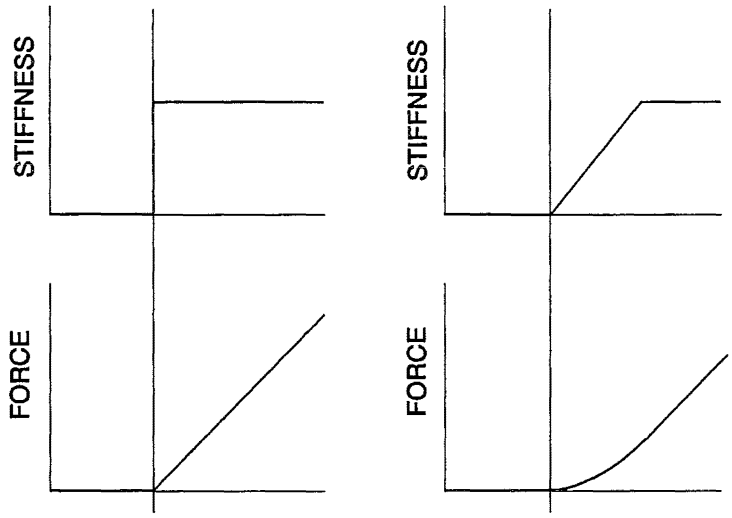

Figure 8-27 *Comparison between step and linear stiffness changes.*

Large Magnitude Stiffness

The numerical value of the jamming stiffness is not only larger than that of the free stiffness, but also than of any other stiffness in the system. One reason for this is the very open nature of the undeformed assembly. An assembly could have an initial packing fraction as low as ten percent, this means that the fibres will not jam until the element width is close to one tenth of the original width. All of the applied transverse forces must be resisted without significant further movement, so the energy gain with deformation must be large, leading to large stiffness.

Numerical processes suffer from the limitations of the computers on which they run, one of the most important handicaps is that of finite precision. Computers cannot store numbers exactly, the implication of this for fibre displacements is that the location of a fibre does not vary smoothly from one position to another. The location jumps from one point to another by the minimum amount that the variable storing the value can be adjusted. Normally this causes no problem but with the large stiffness these small position jumps can represent significant jumps in the resistance force of the element. The consequence can be that convergence of the element is impossible because the position that the fibre must occupy to balance the resistance and applied forces cannot be represented by the finite precision of the computer. This was shown to be the case for the fibrous analysis.

One possible solution to this problem is to adjust the convergence criteria so that convergence could be found at a point that could be represented. No satisfactory system

of adjustment was found and this approach was forgone when a better approach was developed.

If the convergence criterion is not to be adjusted then the stiffness must be made smaller. If the stiffness is reduced then the lateral deformations are increased to excessive levels where the elements develop zero or negative width, an undesirable situation. The solution was to introduce a virtual jam point, then treat the jammed system as if it has low stiffness but continually shift the point at which jamming occurs (within the iterative system) so that the element widths remain at reasonable levels.

Consider the object being forced into a wall of infinite stiffness shown in Figure 8-28 (a), although it is intuitive that the object will come to rest on the wall, numerical treatment of this situation is difficult due to the problems discussed above.

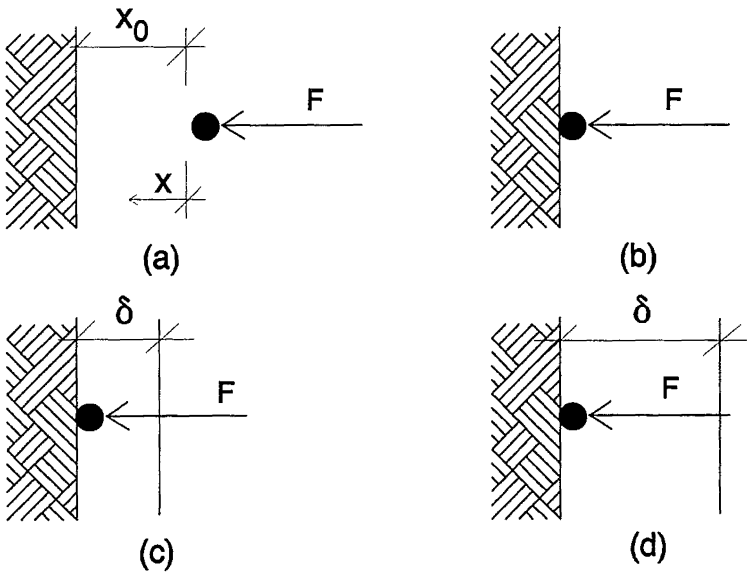

Figure 8-28 *An object is forced into a wall of infinite stiffness.*

Consider that the wall does not have infinite stiffness, but a finite and manageable stiffness K. The resistance force of the wall on the object (if it has made contact) is then:

$$R = K(x - x_0) \tag{8-35}$$

The object will then deform into the wall until the resistance force equals the applied force. Consider now that the object was assumed to contact an imaginary wall a distance δ from the real wall. The resistance force is now:

$$R = K(x - x_0 + \delta) \tag{8-36}$$

If the value of δ were set up so that it was equal to the amount that the object would have deformed into the wall. Then the object would appear to come to rest against the wall, simulating infinite stiffness, Figure 8-28 (d).

The algorithm below could be used within an iterative system to evaluate the virtual displacement factor δ.

- Initially $\delta = 0$
- Do until convergence:
  - $R = K(x-x_0+\delta)$
  - Residual = R - F
  - $x = x +$ Residual/K
  - $\delta = \delta + x - x_0$
- End Do.

This algorithm was applied as a trial to a one degree of freedom system and it was found that for linear stiffness the correct value of δ was found within two iterations. For quadratic stiffness, satisfactory convergence was attained within ten iterations.

Infinite stiffness can now be modelled within the numeric system, but it would be desirable to be able to model stiffness that is finite, but too large to be handled numerically. It will be shown here how a subtle adjustment to the algorithm can give this capability.

If the number of iterations that have been completed in the process is given the index i, then the previous scheme for infinite stiffness can be written:

$$\begin{aligned} \delta_{i+1} &= \delta_i + x_{i+1} \\ R_{i+1} &= K(x_{i+1} + \delta_{i+1}) \end{aligned} \qquad \textbf{(8-37)}$$

Modify the system by the factor α to give:

$$\begin{aligned} \delta_{i+1} &= \delta_i + x_{i+1} \\ R_{i+1} &= K(x_{i+1} + \alpha\,\delta_{i+1}) \end{aligned} \qquad \textbf{(8-38)}$$

Under this system, it can be shown that the virtual displacement factor at the ith iteration may be written as:

$$\delta_i = \frac{F}{K}\left[\sum_{n=0}^{i-1} (1-\alpha)^n\right] \qquad \textbf{(8-39)}$$

As the system converges to the final solution, the value of i tends to infinity, at this point the sum may be written as:

$$\delta_\infty = \frac{F}{K}\sum_{n=0}^{\infty}(1-\alpha)^n = \frac{F}{K}\frac{1}{\alpha} \qquad 0\le\alpha<1 \tag{8-40}$$

The final displacement can then be calculated:

$$x_\infty = \frac{F}{K}\left(\frac{1-\alpha}{\alpha}\right) \tag{8-41}$$

If the stiffness is assumed constant then the simulated stiffness may be calculated as the applied force divided by the displacement:

$$K' = \frac{F}{x_\infty} = K\left(\frac{\alpha}{1-\alpha}\right) \qquad \therefore\frac{K'}{K} = \frac{\alpha}{1-\alpha} \tag{8-42}$$

Assume that the two stiffness values are known (and constant) K' is the true stiffness that is of a high value and that K is the stiffness being used by the numeric process and is of a smaller value to avoid precision difficulties. The value of α to be used within the algorithm is then:

$$\alpha = \frac{K'}{K+K'} \tag{8-43}$$

8.3.4 Extension Stiffness

The fibre is modelled as a rod of elastic material, the extension properties of the rod are proposed to be those that would match a linear elastic helix. The rod would then be formed of nonlinear elastic material.

Equations governing the extension deformation of a helix were derived. Algorithms were found for calculating the internal force and stiffness in the helix given the extension, the elastic properties and the initial geometry.

These assumptions were coded into the finite element analysis. Several test cases revealed that for any reasonable fibrous deformation the helical equations were an unnecessary complication. A far simpler model could be developed for the extension without significant change in the results of the analysis. There are two stages to the extension of a helix, before the fibre straightens the stiffness is almost constant, after straightening the stiffness is orders of magnitude greater. It was found that once a fibre got close to straightening the stiffness would become so large that there would be little further extension of the fibre, a satisfactory result would be given by any sufficiently

large number. Similarly, when the fibre is in compression inevitably the fibre would buckle rather than sustain any significant compression force. A new extension model was therefore developed based on two constant elastic stiffness values, one before and one after straightening. A transition zone was also introduced to aid numerical convergence.

8.3.5 Modal Stiffness Matrix

An example will be shown of how the terms of the modal stiffness matrix are calculated for one energy mechanism.

The modal stiffness matrix requires numerical integration in one direction, the integration can be written over the range h=-1 to h=+1, where h is the height on the element, and is defined in Figure 8-29.

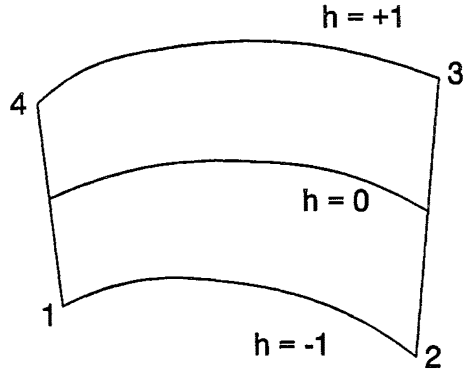

Figure 8-29 *Modal stiffness matrix requires integration over the element height.*

Notice that each value of h represents a different fibre piece within the element, the properties of this fibre must be defined in terms of the modes of the element. As an example, consider the bending modes of the element. The bending energy in a single fibre may be written in terms of the rotations at either end of the fibre:

$$E_B = E_B(r_1, r_2) \tag{8-44}$$

The fibre end rotations may be written in terms of the modal displacements of the element, and the height of the fibre on the element:

$$\begin{aligned} r_1 &= (\beta_9+\beta_7)+h(\beta_6+\beta_8) \\ r_2 &= (\beta_9-\beta_7)+h(\beta_6-\beta_8) \end{aligned} \tag{8-45}$$

Substitution will give an equation for the energy in terms of the modal values:

$$E_B = E_B(\beta_6, \beta_7, \beta_8, \beta_9, h) \tag{8-46}$$

Derivatives of the bending energy will give the contribution of this fibre to the bending terms of the modal stiffness matrix. Integration over the range of h will give the complete bending terms:

$$\int_{h=-1}^{h=1} \frac{\partial^2 E_B}{\partial \beta_i \partial \beta_j} dh \quad i=6...9,\ j=6...9 \tag{8-47}$$

The other sets of terms of the modal stiffness matrix may be found similarly.

8.4 Equation Solution

The finite element system now presents a set of nonlinear equations to be solved. This section describes the scheme that was used for the solution process and the methods that were used to enforce the various constraints and boundary conditions on the solution.

Modifications to the solution scheme were introduced in an attempt to improve the convergence characteristics of the equation system. The modifications described here are only those that could apply to any set of equations, enhancements that are unique to the modal analysis approach are discussed in other sections.

8.4.1 Solution Procedure

Nonlinear structural finite element analysis is usually solved using a form of the Newton-Raphson method and this fibrous analysis is no exception. Newtons method is the natural choice because the Jacobian matrix required within this solution process is the tangent stiffness matrix of the structural system.

The full Newton-Raphson method requires the tangent stiffness matrix to be updated at every iteration, this is computationally expensive and a simpler modified Newton-Raphson method can usually be found which would work out to be more efficient. For the fibrous assembly however, the highly nonlinear nature of the system makes it prudent to use the full method initially, simplifying to a modified method if convergence is attained easily. Convergence was never found without difficulty, consequently the decision was made to use the full Newton-Raphson method for all the analyses.

The analysis is broken into three levels for solution, steps, increments, and iterations.

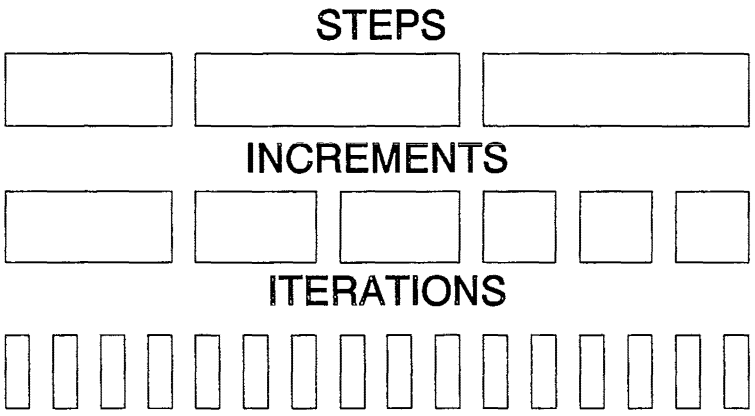

Figure 8-30 *Structure of the solution process.*

Steps

Most simple analyses will only have one step and within a step the boundary conditions, constraints, and applied forces do not significantly change. A linear variation of these is allowed within a step. Multiple steps might be required if a part of the assembly must be held until a force is applied and then released.

Increments

The name of the increment refers to the increase of any linearly varying forces or boundary conditions within the step. Exactly how many increments there are to be within each step would usually be defined. It is numerically more stable for the forces to be slowly increased, rather than fully applied at the start of the step.

Iterations

Each increment requires a nonlinear iterative solution for the equation system with the relevant applied loading for that increment. This requires an unknown number of iterations, continuing until satisfactory convergence is obtained. The geometry of the system is updated after every iteration.

Convergence Criteria

The convergence criteria used by the analysis are limits set on the maximum out-of-balance force and the maximum out-of-balance moment at any node. Convergence limits are set by the user and some care must be taken as results may be significantly affected. If the limits are set too large then the answers may be meaningless because the

resistance forces from the element could be less than the limits giving instant convergence. If the limits are too small then convergence may never be attained, because either it simply takes a long time or the finite precision of the computer precludes such an accurate answer being obtained. A minimum number of iterations within each increment were set, because if an analysis is displacement driven there will be none or very small forces during the early iterations. Without this minimum limit a force based convergence criteria would declare convergence before the system has started to build up any internal stress.

8.4.2 Constraints and Boundary Conditions

Constraints, boundary conditions and applied loads are only applied to the nodes of the system. The applied loads and boundary conditions are very simple to apply to the modal analysis.

If a node is set to have a particular displacement, then the geometry of the element is adjusted before the tangent properties of the element are calculated. The internal force vector of the element then includes all of the internal stress from the displaced node and the element stiffness and forces can be assembled into the complete system without further adjustment.

Applied loads are simpler again to include, the load is added to the system force vector after all the element contributions have been applied.

Nodal constraints are more complicated to enforce. One constraint required is to restrain a node to the extent that it remains on a line between two other nodes, but is free to move along that line. This must be enforced while the position of the two nodes defining the line may be changing. One possible approach would be to modify the element stiffness matrices before adding them into the system matrix, including extra element degrees of freedom linking the nodes of the element to those defining the line.

An alternative approach would be the use of Lagrange multipliers, these modify the system stiffness matrix rather than the element matrix, which is an advantage in the modal analysis. Lagrange multipliers have the disadvantage that they increase the number of degrees of freedom in the total system to decrease the range of deformation patterns (constraint nodes). This was considered acceptable when the flexibility of the approach was taken into account.

Lagrange multipliers work by inserting enough virtual links (one for each degree of freedom constrained) into the system. These links maintain appropriate forces between the constrained nodes to maintain them in their assigned positions.

An equation system can be written in the form:

$$[K]\{D\} = \{R\} \tag{8-48}$$

and could be modified by a constraint:

$$[C]\{D\} = \{Q\} \tag{8-49}$$

Then this may be done by solving the system:

$$\begin{bmatrix} [K] & [C^T] \\ [C] & [0] \end{bmatrix} \begin{Bmatrix} \{D\} \\ \{\lambda\} \end{Bmatrix} = \begin{Bmatrix} \{R\} \\ \{Q\} \end{Bmatrix} \tag{8-50}$$

Assuming that there are three nodes, numbered one to three, it is desirable to constrain the second node to lie on the line defined by the other two. Define that (x,y) for each node are the deformed locations of the nodes. The constraint equation can then be written as:

$$(x_2-x_1)(y_3-y_1)-(x_3-x_1)(y_2-y_1)=0 \tag{8-51}$$

But as the tangent properties are being used within the system, the forms of the equation system and constraint equation are:

$$[K_T]\{dD\} = \{r\} \qquad [C_T]\{dD\} = \{q\} \tag{8-52}$$

The appropriate constraint equation can be found as the derivative of the equation above:

$$\begin{aligned} &du_1(y_2-y_3)+dv_1(-x_2+x_3)+ \\ &du_2(y_3-y_1)+dv_2(-x_3+x_1)+ \\ &du_3(y_1-y_2)+dv_3(-x_1+x_2) = 0 \end{aligned} \tag{8-53}$$

The total system for iterative solution including the Lagrange constraint is then:

$$\begin{bmatrix} [K_T] & [C_T^T] \\ [C_T] & [0] \end{bmatrix} \begin{Bmatrix} \{dD\} \\ \{d\lambda\} \end{Bmatrix} = \begin{Bmatrix} \{r\} \\ \{q\} - \{C'\} \end{Bmatrix} \tag{8-54}$$

Where C' is the value that is found when the original constraint equation is calculated. This value will be zero when the constraint is satisfied.

8.5 ABAQUS

ABAQUS is a nonlinear finite element package and it is one of the most flexible packages available. It is flexible both in terms of the materials and options built in and the amount of user control for strange materials. Initially the fibrous analysis was to be formed as a subroutine to ABAQUS but this was found impractical for reasons stated below.

The USER MATERIAL option from ABAQUS was used for the first attempt at fibrous analysis. In this option the user subroutine supplies the material constitutive properties at every integration point on an element, given the strain conditions at that point. It was found that not enough information was passed from ABAQUS to the subroutine to make it possible for the option to be used for the fibrous analysis.

The USER ELEMENT option was better suited for the fibrous approach. The user subroutine supplies the element tangent stiffness matrix and force vectors, given the current state of the nodes on the element. Using this option means that all that remains for ABAQUS to do is the input, output, element assembly and equation solution. The use of ABAQUS was abandoned in favour of writing a complete package as for all that ABAQUS was doing it was not worth the inflexibility that was brought to the system. The step control algorithms of ABAQUS would be very good in a fully functional system but in development work when the elements may not be behaving properly it was very hard to see what was influencing the solution. The output of variables from within the analysis was also much easier using an independent approach and the ability to track nodal or modal values while the analysis proceeded was important to detecting the problems with the fibrous element.

Although the fibrous analysis is being developed within a fully independent package, once the approach is functional it could be put back into the USER ELEMENT option of ABAQUS. This would then gain the advantages of standardisation of input and output, making applications easier for the users of the fibrous analysis.

9 Elastic Spring Systems

9.1 Model Verification

Verification of the accuracy of a computer model can be obtained in a variety of ways. The results from the model may be compared against the real system which it is intended to model, against a simplified (but still physical) system or against the analytical solution (if it is available) to the governing equation to the problem.

The two dimensional fibrous finite element model was tested against an assembly of springs. This comparison gives better verification of the model than comparison against either an analytical model or a woollen assembly. An analytical model cannot be used as no general governing equation is known for the assembly. It would be possible to find analytic formulae for simpler assemblies but it is likely that solution of these equations could only be found for elementary deformations. It is desirable to test a model in as wide a range of situations as possible and the analytical option is therefore unsuitable. The model could also be compared with a fibrous assembly but this is undesirable as it would be difficult to get good data from an assembly of woollen fibres. Difficulties would arise due to the irregularity of the assembly as well as the very small size of an assembly, even when comprised of a large number of fibres.

A comparison with an array of springs is the best option for testing the model. The springs used were much larger than woollen fibres[9], allowing for simpler experimental technique and the collection of more accurate data. The regularity of the springs meant that a small number could be used, making it possible to keep track of all of the assembly deformations. The physical size of the springs made it possible for them to remain within the two dimensional plane, this would have been difficult with a woollen assembly.

During the modelling process it was necessary to make simplifying assumptions about the material, two of the assumptions were that the fibre material is linearly elastic and that the crimp in the fibres would be modelled by a helical deformation. These assumptions have the effect of making the theoretical fibres act exactly as steel springs,

---

[9] The springs used had a diameter of 23.6mm, a typical yarn diameter would be 1.8mm.

that is, they are linearly elastic and helically wound. The results obtained from the numerical model should therefore be closely related to those from the experiment.

The degree of crimp represented by the springs is considerably more than would ever be found in a woollen fibre but this should not affect the validation of the model. The extra crimp would be interpreted as different theoretical fibre elastic properties. If the model can be shown to be valid for one set of elastic properties, then it follows that it is valid for any other realistic set.

9.2 Experimental Procedure

An assembly of springs was created by attaching nine similar springs to two rigid rods. The springs were attached so that the gaps between them in the lateral direction were equal to the diameter of the springs, and arranged as shown in Figure 9-1. One of the rigid end pieces was attached to the work surface so that it could not move, all of the assembly deformation was therefore achieved by movement of the second rod. The springs were attached to the rods in such a manner as to be fully fixed so that throughout the deformation the springs were perpendicular to the rod and kept a constant position on the rod.

This simple assembly with its limited number of degrees of freedom of movement[10] provided for a surprising variety of deformation patterns. Simple patterns involved only one of either fibre bending or fibre extension. More complicated deformation patterns display some fibre jamming or fibre longitudinal compression, the experiment culminated in deformation patterns exhibiting all of these movements simultaneously.

The assembly of springs was photographed from above, the photographs being the only results from the experiment. A regular grid of 50mm squares was drawn onto the surface underneath the springs. The grid would supply all of the information necessary to both find the correct scale within the photographs and to compensate for any distortion of the images during the photographic process.

---

[10] The assembly has three degrees of freedom, these are the degrees of freedom of movement of the free rigid rod. Two translation degrees of freedom, and one rotation.

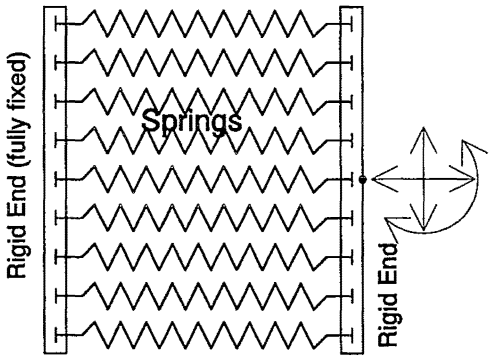

Figure 9-1 *Experimental configuration for spring assembly.*

9.3 Test Configurations

A number of test configurations were photographed, a selection of these were taken for data processing and comparison with the numerical model. The chosen set of configurations were selected such that a wide range of deformations were represented. Eight deformation patterns were chosen, these were labelled *a* through *h* and are in approximate order of increasing difficulty. Pictures of each of these configurations will be provided in the section 9.7.

Configurations were selected which would test the numerical analysis to the fullest extent. The more complicated deformations include a number of features which numerical processes find very difficult to model. Difficult features include lateral compression between the fibres, large openings between the fibres, large deformations and high fibre tension.

9.4 Data Digitization and Transformation

The digitization process was used to extract the coordinates of the centrelines of each spring in the assembly. The transformation was required to allow for the noticeable distortion in the photographs. These two operations result in a set of data describing the displaced positions of the springs in a real coordinate system, ready to be compared directly against any numerical result.

9.4.1 Digitization

A digital planimeter[11] was used to measure the centreline coordinates of each spring in each assembly, this data was then saved to a file. A separate file was used to similarly digitise the coordinates of the grid underneath the springs. In a small percentage of instances the grid point to be digitised was obscured by a spring, a rigid end piece or a hand holding the assembly in place. When this occurred, the position of the grid point was estimated and the effect of this small error was eliminated during the smoothing within the transformation.

It was found to be simple to pick out the centreline of each of the springs in the assemblies. The flash unit of the camera, which was positioned close to the lens, reflected off the top of the curve of the springs, clearly highlighting the top edge (as seen in Figure 9-2).

An example deformation photograph is shown in Figure 9-2, this is the assembly deformation which will be known as test case h.

[11] A digital planimeter can also be called an xy digitiser, it consists of a hinged arm connected to a control box which is in turn connected to a computer. Accurate measurement devices on the hinged joints provide the control box with the information to output the exact coordinate of the crosshair at the end of the arm.

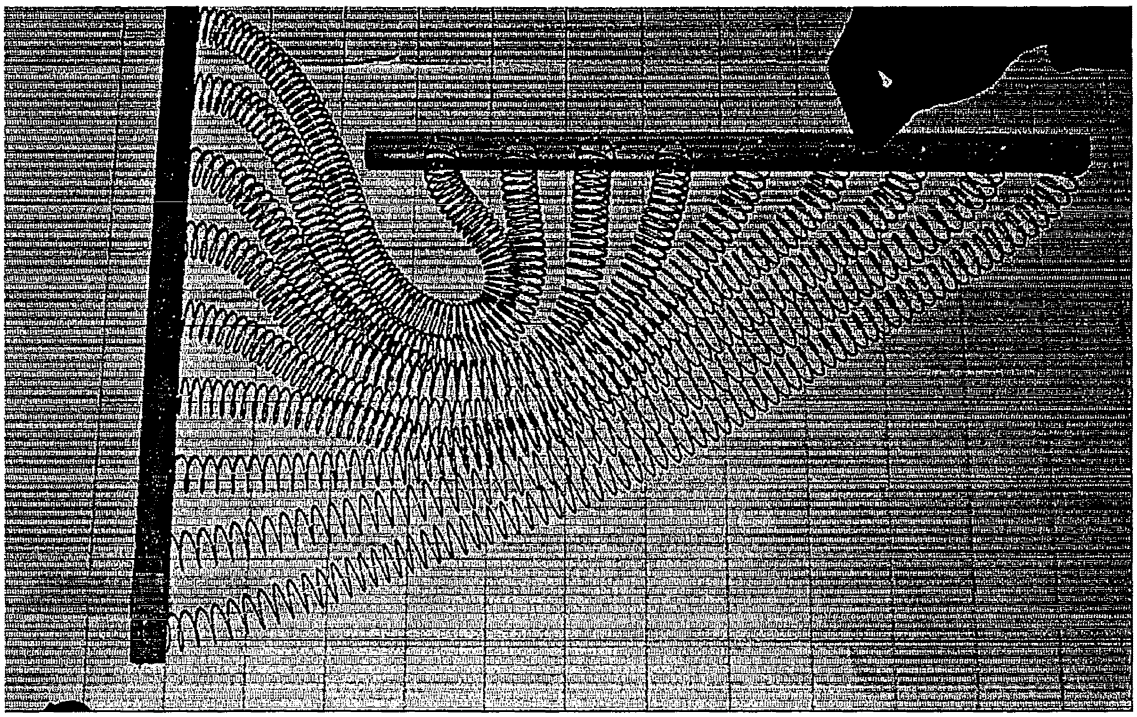

Figure 9-2 *Spring assembly deformation, test case h.*

9.4.2 Transformation

The two reasons which were proposed for requiring the transformation process were both found to have a significant effect on the results. The problem with finding the right scale for the data was complicated by the camera not being exactly vertical or positioned over the centre of the assembly. The scale factor required to convert the digitised data to the real coordinate system then varied over the photograph. The transformation process allowed for this, introducing a smoothly varying scale factor based on the grid digitization. Noticeable distortion was observed in the photographs of the grids and was especially prevalent in straight lines near the edge of the print, which displayed significant curvature.

The transformation also had the advantage of correcting for any consistent error within the digitiser. Both the grid and the springs were digitised from the same photograph at nearly the same time therefore any errors would occur equally in both and be automatically corrected for in the resulting data. One major correction was that the coordinate system used by the digitiser was reversed when compared to the intuitive coordinate system, but the final data was always oriented in the correct manner.

There were occasional small errors in the digitisation of the grid, the process chosen for defining the coordinate transformation also served to smooth the effect of these errors.

The mapping from the digitiser coordinate set to that of the grid was controlled by a parametric mapping. In finite element terms the mapping was that used by a nine point Lagrange element and the mapping is therefore controlled by the coordinates of a three by three grid of points which are spread across the area to be mapped.

The digitized grid was defined by over 200 degrees of freedom, the mapping which relates the photograph grid to the real space is controlled by only eighteen degrees of freedom[12]. This large difference in the number of degrees of freedom introduces the smoothing in the transformation, each digitized degree of freedom can have only a small influence in the mapping. The mapping is capable of reproducing a cubic variation in displacement in each direction over the mapped area. If the photographic distortions are no more complicated than this then the situation would be mapped exactly and only the digitisation errors would be eliminated. This was found to be the case, the matches between the mapping and the original grids were found to be excellent.

The coordinates defining the mapping were found using an iterative process. A Fortran program[13] was written to evaluate these parameters. Based on the knowledge that the original grid was composed of squares with sides of 50mm, an initial (and very rough) approximation was made of the mapping. The initial approximation assumed that the mapping was in error in only a consistent scale factor, ignoring any distortion, rotation or variable scale factor effects. This was found however to be a good starting point and the mapping coordinates were found to converge to satisfactory solutions within three iterations.

The first panel of Figure 9-3 shows the initial guess to the transformation mapping overlaid over the digitised grid. The second panel is the second iteration match, this is visually indistinguishable from the state after any further iterations. It is clear from this figure that although the grid has many more degrees of freedom than the transformation, the distortion is simple enough that it can be mapped sufficiently.

---

[12] There are two degrees of freedom per node (x and y coordinates), and nine nodes defining the mapping.

[13] The program and related programs are discussed in greater detail in Appendix C.

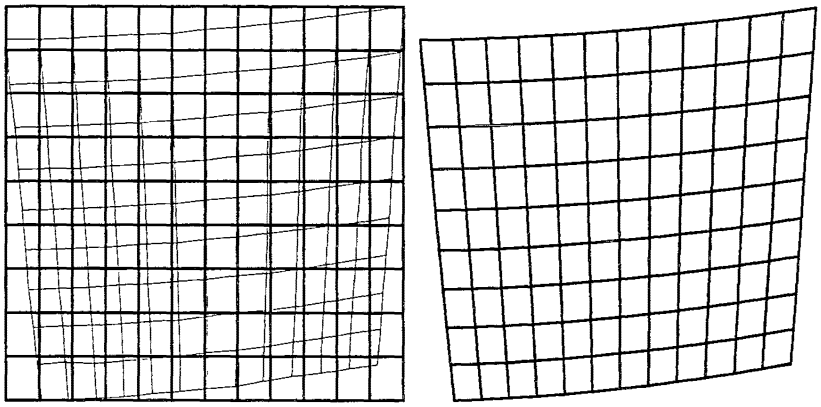

Figure 9-3 *Initial guess and final match for mapping of case h.*

Once the defining coordinates for the mapping were found, they could be used to adjust the spring data. For every coordinate pair defining a point on a spring centreline, a corresponding set of coordinates exists in the real space. This is the reverse transformation of the mapping defined above. Therefore, an iterative scheme must also be developed to find this data. Another Fortran program was written[14] which assumed a initial guess for the coordinate in the centre of the grid. A scheme was used to progressively update the estimates at the coordinates until the proper mapped coordinates were found. This program was found to also have good convergence characteristics for any realistic mapping[15].

Figure 9-4 shows the effect that the adjustment made to the spring data. The two sets of fibre ends most clearly show the influence of the adjustment, both are rigidly attached to straight end pieces and the end points must remain in straight lines. The left hand end should also be in a vertical position. Both of these requirements show considerable improvement from the unadjusted data set to the adjusted data.

[14] Discussed in Appendix C.

[15] If a mapping was multi-valued, or close to singular, the iterative scheme would not converge. However these situations would never arise in a realistic situation.

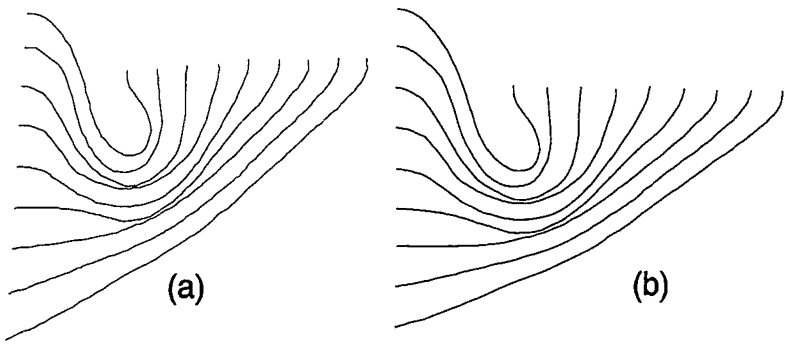

Figure 9-4 *Unadjusted (a) and adjusted (b) spring data for test case h.*

9.5 Assessment of Spring Properties

A typical spring was chosen to be tested to assess the physical properties of the spring. In theory, once the elastic properties of the steel (from which the springs were made) was known then the properties of the spring may be calculated.

The physical dimensions of the spring were measured as:

Spring Length	0.4430m
External Helix Diameter	0.0236m
Wire Diameter	0.00072m
Helix Turns	65 turns

The test spring was then suspended from a hook while weights were added to the other end. The resultant displacement was then measured. Both ends of the spring were restrained so that no end rotation could take place, allowing end rotation would have increased the flexibility of the spring. A plot of the results from this test is given in Figure 9-5.

The measured force/displacement relationship for the spring is shown to be linear and a linear regression fit to this plot has an R-squared value of 0.9998. At the maximum extension the test spring was three times as long as in the undeformed state.

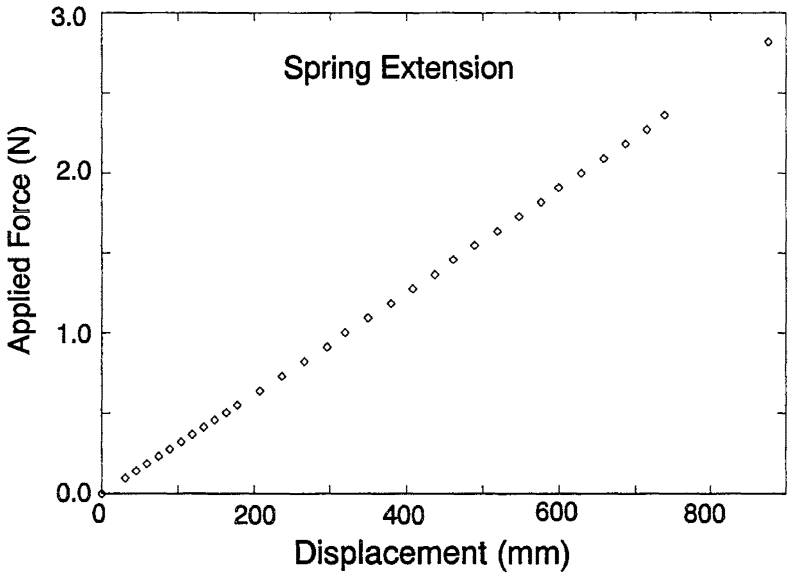

Figure 9-5 *Force vs Extension for test spring.*

The shear modulus of the steel could then be easily calculated and with the assumption of a Poisson's ratio of 0.3 (typical for steel), the Young's modulus. Both the shear and Young's modulus that were calculated are shown below.

G = 76.281 GPa
E = 198.33 GPa

Both are reasonable values for spring steel.

Originally higher order effects were to be included in the material properties, such as stiffening of the spring as the helix tends towards a straight line. But due to the large linear range of the spring compared to the relatively small extensions which the springs undergo during testing, the second order effects were not included. This is because of the high helix angle of the undeformed helix. This does not imply that for a general fibrous assembly it would be accurate to ignore these second order effects, the simplifying assumption only applies for the steel springs.

9.6 Numerical Analysis

The two dimensional fibrous finite element program developed in a previous chapter was used to generate numerical analogues to each of the eight test cases.

9.6.1 Element Mesh

The chosen mesh was composed of 64 elements, arranged in an eight by eight grid. Eight elements were chosen in the direction perpendicular to the fibre direction because this results in nine lines in the fibre direction when the element grid is drawn, which is the same as the number of springs, allowing a simple comparison. Eight elements were chosen in the longitudinal direction, this was assumed to be the minimum to give a reasonable result. Some analyses were attempted with sixteen elements in the longitudinal direction to see if better system convergence properties could be attained using shorter elements. The improvement in convergence was not found to be significant and the extra elements led to an increase in the computational time required.

The enforced displacement on the mesh is controlled by the movement of the two ends. For each test case these displacements were chosen to match that of the real case. Measurements of the values were made from plots of the spring centreline data after it had been adjusted for photographic deformations.

9.6.2 Boundary Conditions

The mesh boundary conditions were initially set using two different methods. The left side of the mesh had to be restrained so that there was no movement, the degrees of freedom along this edge were therefore set to zero. On the right hand end the degrees of freedom had to change so that the nodes remain on a straight line, and that the fibre direction is at right angles to that line. A series of Lagrange constraints were used to enforce these conditions. It was found that the system converged very slowly using this system, part of the problem being the loss in data precision due to the way that the Lagrange constraints adjust the system matrices. The constraint on the right hand side was then re-worked so that the values of each degree of freedom along the edge was specified, this system was found to converge faster for small and moderate deformations.

Under large deformations the assembly often either did not converge or converged to a solution which was very different to the real case. The reasons for these problems were found and both had the same solution, an adjustment to the way in which the boundary conditions were applied to the right hand end was required.

Both problems are due to the fact that the boundary conditions are applied to the system linearly across the step. This linear application applies to both the coordinate positions

of the nodal points and the fibre directions at those points. A linear variation of coordinate does not imply a linear variation in the angle of the line connecting those points, so the fibre direction does not remain at right angles to the mesh end. In extreme cases this can result in the development of impossible situations, including highly jammed or reversed elements, either of which cause extreme convergence difficulties.

The final configuration of the system solution can be path dependent for fibrous systems and this is most likely when the fibres are buckling. Normally a fibre will buckle into a first mode deformation (single curvature) but often certain deformation paths combined with the fibre jamming against other fibres could cause the fibre to find a stable situation in a second or third mode deformation pattern. The linear stepping of the boundary conditions was applying the end movement in an unnatural way and was causing the fibres to find unusual final configurations.

To solve these problems the input data was modified to have multiple (ten) steps rather than one single step. At the start and end of each step the fibres were all at right angles to the assembly end and the end was the same length as it was originally. During the step there would be some variation from these two constraints but as the steps were small it would not change the final solution. The systems were found to have improved convergence after these changes.

Due to the multi-step nature of the input data, the files became very large and cumbersome. To simplify data input a program was written which takes as input the gross size of the assembly and the final position of the rigid end and creates an input file ready for execution. Versions of the program were written to accommodate either eight or sixteen elements along the fibre length.

9.6.3 Lateral Jamming Values

A value for the lateral jam limit for the assembly had to be chosen, this value is the element width (as a percentage of the original width) where the fibres begin to touch one another. In a real fibrous system some fibres touch one another all of the time but there will be a point at which the lateral effects begin to have a significant influence on the system solution. This is the point that the jamming value is assumed to indicate.

The elastic spring system which is being analysed has an initial spacing between each spring of one spring diameter, therefore the theoretical value for the jam limit is 50

percent. Other effects also have an influence on what this value should be, most significantly the possibility that the springs will mesh together. When this happens the springs easily overlap without appreciable energy increase and the jam situation will not occur until a position at a closer spacing than 50 percent.

In order to establish the value which should be used for the jam limit, two test cases were chosen and a number of runs were done on each at a variety of jam limits.

The first of the two cases chosen was test case c, the jam value varied from 0.1 to 0.9 in increments of 0.1. Plots of the deformed finite element mesh (light lines) overlaying the actual spring lines (heavy lines) are given in Figure 9-6.

The effect of the increasing jam limit can be seen in the innermost elements, with the very low jam points the element sides come close to touching in the centre of the mesh. As the jam limit increases, the distance between these element sides at the closest point steadily increases.

It appears that a value of 0.4 for the jam point provides the best approximation to the real situation. This value is reasonable as it is slightly less than the theoretical value of 0.5. It is interesting to note what happens to the deformed mesh as the jam point climbs up to 90%. As the assembly begins to jam earlier, the central elements resist further lateral compression when they are in a more open state. The *larger* elements require more space in the centre of the mesh and the lower elements are forced to move. Eventually (at a value of 0.8) the lower element edges become too compressed longitudinally to be stable and buckle outwards to assume a new stable state. At a value of 0.9 two of the fibres have buckled and the next two in the assembly look as if they are on the point of also buckling.

Test case h was used for the second set of trials, here the range of jam values was from 0.05 to 0.45 in steps of 0.05. The plots of these deformations are shown in Figure 9-7.

The influence that the varying jam point had on the deformed mesh is clear in the plots, the bottom loop of the top element edge moves steadily from left to right as the value increases. This is caused by the near vertical element edges just to the left of that loop progressively jamming and pushing the loop away from the left.

The modelling of the lower edge of the bottom row of elements of this assembly is not accurate, this edge is in tension and develops almost a straight line in the numerical

model. In the real situation the spring helices do not mesh perfectly and they tend to

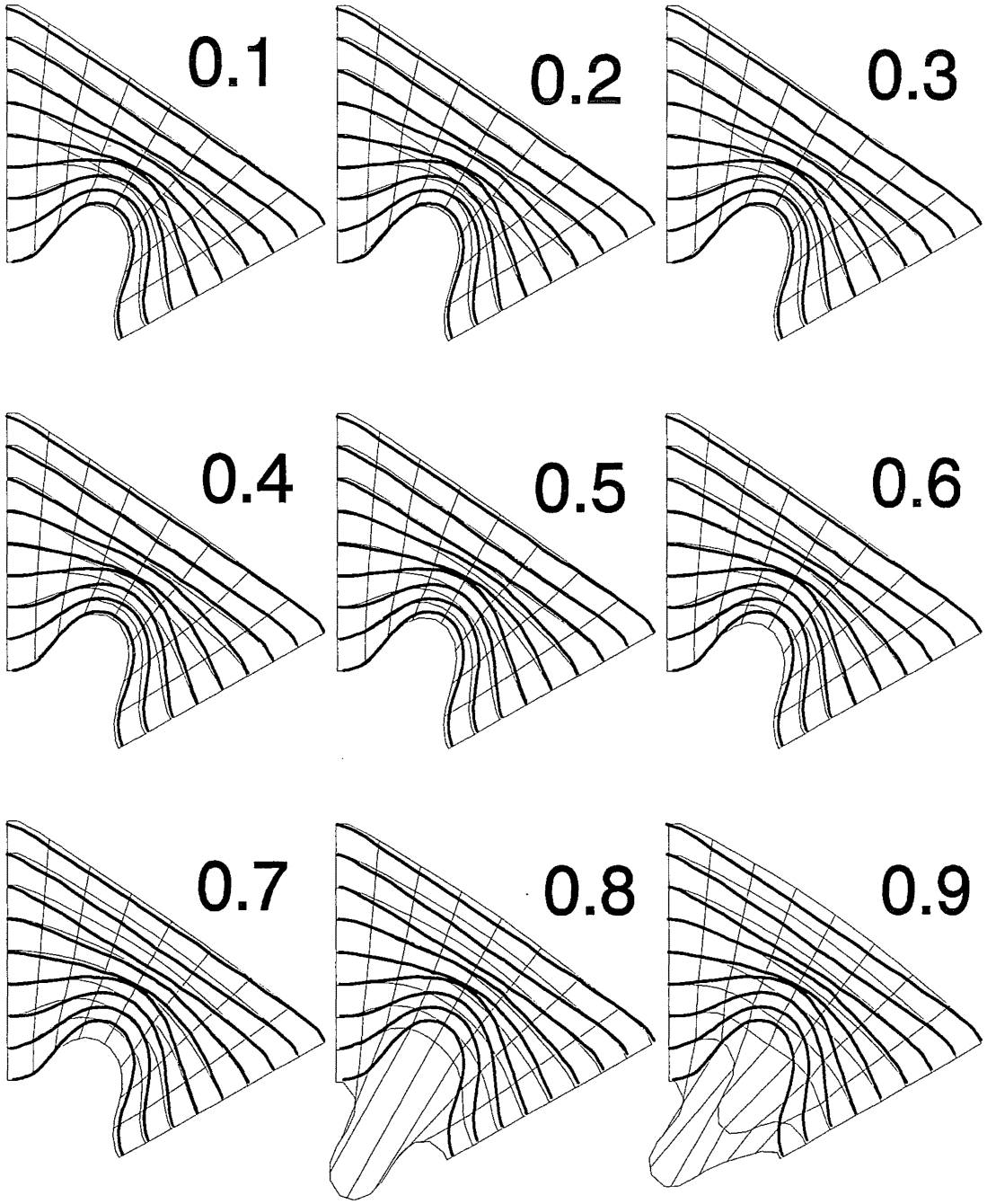

Figure 9-6 *Test case 'c', Numeric solution with a variety of jam values.*

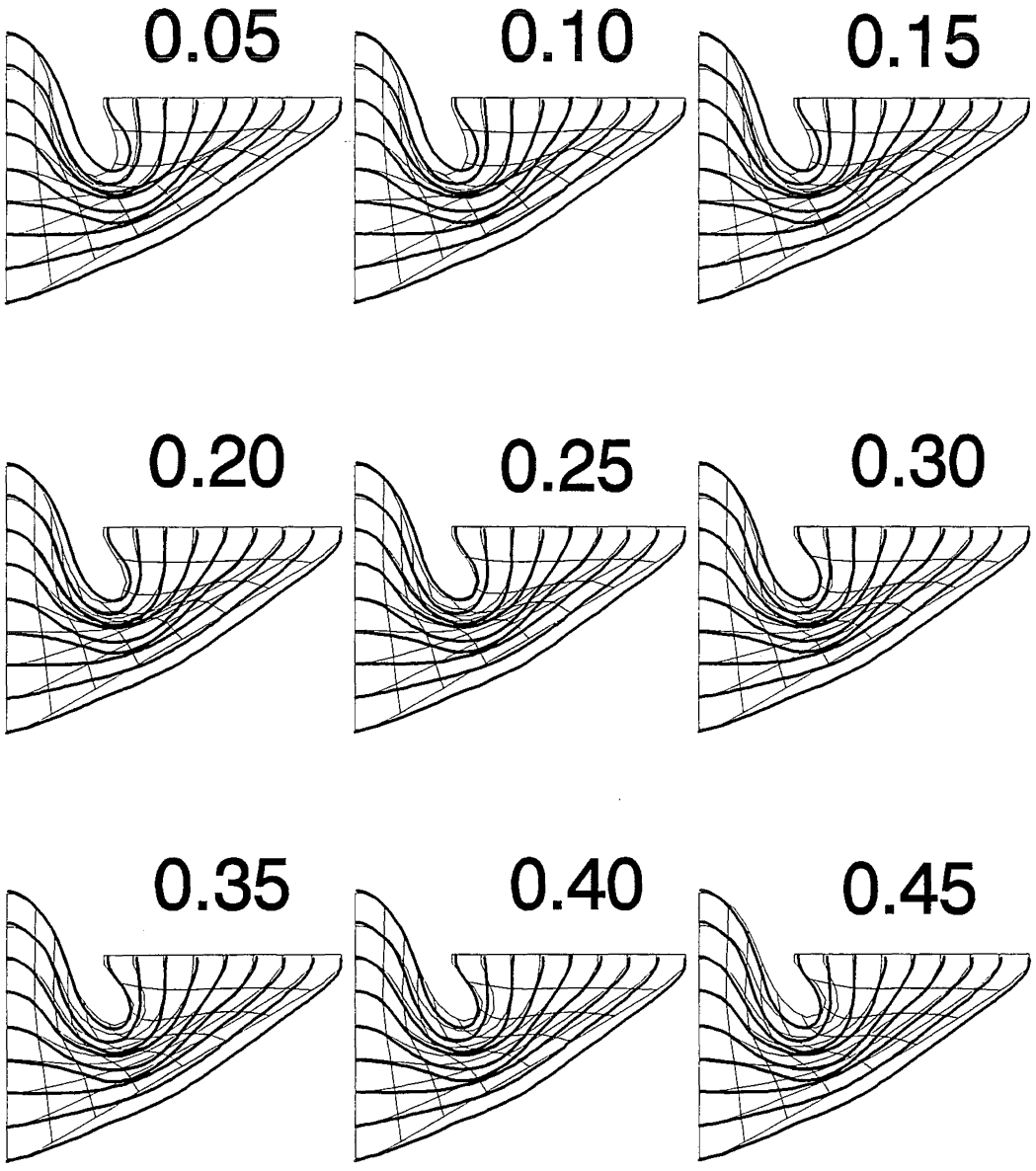

Figure 9-7 *Test case 'h', Numeric solution with a variety of jam values.*

catch on one another. For this reason the model tends to be inaccurate when two edges are aligned over a significant length at the same time as being laterally compressed. A solution for this problem would involve a detailed investigation into how helices merge together and possibly the incorporation of a jam limit which varies over the mesh depending on the deformed configuration. Such an investigation is beyond the scope of this work.

Based on the two cases described above, a jam value of 40% was chosen for the remaining cases. This value was the only used in the final analyses shown in the next section.

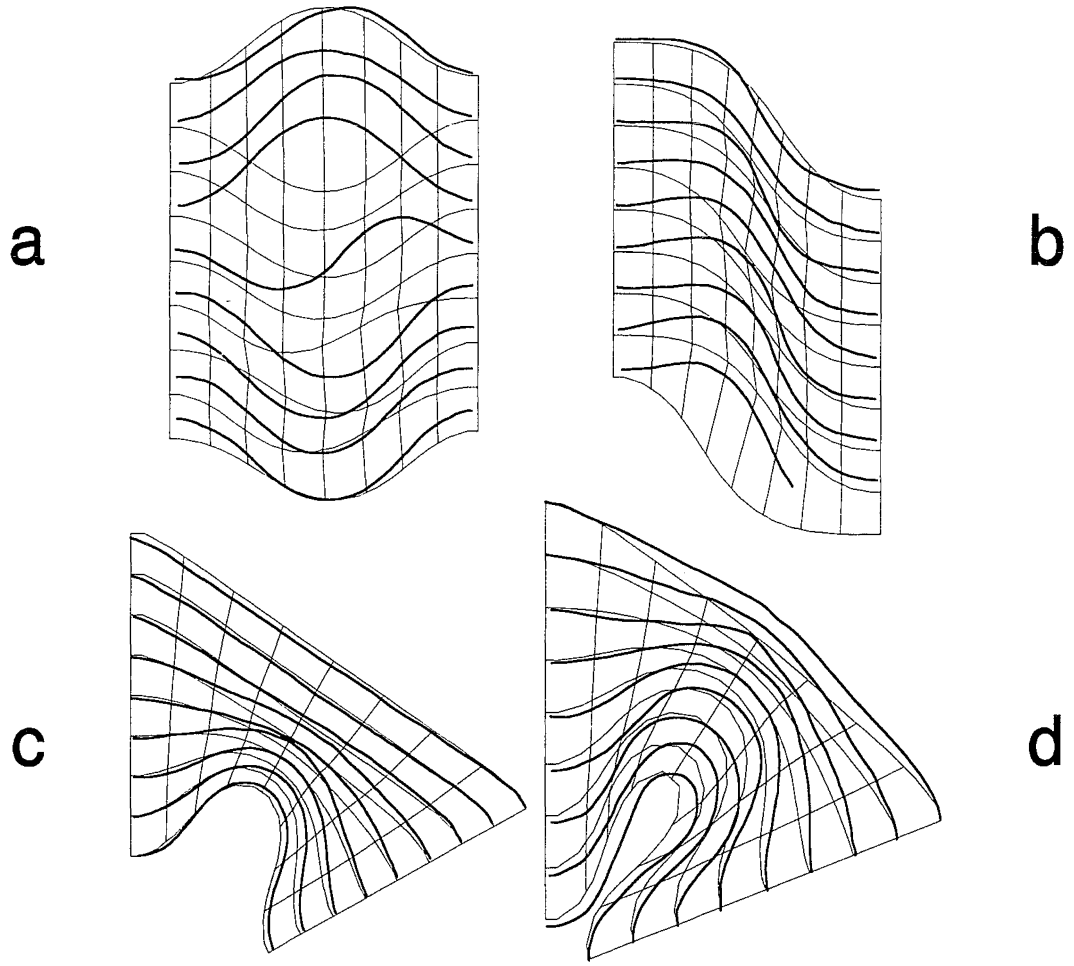

Figure 9-8 *Final Comparison, test cases a-d.*

9.7 Results

This section presents the comparison between the numeric solution and each of the eight test cases, using a jam point of 40%. In an overall sense the numerical model was found to agree well with the spring experiment.

The results are shown in Figure 9-8, Figure 9-9. The measured spring centrelines are the heavy lines and the deformed finite element meshes are the light lines.

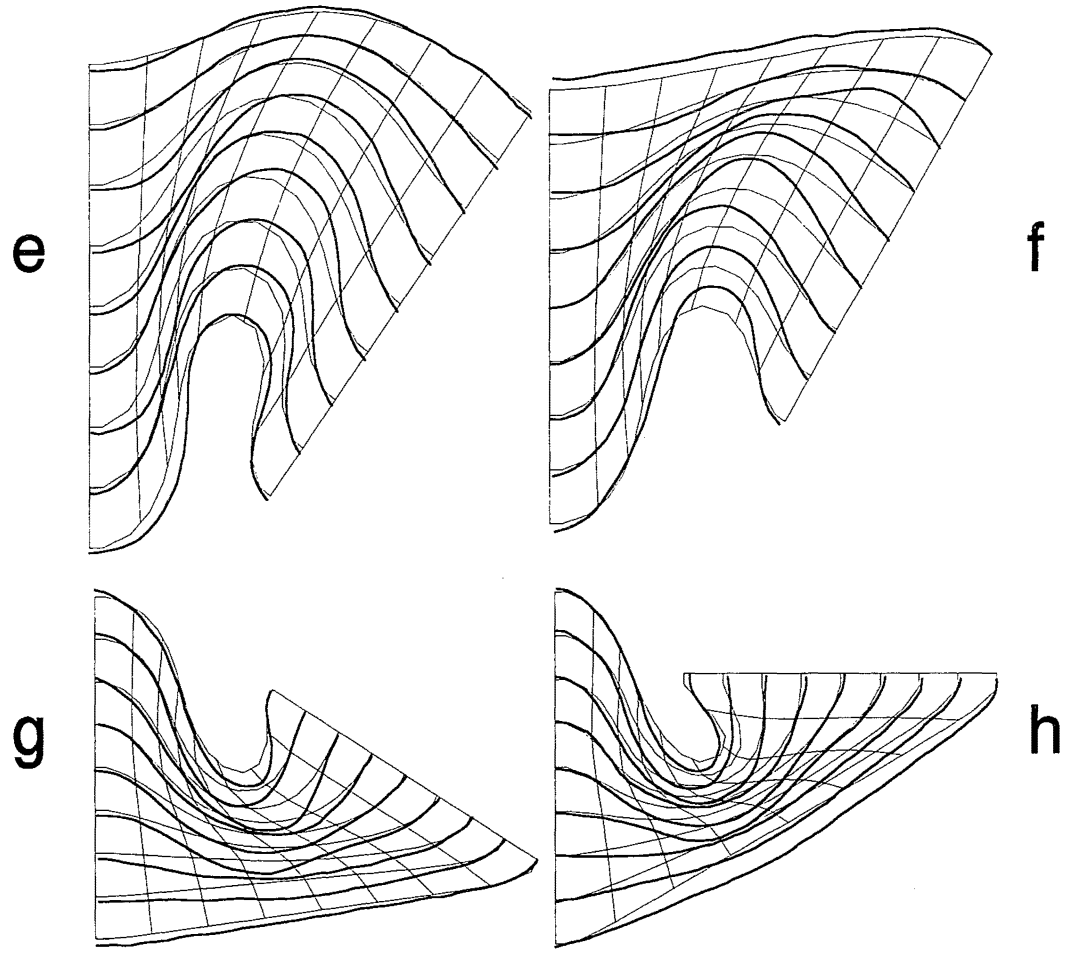

Figure 9-9 *Final Comparison, test cases e-h.*

Case a

This result is not as bad as it might look at first glance. When a straight fibre is compressed axially it will tend to buckle and the direction that it will buckle in is governed by any small imperfections in the fibre. In the case of the numerical analysis, the buckling direction will be decided by the random accumulation of small numerical errors until they become significant enough to influence the solution. Because no attempt is made to measure the initial imperfections of the spring and build these into the numeric model, there is no reason to expect on the buckle in the same direction as the other. What is important to note is that the shape of eight of the nine fibres are similar in the real and numerical cases. There is one spring which has quite a different

shape, the initial imperfections in the middle fibre were such that under compression it deformed into a second mode configuration (double curvature) rather than the normal first mode (single curvature). This can happen in a real situation due to the small amount of friction between the springs and the work surface.

Case b

The curvature in the springs in case b is higher than in the numerical solution, this is caused by the spring-table friction as noted in the discussion of case a. The springs were dragged sideways across the table, dragging the ends a little due to friction, therefore increasing the curvature in the middle section of the assembly.

The bottom fibre of this case is incomplete, this is because the fibre passed off the frame of the photograph and therefore no data was available.

Case c

Case c has a good match between the spring data and the element mesh. The middle fibres are slightly different but this can be blamed on the simple helix meshing assumptions. The sizes of the gaps between parallel fibres through the middle of this assembly are quite irregular. This is due to some of the helices meshing well and others not at all. The numeric process shows a consistent behaviour and the results do not vary too much from the spring lines.

Case d

Case d shows a reasonable match between experimental and numerical results. The bending in the top fibres is not fully represented as this is caused by the complicated helix meshing procedure giving larger jam points. In trials which are not shown here, some runs were performed with very high jam points. This caused the outer fibres to show this bending although the rest of the deformed mesh exhibited a worse fit.

The position of the centre loop of this mesh does not line up with the springs. Both the springs and the mesh should be symmetrical and match in the middle. What has happened is the both have assumed a small degree of asymmetry but in different directions. The springs are out of shape due to the friction problem mentioned earlier. The numerical model does not achieve a fully symmetric state due to the nature of the convergence process. The system does not iterate on the solution for ever, but only

until certain tolerances on the out of balance forces are attained. In this case the point was found with the centre of the fibre still a small distance off the *ideal* position.

Cases e-h

Each of these four cases provided a good comparison between the computational and experimental results. Any differences can be explained using the arguments covered in cases a to d.

10 Three Dimensional Model (I)

The three dimensional model is based on the same modal techniques which were developed and implemented for the two dimensional model. The degrees of freedom describing this element are defined in a manner similar to those of the earlier element.

The highlights of the difficulties which were encountered during the development of this model are outlined. The problems which have been particularly difficult have been presented within individual subsections. The remaining points are covered in the general modelling subsection (10.2).

10.1 Degrees of Freedom

The three subsections below outline the definition of the degrees of freedom and the transformation equations of the three dimensional element. The order in which the three sections are presented does not indicate the order in which they were developed. The definitions within each section influence those in the other sections, forcing them to be developed as a whole.

The configuration presented is the best arrangement that was found but is unlikely to be the optimum solution. Time constraints have meant that early decisions made regarding the form of the three dimensional element have been unable to be changed. Although the major decisions stand firm the development was an iterative process. Many of the options tested during the development process will not be mentioned here, only a small number of the significant changes will be discussed.

10.1.1 Nodal Degrees of freedom

It was decided that the element have a cuboid shape in the neutral configuration with the fibres aligned in a vertical direction. There are eight nodes on the element, one on each corner of the cube. Each node has six degrees of freedom, three translations and three rotations.

This combination of degrees of freedom allowed the element to represent a cubic displacement variation in the direction parallel with the fibre and a linear variation in

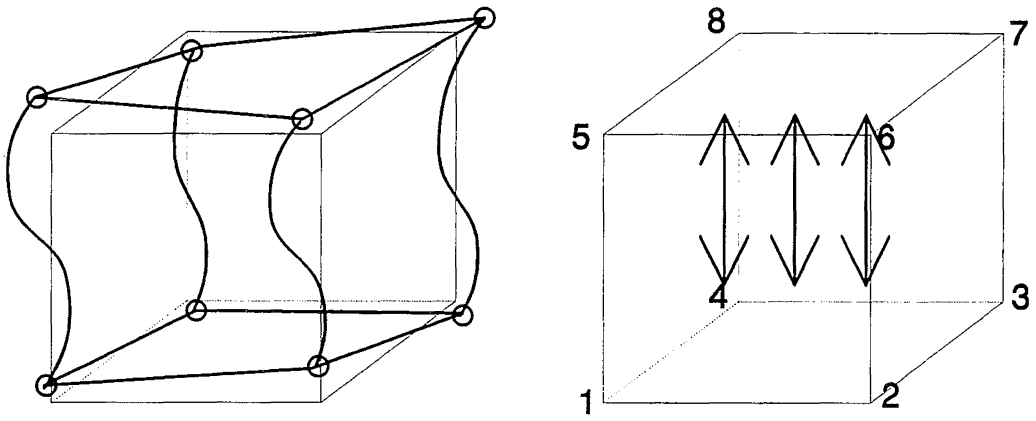

Figure 10-1 *Sample deformation pattern and nodal numbering of the three dimensional element.*

the directions perpendicular to the fibre (Figure 10-1).

Figure 10-1 also shows the numbering of the nodes on the element and the direction of the aligned fibres. The top and bottom of the element as shown are often referred to as the element ends, while the other four faces of the cube are the element sides. These names are based on the fibre alignment and are significant as the permissible displacement patterns for the ends are different from those for the sides.

This element has 48 degrees of freedom[16]. The increase in the storage space required for computing implied by this is significant. The element stiffness matrix and the first derivative tensors now have 48 by 48 elements (2304) as opposed to 12 by 12 (144) for the two dimensional element. The second derivative tensor now has 110592 components (48*48*48) which is significantly larger than the two dimensional element (1728). The space required for the total system matrix is also increased, this is due not only to the larger size of the contributing matrices but also the three dimensional configuration means that each element is now connected to a larger number of other elements,

[16] Six degrees of freedom per node and eight nodes.

increasing the connectivity and complexity of the system matrix. The work required for the formulation of the element stiffness matrix is scaled similarly to the storage space.

This element was chosen as it was thought to be the minimum configuration which would be able to model the fibrous assembly. The analysis would take significant resources on even mid-sized to large computers and it was for this reason that the minimum usable configuration was sought.

The nodal degrees of freedom of the element were numbered from one to 48, all the degrees of freedom of each type were numbered together.

Degrees of Freedom	Description
1-8	X-direction translation for nodes 1-8
9-16	Y-direction translation for nodes 1-8
17-24	Z-direction translation for nodes 1-8
25-32	Rotation about the X axis for nodes 1-8
33-40	Rotation about the Y axis for nodes 1-8
41-48	Rotation about the Z axis for nodes 1-8

Rotation degrees of freedom.

It was found during the writing of the three dimensional finite element program that having the fibre direction at a node defined by three rotations does not work when applied to a large displacement formulation. There are three items of information which must be extracted from these three rotations, the amount of twist in the fibre (one) and the fibre orientation direction (two)[17]. It was found that there is no unique definition that will in general give this data from the global rotations. The program was modified so that for every node in the system a fibre direction vector (which was always normalised to have unit length) and a fibre twist component were maintained. When the global system was assembled for each linear iteration the equations were assembled in terms of the three rotations, but the results from this step were then used to update the fibre direction vector and twist for each node. This solution introduced significant complication into the definition of the transformation equations (see section 10.1.3).

---

[17] A direction would normally be described in three dimensional space using a vector of three components, the assumption of unit length for the vector reduces this to two.

10.1.2 Modal Degrees of freedom

To coincide with the number of nodal degrees of freedom 48 modes are required to describe the deformation of the three dimensional element. The modes are broken into six groups depending on type of deformation being applied to the element.

Mode Numbers	Description
1-6	Element rigid body modes.
7-10	Fibre extension modes.
11-18	Element jam modes.
19-34	Fibre bending modes.
35-42	Fibre torsion modes.
43-48	Element shear modes.

A description of each of the modes is given below. For each mode two diagrams will be shown, the first is a representation of the forces which are induced in the element by the application of force in only that mode. The second diagram is a picture of the displaced shape of the element after a small displacement in only that mode. The induced forces from each mode are found from the respective column of the first derivative matrix of the transformation equations. Each column represents the nodal forces from that mode, these are found by multiplying the matrix by a vector of the modal forces[18].

The displaced shaped of each mode are found from the respective columns of the inverse of the first derivative matrix. The inverse matrix is never calculated during the finite element process but has been calculated for display purposes. These graphic representations of the element mode shapes were critical in determining a number of the faults which the equations developed.

Rigid Body Modes

There are six rigid body modes for the three dimensional element, translations in each of the three axis directions and rotations about each of the axes.

---

[18] Refer to section 7.2.

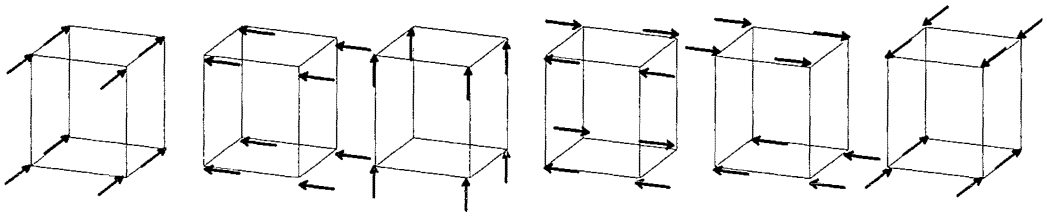

Figure 10-2 *Induced forces in the rigid body modes.*

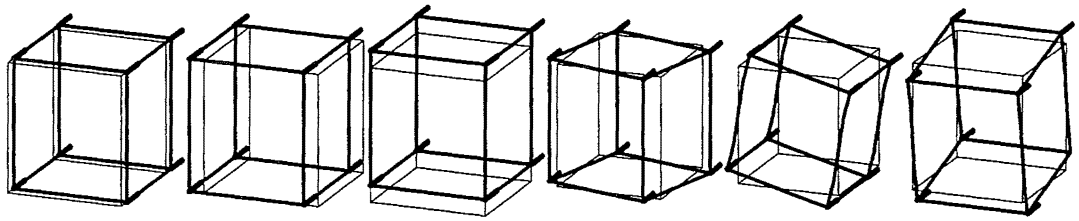

Figure 10-3 *Mode shapes of the rigid body modes.*

The first of the rigid body modes induces exactly eight equal forces, one from each of the corners and all in the same direction. This direction is the x-axis and this first mode represents the rigid body translation of the element in the x direction. The plot of the mode shape indicates the x translation.

Similarly the second and third rigid body modes are translations in the other two coordinate directions.

The fourth mode induced forces indicate that this mode also has eight forces of equal magnitude. In this case, half of the forces are in the opposite direction to the other half, all of the forces are aligned with the y-axis. This arrangement of forces creates a couple about the z-axis and this mode is a rigid body rotation of the element about the z-axis. The mode shape of this fourth mode does show a rigid rotation.

Despite the fact that the couple of induced forces in the fourth mode was generated by forces solely in the y-direction, the resultant mode shape shows no bias towards any of the axis directions. This is a feature of the mode shapes, the inversion of the first derivative (induced forces) matrix has given a matrix where each of the columns is orthogonal to the other. The orthogonality implies that the displacement pattern which comprises each mode contains no part of any other mode.

The fifth rigid body mode is a rigid rotation about the x-axis. The induced force plot in this case looks a little different to that of the previous mode. The couple in this case spans the height of the element and is therefore along one of the fibre sides, because there is no fibre rotation at the nodes of the element there are no induced moments at the nodes. There are still only eight forces of equal magnitude being applied in this case. The mode shape plot has eliminated the bent sides and shows a pure rotation about the x-axis. The remaining rigid body mode is similar and represents a rotation about the y-axis.

By definition these rigid body modes do not introduce any internal stresses into the element, the plots of the mode shapes show that this is the case. In each of the six cases the element is moved as a whole.

The small tag attached to each corner of all of the element plots is a representation of the fibre twist (the rotation component about the fibre axis). In the mode shape plots rotation of the tag indicates a twisting of the fibre at the node. None of the rigid body modes induce any twist moments or give any fibre twist.

Extension Modes

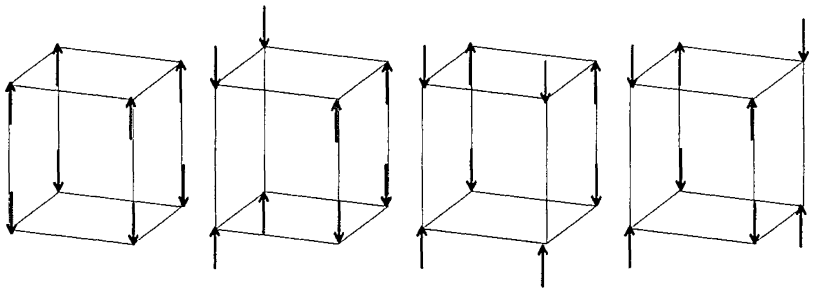

Figure 10-4 *Induced forces in the extension modes.*

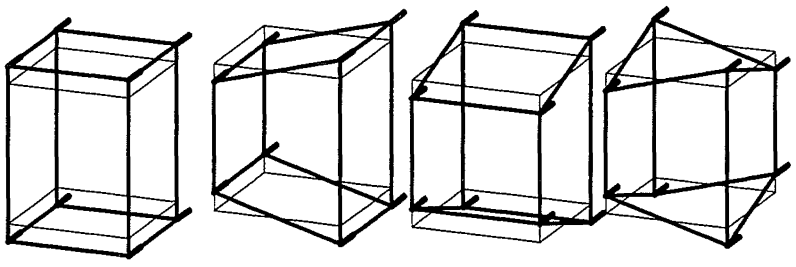

Figure 10-5 *Mode shapes of the extension modes.*

The extension modes are very simple as displayed in the pictures above. There are four modes, the combination can give a linear interpolation of the fibre length across the element. The first mode represents the average fibre length, the other three are different patterns of variation over the element cross section.

The plots for the induced forces and those for the mode shapes are almost identical for these modes. This is because in this configuration the modes are very simple and there is no component from other mode types in the induced forces.

All of these plots are based on an element with an initial distortion of zero, the mode shapes would be different if the element were initially bent or had any other distortion. The mode shapes of the element are dynamically changing throughout the analysis, depending on the state of the element at the start of the iteration.

Jamming Modes

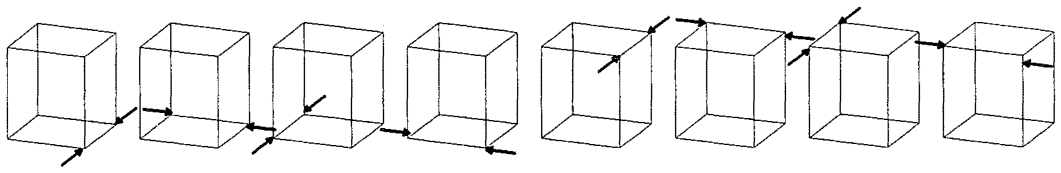

Figure 10-6 *Induced forces in the jamming modes.*

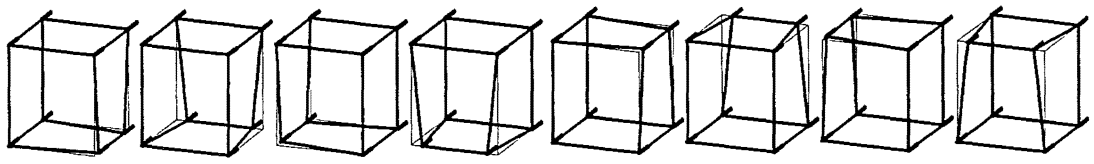

Figure 10-7 *Mode shapes of the jamming modes.*

The jamming modes have proved some of the most difficult modes in which to achieve the correct formulation. There is a compromise in the formulation of these modes between choosing a mode configuration which is too simple to allow the solution of the equation system, or setting the mode up in such a way that the source code becomes far

too cumbersome and complicated to use. It is possible that with the present choice of nodal degrees of freedom there is no suitable selection for the jamming modes. The modes shown above are one of the simplest choices possible as they are based on the length changes of each of the edges around the ends. There is one mode for each edge. In practice the mode moves freely until the length reaches some fixed proportion of the original length (jam limit), after which some resistance force and stiffness is included within the mode. These modes also take account of the fibre direction in calculating the jam length, this is not evident in the plots shown as the fibres are all initially oriented in the vertical direction.

The number of modes to use for jamming is also at issue. If required, the two shear modes which represent the shear in the ends of the element could be used as additional jam modes, bringing the total to ten. This has been tried, but the extra modes tend to be complicated as they are based on area or volume changes and have not proved very successful.

Bending Modes

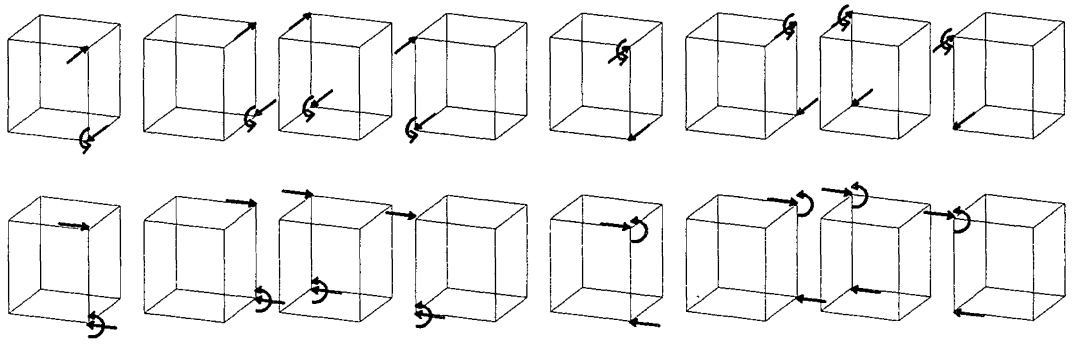

Figure 10-8 *Induced forces in the bending modes.*

The definition of the bending modes is clearly seen on the mode shape plots. Each mode has rotation at only one node, and each node has two rotation components, at right angles to one another.

The induced forces are interesting as each mode has one moment and two forces. The forces are arranged such that they form a couple, ensuring that the total moment on the element is zero.

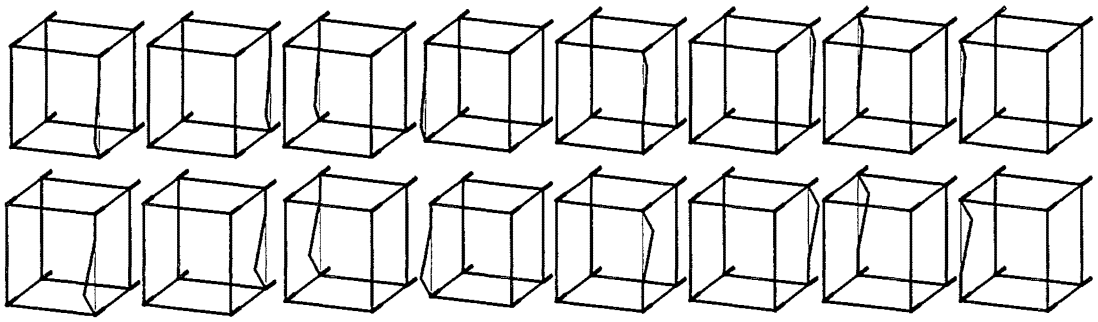

Figure 10-9 *Mode shapes of the bending modes.*

Torsion Modes

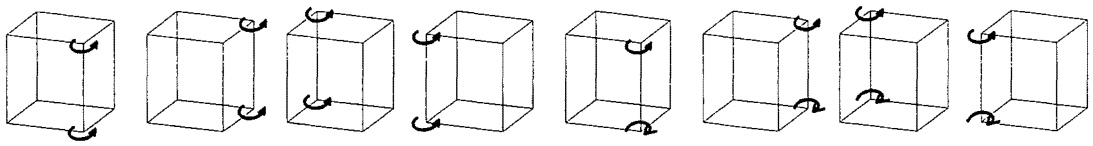

Figure 10-10 *Induced forces in the torsion modes.*

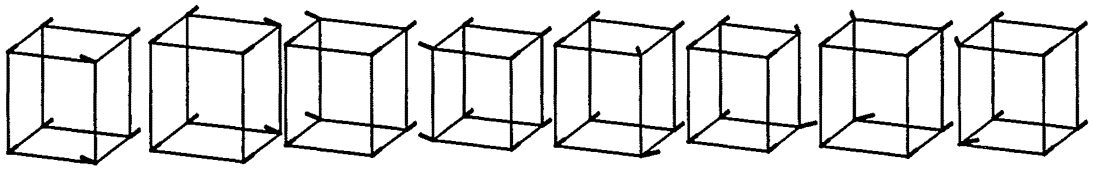

Figure 10-11 *Mode shapes of the torsion modes.*

The torsion modes are similar to the bending modes in that the modes tend to look simple. This is because in the undeformed state there is little or no interaction between the rotational degrees of freedom and the translational degrees of freedom.

The torsion modes are arranged into two groups. The first group of four have equal twists applied to the top and bottom of the fibre, one mode for each of the corners. The second group also have equal magnitude top and bottom twists, but they are in opposite directions. There is also one of these modes for each corner.

Shear Modes

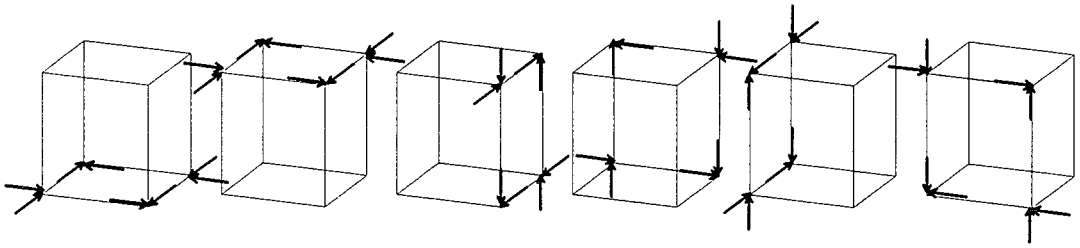

Figure 10-12 *Induced forces in the shear modes.*

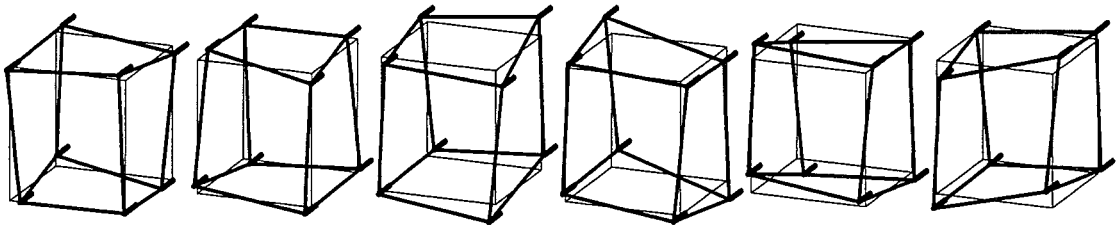

Figure 10-13 *Mode shapes of the shear modes.*

The shear modes display the sort of complicated mode definition which occurs in all of the modes when the deformations become more complicated.

The induced forces force each face in turn into a shear deformation. The first two are the two element ends and the remaining four modes represent the element sides. In the mode shapes plot, the shear in the appropriate face of the fourth and sixth modes can be seen. The other four modes also have similar shear but the view angle makes them hard to identify.

In every shear mode shape, every degree of freedom, both translational and rotation has a contribution to the displacement. This ensures that within a shear mode there is just shear, no fibre is bent or extended and the average rotation and translation of the element is zero.

10.1.3 Transformation Tensors

The definition of the transformation equations for the three dimensional element was significantly more complicated than for the two dimensional element. The basic system

was the same, the relationships between the modal degrees of freedom and the nodal degrees of freedom are written using the MAPLE input language. Fortran code for the calculation of the derivative matrices is then output from MAPLE.

In the two dimensional element, the input consisted of the coordinate set of a reference element and a similar set for the present state of the same element. There were two basic stages to the calculation, initially a series of calculations are carried out on each set of data, resulting in a set of numbers describing the state of the element represented by each set of data. The modes of the element are then calculated from a set of formulae involving both sets of numbers. Up until this point the two data sets were treated independently.

The modal values of the three dimensional element are calculated using a similar method to that used in the two dimensional element. Two sets of numbers are generated[19], each based on either the present or reference state of the element. The formulae for the modes combine the two sets. The computational effort is reduced by calculating the values from the reference element only at the start of the analysis and storing them for later use rather than recalculating the values whenever they are required.

Many of the values calculated have physical meaning for the element and this can be used to model permanent deformation of the element. For example the values which are used to calculated the extension modes are the arc lengths of the corner fibres in the present or reference state. If a fibre was to deform permanently (plastic deformation) then the arc length of that fibre stored for the reference element could be adjusted.

A number of the concepts which were used in the definition of the three dimensional modes are similar to those used within the two dimensional model, these will not be explained in detail.

The input program to MAPLE for the three dimensional case is over 400 lines in length. The way that the program functions will be outlined here and the full code is included on a diskette.

---

[19] These sets of numbers are sometimes referred to as *element measures*.

- **Initialisation.**

  Three vectors are assigned dimensions and prepared for input. When the Fortran subroutine is run these will be the input to the subroutine. The vectors are:

  dp(48) The present coordinates of the element.

  mr(48) The reference measures.

  fd(8,3) The normalised direction vector, representing the fibre direction at each of the eight element nodes.

- **Read in reference measures.**

  The values in the reference measures are all assigned different names to be similar to the names of the present measures to be calculated within the routine.

- **Reorganise data.**

  The translations and rotations are extracted from the dp vector and assigned to more rational names.

- **Rigid body translations.**

  The three rigid body translation measures are calculated as the average of all eight of the translation degrees of freedom in that respective direction.

- **Define edge vectors.**

  A vector (Ep) is defined for each of the 12 edges in terms of the input data.

- **Rigid body rotations.**

  Three vectors are defined which are the average vectors in each of the three principal element directions. The first of the three direction is the fibre direction and the other two are the averages of the top and bottom vectors from each of the two pairs of opposing sides.

  Further vectors are initialised. These temporary vectors will not be defined in terms of the input data until after the derivatives have been calculated, any possibility of these measures having greater than a first order affect on the results is therefore eliminated. These vectors will later contain copies of the direction vectors just calculated.

  The rigid body rotation values are then found as the dot product of the direction vectors with one of the temporary vectors.

- **Chord lengths.**

  The chord lengths of the element edges are calculated.

- **Face vectors (u).**

  Six u vectors are calculated. They each represent an average direction across one of the six faces and are shown in Figure 10-14. On the sides, the vector is in the direction of the fibres and is found as an average of the two vertical chords. The end vectors represent a direction across the element which is

formed as the average of two opposite sides. The vectors are normalised to have unit length.

- **Twist measures.**

  Fibre twist measures at each node are defined as the dot product of the fibre direction vector at that node and the rotation degrees of freedom.

- **Bending measures (i).**

  Measures representing the bending modes are calculated using the nodal translation coordinates and the fibre direction vectors. These measures will be used for calculating the derivatives of the bending modes with respect to the translation degrees of freedom. The second set of bending mode measures will be used for the derivatives with respect to the rotation degrees of freedom. This approach was required as any attempt at a combined measured created a formula which was far too complicated for use.

- **Face vectors (M).**

  A second set of face vectors (M) are calculated. On a cube these vectors would be at right angles to the set previously found (u) and are in the same plane as the face (Figure 10-14). These vectors are also normalised to have unit length.

- **Shear measures.**

  The six shear measures are calculated as the dot product of the six pairs of face vectors.

- **Bending measures (ii).**

  The second set of bending mode measures is calculated as the dot product of the rotation vectors at each nodal point with an orthogonal coordinate system which will be set up on each of the four fibre corner lines. The values will not be assigned to these vectors until after the derivative calculation. This makes the computation simpler and does not affect the result as these measures are only going to have derivatives taken from them with respect to the rotational degrees of freedom.

- **Jam measures.**

  The jam measures are found using a two step process. A set of vectors describing the width of the element along the edge at the ends of each side is constructed. This measure itself could be used to form the jam condition but it was found during the two dimensional model that the system would be more stable if the fibre direction was taken into account. A second set of vectors is formed which represent the average fibre direction along each side of the element. The jam measure is then constructed as the component of the edge vector that is at right angles to the fibre direction vector.

- **Arc length measures (i).**

  The arc length is calculated here based on angular measures. The angles of rotation for the fibres are separated using a series of unit vectors which describe an orthogonal coordinate system for each fibre edge. These vectors are not defined until after the derivatives are taken, in this way the arc length derivative calculation is simplified. These measures are used only for taking derivatives with respect to the angular degrees of freedom. A second set of measures are created for the other derivatives.

- **Edge strains.**

  The edge strains are calculated for each of the four principle fibre edges. These edges are the four edges which are in the fibre direction. The equation system is based on extrapolation from a fibre at each of these edges. The strains are calculated as a simple ratio of the change in length over the original length.

- **Present measure vector.**

  The present measure vector is assembled from the measures which have calculated. Fortran code for the calculation of this vector will be saved separately. This code can then be used to find the initial values for the reference measures.

- **Mode shape definition (i).**

  The various mode shapes are defined in terms of the present and reference measures. Most of the definitions are simple. The bending modes are just the bending measures. More complicated approaches have been attempted in order to make the bending stiffness calculation simpler but the solutions always becomes too complicated and the code too cumbersome for use.

- **Derivative calculation (i).**

  Half of the 48x48 derivative matrix is calculated. This half is related to all of the derivatives with respect to the rotational degrees of freedom.

- **Arc length measures (ii).**

  A second set of arc length measures based on the fibre direction vectors and the nodal coordinates are calculated. Derivatives with respect to the translational degrees of freedom will be taken from these measures.

- **Edge strains.**

  Edge strains are redefined using the new arc length measures.

- **Mode shape definition (ii).**

  The mode shapes which have contributing measures that have been changed are redefined.

- **Derivative calculation (ii).**

  The second half of the derivative matrix is calculated.

- **Fortran output.**

  Fortran code is created for the numerical evaluation of the two vectors representing the mode shapes and the present measures, as well as the matrix of the first derivatives.

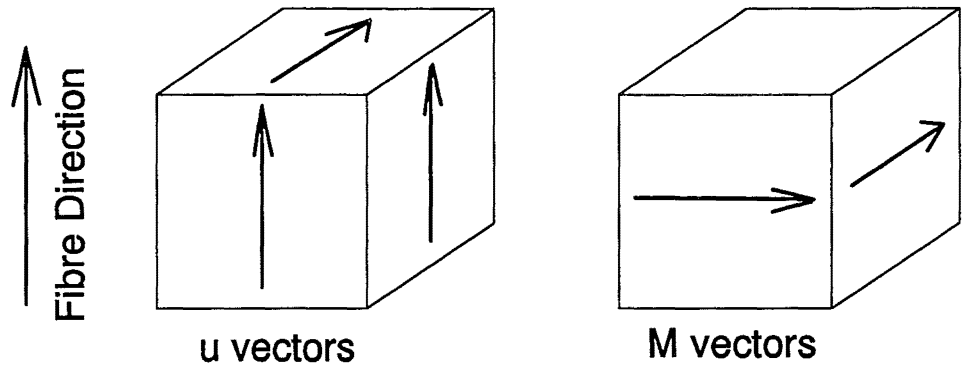

Figure 10-14 *Face vectors, both **u** and **M** vectors.*

Potential Difficulties.

There are three main potential difficulties with the transformation equation formulation.

The transformation equations could be assembled in such a way that they do not resemble either the real situation or the way the modal stiffness vectors have been defined. The major symptom of this problem would be non-convergence of the system to a solution.

One or more modes might be set up as linear combinations of other modes, this would cause the matrix of first derivatives to become rank deficient. This means that there are fewer independent vectors defining the vector space that the number of degrees of freedom. The result of this is that the global stiffness matrix of the system would become singular and impossible to solve. It is easy to define a set of modes which are not independent and it is wise after every mode change to take a matrix of derivative values from a neutral coordinate set and check the rank of the matrix.

The third possible problem with the transformation equations has been mentioned previously. Overcomplication can easily eliminate the usefulness of any system. A complicated system may take too long to generate the symbolic code or when the

routines have been created they may run too slowly. The only solutions to this problem are to either keep everything simple or purchase greater computer resources.

Non-zero Terms in First Derivative Matrix.

The components of the first derivative matrix which have the potential to be non-zero are shown in Figure 10-15.

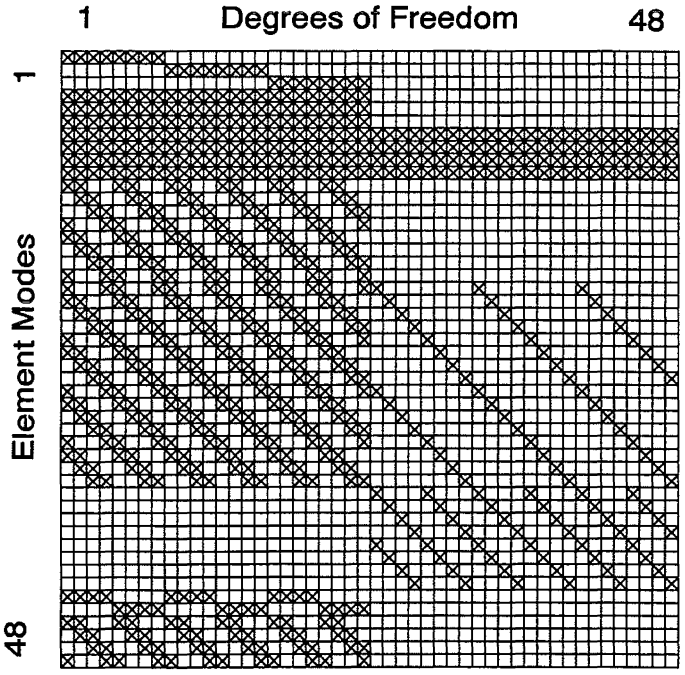

Figure 10-15 *The potential non-zero terms of the first derivative matrix.*

This figure shows which degrees of freedom can influence each element mode. The various classes of modes are clearly differentiated. The simplest of the modes are the translation rigid body modes (modes 1-3) which have contributions from only the eight translational degrees of freedom which are in the same direction as the mode. The most complicated of the modes are the fibre extension modes as these can be influenced by any nodal degree of freedom in the element.

The grids for the non-zero elements of the second degree of freedom tensor are not available, the reasons for this are discussed in section 10.2.2.

10.2 General Modelling

During the rest of the modelling process for the three dimensional element a number of problems were faced and decisions had to be made. Most of these are outlined in this

section (10.2) and a selection of the more significant problems are dealt with in greater depth in sections 10.3 to 10.5.

10.2.1 Single Fibre Model

The model used for three dimensions was a simple extension of the two dimensional model. The fibre piece is formed from three straight sections, the end pieces each being as long as one quarter of the chord length of the element. The position in space of the fibre piece is now fully defined by ten degrees of freedom[20], rather than the six in the two dimensional situation. Two extra degrees of freedom are required to define the amount of twist being applied to each end of the fibre piece.

The extension model of the fibre element was chosen for simplicity, a tri-linear stiffness relationship was used. The first stiffness regime is a constant value up to just before the point where the crimp would be fully removed from the fibre. The stiffness is then ramped linearly over a small strain range spanning the crimp removal point and finishing at the stiffness value used in the third regime which has another constant value.

The extension force relationship is formed to work with the stiffness. The force is linearly varying in the first and third regimes and quadratic in the second. A plot of what these models look like is shown in Figure 10-16.

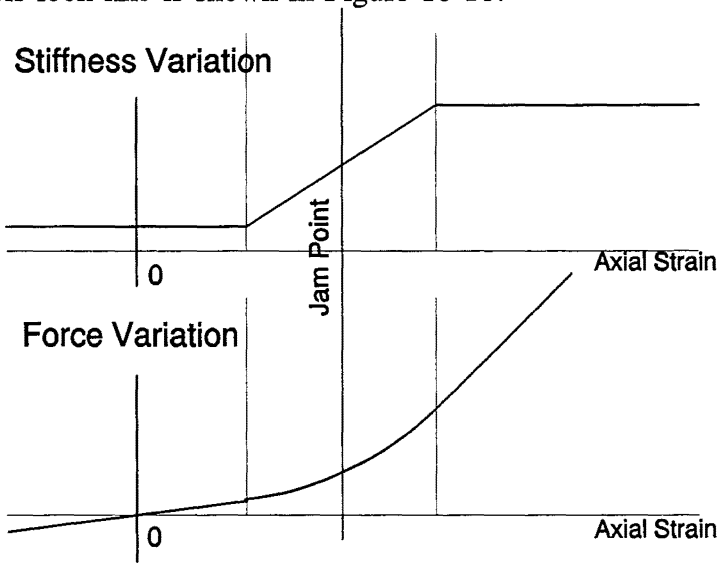

Figure 10-16 *Variation in axial force and stiffness.*

[20] Three coordinates at each end and two degrees of freedom at each end to define the fibre direction.

The stiffness ramp in the second regime is required as it was found that if a step variation in the stiffness similar to the real behaviour was introduced, the solution could iterate about the crimp removal point without convergence.

The bending properties of the fibre were constructed assuming that there was one rotational spring at each of the two fibre bending points. The modal bending degrees of freedom are based on an orthogonal coordinate system along the chord direction and the bending components are transformed into each of the two direction at right angles to the fibre direction. The curvature vectors within each plane are calculated at the locations of the rotational springs and they are summed vectorially to assess the total curvature at that point. The spring rotation, stiffness and force are then calculated at each point in a similar manner to that which was used for the two dimensional bending.

10.2.2 Finite Difference for Second Derivatives

In the three dimensional element, it is impractical to use the same approach of analytically calculating the second derivatives of the modes shapes that was used in the two dimensional element. This is for reasons of both storage and code generation.

The change to three dimensions dramatically increased the number of degrees of freedom in the element. This effect was even more pronounced on the number of components in the second derivative tensor, increasing these by a factor of 64 over the two dimensional model. The storage required for this tensor is large and although it would not be prohibitive, it is one reason for looking for another approach.

The three dimensional MAPLE input code was significantly more complicated than that for the two dimensional element, partly due to the inefficient way that the rotation degrees of freedom had to be dealt with and partly due to the increased number of degrees of freedom on each element. An attempt was made to use MAPLE to generate the second derivatives but the job was too large for the available resources. It was apparent that even if MAPLE had succeeded in generating the necessary Fortran source code, the Fortran compiler would have been unlikely to have been able to compile the code.

The analytic generation of the second derivatives was abandoned for a finite difference approach. Successive calls to the first derivative matrix at slightly varying coordinate

inputs were used to generate the second derivatives using a standard central difference approximation formula.

An attempt was made to use a forward difference formula to half the amount of work which would be required. It was unclear as to whether the bias in the derivatives was causing trouble with the model because it was difficult to separate the effects of this from the other problems in the model. Forward differences were abandoned in preference to the more accurate central difference approximation.

A further argument can be put forward for the use of finite difference techniques. It is possible that the finite difference derivative is a more accurate result than the analytic evaluation. The formulae in the analytic evaluation are very complicated and the loss in precision during the calculations due to the finite precision arithmetic of the computer could degrade the solution. The first derivative formulae are considerably simpler and would not have as great a loss in precision. The finite difference formulae are very simple and should lose very little more precision than that lost already.

10.2.3 Division by Zero from MAPLE

When the Maple generated Fortran code for the three dimensional element was run, the program aborted with a 'division by zero' error. The problem was tracked down to the way in which MAPLE evaluated some expressions and a program was written to post-process the code to eliminate occurrences.

MAPLE evaluates expressions by creating a series of temporary variables. These are then combined to make more variables, continuing until the expression is evaluated. MAPLE optimizes the code by using a temporary variable many times in the subsequent code minimising both the size of the code and the computational effort required.

At times in the code MAPLE would form the construct shown below.

```
t1 = A*A
t2 = SQRT(t1)
B  = t1/t2
```

These lines would not be adjacent in the program and the variable names would be more complicated but this is the form of the problem. The value of B is equal to that of A for all situations except when A is equal to zero, in this case a division by zero

would result. It is likely that this is not a false representation of the formula but if that were the case the result that would be of interest is the limit of B as A tends to zero, which is equal to zero.

A program was written to scan the Fortran code and pick out any examples of this construct, replacing the last line with the simple assignment B = A. This solved the division by zero problem.

10.2.4 'Free' Modes in the Three Dimensional Element

The three dimensional element was constructed on the assumption that it had six 'free' modes, modes which could move without adjusting the energy within the element. The modes were the six rigid body modes, three translations and three rotations. The system was found to be very unstable and the first derivative matrix was found to be rank deficient.

It was found that there are ten zero energy modes in the three dimensional element, the extra modes reflect the possibility of a fibre having a rigid body twist around its own axis. This form of deformation would create no strains in any part of the fibre assembly and represents a zero energy mode. The rank deficiency of the first derivative matrix came about because misunderstanding about the torsion modes had caused four of them to be linear combinations of the other four.

10.2.5 Lateral Compression

The definition of the lateral compression relationship was simplified from that used in the two dimensional model. The iterative approach to define a definite jam point without introducing high stiffness was too complicated to use in a model in which all other aspects had been shown to be not performing as required.

A tri-linear stiffness relationship similar to that used for the extension properties was used (see section 10.2.1). The stiffness in the first regime was set almost to zero, this is the state where there is no jamming, the fibres are free to move. The third regime was set to a stiffness which was a substantial proportion of the extension stiffness. The extension stiffness was chosen because it is the largest stiffness in the fibrous system. The width of the second regime was originally set quite low and the solution was found

to iterate around the jam point without convergence. Increasing the width of this regime introduced some softening to the jam point and allowed satisfactory convergence[21].

10.2.6 Element Meshing

This section concerns the way in which the total assembly is formed from a number of finite elements. The basic assembly is the fibre yarn, this is modelled as a cylinder with the fibres taking a helical path around or through the cylinder.

The yarn cylinder is divided up into layers for meshing, the layer interfaces are planes at right angles to the axis of the cylinder. The number of elements within each layer varies. More elements in a layer gives the potential for a better solution but more computation would be required.

The first layer mesh to be developed was formed from three elements (Figure 10-17).

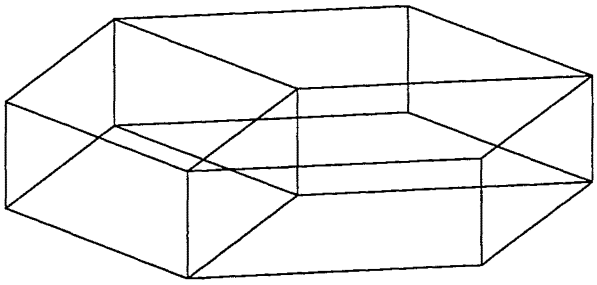

Figure 10-17 *Three element per layer mesh.*

The mesh was then extended to include more elements per layer, this was done by adding rings of elements to the outside of the original mesh (Figure 10-18).
This mesh was found to perform well under yarn extension, but when twisted it refused to converge to a solution. The problem was linked to the corner of an element being positioned at the centre of the yarn, this position is unique in that under yarn twisting the fibre is forced to buckle or compress to reduce its' length, all other fibres can simply bend.

A second mesh was selected, this mesh had no element corners at the centre of the yarn. The simplest version of this mesh had only one element per layer. A three ring version is shown in Figure 10-19 (the centre element counts as the first ring).

---

[21] The jam modes are defined as a ratio, present length over original length. The second regime width was originally 0.001 and was increased to 0.1.

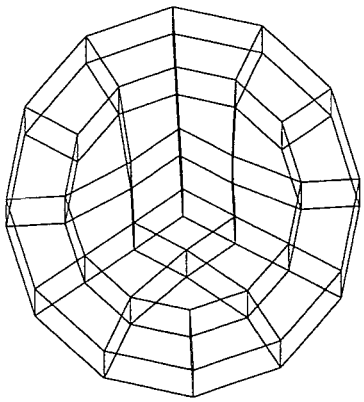

Figure 10-18 *Original mesh with three rings.*

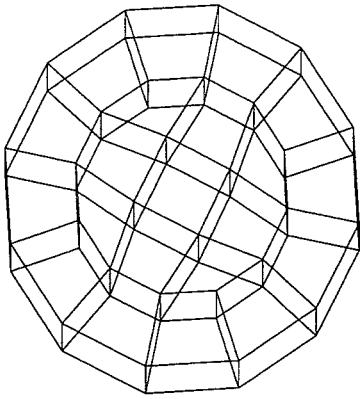

Figure 10-19 *Second mesh, three rings.*

This mesh was found to function well and it remains the most successful mesh.

It was found that under some deformation conditions, the yarn tended to form a cavity in the centre. The mesh did not give very detailed results when this happened as there was only one element surrounding the area. A third mesh was developed which had a small hole in the centre surrounded by eight elements. This was to give good centre resolution as well as the possibility of a hole forming. This mesh is plotted in Figure 10-20.

Satisfactory results were not obtained with this mesh, the small element sides near the middle of the element proved to be unstable in a jamming situation.

A program was written to automatically mesh the assembly given a few parameters defining the element configuration. The program can output any of the meshes above with one, two or three rings, in any number of layers. The helical aspect of the yarn can also be modelled by distorting the elements so that their edges follow a helical path.

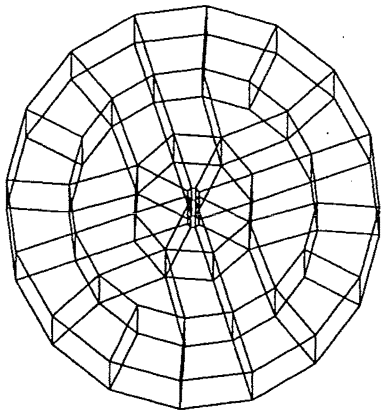

Figure 10-20 *Third element mesh, three rings, with central hole.*

Figure 10-21 shows a sample yarn mesh. Note that the fibre directions at the nodes are defined so that the edges follow the helical path as closely as possible.

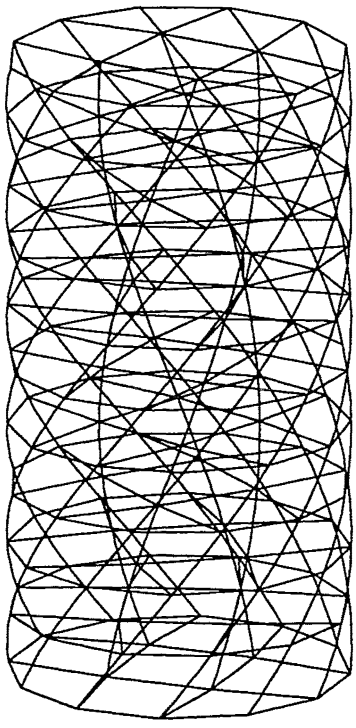

Figure 10-21 *Yarn mesh, using mesh 2, 2 rings, 10 layers.*

10.2.7 Matrix Multiplication

Once the three dimensional model was running it was found to perform far slower than expected in each iteration. Profiling code was incorporated during a compilation and subsequent execution revealed that nearly seventy percent of the computational time was

being spent in one subroutine. This subroutine carried out the transformation of the modal stiffness matrix into the nodal stiffness matrix.

The subroutine had been coded based on the tensor notation version of the equation.

$$K_{ij}^{//} = \frac{\partial \beta_l}{\partial \delta_i} \frac{\partial^2 E}{\partial \beta_l \partial \beta_k} \frac{\partial \beta_k}{\partial \delta_j} \qquad \textbf{(10-1)}$$

Where i,j,k,l all varied from 1 to 48. This was performed by setting up a four deep nested loop, each index varying from 1 to 48 in the same format as the tensor equation. This required 48^4 operations ($\approx$5.31 million operations).

The subroutine was the re-coded based on the matrix notation version, both matrices in this equation are 48 by 48.

$$[A^{-1}]^T [K_T'] [A^{-1}] \qquad \textbf{(10-2)}$$

This way the evaluation is performed as two steps, the first multiplying two of the matrices together and storing the result. The second step multiplies this result by the remaining matrix. This system achieves the same result as above but requires only $2x48^3$ operations ($\approx$0.22 million operations).

This significant advantage comes about from the storage of intermediate results which would have had to be calculated many times with the first system. The program was found to run in less than half of the CPU time of the original version.

10.2.8 Lagrange Constraints

A number of Lagrange constraints were designed for use with the three dimensional program. All of the constraints worked at small displacements and they were used to perform a number of analyses.

It was found that when a constraint involved a rotational degree of freedom, at some point during deformation the constraint would become unstable. The reason for this was that the rotation has a step discontinuity once every rotation (or more often if combinations of inverse trigonometric functions have been used in the constraint definition). Modifications were made to the equations to add or subtract factors of 2π as required. This worked for the simpler assemblies but eventually the more complicated Lagrange constraints were abandoned for any but the simplest assemblies.

The formulation of the constraint equations in three dimensions involved some near zero divisions and it was suspected that there might have been a precision loss within the constraints contributing to their instability.

10.3 Skyline Storage

At each iteration of the program a set of simultaneous equations had to be solved. The equations are represented by the global stiffness matrix and the global force vector. There are a number of different approaches to the solution process and those which had an influence on the present analysis are discussed.

The two dimensional model used a public domain equation solver, the solver accepted the input as a full nxn matrix and performed the solution with pivoting. The input format means that the stiffness matrix given to the solver was a two dimensional array, each dimension having as many terms as there were equations in the system. The amount of storage required was then the square of the number of equations which was not prohibitively large for the two dimensional model. Pivoting is a feature of equation solvers which means that the equations are not solved in the order in which they were given but are solved in the order which would give the most accurate result. Degradation occurs in the answer due to finite precision in computing and row and column interchanges are carried out to minimise the precision loss. The best order is assessed by the solver as the solution progresses.

In three dimensions the number of equations increased dramatically over that of the two dimensional model and the global stiffness matrix became large enough to make storage of the full matrix impractical[22]. A symmetric skyline equation solver was used which reduces the computational effort and storage space required.

Skyline solvers exploit the sparsity of most stiffness matrices in order to reduce the storage and computational requirements. The storage is reduced by not storing a large proportion of the zero terms within the matrix. Storage requirements are also halved when the symmetry of the matrix is exploited.

---

[22] The ability of Unix systems to page to disk when they run out of memory means that a solution can still be reached, at the cost of a considerable increase in CPU time (greater than an order of magnitude).

Upon use of the skyline solver it was found that the equations of the three dimensional system could not be processed in the order in which they were given to the solver. The way in which the Lagrange constraints were implemented meant that the Lagrange degrees of freedom had to be processed after some degrees of freedom and before others. This problem had not occurred with the two dimensional system because the equation solver would have automatically pivoted to find the correct solution order.

Attempts were made to order the equations in the correct order for solution. It was found that as the assembly deformed the parameters governing the Lagrange multipliers changed and the order in which the equations should be processed also changed. It was therefore found to be impossible to pre-order the equations for solution and some sort of pivoting had to be implemented.

An unsuccessful search was made for a skyline solver with pivoting. An investigation into how a skyline solver works revealed that it is impossible to pivot a matrix without changing the skyline of the matrix. It was also found that the symmetry of the matrix could only be preserved if the pivot point is on the main diagonal of the matrix.

In order that the workings of a skyline solver be fully understood a solver was developed. The solver was then modified to solve the systems generated by the three dimensional element assemblies.

Full pivoting on the main diagonal was implemented into the skyline solver. As explained above this cannot be done without adjustment of the skyline storage. A subroutine was written to pivot the skyline, re-arranging the storage vectors as required. The solver will process the equations in the order given as much as possible, pivoting only when it is required for a solution. The routine was written to use as little extra storage as possible, the skyline was re-arranged by shifting the terms about within the space allocated for the vector[23]. Most of the terms of the skyline matrix are stored in a single storage vector. One extra storage vector, the same length as the number of degrees of freedom is used for temporary storage during the pivot process. This algorithm is discussed in more detail in the Appendix E.

---

[23] A little extra space is inevitably allocated for any array when using Fortran, this is because the allocation cannot be dynamically adjusted during execution. This extra space is used to facilitate the re-arrangement.

10.4 Integration Points

The three dimensional element requires numerical quadrature to integrate in the plane at right angles to the fibre direction, the number of integration points proved to have a significant influence on the convergence properties of the assembly.

A two dimensional vertical stand of fibres has forces applied so that the top is forced to open and the fibrous assembly deforms as a continuum. The deformed pattern is shown in Figure 10-22(b).

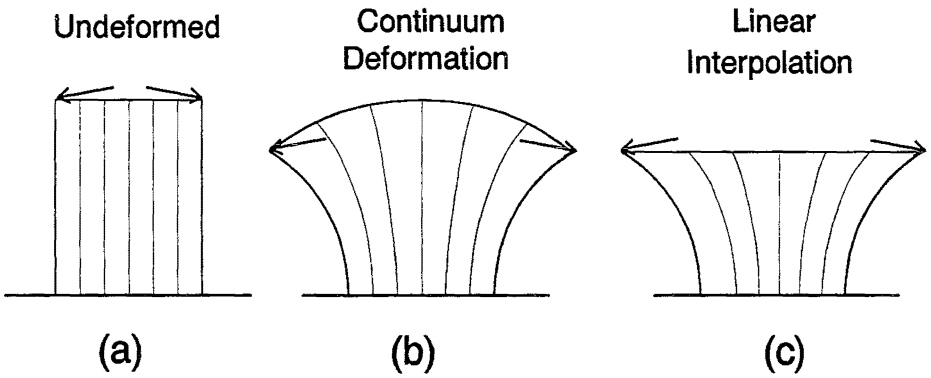

Figure 10-22 *Opening of a vertical assembly.*

If a single element was used to model this situation, the best approximation would be that shown in (c) of this figure. The element has only linear interpolation in a direction perpendicular to the fibre orientation. If this element were integrated analytically the resultant stiffness terms would be significantly greater than in the yarn. Large artificial stiffness would result from the axial compression of the fibres near the middle of the element. There are two ways to overcome this problem without abandoning the concept of a continuum approach.

Limited (or selective) integration could be used within the element. Only two integration points in two dimensions (or four in three dimensions) are used so that the contribution to the stiffness matrix would come from only those two fibres passing through the integration points. The linear interpolation between the integration points would allow a stable solution.

A higher order interpolation could be used across the element such as quadratic or cubic, allowing the element to achieve a more realistic deformation pattern. Care still has to be taken so that the number of integration points are not too great. The deformation pattern would still not exactly model the fibrous solution.

Integration points and interpolation problems are more significant in the fibrous finite element than in a more conventional finite element formulation. The considerably greater stiffness in the fibre direction when compared to those in the lateral direction amplifies the effect.

The three dimensional finite element required that the number of integration points be reduced to four in the plane normal to the yarn axis to give stability. It was also found that unless the points were placed at the corners of the element the system converged poorly. This is because the modal equations are designed based on the assumption of a fibre at each corner. For better integration the equations could have been developed assuming the presence of a fibre at each Gaussian integration point.

10.5 Poor System Convergence

The three dimensional model converged well in only a small number of cases. Investigation showed that the cases which converged were only those that the fibres were initially straight and were all under tension throughout the test or cases where every fibre was bent only within a plane.

Assembly deformation from one iteration to the next was observed during a non-convergent test case. All fibres which were not under tension were found to be varying their position at every iteration, the fibres were not settling to a unique position. This effect was caused by the torsion within a fibre piece being modelled incorrectly. Without torsion resistance the position in space of a three dimensional fibre is non-unique. The influence on the torsion in the fibre from the twisting of the fibre path was not being fully included.

The path torsion was incorrect for two reasons, both of which are linked to the nodal rotational degrees of freedom. The formula for path torsion had to be simplified in order to obtain workable MAPLE output because the formula had to be written in terms of the nodal rotations any realistic attempt tended to be too complicated. The second reason that the path torsion was being incorrectly represented was that the translation of the nodal global rotations into fibre end rotations could not be uniquely specified.

The next chapter will modify the nodal degrees of freedom of the element and reconfigure the analysis to allow better torsion modelling.

10.6 Twisting Model

Due to the lack of correct fibre torsion modelling the model is only able to represent a small number of test cases. One interesting case involving the twisting of a small assembly of fibres is presented here along with theory to demonstrate the accuracy of the solution.

10.6.1 Model Description

In order for the analysis to give a stable solution every fibre must be in tension at all times, the fibre torsion component is not then necessary to define the fibre position. The number of fibrous assemblies which can be tested under this restriction is small. The possibility explored here is the twisting a set of initially parallel straight fibres under tension.

The total assembly has a height to width ratio of over ten and is formed from twenty elements, one element for each layer of the assembly. The properties of the fibres within the model are chosen to be similar to those of a typical woollen fibre within the limits of the assumptions made within the numerical analysis.

The assembly deformation is enforced through rotation of the top face. The bottom face is held still while the top face nodes are progressively moved around in circles of constant radius. The top face is free to move in the vertical direction although all of the nodes must move together. A small vertical load is applied to the top face using a lagrange multiplier, ensuring that the load is correctly distributed over the top face nodes.

A plot of the element mesh at various steps during the analysis is shown in Figure 10-23. The light line within each plot is the undeformed mesh and this is the same in all eleven plots. The heavy lines are the deformed positions of the elements and the actual fibres in the system are along the long axis. The fibres in this analysis have been defined to jam when the lateral distance between them is one third of the original distance.

Top face rotation is increased by one quarter turn between each plot, the final plot having a top rotation of two and three quarter turns.

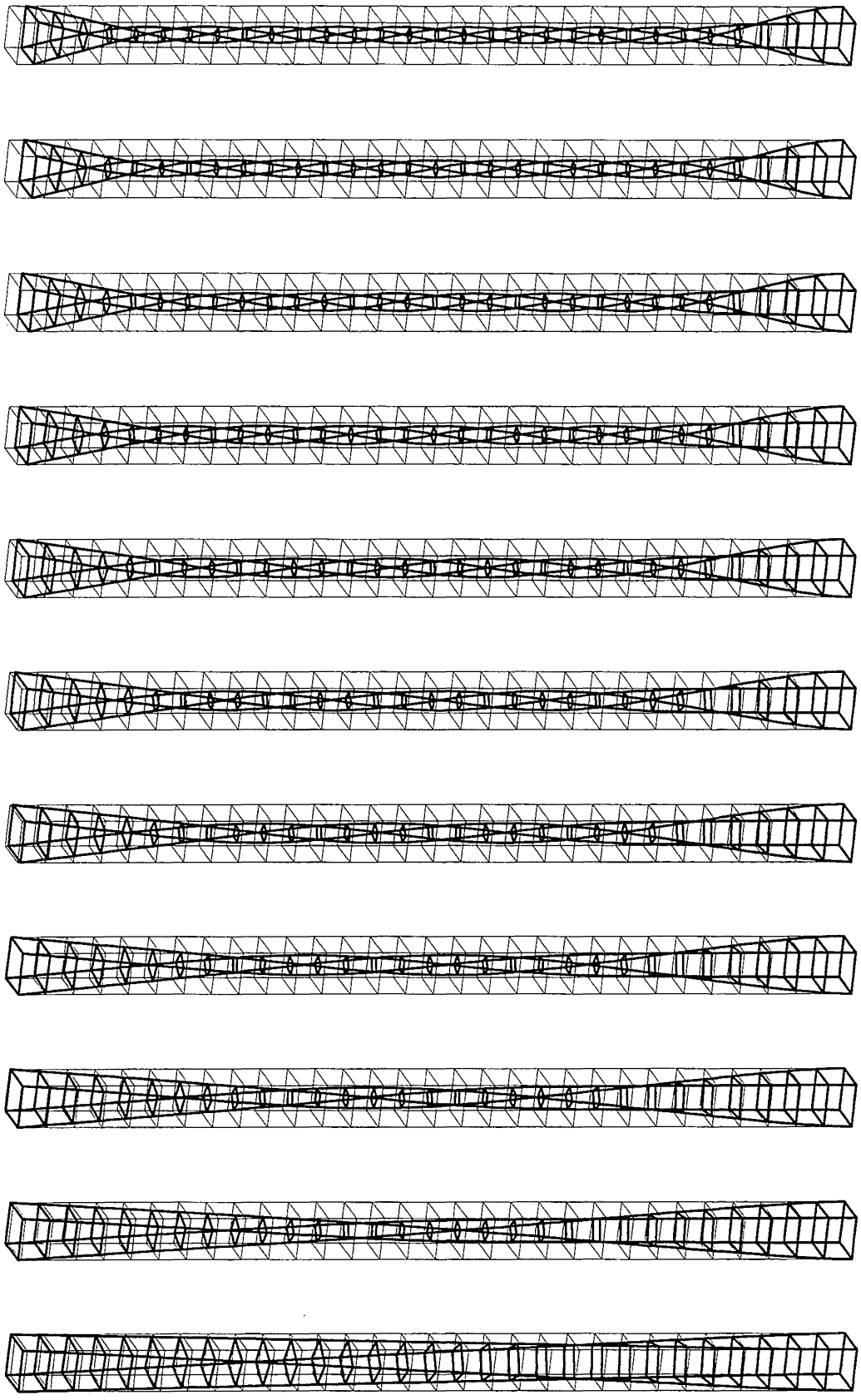

Figure 10-23 *Assembly twisting, each plot is one quarter turn to top face.*

No lateral fibre jamming has occurred in the first plot, the fibres in this case travel an almost straight line from the bottom node to the quarter node, displaced one turn from the original position. The straight line solution is the lowest energy path as the elements at mid height (which would be the first to jam) have not been compressed laterally enough to reach the jam limit. The axial force being applied to the assembly causes the slight extension shown in this plot.

The second plot shows some curvature in the fibres as they start to jam at mid height and the fibres bend around the central core. This pattern is continued through the remaining nine plots, the final plot having over two full twists wrapped around a central cylindrical core.

The displacement of the top face is as would be expected, slowly dropping as the twist in the fibre assembly increases.

10.6.2 Theoretical Development

A relationship is found between the angular rotation of the assembly and the top face displacement. The assumptions made are:

- the arc length of the fibre remains constant throughout deformation.
- the fibre remains straight if not jammed.
- the fibre curves around a cylindrical core of constant radius when jammed.

The state of the fibre is defined by the variables defined in (10-3) and are shown in Figure 10-24.

$$
\begin{aligned}
r_0 &= \text{initial radial position of the fibre.} \\
L &= \text{fibre arc length.} \\
x &= \text{length of assembly along axis} \\
r &= \text{radial position of fibre (function of height).} \\
\phi &= \text{jam limit, jam occurs when } \frac{r}{r_0} = \phi \text{ .} \\
\theta &= \text{top face rotation.}
\end{aligned}
\qquad \textbf{(10-3)}
$$

The relationship must be defined in three parts, the state of the fibre before any jamming occurs, the position at which jamming first occurs and the deformation after

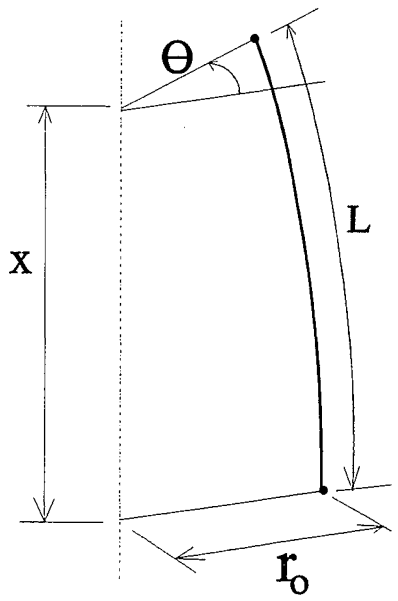

Figure 10-24 *A single fibre under twist, variable definition.*

jamming.

Before Jamming

The fibre in this situation is assumed to be straight and at an angle from the vertical defined by the rotation of the top face. The arc length is constant and the horizontal component of the fibre path is easily determined. Looking down the assembly axis, the plan view of the arrangement is Figure 10-25, the horizontal component is shown as y.

The value of y is shown to be:

$$y = 2r_0 \sin\left(\frac{\theta}{2}\right) \tag{10-4}$$

and the relationship for the assembly axis length can then be calculated as

$$\frac{x}{L} = \sqrt{1 - 4\left(\frac{r_0}{L}\right)^2 \sin^2\left(\frac{\theta}{2}\right)} \tag{10-5}$$

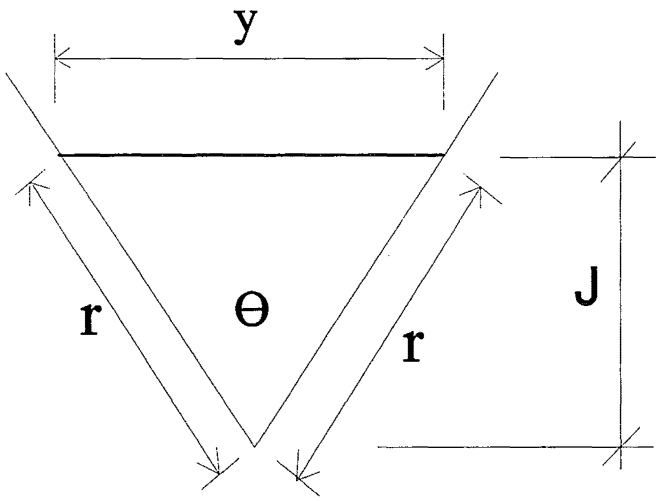

Figure 10-25 *Plan view of a fibre before jamming.*

At the Jam Point

Jamming occurs when the value shown as J in Figure 10-25 reaches the jam point. This can be shown to occur when

$$\sin^2\left(\frac{\theta}{2}\right) = 1 - \phi^2 \qquad \textbf{(10-6)}$$

which gives the height relationship at the point of jamming as

$$\frac{x}{L} = \sqrt{1 - 4\left(\frac{r_0}{L}\right)^2 (1 - \phi^2)} \qquad \textbf{(10-7)}$$

The top rotation angle at the jam point is

$$\theta_J = 2\cos^{-1}\phi \qquad \textbf{(10-8)}$$

and the length y at this point is

$$y_J = 2 r_0 \sin\left(\frac{\theta_J}{2}\right) \qquad \textbf{(10-9)}$$

After Jamming

After jamming the fibre is assumed to travel a straight line between the end point and the point at which it reaches the cylindrical core. The fibre wraps around the core until near the top when another straight line is travelled to the end point. It is assumed that there is no friction between the fibre and the central core. This implies that the slope

of the fibre would be constant along the full length of the fibre. The constant slope is required to balance the vertical forces of any small piece of the fibre.

If a development of the fibre is made by cutting the length of the cylinder and folding the resulting sheet out flat, then the fibre path would appear as a straight line. This is shown in Figure 10-26.

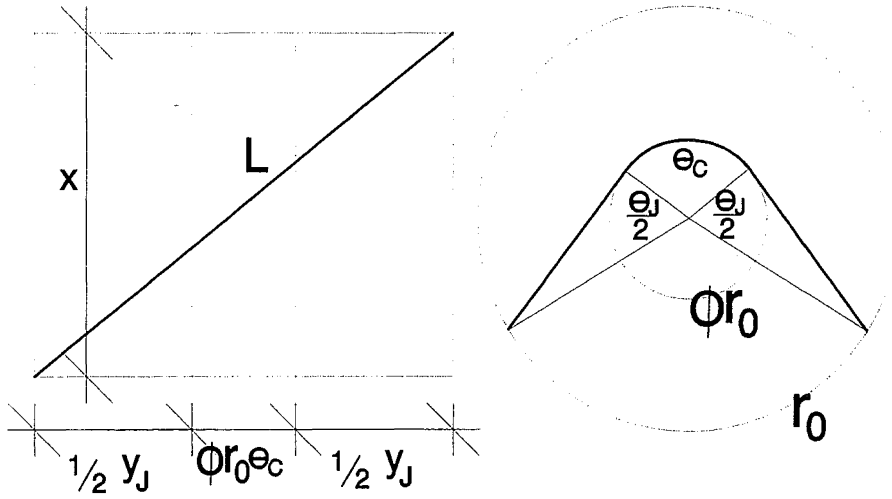

Figure 10-26 *Development and plan view of the jammed fibre.*

Then the horizontal component of the fibre development path is

$$y_J + \phi r_0 \theta_C \qquad \textbf{(10-10)}$$

where the angle wrapped around the core is

$$\theta_C = \theta - \theta_J \qquad \textbf{(10-11)}$$

The relationship between the original and deformed length may now be written

$$\frac{x}{L} = \sqrt{1 - \left(\frac{r_0}{L}\right)^2 \left(2\sin\left(\frac{\theta_J}{2}\right) + \phi(\theta - \theta_J)\right)^2} \qquad \textbf{(10-12)}$$

which can be re-written in terms of the jam limit as

$$\frac{x}{L} = \sqrt{1 - \left(\frac{r_0}{L}\right)^2 \left(2\sqrt{1-\phi^2} + \phi(\theta - \cos^{-1}\phi)\right)^2} \qquad \textbf{(10-13)}$$

Result

The relationship for the length of the wrapped fibre in terms of the rotation angle can be written as (10-14).

$$\frac{x}{L} = \begin{cases} \sqrt{1 - 4\left(\frac{r_o}{L}\right)^2 \sin^2\left(\frac{\theta}{2}\right)} & , \ \theta \le 2\cos^{-1}\phi \\ \sqrt{1 - \left(\frac{r_0}{L}\right)^2 \left(2\sqrt{1-\phi^2} + \phi\left(\theta - 2\cos^{-1}\phi\right)\right)^2} & , \ \theta \ge 2\cos^{-1}\phi \end{cases} \quad \textbf{(10-14)}$$

10.6.3 Comparison

The comparison between the results obtained for the top face displacement from the numerical model with those from the theoretical model is shown as Figure 10-27.

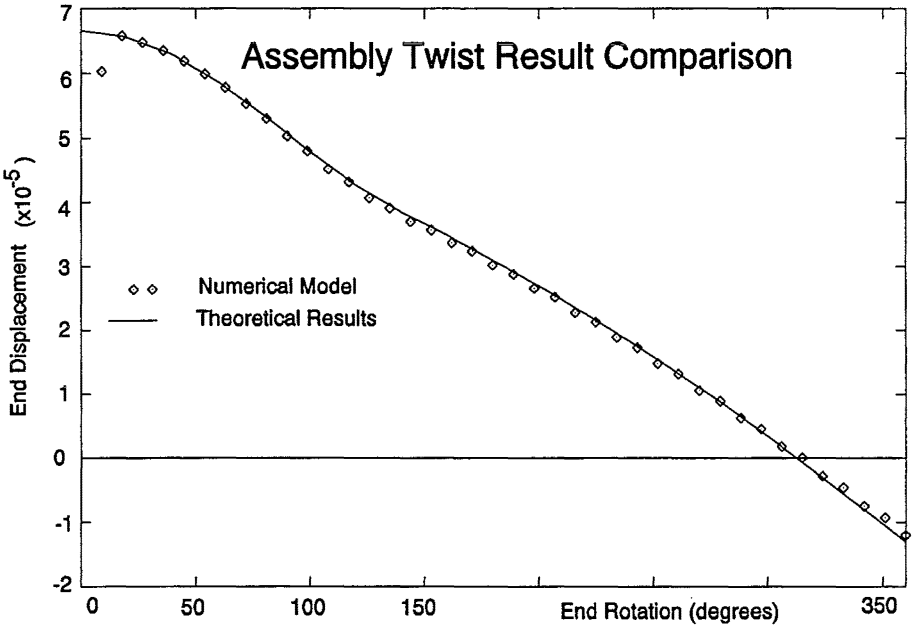

Figure 10-27 *End displacement during twist, numerical model and theory.*

The output from the theoretical model has been modified to put it in the same terms of reference as the data from the numerical model. The arc length has been set to the length of the numerical fibre in straight extension after the axial load has been applied, but the data is plotted as if this represents an initial displacement.

The top face rotation was applied over a number of steps. The steps were each split into two increments so one intermediate point is presented. Each step represents a change in rotation of the top face nodal points as they move in circular arcs about the yarn axis. Within each step the coordinates are interpolated linearly resulting in the intermediate node being on the chord between the two end points rather than the arc

between them. This accounts for the slight mis-alignment of every second point throughout the data set.

The first point of the data set is significantly different from the theoretical model. The axial force was applied linearly over the first step. This initial point is the intermediate point of the first step and only half of the total axial load has been applied. The nonlinear nature of the fibre axial properties stands out in this example as the point has achieved over 90 percent of the displacement after application of only half of the force.

The comparison between the two models was found to be acceptable, despite a number of factors the theoretical formula fails to take into account and which were modelled numerically. The sections of fibre between the ends and the central core must have some bending but the numerical model did exhibit this. The slope of the fibre would rise as the amount of twist increased and this would increase the axial force in the fibre resulting in a change of the assembly axial length. It is assumed that the nonlinear fibre extension properties prevented this affect from making any significant change to the relationship although it would not be difficult to include this in the theoretical model. The fibres at the bottom of the numerical assembly were restrained so that they could not rotate but this would make only a small change to the result.

11 Three Dimensional Model (II)

The three dimensional model is rebuilt to allow a more complicated fibre torsion formula than was possible with the previous configuration. Problems encountered during testing of the adjusted model are discussed and results are presented.

11.1 Model Adjustments

Problems with the path torsion evaluation have been blamed on the complication required for a good model as well as the nodal rotation degrees of freedom not being a good arrangement. The first stage to solving both problems requires the matrix of the first derivatives of the mode shapes with respect to the nodal degrees of freedom to be evaluated numerically. The element nodal degrees of freedom can then be re-arranged and the fibre torsion evaluated. The three changes to the analysis outlined below were performed simultaneously but for simplicity they will be explained as if they were applied sequentially.

11.1.1 Numerical Calculation of First Derivatives

The previous model used MAPLE to analytically evaluate the first derivative of the mode shapes with respect to the nodal degrees of freedom, the second derivatives were calculated numerically to simplify the procedure. The inclusion of any realistic model for the path torsion of the fibre requires further simplification of the analysis procedure by evaluating the first derivatives numerically.

Numerical evaluation of the first derivatives approximately doubles the amount of work required to evaluate the transformation matrices for each element. The increase in computation time is offset by a number of effects.

The previous three dimensional analysis was restricted in the degree of complication that the equations defining the mode shapes could have. Complicated relationships led to cumbersome MAPLE output for the first derivative matrix. Significantly more complicated equations can be used when the derivatives are calculated numerically, leading to a better model.

It is possible that the numerical precision of the numerically evaluated derivative is superior to that of the analytically calculated derivative. The lower accuracy within the analytic calculation would be due to the more complicated algebra required to calculate the derivative combined with the effects of finite precision computer calculations.

The equations defining the modes no longer need to be described for input into MAPLE, no symbolic calculation is required and therefore MAPLE is not required. The ability to program the equations directly would allow a greater flexibility in the form of the equations but would require more coding effort and might result in less optimal code. MAPLE was still used in the generation of the code for the modified three dimensional model.

MAPLE Code Adjustments

The basic framework from the previous MAPLE code was re-used within the modified model but considerable simplification was possible. The nodal rotation degrees of freedom were removed, all modes were calculated in terms of just the nodal displacements and the nodal fibre direction vectors and the vector of reference state measures.

11.1.2 Element Nodal Degrees of Freedom

The nodal rotation degrees of freedom were adjusted so that they represented changes in the direction of the nodal fibre direction vector.

Each of the three old degrees of freedom had represented a rotation about one of the three global axis directions. The degrees of freedom were defined in terms of a global coordinate system. This is a minimum requirement for the nodal degrees of freedom as it allows the values at one node to be compared with a node on another element. The replacement degrees of freedom must also have this property.

The first two of the new degrees of freedom represent the change in orientation of the unit vector describing the fibre direction. The third degree of freedom is the amount of twist in the fibre. Both the old and the new degrees of freedom are shown in Figure 11-1.

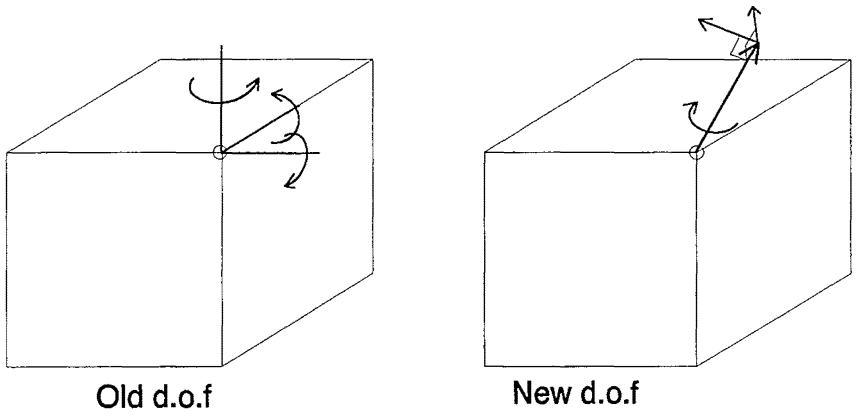

Figure 11-1 *Old and new nodal rotation degrees of freedom.*

The two orthogonal degrees of freedom describing the orientation change of the fibre direction are treated as linear degrees of freedom. Within a small displacement increment the linear movement of the end and the angle of rotation of the unit vector can be considered to be the same. The linear measure of these degrees of freedom is simpler to calculate. Three coordinates are used within the program to store the fibre direction at every node, the values for the movement of the end of the vector resulting from the solution process are used at the end of each iteration to calculate the new fibre direction.

The directions of the two degrees of freedom orthogonal to the fibre direction must be specified uniquely, this is to allow the values at this node to be matched with those on a node connected to an adjacent element. The degrees of freedom can depend on only the nodal or global variables.

An orthogonal coordinate system was built around the fibre direction vector. This vector formed the first axis of the local nodal coordinate system. It was then found which of the three global coordinate axes formed the smallest dot product with the fibre direction vector (which is closest to being orthogonal). The second local axis was found as the vector which is orthogonal to the fibre direction and within the plane formed from the fibre direction vector and the chosen coordinate axis direction. The third local axis direction is the cross product of the first two, forming an orthogonal basis. A diagram of this process is given in Figure 11-2.

The replacement degrees of freedom were found to be an improvement on the earlier choice as they were more logical, simpler and gave better results.

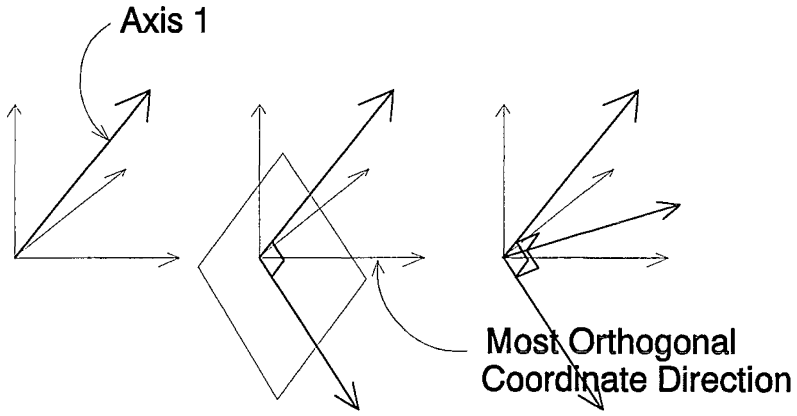

Figure 11-2 *Development of local nodal coordinate basis.*

11.1.3 Fibre Torsion

After the modifications described above were made to the program a better approximation to the fibre torsion could be coded. A number of methods of calculating the path torsion were attempted before one was chosen. These options will be briefly outlined below starting with the calculation of torsion for a general smooth three dimensional curve.

Torsion in a smooth three dimensional curve.

The coordinates of a curve are defined by the vector **r**, which has components (x,y,z) that are functions of the arc length s. The unit tangent vector (**u**) to the curve at any point can be calculated as:

$$\boldsymbol{u} = \frac{d\boldsymbol{r}}{ds} = \frac{dx}{ds}\boldsymbol{i} + \frac{dy}{ds}\boldsymbol{j} + \frac{dz}{ds}\boldsymbol{k} \qquad \textbf{(11-1)}$$

The derivative of the unit vector with respect to the arc length forms the product of the inverse of the radius of curvature and the unit principal normal vector.

$$\frac{d\boldsymbol{u}}{ds} = \frac{1}{\rho}\boldsymbol{n} \qquad \textbf{(11-2)}$$

The radius of curvature can then be written in terms of the coordinates.

$$\rho = \frac{1}{\sqrt{\left(\frac{d^2x}{ds^2}\right)^2 + \left(\frac{d^2y}{ds^2}\right)^2 + \left(\frac{d^2z}{ds^2}\right)^2}} \qquad \textbf{(11-3)}$$

The binormal vector can be defined in terms of the previous two.

$$\boldsymbol{b} = \boldsymbol{u} \times \boldsymbol{n} \qquad \textbf{(11-4)}$$

The derivative of the binormal vector with respect to the arc length can be shown to be the product of the inverse of the radius of torsion and the principal normal vector.

$$\frac{db}{ds} = -\frac{1}{\tau}n \qquad \textbf{(11-5)}$$

Therefore the radius of torsion at a point in a curve can be found as the inverse of the magnitude of this derivative.

With some manipulation the torsion in the curve can be re-written in the two forms shown below.

$$\frac{1}{\tau} = \rho^2\left(u \times \frac{du}{ds} \cdot \frac{d^2u}{ds^2}\right) \qquad \textbf{(11-6)}$$

$$\frac{1}{\tau} = \rho^2 \begin{vmatrix} \frac{dx}{ds} & \frac{dy}{ds} & \frac{dz}{ds} \\ \frac{d^2x}{ds^2} & \frac{d^2y}{ds^2} & \frac{d^2z}{ds^2} \\ \frac{d^3x}{ds^3} & \frac{d^3y}{ds^3} & \frac{d^3z}{ds^3} \end{vmatrix} \qquad \textbf{(11-7)}$$

Numerical Calculation.

The fibre element for which the torsion had to be calculated was modelled as three straight lines. This is the minimum number of lines to form torsion, two lines must always lie in the same plane and therefore cannot have any twist.

All of the torsion calculation methods start by assuming that the unit tangent vector has three distinct values over the length of the fibre piece, one for each of the line segments.

Method One.

The first method derives approximations for each of the vectors describing the path deformation. The principal normal vector can be evaluated at the two corners within the fibre segment. A finite difference formula is used to approximate the vector derivative.

$$n_A = \frac{du_A}{ds} \approx \frac{u_2 - u_1}{\Delta s} \qquad \textbf{(11-8)}$$

Where A and B denote the two corners and 1,2,3 denote each of the three fibre segments.

The binormal vectors can then be found at each corner using (11-4). The derivative of the binormal vector (and hence the torsion) could then be calculated using another finite difference approach between the two corners A and B.

This method of torsion calculation was found to give good results as long as the fibre piece was in single curvature. If the piece was in double curvature the binormal vectors would be co-axial but in opposite directions, the resultant derivative would have a large value instead of zero.

Method Two.

The second method used equation (11-6) numerically calculating the various derivatives. This avoided the problems found in method one while in double curvature. The first derivatives of the tangent vectors were calculated at the corners and then averaged to give a value at the centre of the fibre piece. The cross product was then formed with an average tangent vector. The second derivative of the tangent vector was found from the difference of the first derivative vectors already calculated. The torsion at the centre could then be calculated. If the point C is called the centre of the fibre then this approach could be written as:

$$\frac{1}{\tau} = \left(\frac{\rho_A + \rho_B}{2}\right)\left(u_C \times \left[\frac{du}{ds}\right]_C \cdot \left[\frac{d^2u}{ds^2}\right]_C\right) \qquad \textbf{(11-9)}$$

This was found to give good results at small values of torsion but would give unrealistic answers at larger values.

Method Three

Method two was modified to calculate the values at the corners before averaging to give the torsion for the whole segment.

$$\frac{1}{\tau} = \frac{\rho_A}{2}\left(u_A \times \left[\frac{du}{ds}\right]_A \cdot \left[\frac{d^2u}{ds^2}\right]_C\right) + \frac{\rho_B}{2}\left(u_B \times \left[\frac{du}{ds}\right]_B \cdot \left[\frac{d^2u}{ds^2}\right]_C\right) \qquad \textbf{(11-10)}$$

This formula was found to give a better approximation to the curve torsion.

The torsion formula was then coded into the three dimensional analysis. The program was convergent for small displacement analyses but unstable at larger displacements. It was shown that the convergence problem was caused by the torsion modes. Another method for calculating the torsion was then developed which had a less rigorous definition but a more successful result.

Method Four

In order to find the problem with the results of method three an accurate assessment of what the fibre torsion should be was found. A cubic curve was fitted through the four points defining the three line segments in space. The torsion was then evaluated by using equation (11-7), calculating the derivatives of the fitted curve numerically at a large number of points along the curve.

It was found that torsion is introduced into the fibre gradually as the points are moved from an initial position which is almost straight. If the fibre is bent within a plane before moving the nodes to introduce torsion then the rate of torsion increase is considerably greater. The high rate of increase was causing the system to become unstable and preventing convergence.

The fourth method of torsion calculation is based on intuition more than rigorous mathematics. Consider the fibre segment formed from three segments each with a unit tangent vector defining the direction of the segment. If the segment is observed along the line formed by the second unit vector then the torsion must be related to the area of the triangle formed from the two other vectors (Figure 11-3).

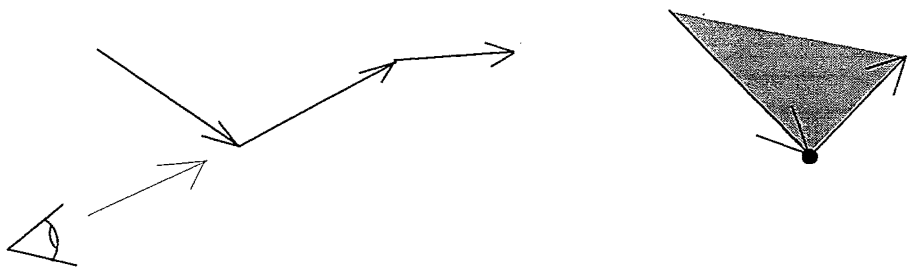

Figure 11-3 *Torsion approximation, view of three segment fibre along axis.*

The actual value is then calculated by finding the two vectors which are the parts of the first and third unit tangent vectors that are orthogonal to the second. The component of the cross product of these two vectors in the direction of the second tangent vector gives the torsion approximation.

The final dot product will not change the magnitude of the result as the vectors are coaxial and one is of unit magnitude but the torsion value is given direction (positive or negative) from this operation.

This formula has little justification but after coding it into the program the analysis converged in a significantly wider range of cases. Further work would require a validation of this formula or the presentation of a better substitute.

11.2 Test Run Convergence

Test runs on the three dimensional model encountered some difficulties, mostly concerned with the boundary conditions or the element jamming. These difficulties will be discussed in this section while the results will be presented in section 11.3.

11.2.1 Element Pinching

It was found that under certain circumstances one of the elements within the central core of a yarn would become *pinched*. A *pinched* element has been twisted so much that the edges touch in the centre, the element is unstable in this state as it can freely pivot, Figure 11-4.

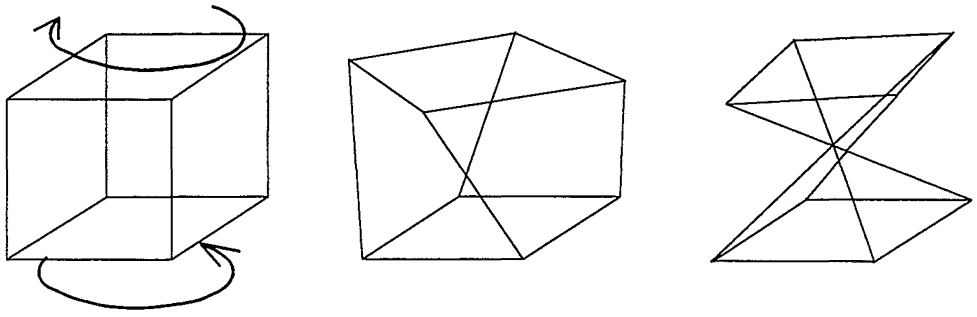

Figure 11-4 *'Pinching' of a single element under twisting.*

There were three reasons why the element pinching occurred. The first is a combination of the initial mesh geometry and the value of the continuum jam point. Elements typically have the initial geometry of a distorted cube with a height to width ratio of about one. During deformation the elements often compress at right angles to the fibre direction causing them to become tall and narrow. A tall narrow element becomes susceptible to the pinching problem as only a small amount of twist is required to cause the edges to cross. The solution to this problem is to design the initial mesh so that the elements are short and wide, after deformation they will deform into a more normal element shape[24].

The second problem which increased the chance of *pinching* occurring within a mesh was the type of boundary conditions being enforced on the assembly. It was clear during the two dimensional analysis that the more realistic the boundary conditions were then the better convergence to a solution was found. This is also the case with the three dimensional model. Preliminary runs restricted the position of the fibre ends at the top of the yarn during torsion while the rotation of the fibre was not controlled. This condition was quite unrealistic as the fibres tended to deform to a path which left the top node and cut close to the yarn axis, causing element *pinching* to occur (an example of this deformation is given in section 11.3). The solution for this was to enforce more realistic boundary conditions at the top of the yarn.

The third reason for the *pinching* problem is the lack of a jam condition anywhere except at the ends of the element. If there were some resistance to the central portion of the element closing to zero then *pinching* would not occur. This problem is however too complicated to fix within this analysis and a solution will have to be left for future elements.

11.2.2 Restraint Conditions

Almost all test runs were controlled by enforcing displacements onto control nodes, typically an entire layer of nodes. It was established after preliminary runs that to get meaningful results the fibre rotations must be enforced at the control nodes as well as the displacements.

---

[24] The problem can also be solved by increasing the continuum jam point, but this would not normally be possible as it is a function of the material being tested.

An attempt was made to modify the three dimensional analysis program so that the fibre direction could be specified at any node but this adjustment proved to be too complicated. The program has been modified to put in so many additional features that the code has become cumbersome and further significant adjustment almost impossible.

Displacement restrictions were placed on the top two layers of the mesh providing adequate directional restraint to the fibres. The extra storage required for this system is small as it requires restricting three degrees of freedom per node over two layers as opposed to five degrees of freedom per node over one layer if the fibre directions could be restricted. There is a degree of extra computational effort required as the total number of elements is increased.

11.2.3 Element Jamming

With torsion resistance being provided within the fibre, the range of possible test cases increased from those of the previous chapter. The new cases revealed further problems with the jamming of the fibrous finite element.

One of the new cases was the twisting of a yarn without the application of an axial force and both initially straight and twisted yarns were tested. Without significant tension force in the fibres the jamming of the central element (the element in the yarn core) was found to be unstable. The edges of the central element are all moved towards the axis of the yarn as the twist increases until jamming. Once jammed the force being applied to enforce the jam condition is generated largely from the increased bending in the fibres. This force is considerably smaller than the force which that would come from an extension of the fibre. The square shape of the element proved to be unstable in this situation as the square would deform into a diamond or some more irregular shape. The orientation of the element distortion would alternate at different layers up the yarn to avoid introducing any fibre extension.

This problem can only be solved by defining a new jam condition which is stable under a greater range of situations. The new condition could be defined for the present element or a new element could be developed for which such a formula could be defined in a simple manner. Neither of these options has been applied to the present analysis.

11.2.4 Increment Size

It was found that the magnitude of the displacement increments was critical to the convergence of the system. If the displacement was greater than a certain value then the system would not converge but at a slightly smaller increment convergence would be easily obtained. This limit was found to increase with the length of the element at which the displacements is being enforced. Shorter elements required smaller increments of displacement. If the system failed to converge at the first step often a smaller increment would give a solution.

The requirement that a small step size be used resulted in a large number of steps being required within each analysis. Fewer iterations were required to achieve the final result if a number of the intermediate steps were set to have large convergence tolerances. The speed increase was at the expense of detailed information at the end of every step.

11.2.5 Computational Effort

To show the amount of computational time that was required for these analyses a simple test case was run on each of the three types of machine used. The three machine types are listed below followed by the CPU time taken for the test case.

SUN SPARCcenter 2000
The SUN is managed by the Computer Services Centre of the University of Canterbury. It has two SPARC 40 MHz processors and uses SunOs, a variant of the Unix operating system.

DECStation 3100
The Civil Engineering department of the University of Canterbury has two of these machines. The machines run Ultrix, a variant of Unix.

DECStation 2100
Civil Engineering also has five DEC 2100's, these machines also run Ultrix and were used for the bulk of the calculations. Their low rate of use by other users combined with the fact that there were five of them made them the most attractive option despite the fact that they were the slowest machine.

The CPU time figures quoted below are actual processor time, if more than one user were using a machine at the same time then the clock time could be a small fraction of this time (often the case with the SUN machine).

Machine	CPU Time	Ratio
DECStation 2100	1183.2 secs	6.0
DECStation 3100	822.0 secs	4.2
SUN SPARCcentre 2000	196.4 secs	1.0

The Ratio given in this table is the ratio of the CPU time against that for the fastest computer.

The test case was a four element vertical stack, with an axial load applied in two steps. Nine iterations were required during the analysis.

11.3 Results

The following pages show eight sets of results from the three dimensional model. These results demonstrate both the problems with the present model and the potential of fibrous finite element analysis.

In all of the figures the light lines represent the undeformed state of the assembly and the heavier lines are the deformed state. In some figures all of the lines defining the fibrous elements are shown but at times this is confusing and these are removed to leave just the element fibre corners. These corners are those which are parallel to the fibre direction, they trace the fibres through the assembly.

It is clear from the figures that the problems with the three dimensional analysis are almost exclusively caused by the failure of lateral jamming modes of the element.

11.3.1 Torsion Pinching

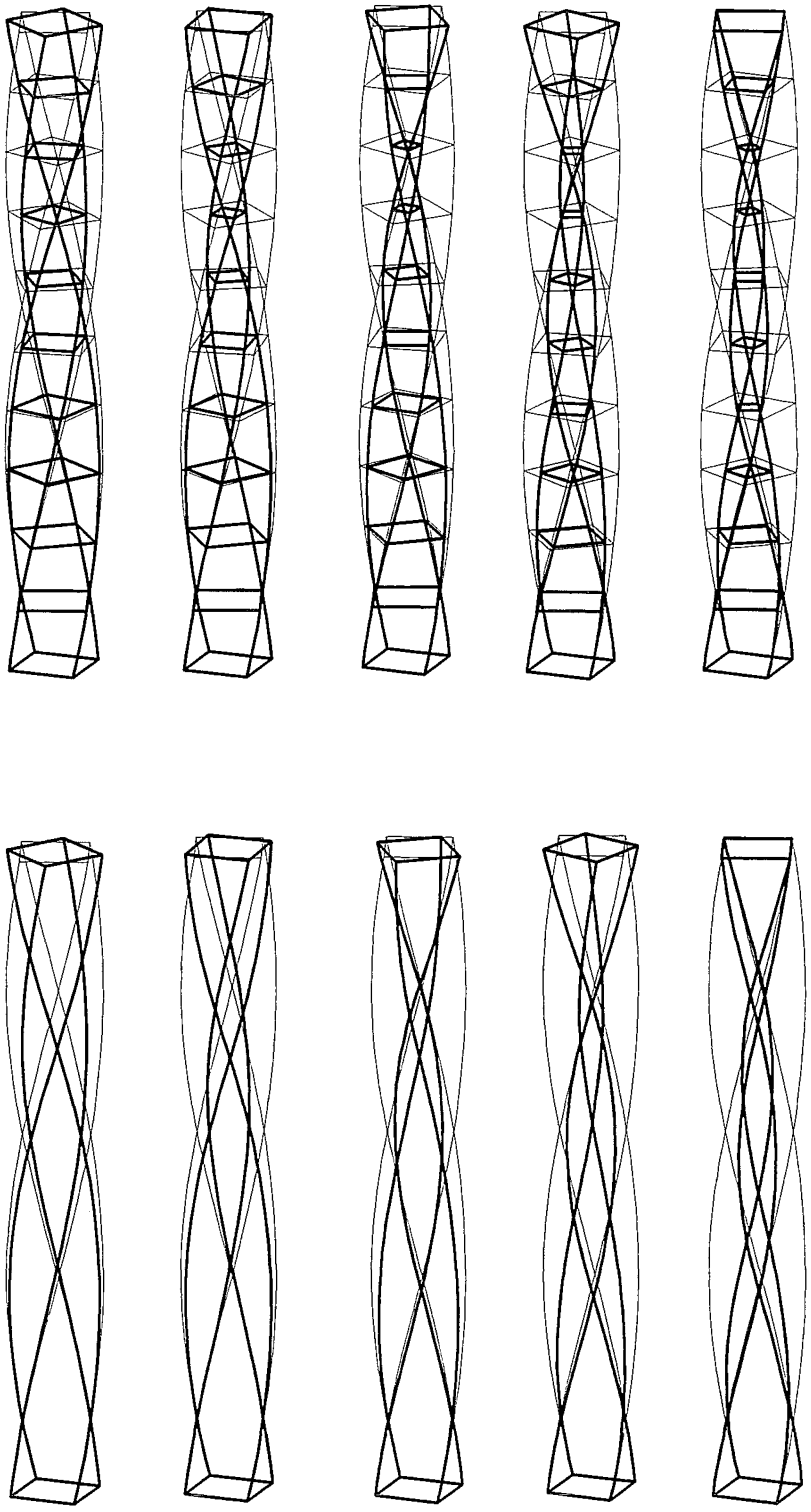

Figure 11-5 *Simple yarn torsion model, tendency to pinch in third element.*

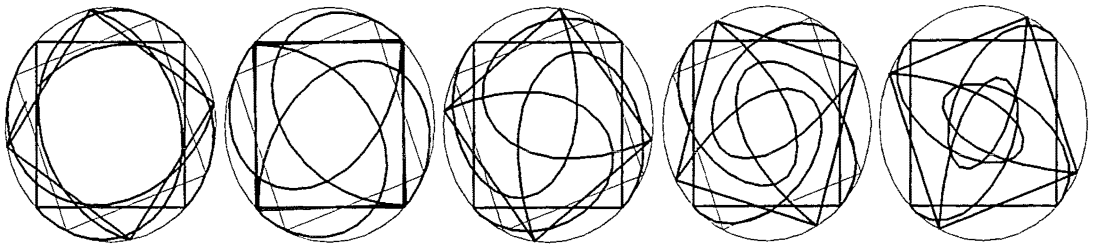

Figure 11-6 *Torsion model from above, element lines not shown*

An attempt at a yarn torsion model is shown in Figure 11-5, the five plots at the top of the figure show the progressive deformation of the element mesh as the top face is rotated. The top face is free to move vertically during the analysis and zero axial load is applied.

The boundary conditions imposed on this mesh are unrealistic, the bottom face fibres were held fully fixed while the top face fibres had an enforced displacement but were free to change direction. This boundary condition discrepancy is the reason that the deformation in the yarn model is biased towards the top during deformation.

The third element from the top of the mesh is almost pinching in the fifth plot, the analysis failed to converge after this point due to pinching in this element. The views of the same deformation from above (Figure 11-6) clearly shows that the boundary conditions are a cause of the pinching problem.

As the top face rotation increases the fibre curvature normal to the axis increases. The fibre takes a shape in which the fibre meets the top face at an angle significantly different from the initial angle. In the fifth plot the fibre passes close to the yarn axis near the top of the mesh, a small amount of additional rotation causes the fibres to cross the axis resulting in a pinching problem.

A better jamming condition would prevent this from occurring, but the boundary conditions are unrealistic and it is shown in a later test that adjusting these boundary conditions eliminates this type of problem.

11.3.2 Compression Pinching

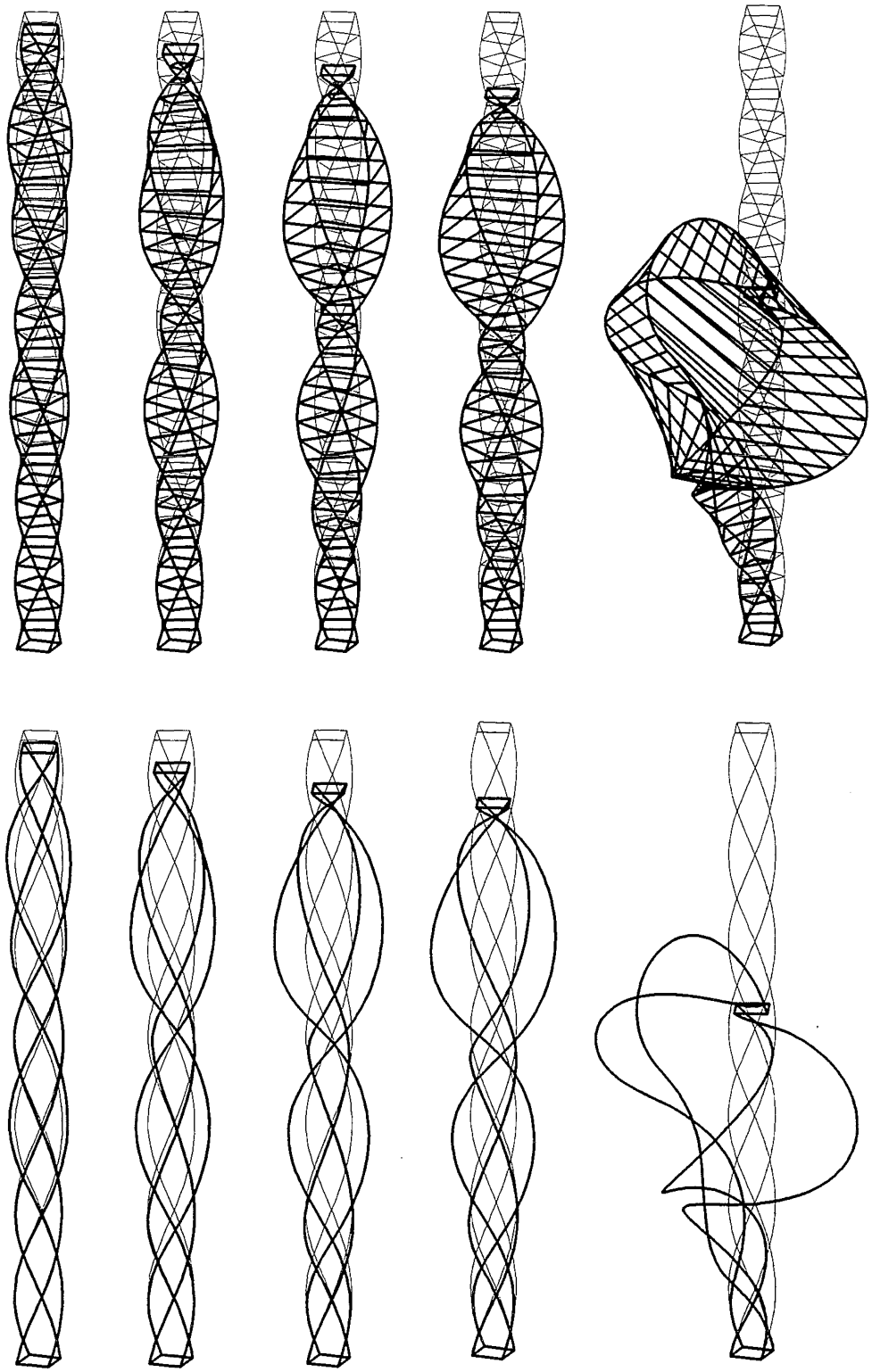

Figure 11-7 *Compression under applied force, non-convergence due to pinching.*

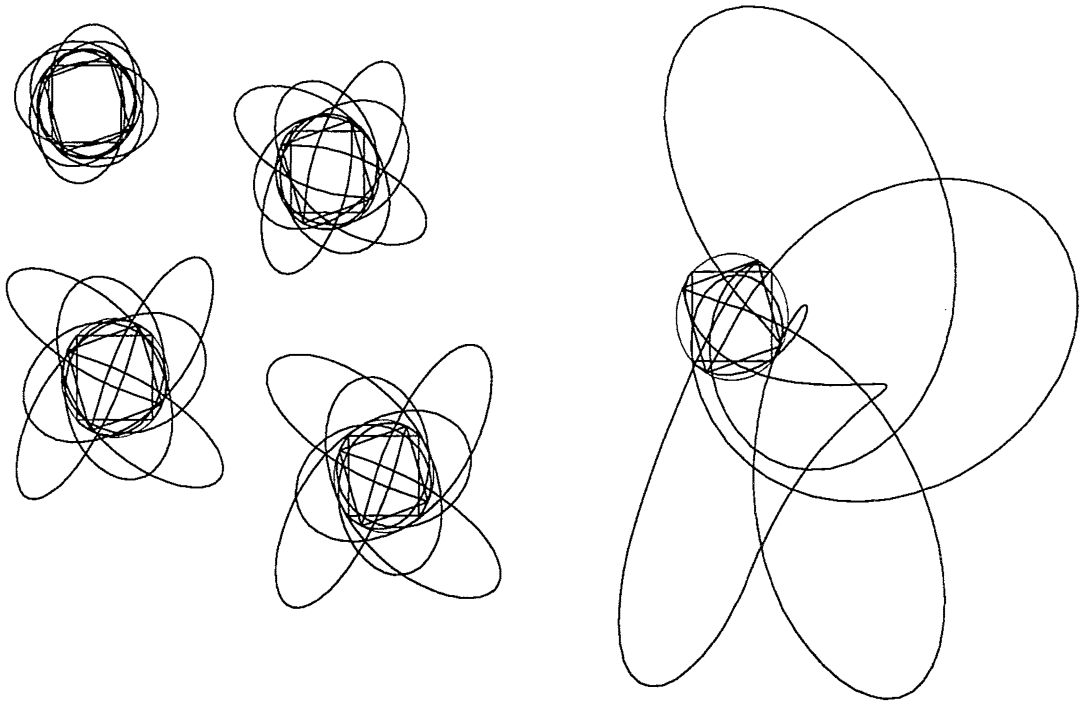

Figure 11-8 *Compression pinching view down the yarn axis.*

An axial compressive load is progressively applied to the element assembly. This test suffers an element pinching problem which is more apparent than that on the previous pages. The second element from the top is pinching from the second plot shown but as the element is not under torsion the system still converges. The effect of this unrealistic deformation is to reduce the resistance of the model. The fibres can assume a minimum energy position that would not be available in a better model.

In the final plot the system has failed to converge, the fibres have effectively buckled and are incapable of resisting the force being applied. It is interesting to note from the views from above that the fibre deformation remains axisymmetric up until the non-convergent step.

11.3.3 Torsion - I

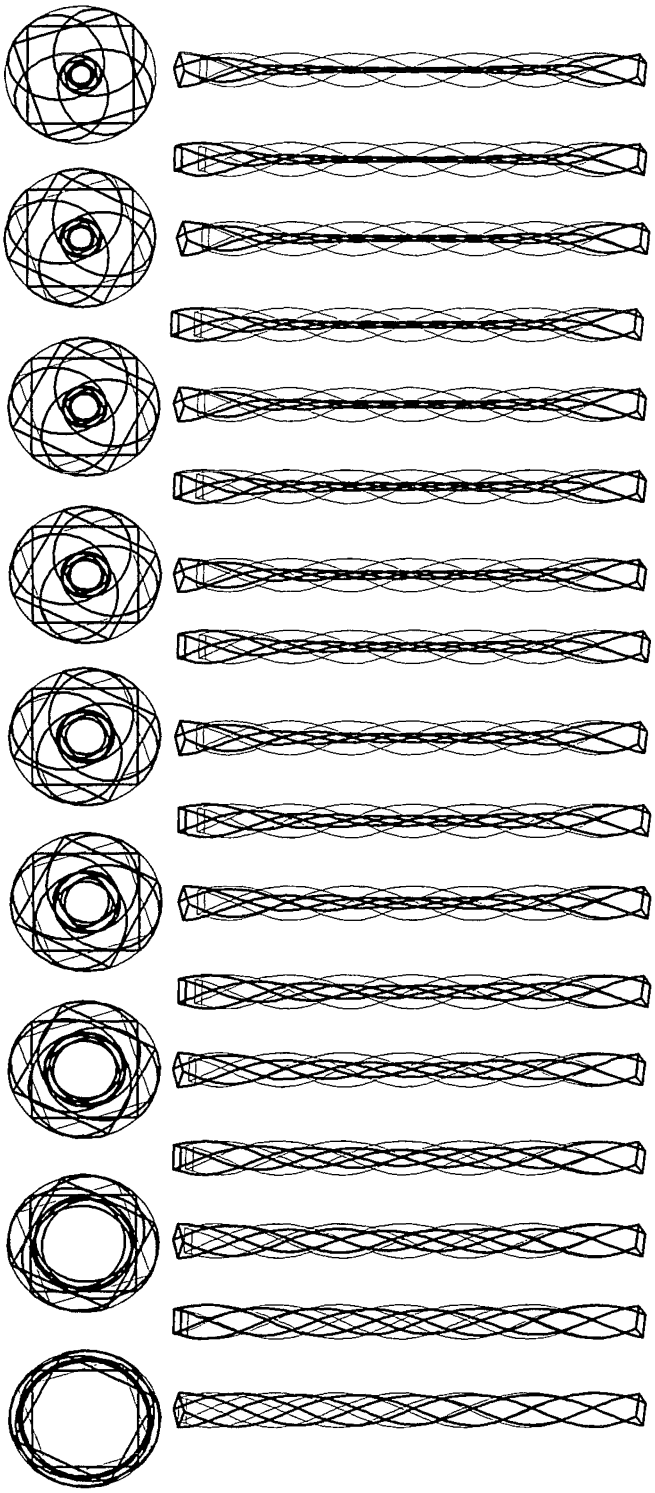

Figure 11-9 *Deformation plots from the side and top with increasing twist.*

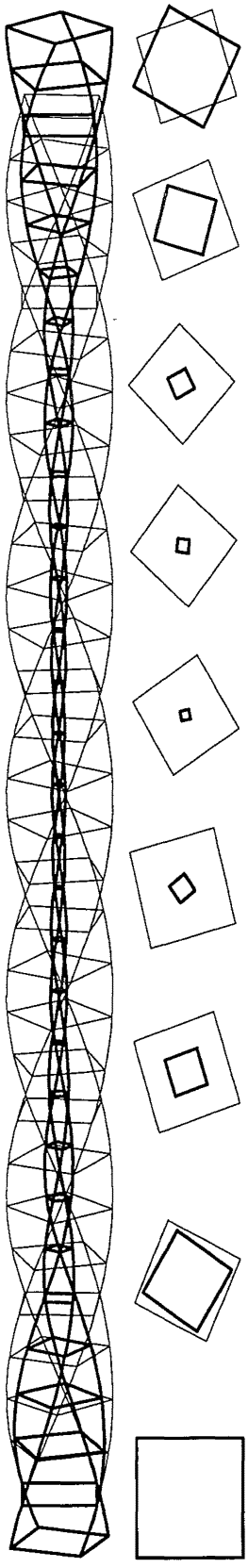

This test underwent a rotation of the top face under zero axial load. The boundary conditions are configured so that the fibres meeting the top face do not change the angles at which they intersect the face. This condition was enforced by restraining the displacements of all of the nodes in the top two layers. For symmetry the bottom two layers were given the same restraint.

The scaling of the plots within the figure opposite is variable, each plot is scaled to have the same length. To assess the extension of a deformed mesh it must be compared against the undeformed mesh on the same plot.

The plots of the view along the axis clearly show the differences between this zero tension torsion model and the torsion model of the previous chapter. The fibres can be seen bending from their starting points, reaching a constant curvature as they wrap around the jammed core and then flaring out to the top.

The central core of this model becomes quite small, the stiffness of the jam condition of this run was based on the fibre extension stiffness. The fibre was not in tension and so the stiffness was quite low, later models increase this value to give better jamming behaviour.

The adjacent figure shows the element mesh in the final state, cross-sections are shown at various positions along the length.

11.3.4 Torsion - II

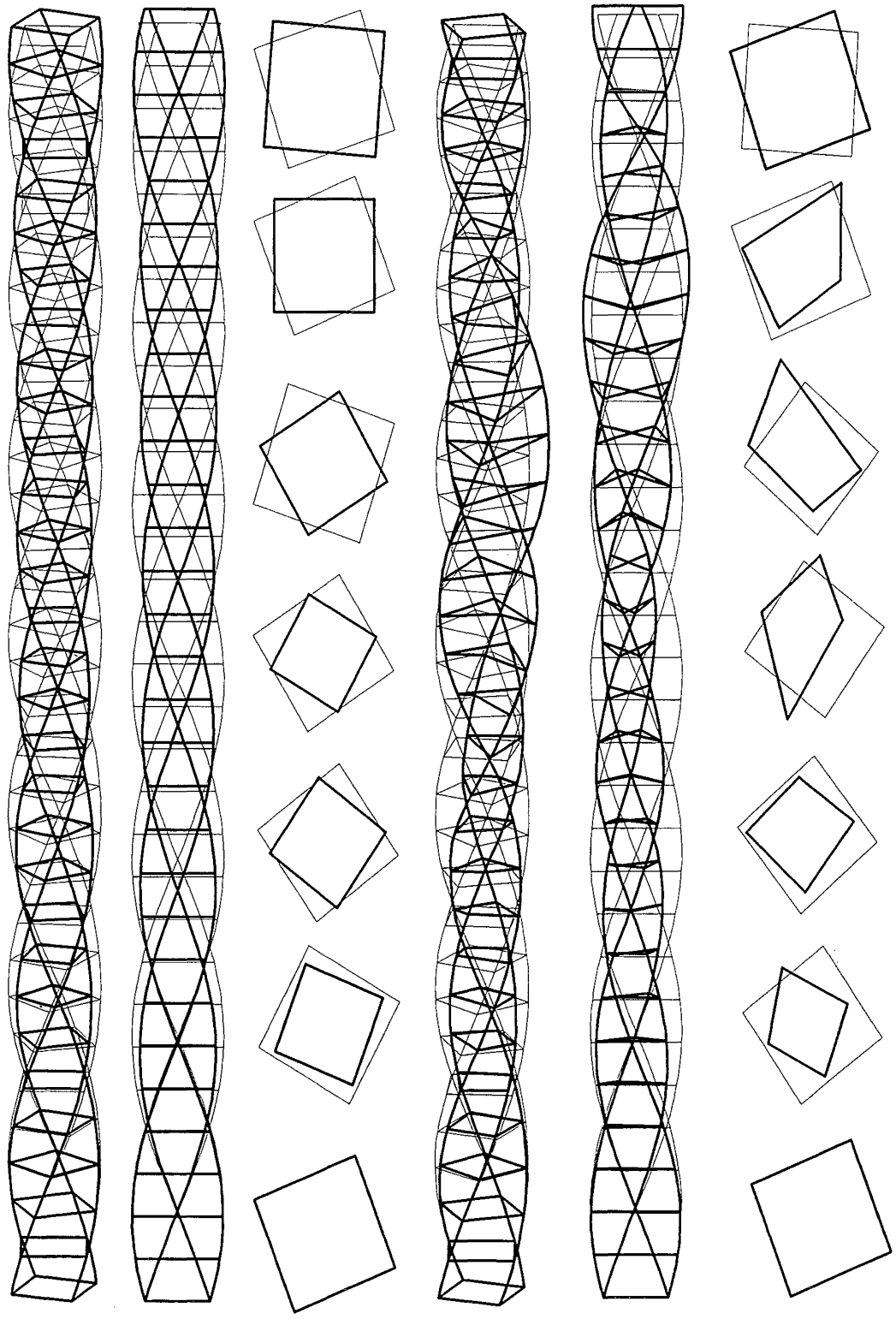

Figure 11-10 *Mesh under torsion, jamming modes cause non-convergence.*

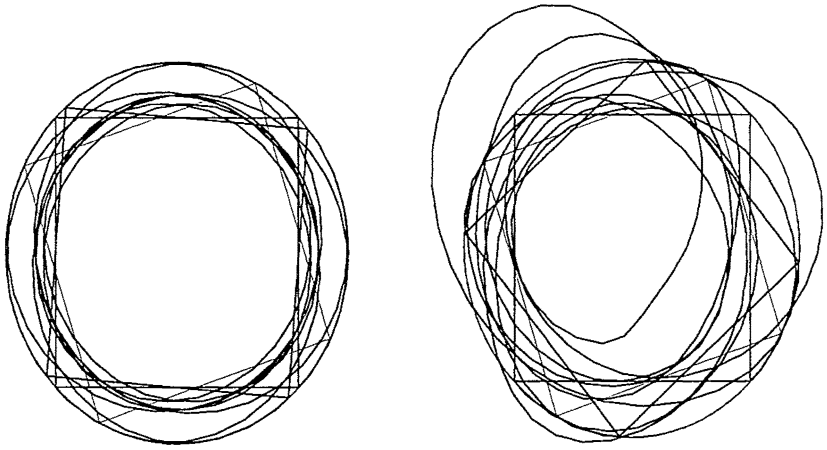

Figure 11-11 *View down axis of torsion model, element lines not shown.*

The figure opposite shows a mesh under torsional deformation similar to that of the previous test. The jam limit in this case has been set at 0.9 rather than the value of 0.25 which is commonly used in other tests. It was intended to assess the stability of the lateral jamming modes of the element in a slightly different situation to what they had previously been exposed. The elements were revealed to be unstable.

The first three columns of the figure represent the model at in intermediate stage. The first column is a three dimensional view and gives a clearer picture of the mesh than the second column which views the mesh from the side. Side views of the mesh allow assessment of how much each layer has moved out of plane, the intermediate plot has experienced no noticeable out of plane movement. The third column shows layer cross sections at various height on the model, it is clear that the model remains axisymmetric at this stage.

The final set of columns show the mesh in the final state. Jamming modes in the element have become unstable and have been able to minimise energy by warping the layer shapes out of plane. Layer plots clearly show that the mesh is no longer axisymmetric.

The views along the axis show how little lateral contraction occurred and verify the unsymmetric nature of the deformation.

11.3.5 Bending - I

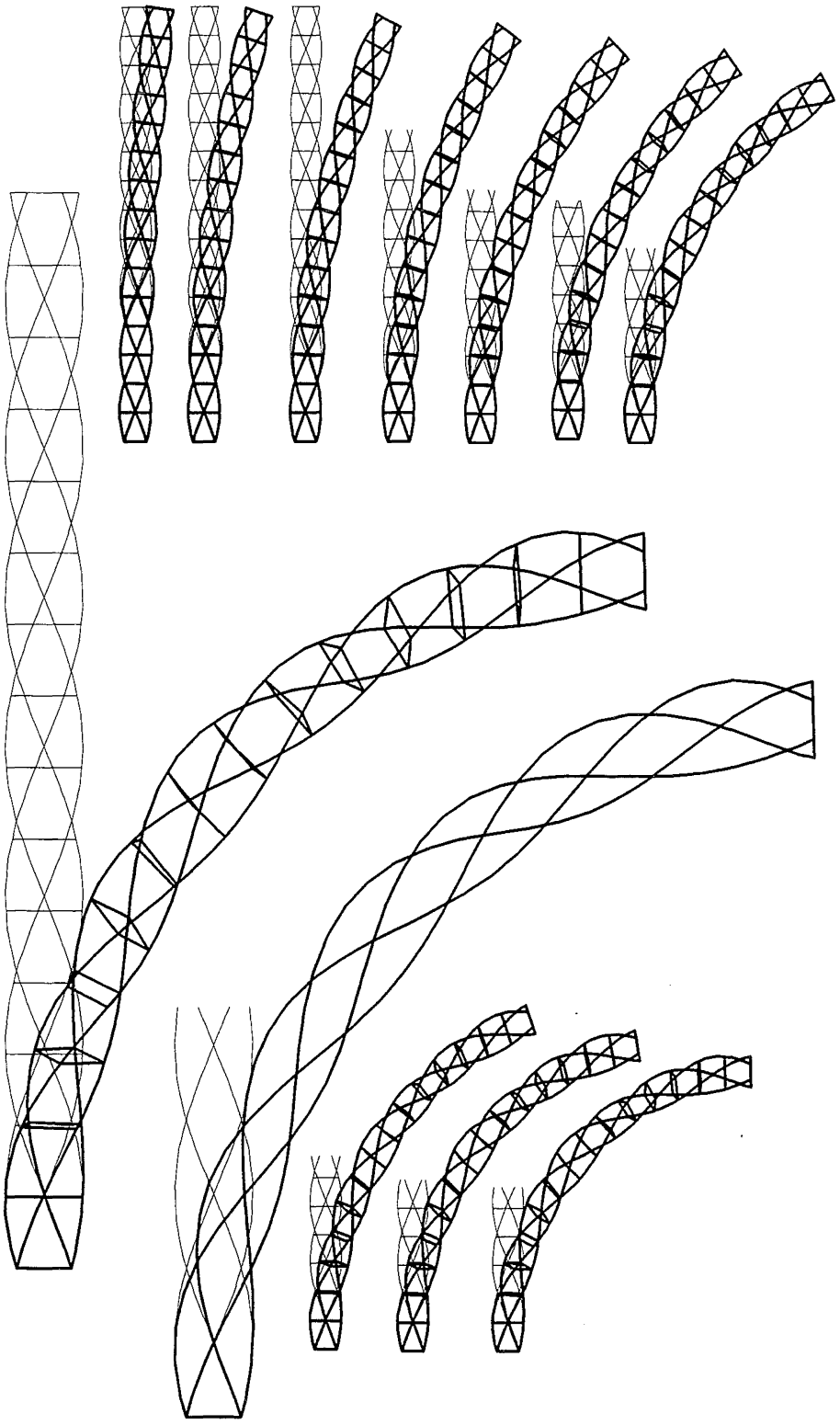

Figure 11-12 *Bending of a simple initially twisted mesh.*

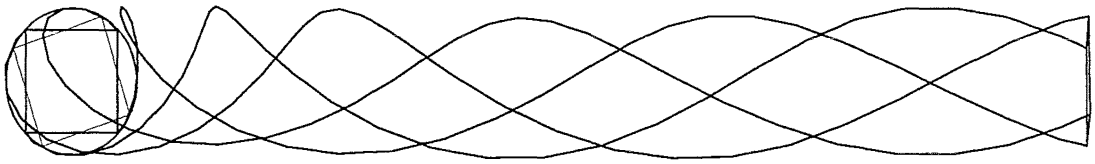

Figure 11-13 *Bending of a simple initially twisted mesh, top view.*

The figure opposite shows the progressive bending of a mesh of 15 elements. The elements are twisted in the undeformed state.

The model is bent by enforcing displacements on all three translation degrees of freedom on each node of the layer. Two layers at each end of the mesh are restrained giving directional and positional control over the fibre ends.

At each step the location and angle of the top end is calculated on the assumption that the yarn is bending in a circular arc. The end nodes are then enforced to the calculated position. The plot represents every fifth step of the analysis, a large number of steps were required due to the size of the total displacement being applied to the top face.

During deformation the cross-sections of the yarn did not remain plane. The side view with the elements visible shows the fibres tending to move along their axis towards the outside of the curve. The top view of the yarn shows that there was no movement of the assembly out of the vertical plane.

11.3.6 In Plane Bending

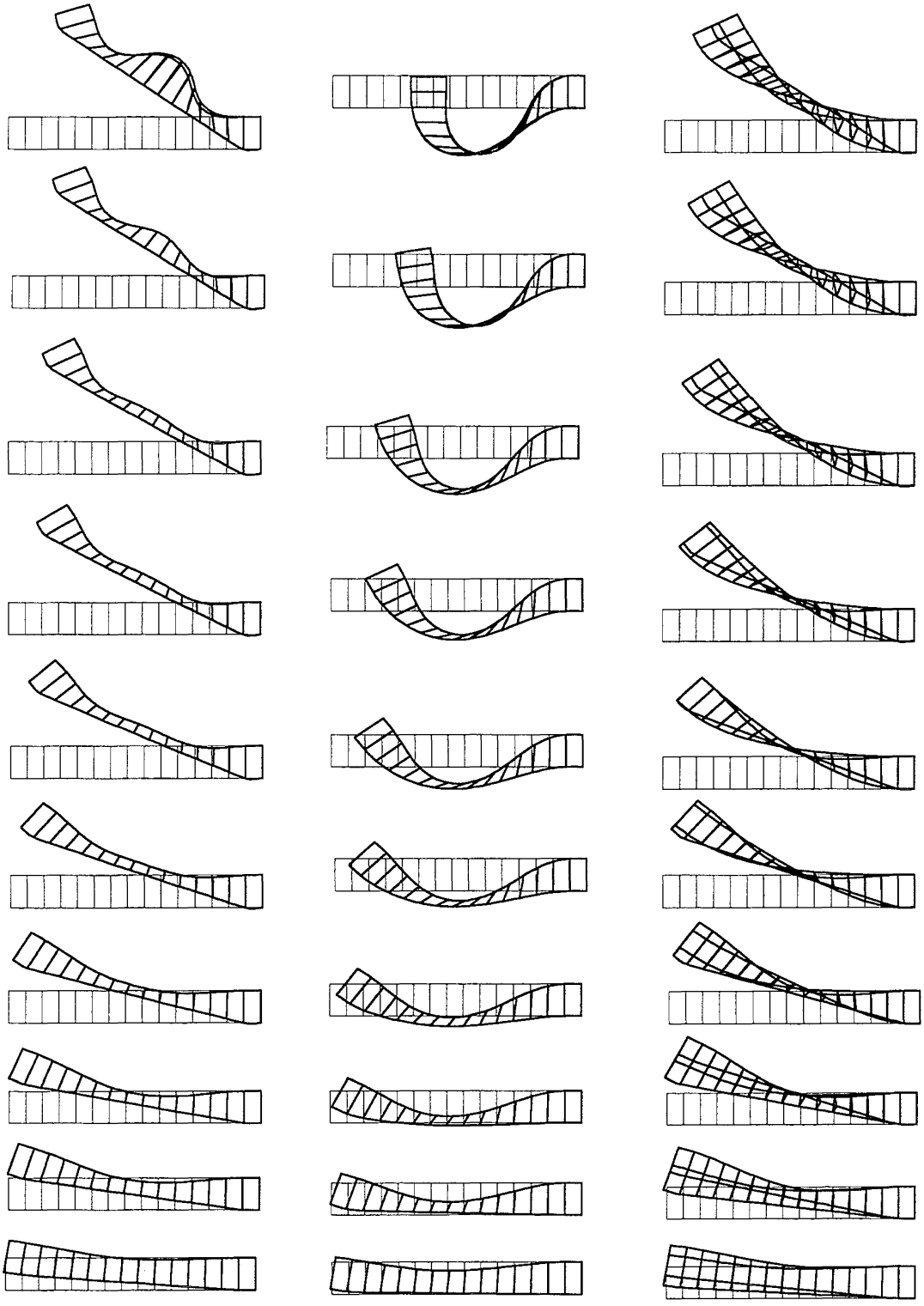

Figure 11-14 *Three simple test cases illustrating bending in a plane.*

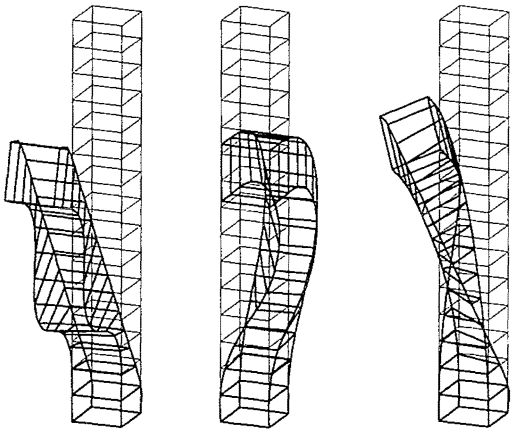

Figure 11-15 *Three dimensional view of the bending tests.*

Results from three test cases are shown on these pages, all three are a simple arrangement of straight fibres in the undeformed state.

The first test has been bent so that the end positions are the same as if it were bending in a circular arc. The lack of initial twist prevents the fibres from minimising energy by moving around the section towards the outside of the curve. The outside fibres go into tension while the fibres on the inside of the curve are in compression. The inside fibres quickly jam against the taut outside fibres and continue to increase their compressive load until buckling. The jamming of the elements works well in this situation.

The second test is similar to the first, except that as the mesh bends over a displacement is added which moves the top back to its original lateral position. The different deformation has the effect of preventing any of the fibres from going into tension. The jamming condition behaves badly as the thickness of the deformed mesh is smaller than the jam condition should allow. The poor performance of the jam condition in this case is linked to the large shear in the elements when they jam. There is a significant longitudinal displacement between either side of an element in the jam region, this does not occur in the first test.

The third test has the same enforced displacements as the first except that the top face is rotated by almost half of a turn. The top face rotation allows the fibres to take a shorter path but does not prevent all of them from going into tension. The jam condition behaves very badly in this case, the combination of unsymmetric deformation and the large differences in the axial force in the fibres causes large out of plane deformation in the layers.

11.3.7 Extension

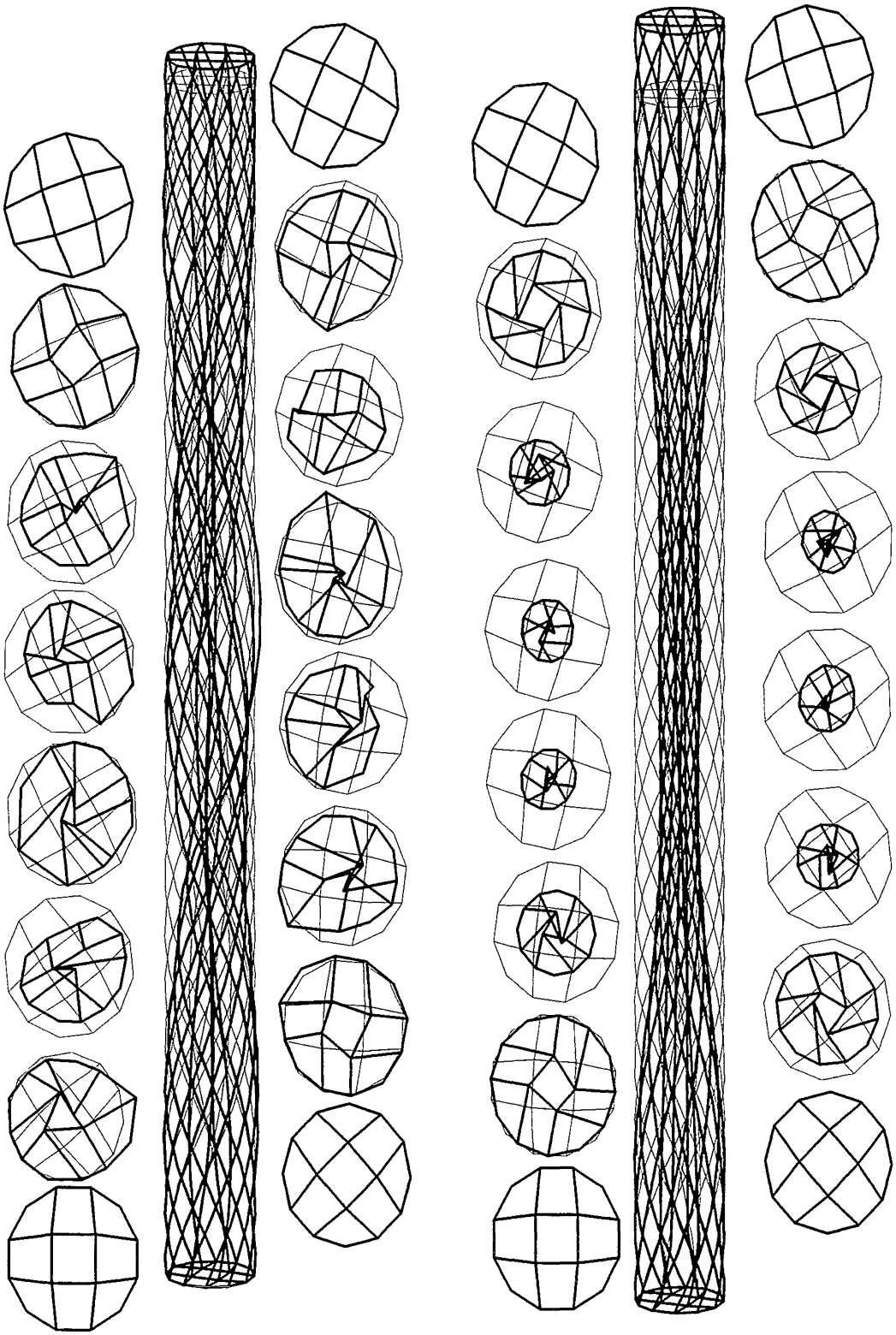

Figure 11-16 *Final deformation from two extension tests.*

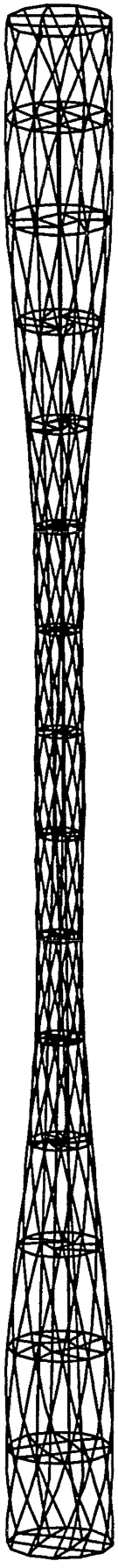

The final deformed shapes from two attempts at modelling yarn extension are shown on the opposite page. Neither model was wholly successful but they both help to point out the problems with both the element jamming modes and with modelling yarn extension. Extension was enforced in both case by specifying the displacements of the end layers.

The first model failed to converge after only one step. It is clear from the cross-section plots (either side of the three dimensional image) that the jamming of the central element has caused the failure. A view from the side of the mesh (not shown) revealed that the end faces of the central elements had twisted significantly out of plane, increasing the chance of failure of the jamming modes.

The second model is identical to the first except that the middle layers are all constrained so that each layer has only one longitudinal degree of freedom. Therefore the nodes on one layer must remain on the same horizontal plane and the central element ends cannot buckle.

The modified model was significantly more stable, a number of steps were performed before a failure to converge occurred. Examination of the layer cross-section reveals that this model also failed due to gross distortion of the elements. The element distortion in this case came about due to the large differential rotations between the elements near the centre of the yarn and those on the outside. Incorrect element jamming can still be blamed for this failure, the elements should not be able to be distorted to the degree that they are in this case. More elements within each layer would give a better solution, allowing the differential rotation within any one element to be reduced.

11.3.8 Axial Compression

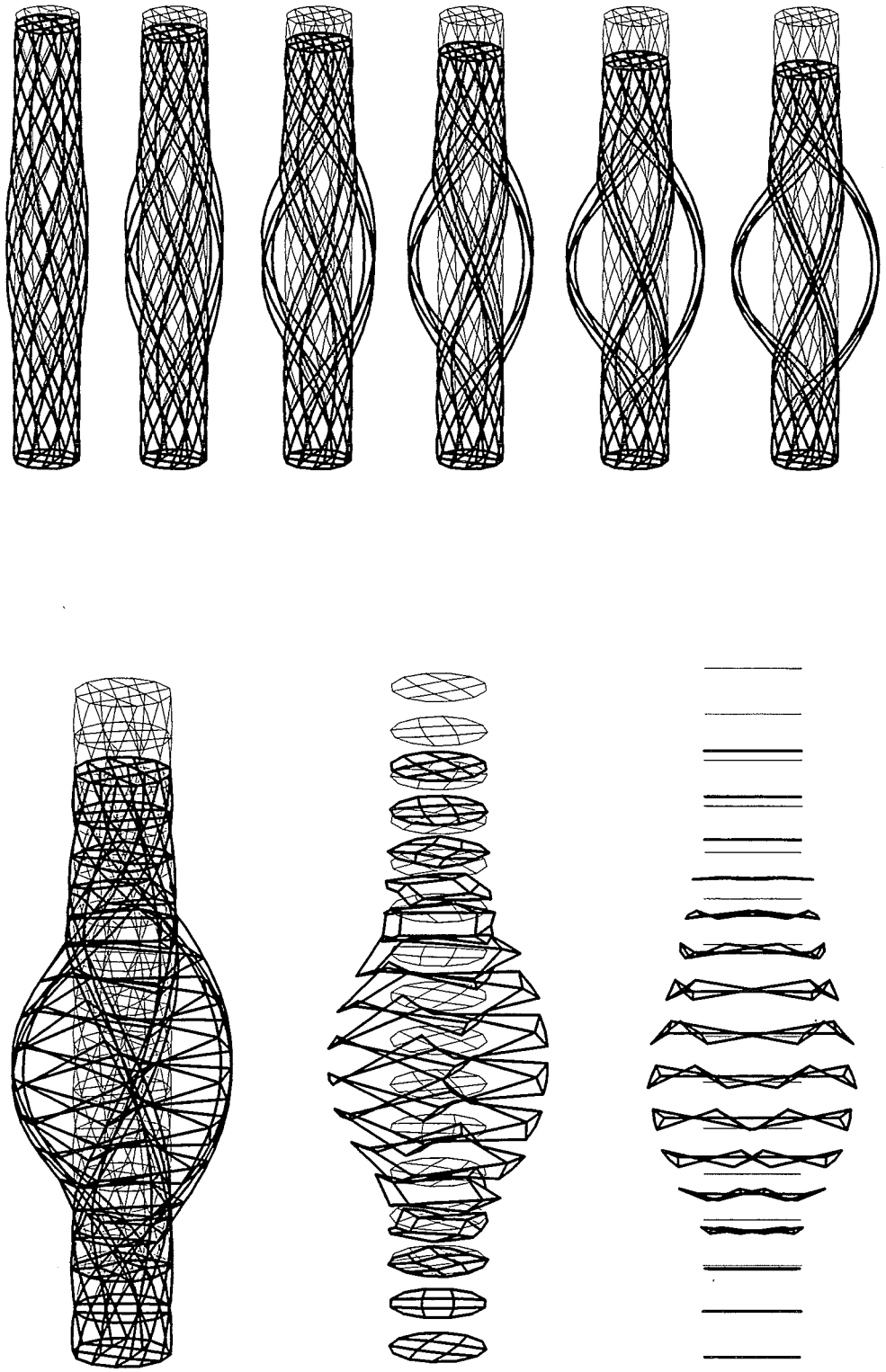

Figure 11-17 *Axial compression.*

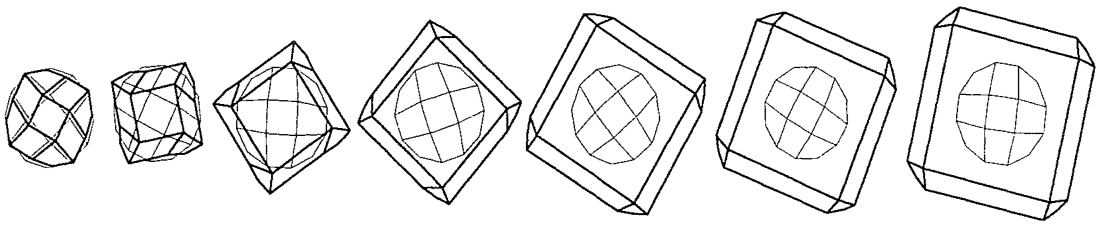

Figure 11-18 *Sample cross-sections of axial compression model.*

This test put the yarn model into axial compression by specifying the displacement of the top two layers of the mesh. Using the top two layers provided fibre directional restraint as well as positional constraint. The extra restraint avoided the pinching problem which was found with the earlier compression model.

At the top of the figure on the opposite page three dimensional views are shown of the fibres as the displacement is applied. It is clear that the fibres have not spread around the yarn in a uniform manner but bulged from the axis. The fibres have grouped based on the definition of the finite element mesh. The fibres closest to the yarn axis buckle first and have the greatest outward bulge, these fibres then press against the outer fibres, forcing them outwards. The central element is four sided in section and this is part of the reason for the way that the outer fibres group.

A plot of selected cross-sections from the deformed mesh (above) clarify the way that the outer fibres are being forced to deform. Only every second element around the circumference is jamming, and the mesh is deforming into a square shape.

A better shape to the deformation pattern could be achieved by either (or preferably both) of two methods. The number of elements in each layer of the mesh could be increased as more elements would diffuse the effect of the central fibres. A better lateral jamming formula could be found for the element, causing the lateral compression force to be better spread across elements.

12 Conclusions and Recommendations

12.1 Review

Prior to this study, finite element analysis had not been applied in a rigorous manner to yarn mechanics. There was difficulty in establishing how to approach the problem which is shown by the investigations of chapter five. Attempts to overcome the limitations of the two point bending element with regard to fibre direction continuity using a statistical approach were unsuccessful. The definition of the two point element properties were calculated in terms of the continuum strain parameters for both large and small deformations. These sections contributed to a better understanding of fibrous systems although there were few useful results.

Chapter six introduced the treatment of the fibres as fixed to a continuum material using a conventional finite element approach. The fibres were assumed to deform with the continuum and the strains in the fibre could be calculated as functions of the continuum strains. The analysis quickly became cumbersome and threatened to be too computationally expensive to be useful. This type of continuum approach was abandoned and the modal approach of chapter seven was investigated in preference.

The concepts of modal analysis were explained in chapter seven. The stiffness matrix controlling the actions of a single element were defined based on the deformation modes of the element. A coordinate system was developed for the element where deformation in the direction of each basis vector causes deformation of only one type in the element fibres. The fibre deformation types are the fibre extension, bending or torsion. Remaining basis vectors represent the deformation patterns which describe the movement of the continuum. In this modal coordinate system the element stiffness matrix could be easily constructed but it had to be transformed to conventional nodal coordinates so that it could be interfaced with the other elements in the mesh. Because the different fibre properties are treated independently, a separate routine could be called to define each property making it simple to use nonlinear material properties.

The equations used to transform the element properties to the global coordinate system were initially defined intuitively. This approach to the transformation used an iterative approach to find the mode shapes which separated the deformations and these mode

shapes were then used to transform the element matrices. The approach was simplified after it was shown that the first order transformation matrix could be derived directly.

A two dimensional analysis was programmed and used for testing the modal approach. The system remained unstable at large displacements and formal definition of the transformation equations was sought. When the stiffness matrices in each of the two coordinates system were written in terms of derivatives of the global energy it was clear that a second order term was omitted from the previous equation. The extra term added a component to the nodal stiffness matrix which depended on the modal force vector as well as the equations defining the mode shapes.

If the element modal coordinates are β_i, the nodal coordinates are α_j and the energy in the system is E then the transformation of the modal stiffness matrix to the nodal stiffness matrix can be written as:

$$\frac{\partial^2 E}{\partial \alpha_i \partial \alpha_j} = \frac{\partial^2 E}{\partial \beta_k \partial \beta_l} \frac{\partial \beta_k}{\partial \alpha_i} \frac{\partial \beta_l}{\partial \alpha_j} + \frac{\partial E}{\partial \beta_k} \frac{\partial^2 \beta_k}{\partial \alpha_i \partial \alpha_j} \qquad \textbf{(12-1)}$$

where the nodal stiffness matrix is $\frac{\partial^2 E}{\partial \alpha_i \partial \alpha_j}$, the modal stiffness matrix is $\frac{\partial^2 E}{\partial \beta_k \partial \beta_l}$ and the modal force vector is $\frac{\partial E}{\partial \beta_k}$.

The analysis was stable at large deformation after this transformation had been included.

Chapter eight detailed the process of defining the modal coordinate system of the two dimensional element in terms of the nodal coordinates. The highly variable resistance of the element in compression normal to the fibre direction causes problems but schemes are presented to overcome the difficulties. Programming the two dimensional model was a process of learning what can go wrong with a modal fibrous finite element.

The two dimensional element was verified against experiment in chapter nine. An array of springs was photographed under deformation and the numerical system was used to model the springs. Satisfactory matches were obtained between the springs and the model. Differences were explainable as being caused by effects that the numerical system was not designed to model properly.

Chapter ten introduced the three dimensional modal fibrous finite element. The new element was significantly larger and more complicated than the two dimensional element. The second derivative matrices had to be calculated numerically rather than analytically to ensure a useful system. The size of the numerical system required that a skyline matrix storage formulation be used while the Lagrange constraints being used meant that a pivoting equation solver had to be used. A pivoting skyline equation solver was written for use in the fibrous analysis.

A small number of tests were run with the three dimensional model but it was revealed that the torsion within the fibre was being misrepresented by the analysis. Systems would only converge if either all of the fibres were in tension or all were bending within one plane resulting in no fibre torsion.

Investigation into the lack of torsion revealed that both the rotation nodal degrees of freedom and the path torsion modelling were at fault. This is presented in chapter 11. The nodal degrees of freedom of the element were changed and the path torsion modelling was adjusted to give a solution. Limitations of the cuboid element with regarded to continuum jamming are revealed in the model and solution of the problem was too complicated to be adjusted within the present model.

Boundary conditions on the system were found to have a significant influence on the convergence and the more realistic the boundary conditions are modelled then the better the system convergence. This trend was duplicated in both the two and three dimensional models.

A greater range of test cases were found to converge with the improved three dimensional model, a selection was presented including yarn torsion, extension and bending.

12.2 Conclusions

This study has produced the most sophisticated yarn model to date. Never before has a single model simulated as wide a range of yarn deformations. The model supports yarn bending, torsion, extension, lateral compression or any combination of these deformations. The versatility of the approach allows the extension of the model from the present continuous filament single ply configuration to a staple fibre multi-ply configuration. With sufficient computing power the model could be used not only for any yarn situation but for any aligned fibre assembly problem. The degree of nonlinearity allowed in the fibre property specification is not limited allowing a realistic fully nonlinear yarn model to be developed.

The initial literature review indicated that the two contact point bending element would be the most likely development path for the fibrous analysis. Investigation of the two point element revealed that the lack of fibre direction continuity between bending elements would introduce an unacceptable degree of error. It was concluded that any accurate fibrous finite element analysis must maintain fibre direction continuity. This is necessary in any model that utilises fibre flexure.

The modal separation approach allows the definition of the material properties of the element in a coordinate system based on the element deformation modes. The nonlinear behaviour of the different modes may then be defined without consideration of the geometric linking between the modes. There is a clear distinction between those modes which are based on the relative positions of the fibres within the element (such as the lateral fibre jamming or the element face shear) and those modes which depend only on the fibre deformation within the element (such as the fibre extension). Defining the nonlinear response of each of these modes individually considerably simplifies the specification of the element properties.

The finite element program has separate program units to define the response of each mode type. The user has only to modify the code within each unit to adjust the material properties of the assembly allowing any type of nonlinear response to be included.

The analysis defines the element properties in terms of a coordinate system based on the deformation modes of the element and transforms the properties to a coordinate system based on the nodal degrees of freedom of the element. It was shown that the matrices describing this transformation can be defined in terms of the equations defining the mode shapes.

The fibrous finite element program developed along with this study must be regarded as preliminary. Limitations of the program with regard to lateral fibre jamming and torsion representation reduce the usefulness of this program as a general investigative tool. There is confidence that the element outlined in the next section will overcome the remaining few difficulties and produce an element to analyze the vast range of aligned fibre problems.

It is clear that dealing with fibrous deformations introduces an extra degree of complexity to the finite element method. Fibres in three dimensional space have the added complication of twist within the fibre. Specifying the position in space of the fibre is insufficient to resolve all forces along the length, the amount of twist must also be known. Any approach treating the fibres as part of some continuum material must maintain a record of the fibre twists as well as the spacial displacements. Great care must also be taken with the boundary conditions. The method of application can have a critical effect on whether a result is achieved.

The amount of calculation required for the fibrous element can easily make an analysis impractical. The equations defining the mode shapes must be defined in as simple a manner as possible without sacrificing the final result. The present analysis progressively simplified the bending, extension and torsion modes to achieve a practical system. In early models the derivatives were evaluated analytically but the large amount of computation required for the mode shape equations resulted in all internal derivatives being calculated numerically in the final model.

The finite element method has been shown to provide useful results when applied to fibrous assemblies. Future programs will only improve the quality of the results attained as well as provide greater insight into the mechanics of fibrous assemblies. This study has shown that the assumption of a continuum can be justified for a fibrous assembly but it must be remembered that in some situations the continuum assumption may be restrictive and lead to incorrect results.

The finite element approach which has been developed has application to a range of problems of which yarn mechanics is only a small part. Any material which has a high degree of anisotropy and nonlinear properties could benefit from the modal decomposition approach. It is likely that this approach would be useful in the design of large tent or sail structures where the in-plane deformation modes of the element could be separated. Materials used in these structures tend to have anisotropic material behaviour and nonlinear geometry due to high flexibility in the out of plane directions.

12.3 Recommendations for Future Research

There are a number of options for extending the fibrous finite element. The three most significant options are outlined below. The Author's recommendation will be explained in more detail.

- Fibres fixed in continua using a non-modal approach.
  This concept was abandoned in chapter six due to complication. It is possible that an analysis based on this method would be competitive with the modal analysis. The approach has the advantage of being better able to deal with an assembly of fibres that are not aligned with the element.

- Continue with six faced modal finite element.
  A jam condition could be designed for the element giving stability under a greater range of situations.

- Develop a simpler modal element.
  A new modal finite element could be developed based on a triangular prism. Three side faces in the fibre direction and two end faces perpendicular to the fibre direction.

The author's recommendation is the development of the triangular prism modal element. There are two reasons why the triangular element should be the next step in yarn finite element analysis. It can be shown that the computational cost of generating the element transformation matrices is related to at least the square of the number of degrees of freedom of the element. The triangular element would have only 36 degrees of freedom saving computational time. The most significant problem with the square sectioned element was the determination of the jamming condition. A triangle is a much simpler shape to deal with in this respect. The equations defining the jamming modes of the triangular element would be simpler and the overall computation would be reduced. It is clear that under deformation and jamming the triangular cross-section of this element would be more stable than the four sided cross-section of the previous element.

An outline for the development of the triangular element is given. A number of the steps which are to be recommended for this element would also be required for either or both of the other two options.

A three dimensional single fibre modal analysis should be developed. An element representing just a piece of fibre would have twelve degrees of freedom. This element would accomplish a number of tasks that cannot be done once a fibre model is assembled into a continuum element. Each of the three models for bending, extension and torsion could be assessed in three dimensions and their stability and accuracy under a range of deformations could be verified. The fibre direction nodal degrees of freedom could be fully tested under a greater range of displacements than those under which they have already been shown to work.

Better material models must be found, in particular to replace the simplistic jamming model used in the present program. A better jamming model would most likely have a more gradual initial jamming phase and lead to a more stable system.

It was proposed that finite precision computing could mean that the numerical calculation of the derivatives of the shape functions would give better answers than that achieved by the symbolic approach. It would be interesting if a study were done to verify this assumption, although for reasons of simplicity it is likely that the numerical approach would remain the most practical.

During the numerical derivative calculation the symmetry of the second derivative matrix could be used to reduce the computational effort by approximately a factor of two. Small reductions in effort could be gained by finding the unmixed second derivatives using the information calculated to evaluate the mixed second derivatives. An alternative three point finite difference stencil could be used to find the mixed derivatives, saving another eighth of the computation.

An investigation should be made into using nonlinear equation solving techniques other than the Newton-Raphson method within each increment. Significant advantage could be found from other systems such as modified Newton methods when the calculation of the material properties is such an computationally expensive procedure.

The new element program should be able to implement boundary conditions to restrict the fibre direction at nodes. Complicated boundary constraints such as those implemented using the Lagrange multipliers must be introduced in the element. More realistic yarn boundary conditions can be enforced with this type of constraint.

The fibre density in the continuum should be allowed to vary at least between different elements. This will not only allow more realistic modelling but is necessary if fibre

slippage in extension is to be included. If a fibre slips then it will lengthen, increasing the volume of the element while the total amount of fibre within the element should remain constant. A value of the mass of fibre material within each element should be maintained so that this would remain constant throughout the analysis.

The triangular element would have 36 degrees of freedom, the minimum to model the cubic variation of the three element corners and to cover the continuum deformation. The number of degrees of freedom of the element could be increased if an interpolation scheme greater than linear were to be used in the direction normal to the fibres. The extra calculation required for this would be prohibitive and selective integration should be used to compensate for the limitations of the linear interpolation.

The modes of the element could be arranged as:

Rigid body modes	6
Extension modes	3
Bending modes	12
Torsion modes	6
Face shear modes	3
Jam modes	6

The number of jam modes could be reduced to two, the other four modes would have zero energy and describe the shear distortion of planes normal to the fibre direction.

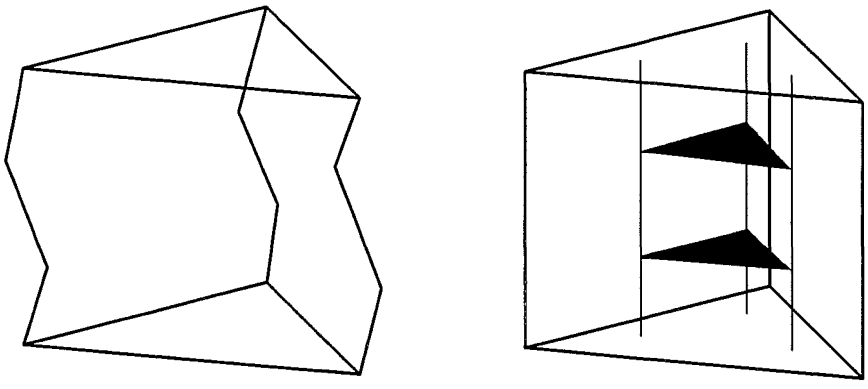

Figure 12-1 *Triangular modal element, showing cubic deformation and integration point fibres.*

A diagram of the proposed element is shown in Figure 12-1. The second part of this figure shows the control points for the modal analysis.

The three integration points for the element will be placed within the triangular cross-section, rather than at the nodes as in the square element. For this reason the modes must be based on the fibres passing through these points, such fibres are dotted into the element on the right hand side of Figure 12-1.

Having the element integration points away from the element corners will greatly improve the ability of the element to model the continuum. When the points were coincident with nodes the points from an adjacent element would be on the same point which is inefficient.

The two areas which could be used to calculate the jam modes are shown shaded in the figure, these areas are placed at the height of the bend in the fibre. This is the most efficient place to have the measures as it prevents the element connected longitudinally measuring the same area, a similar problem to that of the integration point placement. The area of only the small central core between the integration point fibres is measured, this is not an approximation as this area is a linear interpolation from the full element cross-sectional area. If linear jam measures are preferred, then the three sides of this triangle could be used. A combination of the two could be used as the area of a triangle is easily calculated from the lengths of the three sides.

The author is confident that the analysis resulting from this description would be a useful general analysis tool for aligned fibre assemblies.

References

1 Backer, S. (1952), Textile Res. J, **22,** 668.

2 Brebbia, C.A. and Dominguez, J. (1989), 'Boundary Elements, an Introductory Course', McGraw-Hill, New York.

3 Carnaby, G.A. and Curiskis, J.I. (1987), J. Textile Inst, **4,** 293.

4 Carnaby, G.A. and Grosberg, P. (1976), J. Textile Inst, **67,** T229.

5 Cook, Malkus, and Plesha. (1989), 'Concepts and Applications of Finite Element Analysis', John Wiley & Sons, Inc.

6 Djaja, R.G. (1989), 'Finite Element Modelling of Fibrous Assemblies',Master of Engineering Thesis, Dept of Civil Eng., Univ. of Canterbury.

7 Duckett, K.E. and Cheng, C.C. (1978), J. Textile Inst, **69,** 55.

8 Dunlop, J.I. (1974), J. Textile Inst, **65**, 532-536.

9 Dunlop, J.I. (1981), J. Textile Inst, **72,** 154.

10 Eggert, M. and J. (see H.Mark: Beitrage zur Kenntnis der Wolle und ihrer Bear beitung, Berlin 1925).

11 Felippa, Carlos A. 'Incremental Finite Element Matrices', Journal of the Structural Division ASCE, No ST12, 1984.

12 Fung, Y.C. (1969), 'A first Course in Continuum Mechanics', Prentice-Hall, Inc. Eaglewood Cliffs, N.J.

13 Galileo, Galilei (1638), Dialogues Concerning Two New Sciences, Leyden; translated by A. De Salvio and A. Fabaro (1914), Evanston, Ill.

14 Gégauff, G. (1907), Bull. Soc. Ind. Mulhouse, **77,** 153.

15 Grosberg, P. (1963), J. Textile Inst, **54,** T223.

16 Hearle, J.W.S. (1958), J. Textile Inst, **49,** T389.

17 Hearle, J.W.S. and Bose, O. N. (1965), Textile Res. J, **35,** 693.

18 Hearle, J.W.S, Grosberg, P. and Backer, S. (1969), 'Structural Mechanics of Fibres, Yarns and Fabrics', Vol. 1, New York, Wiley-Interscience.

19 Hearle, J.W.S. (1962), J. Textile Inst, **53,** T537.

20 Hearle, J.W.S, Gupta, B.S. and Merchant, V.B. (1965), Textile Res. J, **35,** 329.

21 Hearle, J.W.S., H. M. A. E. El-Behery, and V. M. Thakur (1961), J. Textile Inst, **52,** T197.

22 Hickie, T. S. and Chaikin, M. (1974), J. Textile Inst, **65,** 546.

23 Holdaway, H.W. (1945), J. Textile Inst, **56,** T121.

24 Kallmes, O. and Corte, H. (1960), 'The Structure of Paper', Vol. **43,** No. 9, 737-752, Tappi, 1960.

25 Komori, T. and Makishima, K. (1977), Textile Res. J, **47,** 13.

26 Lai, Rubin and Krempl, (1993), 'Introduction to Continuum Mechanics', Oxford; New York, Pergamon Press.

27 Lambert, J.D, (1973), 'Computational Methods in Ordinary Differential Equations', John Wiley & Sons.

28 Lee, D.H, Carnaby, G.A. and Tandon, S.K. (1992), 'Compressional Energy of the Random Fiber Assembly, Part II', Textile Res. J, **62,** 5, 258-265.

29 Lee, D.H. and Carnaby G.A. (1992), 'Compressional Energy of the Random Fiber Assembly, Part I', Textile Res. J, **62,** 4, 185-191.

30 Lee, D.H. and Lee, J.K. (1985), The Text. Mach. Soc. of Japan, 613-622.

31 Lee, D.H, Carnaby, G.A, Carr, A.J, and Moss, P.J. (1990), 'A Review of Current Micromechanical Models of the Unit Fibrous Cell', WRONZ Communication, No. C113.

32 Malvern, L.E. (1969), 'Introduction to the mechanics of a continuous medium', Englewood Cliffs, N.J.: Prentice Hall.

33 Martin, H.C, and Carey, G.F. (1973), 'Introduction to Finite Element Analysis',
McGraw-Hill, Inc.

34 Moore, T.A, (1975), 'Finite Element Analysis of Box-girder Bridges', Ph.D. Thesis, Dept of Civil Eng., Univ. of Canterbury.

35 Morton, W.E. (1956), Textile Res. J, **26,** 325.

36 Morton, W.E. (1956), Textile Res. J, **26,** 325.

37 Morton, W.E. and Yen, K. C. (1952), J. Textile Inst., **43,** T60.

38 Oden, J.T, (1972), 'Finite Elements of Non-Linear Continua', McGraw-Hill, New York.

39 Onogi and Sasaguri, (1961), 'The Elasticity of Paper and Other Fibrous Sheets', Tappi, **44,** 874-80.

40 Pan, N. and Carnaby, G.A. (1988), 'The initial Shear Modulus of a Unit cell of Wool Fibres', WRONZ Report No. R106.

41 Pan, N. and Carnaby, G.A. (1989), Textile Res. J. 285.

42 Pierce, F.T. (1947), Textile Res. J, **17,** 123.

43 Platt, M.M, Klein, W.G. and Hamburger, W.J. (1959), Textile Res. J, **29,** 611.

44 Platt, M.M. (1954), Textile Res. J, **24,** 132.

45 Platt, M.M, Klein, W.G. and Hamburger, W.J. (1958), Textile Res. J, **28,** 1.

46 Platt, M.M. (1950), Textile Res. J, **20,** 1.

47 Platt, M.M. (1954), Textile Res. J, **24,** 132.

48 Postle, R, Burton, P.G. and Chaikin, M. (1964), J. Textile Inst, **55,** T448.

49 Riding, G. (1964), J. Textile Inst, **55,** T9.

50 Riding, G. (1959), J. Textile Inst, **50,** T425.

51 Scipio, L. Albert. (1966), 'Principles of continua with applications'. New York: Wiley.

52 Stearn, A.E. (1971), J. Textile Inst, **62,** 353.

53 Strang, G, and Fix, G.J, (1973), 'An Analysis of the Finite Element Method', Prentice-Hall, Inc., Eaglewood Cliffs, N.J.

54 Sullivan, R.R. (1942), J. Appl. Phys, **13,** 157.

55 Thwaites, J.J. (1980), 'Mechanics of Flexible Fibre Assemblies', eds Hearle, J.W.S, Thwaites, J.J. and Amirbayat, J, Sijthoff and Noordhoff, Alphen aan den Rijn, 87.

56 Treloar, L.R.G. (1965), J. Textile Inst, **56,** T359.

57 Treloar, L.R.G. and Riding, G. (1963), J, Textile Inst, **54,** T156.

58 Van Luijk, C.J. (1981), 'Structural Analysis of Wool Yarns', Ph.D. Thesis, Dept
of Civil Eng., Univ. of Canterbury.

59 Van Wyk, C.M. (1946), J. Textile Inst, **37,** T285.

60 Zienkiewicz, O.C, (1971), 'The Finite Element Method in Engineering Science', McGraw-Hill, London.

A Updating the Orientation Density Function

A.1 Orientation Density Function

The orientation density function is a function which is used to define the orientation of the fibres in an assembly. The function is defined in a spherical coordinate system, where a direction is represented by the angles θ, and ϕ. θ is the angle from the vertical, and ϕ is the horizontal angle. The function is defined such that the probability of finding a fibre within a small angular segment described by dθ and dϕ is:

$$\Omega(\theta,\phi)\sin\theta \; d\phi\, d\theta \tag{A-1}$$

and the limits on θ and ϕ are chosen such that:

$$\int_0^{\frac{\pi}{2}} \int_0^{2\pi} \Omega_b(\theta,\phi)\sin(\theta)\, d\theta\, d\phi \;=\; 1 \tag{A-2}$$

The various terms which make up the material constitutive matrix for the continuum may be calculated in terms of the orientation density function along with the fibre properties including length distributions and frictional properties. Once these are found, the system may be easily analyzed for a small load step and the appropriate strain parameters may be calculated.

The situation being modelled here is uniaxial compression as an axisymmetric problem it can be easily modified due to symmetry to be a two rather than three dimensional problem, considering only the radial and the longitudinal directions. The relevant strain parameters in this situation are the strains in each of the two directions. The orientation density function must be redefined for this situation, leaving it in terms of θ only:

$$\int_0^{\frac{\pi}{2}} \Omega_b(\theta)\sin\theta\, d\theta \;=\; 1 \tag{A-3}$$

A.2 Small Displacement Deformation of a Line

The case of the deformation of a line of original angle θ', which changes to θ, under the relevant strains, is investigated. The simple relationship is derived using two methods, the first graphical and the second analytical in nature.

The continuum is thought to be subject to two strains, one in the radial direction (ε_r), and one in the axial direction (ε_a). These may also be interpreted as a strain in the axial direction and a poissons ratio governing deformation in the radial direction (ν_a). The relationship between these two systems is easily defined:

$$\nu_a = \frac{\varepsilon_r}{\varepsilon_a} \qquad \textit{therefore} \quad \varepsilon_r = \varepsilon_a \, \nu_a \tag{A-4}$$

Both methods assume that the line deforms as shown in Figure (A-1).

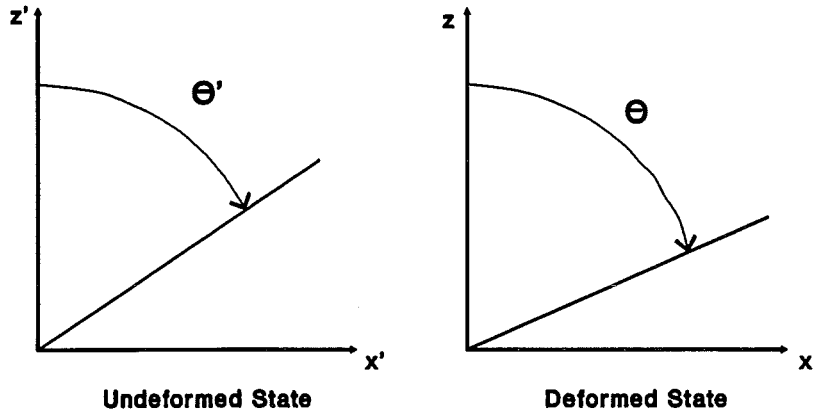

Figure (A-1) *Deformation of a line.*

The relationships can then be derived that for a point on the line:

$$\varepsilon_a = \frac{z-z'}{z'} = \frac{z}{z'} - 1$$
$$\varepsilon_r = \frac{x-x'}{x'} = \frac{x}{x'} - 1 \tag{A-5}$$

Simple trigonometry dictates:

$$\frac{\tan\theta'}{\tan\theta} = \frac{\frac{x'}{z'}}{\frac{x}{z}} = \frac{x'}{x}\frac{z}{z'} = \frac{1+\varepsilon_a}{1+\varepsilon_r} = \frac{1+\varepsilon_a}{1+\varepsilon_a \nu_a} = c \tag{A-6}$$

Therefore the relationship between θ' and θ is found as:

$$\tan\theta' = c\tan\theta \tag{A-7}$$

A more analytical approach is given by initially assuming only the definition of the strain, for the small displacement case, this is:

$$\varepsilon_r = \frac{\partial u}{\partial x'}$$
$$\varepsilon_a = \frac{\partial w}{\partial z'} \tag{A-8}$$
$$\varepsilon_{ra} = \frac{1}{2}\left(\frac{\partial u}{\partial z'} + \frac{\partial w}{\partial x'}\right)$$

Where the displacement vectors, u and w, are described as:

$$u = x - x'$$
$$w = z - z' \tag{A-9}$$

Substitution of equation (A-9) into equation (A-8) leads to:

$$\begin{aligned} \varepsilon_r &= \frac{\partial x}{\partial x'} - 1 \\ \varepsilon_a &= \frac{\partial z}{\partial z'} - 1 \\ \varepsilon_{ra} &= \frac{1}{2}\left(\frac{\partial x}{\partial z'} + \frac{\partial z}{\partial x'}\right) \end{aligned} \qquad \textbf{(A-10)}$$

The mapping for the deformation is assumed as:

$$\begin{aligned} x &= Ax' + By' \\ y &= Cx' + Dy' \end{aligned} \qquad \textbf{(A-11)}$$

Where A,B,C,D are constants.

The linear deformation mapping defined in equation (A-11) is justified because the assumption has been made that a straight line will deform to a straight line, it can also be shown that any terms greater than first order will not fulfil equation (A-10). No constant terms are present as the origin is assumed to remain fixed.

Substitution of equation (A-11) into (A-10), and the assumption that the shear is zero, leads to a set of equations, the simplest solution of which is:

$$\begin{aligned} A &= (1+\varepsilon_r) \qquad \textit{therefore } x = (1+\varepsilon_r)x' \\ B &= (1+\varepsilon_a) \qquad z = (1+\varepsilon_a)z' \\ C &= 0 \\ D &= 0 \end{aligned} \qquad \textbf{(A-12)}$$

The same relationship between the deformed and undeformed angle can be found:

$$\tan\theta' = \frac{x'}{z'} = \frac{(1+\varepsilon_a)}{(1+\varepsilon_r)}\frac{x}{z} = c\frac{x}{z} = c\tan\theta \qquad \textbf{(A-13)}$$

$$\textit{therefore} \quad \tan\theta' = c\tan\theta$$

A.3 Segment Deformation

To calculate how the orientation density function updates with deformation, the change in position and size of a segment must be considered. The probability of a fibre being within a segment in the undeformed state must be the same as the probability of it being within the deformed position of the segment in the deformed state. This may be written more clearly:

$$\Omega_a(\theta)\sin\theta\, d\theta = \Omega_b(\theta')\sin\theta'\, d\theta' \qquad \textbf{(A-14)}$$

Where a and b refer to the deformed and undeformed states respectively.

A relationship must be found between the infinitesimal angles $d\theta'$ and $d\theta$, this may be achieved by differentiation of equation (A-7):

$$\sec^2\theta'\, d\theta' = c\sec^2\theta\, d\theta \qquad \textbf{(A-15)}$$

The deformation of a segment is given:

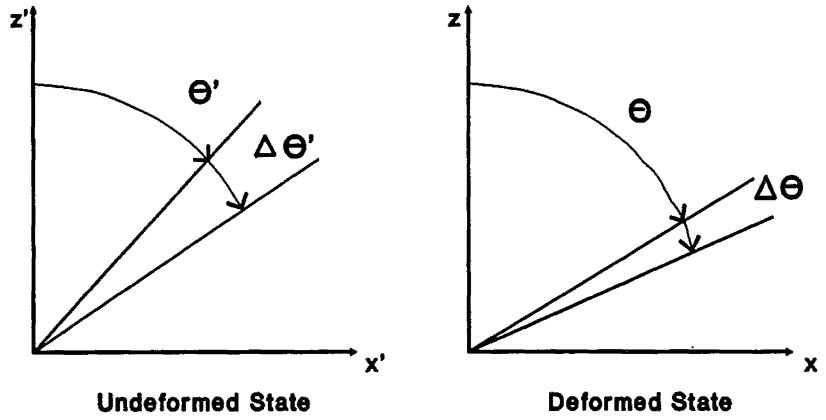

Figure (A-2) *Deformation of a segment.*

It is obvious that the relationship below can be written for segment deformation directly from equation (A-7), as the other side of the segment is simply considered as another straight line in the continuum which deforms according to the rule previously defined.

$$\tan(\theta' + \Delta\theta') = c\tan(\theta + \Delta\theta) \qquad \textbf{(A-16)}$$

However a comparison of equations (A-15) and (A-16) shows two different definitions of what appears to be the same situation. This *discrepancy* comes about as the quantities

$d\theta$ and $\Delta\theta$ cannot be directly compared, $d\theta$ represents an infinitesimal angular segment, while $\Delta\theta$ represents a finite angular segment. A relationship can be written between the two, and then that can be used to show that the equations above do indeed represent the same situation.

The size of the deformed segment is calculated as the sum of the infinitesimal deformed pieces, which may be written in mathematical terms as:

$$\Delta\theta = \int_{\theta}^{\theta+\Delta\theta} d\theta \tag{A-17}$$

A change of variables using equation (A-15) leads to:

$$\Delta\theta = \int_{\theta'}^{\theta'+\Delta\theta'} \frac{\frac{1}{c}\sec^2\theta'}{\frac{1}{c^2}\tan^2\theta'+1}\, d\theta' \tag{A-18}$$

If a substitution for u is made where u is defined as:

$$\begin{aligned} u &= \frac{1}{c}\tan\theta' \\ du &= \frac{1}{c}\sec^2\theta' d\theta' \\ d\theta' &= \frac{du}{\frac{1}{c}\sec^2\theta'} \end{aligned} \tag{A-19}$$

Therefore:

$$\begin{aligned}
\Delta\theta &= \int_{\theta=\theta'}^{\theta=\theta'+\Delta\theta'} \frac{1}{u^2+1}\,du \\
&= \left[\tan^{-1}(u)\right]_{\theta=\theta'}^{\theta=\theta'+\Delta\theta'} \\
&= \left[\tan^{-1}\left(\frac{1}{c}\tan(\theta'+\Delta\theta')\right)-\tan^{-1}\left(\frac{1}{c}\tan\theta'\right)\right] \\
&= \left[\tan^{-1}\left(\frac{1}{c}\tan(\theta'+\Delta\theta')\right)-\tan^{-1}(\tan\theta)\right] \\
&= \left[\tan^{-1}\left(\frac{1}{c}\tan(\theta'+\Delta\theta')\right)-\theta\right] \\
\textit{therefore}\quad \theta+\Delta\theta &= \tan^{-1}\left(\frac{1}{c}\tan(\theta'+\Delta\theta')\right) \\
\tan(\theta'+\Delta\theta') &= c\tan(\theta+\Delta\theta)
\end{aligned} \tag{A-20}$$

Which proves the consistency of the two apparently different equations.

A.4 Updating the Density Function

It is desired to now derive an equation for the orientation density function in the deformed state, in terms of only the constant c, the position in the deformed configuration, and the original orientation density function.

From equation (A-7), it can be written:

$$\begin{aligned}
\theta' &= \tan^{-1}(c\tan\theta) \\
\textit{therefore}\quad \theta'+\Delta\theta' &= \tan^{-1}(c\tan(\theta+\Delta\theta))
\end{aligned} \tag{A-21}$$

Manipulation of the same equation can result in:

$$\sin\theta' = \frac{c\tan\theta}{\sqrt{1+c^2\tan^2\theta}} \tag{A-22}$$

Substitution of equations (A-15), (A-22) and (A-21) into (A-14) reveals with some manipulation, the desired equation:

$$\Omega_a(\theta)\sin\theta = \frac{c^2(1+c^2\tan^2\theta)^{-\frac{3}{2}}}{\cos^3\theta}\,\Omega_b(\tan^{-1}(c\tan\theta))\sin\theta \qquad \textbf{(A-23)}$$

A.5 Large Displacement Deformation

The use of the large displacement strain equations in the derivation in place of equations (A-8), leads to a relationship which is valid for large displacement problems. The large displacement strain equations are:

$$\begin{aligned}
\varepsilon_r &= \frac{\partial u}{\partial x'} + \frac{1}{2}\left(\frac{\partial u}{\partial x'}\right)^2 + \frac{1}{2}\left(\frac{\partial w}{\partial x'}\right)^2 \\
\varepsilon_a &= \frac{\partial w}{\partial z'} + \frac{1}{2}\left(\frac{\partial u}{\partial z'}\right)^2 + \frac{1}{2}\left(\frac{\partial w}{\partial z'}\right)^2 \\
\varepsilon_{ra} &= \frac{1}{2}\left(\frac{\partial w}{\partial x'} + \frac{\partial u}{\partial z'}\right) + \frac{1}{2}\left(\frac{\partial u}{\partial x'}\frac{\partial u}{\partial z'} + \frac{\partial w}{\partial x'}\frac{\partial w}{\partial z'}\right)
\end{aligned} \qquad \textbf{(A-24)}$$

Using the same linear deformation mapping as was used for the small displacement case, equation (A-11), and substituting into equation (A-24) and (A-9) gives the system of equations:

$$\begin{aligned}
2\varepsilon_r + 1 &= A^2 + C^2 \\
2\varepsilon_a + 1 &= B^2 + D^2 \\
2\varepsilon_{ra} &= AB + CD
\end{aligned} \qquad \textbf{(A-25)}$$

And similarly to the small displacement case the simplest solution of this system when the shear is zero, is given by:

$$\begin{aligned} A &= \sqrt{2\varepsilon_r+1} & x &= \sqrt{2\varepsilon_r+1}\,x' \\ B &= \sqrt{2\varepsilon_a+1} & z &= \sqrt{2\varepsilon_a+1}\,z' \\ C &= 0 \\ D &= 0 \end{aligned} \qquad \textbf{(A-26)}$$

It is interesting to note that the first two parts of the binomial expansion of this term represent the small displacement relationship.

$$\sqrt{2\varepsilon_r+1} = 1+\varepsilon_r-\tfrac{1}{2}\varepsilon_r^{\,2}+\tfrac{1}{2}\varepsilon_r^{\,3}-\tfrac{15}{24}\varepsilon_r^{\,4}+\ldots \qquad \textbf{(A-27)}$$

Similar reasoning to that used for the small displacement case leads to almost identical conclusions regarding the updating of the orientation density function, the only difference being that the constant c is replaced by the appropriate large displacement constant c_L:

$$\Omega_a(\theta)\sin\theta = \frac{c_L^2(1+c_L^2\tan^2\theta)^{-\frac{3}{2}}}{\cos^3\theta}\,\Omega_b(\tan^{-1}(c_L\tan\theta))\sin\theta \qquad \textbf{(A-28)}$$

$$c_L = \frac{\sqrt{2\varepsilon_a+1}}{\sqrt{2\varepsilon_r+1}}$$

B Self Locking of Ideal Migration

The equations developed by J.W.S. Hearle for the case of ideal migration in staple fibre yarns are given (B-1) [B1].

$$
\begin{aligned}
A.\quad f_i &= \frac{q_i}{Q} - \frac{(u_E^2 - c^2)}{2(1-c^2)} \\
B.\quad f_o &= \frac{q_o}{Q} + \frac{(u_E^2 - c^2)}{2(1-c^2)} \\
C.\quad m_i &= \text{integer nearest to } f_i \\
D.\quad C_i &= +1 \text{ for } m_i \le f_i \le \left(m_i + \frac{1}{2}\right) \\
&= -1 \text{ for } \left(m_i - \frac{1}{2}\right) \le f_i \le m_i \\
E.\quad u_i^2 &= 2C_i(1-c^2)(f_i - m_i) + c^2 \\
F.\quad x_{E,c} &= \frac{c^2}{u_E^2} - \sigma_y\left(1 - \frac{c^2}{u_E^2}\right) - 2\sigma_1 g_E \\
G.\quad x_{E,i} &= \left(\frac{2\mu}{a}\right)\int_0^{s_i} g_i\left[1 - \frac{2(s_i - q_i)}{L_f}\right]dq_i \\
H.\quad & s_{ic} \text{ is the value of } s_i \text{ when } x_{E,i} = x_{E,c} \\
I.\quad x_E &= \frac{1}{L_f}\left[\int_0^{s_{ic}} x_{E,i}\,ds_i + \int_0^{s_{oc}} x_{E,o}\,ds_o + (L_f - s_{ic} - s_{oc})x_{E,c}\right] \\
&= \text{value of } x \text{ at } E, \text{ when } u = u_E \\
J.\quad \frac{dg}{du} &= -\frac{x+g}{u} \text{ with } g = 0 \text{ at } x = 1 \\
K.\quad F &= \frac{2}{(1-c^2)}\int_c^1 \left\{x\left(\frac{c^2}{u^2}\right) - g\left[1 - \left(\frac{c^2}{u^2}\right)\right]\right\} u\,du
\end{aligned}
\qquad \textbf{(B-1)}
$$

Where the input parameters are:

$$
\begin{aligned}
c &= \cos\alpha \text{ where } \alpha = \text{twist angle} \\
Q &= \text{Length of fibre in One migration cycle} \\
\sigma_y &= \text{Yarn'poissons ratio'} \\
\sigma_1 &= \text{Fibre poissons ratio} \\
\left(\frac{2\mu}{a}\right) &\quad \text{Where } \mu = \text{coefficient of friction} \\
&\qquad\quad a = \text{fibre radius} \\
L_f &= \text{Fibre length}
\end{aligned}
\qquad \textbf{(B-2)}
$$

The solution of these equations using a numerical iterative technique as outlined by Hearle was coded in the FORTRAN language.

Initially results were found by choosing the initial values of the lateral stress ratio (g) as constant and equal to 0.01. The other input parameters were arbitrarily chosen ?. The value of $2\mu/a$ was allowed to vary to give an impression of how the normalised force (F) varied with changing frictional parameters, this would also give some indication as to any serious bugs in the coding of the solution.

$$
\begin{aligned}
c &= 0.866 \\
Q &= 50 \\
\sigma_y &= 0.5 \\
\sigma_1 &= 0.5 \\
\left(\frac{2\mu}{a}\right) &= \textit{Varies} \\
L_f &= 200
\end{aligned}
\qquad \textbf{(B-3)}
$$

Graphs of g, x, and the amount of fibre slippage are shown, the value of F over a range of $2\mu/a$ is also given.

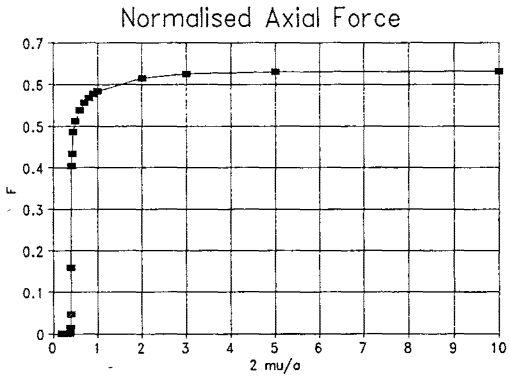

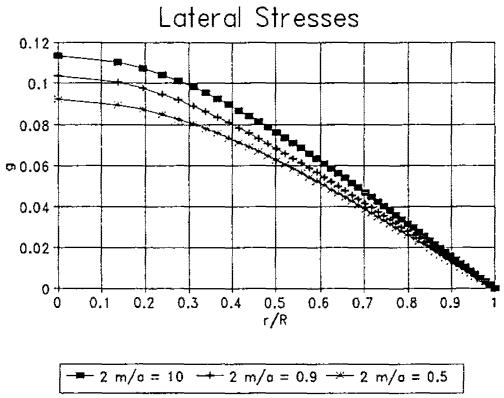

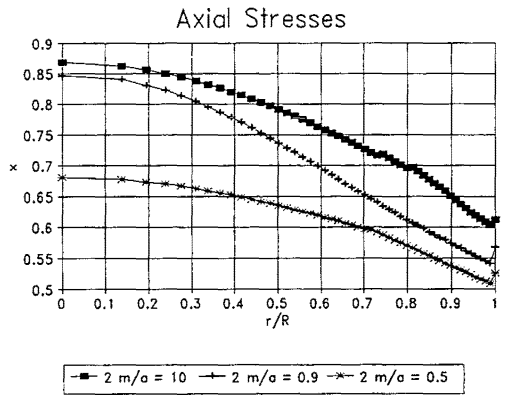

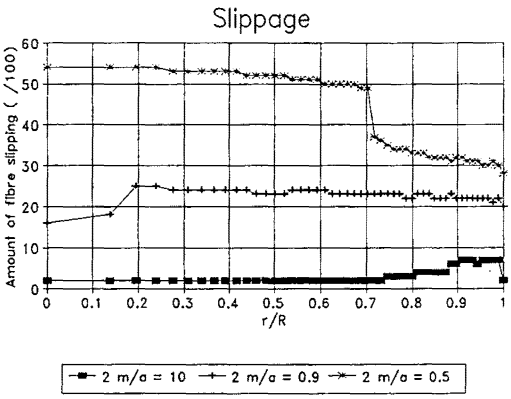

These results would seem to indicate that the equations of ideal migration would self lock in the absence of the WF_0 term in the equation of friction (B-4).

$$F = \mu P + WF_o \qquad \textbf{(B-4)}$$

However the solution above is found by using an iterative technique to solve a system of nonlinear equations ?, as the system is nonlinear there is the possibility of the final result being critical to the solution path. Therefore, the choice of starting point (vector of lateral stress values) could determine the result, the correct choice of these values is essential for an accurate answer. Analyses were performed with various starting vectors (although far from a complete set), these were divided into three main classes which are outlined below:

1) Positive, all non-zero components (of which there were at least one) were greater than zero. The solutions above were obtained with a member of this set, a constant vector with every component at value 0.01. Variations of this set

were attempted, (including a vector with only one non-zero component, and that at a value of 1e-6) but with more or less iterations the same final answer was always found.

2) Negative, all non-zero components (at least one) were less than zero. The solution for this case were found to rapidly diverge with iteration, this may be due to a bias in the coding towards the assumption of positive values for g, or due to the actual equations, but this was felt to be unimportant.

3) Zero, all components of the vector were zero. It was found that with iteration the solution never diverged from the initial zero state, that this will happen is obvious from a careful study of equations ?. Equation G calculates the axial stress which will be at a position in a fibre on the assumption that the fibre is slipping from that point to the fibre end. As the values of lateral stress (g) are a multiplier inside the integral all along the fibre, an all zero g vector can only result in an all zero $x_{E,i}$ vector. As the value of fibre axial stress if fibre is not slipping will always be positive, the minimum of the slipping and non-slipping options which will be chosen will always be the all-zero slipping case. Therefore no axial stresses may be formed, and the differential equation J may be solved to give g=0 again.

Conclusion

It has been shown that the equations of ideal migration with slippage ? only self-lock in the presence of an initial stress. Using the valid initial state for a 'stress free' starting point can not result in the generation of any internal stresses.

References

B1 Hearle, J.W.S., Theoretical Analysis of the Mechanics of Twisted Staple Fibre Yarns, Textile Research Journal, December 1965, 1060-1071.

C Processing Spring Data

The software designed for processing the spring data is outlined. Detailed comment about the source code for the programs will be omitted as it is to be included on an accompanying diskette.

The data processing is in two steps, the determination of the transformation to orthogonal coordinates and the data transformation. The two programs will be explained separately.

C.1 Transformation Determination

The transformation to be determined is the mapping of the digitizer coordinates of the grid to the known real coordinates of the grid. Once this has been found then it can be used to adjust the spring data for any distortion from the digitizer or the photographic process (the distortion from the photograph was clearly noticeable).

The program for determining the parameters controlling the transformation is called **GRIDIT**. Input to the program consists of the digitized coordinates of the background grids on the spring photographs (see section 9.4). The grids are known to be 50mm squares and the actual measurement of the coordinates gives the basis for assessing the transformation.

The grid data is presented as a continuous stream of coordinate pairs, one pair per line in an ASCII file. The program is set up on the assumption that the data has been digitized from left to right, starting from the bottom left of the grid. When the end of each row is reached the data simply restarts from the left, no special mark is used to denote the end of the row.

The distance between each of the grid points is measured, an upper and lower tolerance is set as proportions of the average value. Any points which differ from the previous by less than the lower value are ignored, it was common for the digitizer to record two or three records at one point and this limit eliminated these extraneous points. When the distance was greater than the upper limit then it was assumed that the two points were at the right hand end of one row and the left of the next, this is the only mechanism for separation of the rows. Using this approach the data is read in and

sorted into an array for use within the program. The maximum number of columns and rows are assessed (maximum allowed within the program was 15).

Real coordinates were then assigned to each of the grid points, the bottom left grid point was at (0,0) and each x coordinate increased by 50mm and each y coordinate by 50mm as the grid points were left or up the mesh respectively.

The mapping function for the transformation is the same mapping that would be used for a nine noded Lagrangian finite element. The displacements of the mapping are defined by the coordinates of a three by three array of nodes, the internal displacements are calculated assuming a two dimensional cubic surface. The mapping is therefore defined by eighteen degrees of freedom (two coordinates at each of the nine nodes). The original grid is represented by up to 225 degrees of freedom (15 by 15 nodes), so some form of fitting procedure would be required to find the transformation.

A least squares fit was used to form the best transformation coordinates. The first approximation to the mapping was made by fitting a square mapping oriented to the global coordinate system around the grid points. Although this initial guess was often significantly incorrect good convergence to a solution was always found.

A subroutine (**GETERR**) evaluated the total square error of the system. For each grid point the coordinates of the grid point was established in a system which had plus or minus one at each of the four sides of the grid. Using this grid coordinate the real coordinate of the point in the mapping could be calculated. The square of the distance between the calculated coordinate and the real location of the point was added to the total error value. This process was carried out for every point in the grid.

The error subroutine was used to numerically generate the vector of first derivatives of the error with respect to the coordinates defining the mapping. The matrix of second derivatives was also calculated numerically.

Newtons method was used to find the next estimate of the mapping coordinates. Convergence was very fast as the error function varies quadratically for which Newtons method is exact.

A significant advantage of this reduction in the number of degrees of freedom and subsequent fitting procedure is that any small (or sometimes large) errors in the input

data were eliminated. The resultant fits to the data were close enough that it would have been pointless to use a higher degree of approximation.

The program then output the nine pairs of coordinates to a temporary file (**gridcood.dat**) for use by the next stage of the process.

C.2 Data Transformation

The program for transforming the data was called **TRDATA** and like **GRIDIT** the input file was taken from the standard input.

The data file containing the coordinates of the centrelines of the springs is in the same format as that for the grid data. The data is interpreted in the same manner as was the grid data, the distances between adjacent points being used to separate the different springs.

Each point of the spring data was then transformed by applying the mapping in reverse, the data was changed from digitizer coordinates to real coordinates.

An iterative approach was used for the reversal of the mapping (subroutine **GETCOOD**). The initial guess for the coordinates of the point were always selected as the centre of the grid. Convergence was always found as long as the mapping was single valued at every point (which is the case for any realistic situation). The iterative approach used here was similar to that used in the previous section, basically a least squares fit using Newtons method to minimize the error function. The error function was calculated as the square of the distance between the given digitizer coordinates and the mapped coordinates generated from the present guess.

Using this process the data was adjusted. The resultant data was smoothed using a running average technique to eliminate some of the worst kinks in the digitized data.

D Fibrous Finite Element Program

The program which was used to generate the three dimensional model results is presented. Only a brief outline is given, the source code being supplied on an accompanying diskette. It should be pointed out that although sufficient instructions are given, this program is not intended for general use.

An explanation of the two dimensional program will not be given but the structure is identical to that of the three dimensional model as the three dimensional was developed by extending the two dimensional. The source code for the two dimensional program will be included on the diskette.

As well as outlining the program function, this section will include a sample program and sample output (with explanations).

D.1 Program Outline

An outline of the main program will be given, quick explanations of minor subroutines will be included in this outline. Significant subroutines will be outlined separately.

The main program is called **FIBRE3** within the program code, but has been given a lowercase name for the executable (**fibre3**).

- Program start.
- Initialise variables.
  All variables are specified to help eliminate errors.
- Read debug status from file **.debug**.
  The debug status determines the amount of internal data which is sent to the standard oulput during program execution.
- Call to **RPLOTE**.
  Initialise plot output
- Open output files.
- Call **INPUTDAT.**
  Read all of the input data from the inputfile (assumed to be input.dat). The input data is the definition of; the nodes, the elements, the boundary conditions, the material properties and the solution control parameters.
- Call **ORGDAT**.

The ordering of the loadings and boundary conditions changed to reflect the internal nodal numbering rather than the user ordering, the element connectivity lists are adjusted as well.

- Call **INITIAL**.

  This subroutine is called to allow any nonlinear properties that required initial configuration to be processed. The original intention of this subroutine was to allow the extension relationship of the fibre helix to be numerically calculated only once. This subroutine has no effect in the three dimensional analysis.

- Call **GETIMD**.

  This subroutine calculates the reference element parameters. It is effectively a call to the GETMP subroutine using the undeformed nodal coordinates. The reference values for all elements are stored in an array for later use.

FOR EACH STEP IN THE ANALYSIS DO...

- Call **BOUND.**

  Given the number of the step this subroutine calculates the boundary conditions which apply. Boundary conditions is taken to be a general term including; enforced displacements, applied loadings, Lagrange multipliers and linked degrees of freedom.

- Call **GETEQN**.

  The equation numbering for the step is defined, this must be re-done with each step as changing boundary conditions necessitates different numbers of equations.

FOR EACH INCREMENT DO...

- Increment the step pseudo-time.

FOR EACH ITERATION DO...

- Set relevant variables to zero

FOR EACH ELEMENT DO...

- Call **GETELC**

Finds the initial coordinates of the particular element which is being treated.

- Add the contribution from the global displacement vector to each of the element coordinates to convert them to present coordinates.
- Any enforced displacements are put on to the element degrees of freedom.
- Relax the element if required.

  Element relaxation was introduced as a way of getting around the large effect that the end boundary conditions had on the solution. This was not found to be useful.
- Call **GETELM**.

  This is one of the principle subroutines, it returns the element stiffness matrix and the element force vector. This subroutine will be detailed later.
- Call **ASSEMB**.

  The element stiffness matrix and force vector are assembled into the global matrices and vectors.

END LOOP ON ELEMENTS

- Applied forces and Lagrange constraints are added to the system matrices.
- The total and maximum out of balance forces are calculated
- Call **WSOL**

  The equation solver is called, this subroutine is explained in more detail in appendix E.
- The maximum nodal displacements and rotations are calculated
- A factor is calculated to limit the nodal displacements and rotations to the allowed maximums.
- The global displacement vector is updated
- The fibre directions at each node are updated

END LOOP ON ITERATIONS

The loop is completed if either the convergence criteria have been satisfied or the number of iterations allowed has been exceeded. If the number of iterations was exceeded then jump to the end of the program and exit.

- Write output for the step to the output file (**outdata dat**)

  The outputfile is given all of the nodal data, both displacements and forces.

END LOOP ON INCREMENTS

END LOOP ON STEPS

- End program

The subroutine **GETELM** calculates the element stiffness matrix and the element force vector The effects of the modal analysis are apparent in this subroutine and a significant proportion of the computational time is spent in **GETELM** Due to this importance the subroutine is outlined in more detail below

- Subroutine Start
- Call **GETCENT**

  The values of the three vectors defining the element directions for the rigid body rotations are calculated. These values are sent to the subroutines which calculate the modal values, this was done to ensure that they would be invariant while the derivatives were calculated.
- Call **GETMP**

  The element measures for the deformed element coordinates are calculated.
- The weighting to apply to each integration point is calculated, the initial packing fraction is taken into account to asses how many fibres pass through the element.

FOR EACH INTEGRATION POINT DO...

- Calculate the length and bending properties of a fibre passing through the integration point, end positions and rotations are linearly interpolated from the element nodes.
- Call **EXTEND**

  The extension stiffness and force of the integration pointfibre are assessed, this subroutine could be adjusted by the user to provide any force relationship desired.
- Call **BEND**

The program unit which the user can adjust for the bending properties of the fibre, this routine returns a four by four bending stiffness matrix and a four by one bending force vector. Future versions could simplify this so that the routine need only supply the moment curvature relationship of the fibre material.

- Call **TWIST**

  This subroutine provide the torsion relationship of the fibre passing through the integration point.

- The contributions of the integration point fibre are added to the modal stiffness matrix and the modal force vector.

END OF LOOP ON INTEGRATION POINTS

- A few of the remaining modes are given small stiffness values to facilitate equation solution.
- Call **JAM**

  The Jam properties of the continuum are assessed for each of the jam modes.

- The jam stiffness and forces are added to the appropriate modal arrays
- Call **GETAI**

  This subroutine calculates the matrix of the first derivatives of the mode shapes with respect to the nodal degrees of freedom.

- Call **S1**

  Stage one of the coordinate transformation from modal coordinates to nodal coordinates, the force vector is changed.

- Call **S2**

  Stage two of the transformation, the part of the transformed stiffness matrix which depends of the first derivative matrix is calculated.

FOR EACH DEGREE OF FREEDOM OF THE ELEMENT DO...

- Call **GETAJ**

  Calculates the second derivative matrix of the element.

- Call **S3**

  Modifies the element nodal stiffness matrix using the second part of the transformation equation, depending on the modal force vector and the second derivative matrix.

END LOOP ON ELEMENT DEGREES OF FREEDOM...

- End Subroutine.

D.2 Program Execution

The program is specific in the names of the input and output files. This is a symptom of the rogram being only a preliminary version, in a fuller version the user would be able to specify the names of both files.

The program is run by typing the command:

fibre3

As well as the data saved to the output files, a large amount is sent to the standard output. This information is for debugging purposes and is usually redirected to a file by starting using the UNIX command:

fibre3 > &! outdat &

The input file is taken to be: **input.dat**

The output is written to three principal files: **outdata.dat**
output.dat
echo.dat

The file **outdata.dat** has the state of every node at the end of each step, **output.dat** has one line for each iteration giving the convergence data. The **echo.dat** file is an echo of the input data, for checking purposes.

D.3 Input File

A simple data file is used as a test case, the input file is presented below with explanation inserted in italics.

Start of input file

```
20    4    2
```

These three numbers are the number of nodes, the number of elements and the number of steps respectively.

```
1   0.70711E-03   0.70711E-03   0.00000E+00   0.00000E+00   0.00000E+00   0.10000E+01
```

Nodal data, one line for each node, the first number is the node number, the next three are the (x,y,z) coordinates of the node, the last three are the initial fibre direction vector at the node.

```
 2  -0.70711E-03   0.70711E-03   0.00000E+00   0.00000E+00   0.00000E+00   0.10000E+01
 3  -0.70711E-03  -0.70711E-03   0.00000E+00   0.00000E+00   0.00000E+00   0.10000E+01
 4   0.70711E-03  -0.70711E-03   0.00000E+00   0.00000E+00   0.00000E+00   0.10000E+01
 5   0.70711E-03   0.70711E-03   0.25000E-02   0.00000E+00   0.00000E+00   0.10000E+01
 6  -0.70711E-03   0.70711E-03   0.25000E-02   0.00000E+00   0.00000E+00   0.10000E+01
 7  -0.70711E-03  -0.70711E-03   0.25000E-02   0.00000E+00   0.00000E+00   0.10000E+01
 8   0.70711E-03  -0.70711E-03   0.25000E-02   0.00000E+00   0.00000E+00   0.10000E+01
 9   0.70711E-03   0.70711E-03   0.50000E-02   0.00000E+00   0.00000E+00   0.10000E+01
10  -0.70711E-03   0.70711E-03   0.50000E-02   0.00000E+00   0.00000E+00   0.10000E+01
11  -0.70711E-03  -0.70711E-03   0.50000E-02   0.00000E+00   0.00000E+00   0.10000E+01
12   0.70711E-03  -0.70711E-03   0.50000E-02   0.00000E+00   0.00000E+00   0.10000E+01
13   0.70711E-03   0.70711E-03   0.75000E-02   0.00000E+00   0.00000E+00   0.10000E+01
14  -0.70711E-03   0.70711E-03   0.75000E-02   0.00000E+00   0.00000E+00   0.10000E+01
15  -0.70711E-03  -0.70711E-03   0.75000E-02   0.00000E+00   0.00000E+00   0.10000E+01
16   0.70711E-03  -0.70711E-03   0.75000E-02   0.00000E+00   0.00000E+00   0.10000E+01
17   0.70711E-03   0.70711E-03   0.10000E-01   0.00000E+00   0.00000E+00   0.10000E+01
18  -0.70711E-03   0.70711E-03   0.10000E-01   0.00000E+00   0.00000E+00   0.10000E+01
19  -0.70711E-03  -0.70711E-03   0.10000E-01   0.00000E+00   0.00000E+00   0.10000E+01
20   0.70711E-03  -0.70711E-03   0.10000E-01   0.00000E+00   0.00000E+00   0.10000E+01
```

```
1    1    1    1    2    3    4    5    6    7    8
```

Element connectivity data, one line for each element, the first number is the element number, the second is the element type (there is at present only one type). The remaining eight numbers are the eight nodes forming the element.

```
2    1    1    5    6    7    8    9   10   11   12
3    1    1    9   10   11   12   13   14   15   16
4    1    1   13   14   15   16   17   18   19   20
```

```
0
```

The number of relaxed elements, if the number were not zero then this would be followed by one line for each element, containing only the number of the element to be relaxed.

```
0   28    0    0    3
```

Data for step zero, srep zero is the default step, any conditions applied to this step are applied to every step. First number is the step number, this is followed by the number of displacement boundary conditions, the number of applied loads, the number of Lagrange Constraints and the number of eliminated degrees of freedom (note that due to a program bug, degrees of freedom may only be eliminated in step zero).

```
1    1    1    0
```

Boundary condition data; Node, degree of freedom, index, value. The particular degree offreedom (1-6) on the node is set to the value given. If the index is one then the value is constant over the step, a value of two will ramp the value from that at the previous step.

```
   1    2    1    0
   1    3    1    0
   1    6    1    0
   2    1    1    0
   2    2    1    0
   2    3    1    0
   2    6    1    0
   3    1    1    0
   3    2    1    0
   3    3    1    0
   3    6    1    0
   4    1    1    0
   4    2    1    0
   4    3    1    0
   4    6    1    0
   5    1    1    0
   5    2    1    0
   5    3    1    0
   6    1    1    0
   6    2    1    0
   6    3    1    0
   7    1    1    0
   7    2    1    0
   7    3    1    0
   8    1    1    0
   8    2    1    0
   8    3    1    0
```

If there had been any applied loads or Lagrange constraints, they would have been defined here.

```
3    14   13
```

Eliminated degrees of freedom; degree of freedom (1-6), node number one, node number two. The degree of freedom at node number one is eliminated from the equation system by setting it equal to the same degree of freedom on node number two.

```
   3    15   13
   3    16   13

   1   8    4    0    0
```

Similar node data is given for step number one.

```
  17    1    2   0.00000E+00
  17    2    2   0.00000E+00
  18    1    2   0.00000E+00
  18    2    2   0.00000E+00
  19    1    2   0.00000E+00
  19    2    2   0.00000E+00
  20    1    2   0.00000E+00
  20    2    2   0.00000E+00

  17    3    2   1.0
  18    3    2   1.0
  19    3    2   1.0
  20    3    2   1.0

0.5E+00   50 0.100E+05 0.100E+03 0.125E-02 0.100E+00
```

All steps except number zero have this line of control data. The data is; the size of the pseudo-time increment within the step (1.0 is the whole step, the inverse of this number is the number of increments within the step), the maximum number of iterations allowed within one increment, the force convergence tolerance, the moment convergence tolerance, the maximum displacement allowed within one iteration, the maximum rotation allowed within one iteration.

```
  2   8    4    0    0
```

Data for the second step.

```
 17    1    2   0.00000E+00
 17    2    2   0.00000E+00
 18    1    2   0.00000E+00
 18    2    2   0.00000E+00
 19    1    2   0.00000E+00
 19    2    2   0.00000E+00
 20    1    2   0.00000E+00
 20    2    2   0.00000E+00

 17    3    2   10.0
 18    3    2   10.0
 19    3    2   10.0
 20    3    2   10.0

1.0E+00   50 0.100E-03 0.100E-05 0.125E-02 0.100E+00

  7
```

The number of material properties. Followed by one line for the value of each of the properties.

```
 0.371000E+10
 0.100000E+10
 0.400000E+00
 0.361000E-04
 0.100000E-01
 0.200000E+00
 0.250000E+00

 10    3
```

The monitor degree of freedom (node, local dof), the value of this degree of freedom is printed at every iteration during the program run, allows some monitoring of the system during a run.

D.4 Output Files

The two principle output files are outdata.dat and output.dat. The outputs from the sample input file are given with explanation.

output.dat

This file is a record of the iteration by iteration convergence of the system. The meaning of each of the columns is:

Column Number Explanation

1 *Step Number*

2 *Pseudo time within the step, varies from zero to one within the step.*

3 *Iteration number within the step.*

4 *Maximum residual force.*

5 *Maximum residual moment.*

6 *Value of the monitor node.*

```
 OUTPUT FROM THREE DIMENSIONAL FIBROUS ANALYSIS
================================================

STEP      TIME         ITER       MXRESF       MXRESM    MNODE

   1   0.500000E+00     1   0.500000E+00   0.000000E+00   0.269539E-03
   1   0.500000E+00     2  -0.415256E+02  -0.488736E-20   0.215485E-04
   1   0.100000E+01     1   0.364063E+00  -0.636402E-20   0.242727E-04
   1   0.100000E+01     2  -0.529116E-01  -0.597837E-20   0.239671E-04
   2   0.100000E+01     1   0.899920E+01   0.577194E-20   0.773087E-04
   2   0.100000E+01     2  -0.570634E+00   0.534171E-20   0.741374E-04
   2   0.100000E+01     3  -0.123198E-01   0.537153E-20   0.740690E-04
   2   0.100000E+01     4  -0.265661E-03   0.538779E-20   0.740675E-04
   2   0.100000E+01     5  -0.572850E-05   0.540702E-20   0.740675E-04
```

outdata.dat

This file contains enough information for the post-processor to generate the state of the mesh at the end of any step.

An example file is not presented due to the length of the file. The basic structure of the file is simple:

- First line is two numbers, the number of nodes and the number of elements.
- The initial nodal coordinates, one line for each node consisting of the node number and then the six numbers representing the coordinates and fibre direction.
- The element connectivity information, one line per element. The line has the element number followed by the node numbers of the eight nodes.
- Then follows one data block for the end of each increment.
  - The first line starts with a '*' and is followed by the step number, the pseudo time and the number of Lagrange multipliers.

- One line then follows for each node. Each line has the node number, the three displacements in the translation direction, the three components of the fibre direction vector and the amount of twist in the fibre at the node.
- A similar block then follows giving the forces at each degree of freedom at each node.
- The last block gives the force values within each Lagrange multiplier.

D.5 Auto-mesh Programs

It is clear that it would be tedious to compile the input files by hand. When the input configurations are complicated, the initial fibre directions could be different at every node. A series of programs were written to automatically generate the input meshes. These programs are included on the disk. The program used to compile most of the input files for the three dimensional test cases in the results section was **mesh6**. This program sets up a single yarn model of arbitrary height and twist. The bottom two layers of the element are fixed in place. The displacement of the top two layers is defined by a small number of user input parameters. The user can specify the displacements of the top in each of the three directions, as well as the amount of rotation of the top face about the yarn axis. The other parameter is the lean of the yarn, this value (in radians) moves the top face to the position that it would take if the yarn was bent through a circular arc of rotation angle given.

Auto meshing programs were also written for the two dimensional model, these are also included on the accompanying diskette.

E Pivoting Skyline Equation Solver

The requirements of the three dimensional modal fibrous finite element with Lagrange multipliers required a pivoting symmetric skyline equation solver. A search did not result in such a solver and consequently one was written. An outline for this subroutine is presented here while the source is contained on the accompanying diskette.

When an equation solver pivots the order in which two equations are processed is swapped. This is normally done to increase the accuracy of the solution but in some cases (such as the three dimensional model) pivoting may be required in order to get a solution. Failure to pivot would result in the system having to perform a divide by zero.

In a symmetric skyline system terms are stored only from the leading diagonal of the matrix up to the last non-zero term (within each column). This reduced storage has two main effects on the solution, the total storage required is approximately halved and the number of calculations required is also reduced (multiplications by zero are avoided) Rather than store the terms in a two dimensional array, the information is stored in three vectors, two real and one integer. The first real vector is the vector of the terms in the main diagonal. The second real vector is the remainder of the terms in the matrix, starting from the second column and listing the terms from the row above the leading diagonal. The integer vector contains an index which has the number of the term in the second real vector which contains the top term of each column. The information in these three vectors is sufficient to reproduce the full matrix.

Skyline solvers normally solve the equations sequentially, this means that all of the calculations required for solution can be done using only the storage within the skyline system. Solvers effectively use Gaussian elimination to solve the equations, although the system becomes asymmetric as gaussian elimination is employed, the lower triangular halve also changes to all zeros. This property is exploited to make symmetric skyline solvers work within the available storage.

The pivoting skyline solver must pivot on two terms which are both on the main diagonal, this maintains the symmetry of the matrix and makes the solver possible. This implementation only pivots as a last resort. It is not possible for the solver to pivot within the skyline, this solver has a subroutine which pivots the system, reorganising

the skyline vectors. It is likely that this operation will increase the size of the skyline storage, but the increases do not appear to be rapid.

The solver pivots when the divisor in the elimination step is less than a tolerance. The tolerance is set as 1E-50 multiplied by the maximum diagonal component.

The pivoting operation needs a degree of temporary storage in order to complete the skyline re-organisation. One of the main reasons for using a skyline formulation is to reduce storage, it is therefore impractical to re-organise the skyline into a new vector. One temporary storage vector is used, the same dimension as the number of degrees of freedom in the system. Fortran variables must have their size defined at the start of the program, often the actual storage required falls far short of the amount of space which has been reserved, this spare space is used to facilitate the pivot. The skyline matrix is copied to the end of the reserved storage space and then strategically copied back to the front of the vector as the pivot progresses. It is ensured that these two areas do not overlap. It is possible that there could be insufficient spare space to re-organise at which point the pivoting becomes impossible although it seems that only a small percentage of the total space is required spare.

The equation solving routine (**WSOL**) is outlined below, followed by an outline of the pivoting subroutine.

The call list for **WSOL** is:
WSOL(MXEQN,MXK,NEQN,ORDER,KLD,KD,KU,LOADS,TEMP,ERROR)

Where:

MXEQN the maximum number of equations in the system.
MXK the number of terms that the skyline storage vector has had space reserved for.
NEQN the number of equations in the system.
ORDER a vector which is used to store the order changes of the equations.
KLD the integer indexing array for the skyline storage.
KD the leading diagonal of the matrix.
KU the upper triangular part of the symmetric skyline matrix.
LOADS the right hand side of the equation system.
TEMP the temporary storage vector which is required.
ERROR an error flag, this is set to one if a solution is not obtained.

An outline of **WSOL** is:

- set up the tolerance variable as a proportion of the maximum diagonal.
- if the first term of the leading diagonal is zero, then pivot on the next non-zero term. (in this context zero implies an absolute value of less than the tolerance value) The pivot is performed by calling the subroutine **DOPIV**.

FOR EACH REMAINING DEGREE OF FREEDOM DO...

- if the diagonal term is zero, then find the next non-zero term and call the subroutine **DOPIV** to pivot the skyline.
- continue to do the forward elimination of the skyline to leave the upper triangular form.

END OF LOOP ON DEGREES OF FREEDOM.

- do the back substitution to find the solution.
- re-order the answer to eliminate the effect of the pivoting.
- end of subroutine.

The subroutine **DOPIV** is outline briefly below. The variables **P1** and **P2** are the equation numbers to be swapped.

- calculate the variable **BUF**.

  This variable is the amount of space between the copy of the skyline at the end of the vector and the start of the vector (buffer), during the process this value is compared against the variable **DIFF** *which is a measure of the expansion of the skyline to check if there is an overlap.*
- swap over the diagonal terms and the force vector terms.
- copy the skyline matrix to the end of the vector.
- copy the part of the skyline before the first swapping column back to the start of the vector (up to the **P1**th column).
- Store the **P1**th column into temporary storage.

  This column is not just the information from the leading diagonal upwards, but includes all of the terms on either the row or column of the equation number (as the matrix is symmetric the contents of an entire row and an entire column are the same.

- Copy terms from the **P2**th column over into the **P1**th space.

  Only the top part of this column will be copied, the new height of this skyline column can be calculated from the old height of **P2**. *A check must be made to ensure that the height is above the leading diagonal. The skyline size is adjusted to account for the new height.*

- Copy the columns between **P1** and **P2**.

  The columns are copied over, the **P1***th row is filled in from the data taken from the* **P2***th column. A check is made to see if the term is zero and is the top of the column, in which case the column height can be reduced.*

- Copy the **P1**th vector from storage into the **P2**th.

  The **P1***th row is a special case, a similar height adjustment is made as with the first column (with corresponding skyline adjustment).*

- Insert the remainder of the columns.

  The rest of the columns are copied over, with special cases for the two rows which are the swapped degrees of freedom. Careful attention is made to increase the column height where required, if a previously zero term is being swapped with a non-zero term then an increase in skyline height may occur.

- end of subroutine.

F Program Disk

The diskette accompanying this thesis contains the necessary source code for both the two dimensional and the three dimensional fibrous analyses.

Each collection of files has been compiled into a **tar** file and then compressed using the Unix **compress** command. This maintains the file names of the programs which in some cases are outside of the DOS filename conventions. A **makefile** is supplied with each program to control the compilation.

The contents of the disk are:

Directory	**File**	**Description**
2D	FIB2TAR.Z	The source code for the two dimensional program.
	MSH2TAR.Z	Auto-meshing program for two dimensions.
	MAP2TAR.Z	MAPLE input for two dimensional analysis.
3D	FIB3TAR.Z	Source code for three dimensional program.
	MSH3TAR.Z	Auto-mesh for three dimensions.
	MAP3TAR.Z	MAPLE input for three dimensions.
WSOL	WSOLTAR.Z	Source code for WSOL subroutine.
SPRING	SPRTAR.Z	Code for spring data processing.
MOD	MODTAR.Z	The code for modifying the MAPLE output for eliminating the divide by zero problems.